Invited Speaker

146 In and ex situ (S)TEM manipulation of 2D materials without air exposure
Manuel Längle, Alberto Trentino, Georg Zagler, Barbara Mayer, Clemens Mangler, Harriet Ahlgren, Kimmo Mustonen, Toma Susi, Jani Kotakoski[1]
[1]University of Vienna, Vienna, Austria

Oral Presentation

222 In-situ observation of rheotaxy: 2D materials' growth on liquid substrates
Ms Kristyna Bukvisova[2,4], Mr Radek Kalousek[1,2], Mr Marek Patocka[2], Mr Suneel Kodambaka[3], Mr Libor Novak[4], Mr Tomas Sikola[1,2], Mr. Miroslav Kolibal[1,2]
[1]CEITEC, Brno University of Technology, Brno, Czech Republic, [2]Institute of Physical Engineering, Brno University of Technology, Brno, Czech Republic, [3]Virginia Polytechnic Institute and State University, Blacksburg, United States, [4]Thermo Fisher Scientific, Brno, Czech Republic
262 Two-dimensional few-atom noble gas clusters in a graphene sandwich
Manuel Längle[1], Kenichiro Mizohata[2], Clemens Mangler[1], Alberto Trentino[1], Kimmo Mustonen[1], E. Harriet Åhlgren[1,2], Jani Kotakoski[1]
[1]Faculty of Physics, University of Vienna, Vienna, Austria, [2]Department of Physics, University of Helsinki, Helsinki, Finland
377 A twist to superlubric sliding in bilayer graphene uncovered by in situ TEM
Dr. Xin Zhou[1], Dr. Mingjian Wu[1], Prof. Erdmann Spiecker[1]
[1]Institute of Micro- and Nanostructure Research (IMN) & Center for Nanoanalysis and Electron Microscopy (CENEM), Friedrich-Alexander-Universität Erlangen-Nürnberg, Erlangen, Germany
409 Surface Polarity Dynamics and Strong Reconstruction in Partially Reduced Nickelate Films
Prof. Dr. Peter A. Van Aken[1], Mr. Chao Yang[1], Mrs. Rebecca Pons[1], Mr. Wilfried Sigle[1], Mr. Hongguang Wang[1], Mrs. Eva Benckiser[1], Mr. Gennady Logvenov[1], Mr. Bernhard Keimer[1]
[1]Max Planck Institute for Solid State Research, Stuttgart, Germany
645 Intralayer modification on Ti3C2Tz MXene Multilayer by Tailoring Surface Terminations
Mr Hari Hara Sudhan Thangavelu[1], Assoc. Prof. Fredrik Eriksson[1], Asst. Prof. Leiqiang Qin[2], Assoc. Prof. Jonas Björk[2], Prof. Johanna Rosén[2], Prof. Per Persson[1]
[1]Thin Film Physics Division, Department of Physics, Chemistry and Biology (IFM), Linköping University, SE - 58183, Sweden, [2]Materials Design Division, Department of Physics, Chemistry, and Biology (IFM), Linköping University, SE - 58183, Sweden
660 Enabling atomic resolution electron microscopy at elevated temperature and beyond pressures of a few bar
Hjalte Ambjørner[1], Anton Bjørnlund[1], Tobias Bonczyk[2], Edwin Dollekamp[2], Lau Kaas[1], Sofie Colding-Fagerholt[1], Kristian Mølhave[3], Christian Damsgaard[3], Stig Helveg[1], Peter Vesborg[1,2]
[1]Center for Visualizing Catalytic Processes (VISION), Department of Physics, Technical University of Denmark, 2800 Kgs. Lyngby, Denmark, [2]Surface Physics and Catalysis (SURFCAT), Department of Physics, Technical University of Denmark, 2800 Kgs. Lyngby, Denmark, [3]National Centre for Nano Fabrication and Characterization (Nanolab), Technical University of Denmark, 2800 Kgs. Lyngby, Denmark
87 Temperature-driven in-situ TEM cation exchange at the solid state: a combined experimental and computational study
Alberto Casu[1], Mr. Claudio Melis[2], Mr. Luciano Colombo[2], Mr. Andrea Falqui[1,3]
[1]Department of Physics, University of Milan, Milan, Italia, [2]Department of Physics, University of Cagliari, Monserrato, Italy, [3]Interdisciplinary Centre for Nanostructured Materials and Interfaces (CIMaINa)- Department of Physics, University of Milan, Milan, Italy
365 Electron-beam-induced surface diffusion of contaminants and growth of carbon contamination

Dr. Erich Müller[1], Mr. Arne Johan Schwartz[1], Mrs. Yolita M. Eggeler[1,2]
[1]Laboratory for Electron Microscopy, Karlsruhe Institute of Technology (KIT), Karlsruhe, Germany, [2]3DMM2O - Cluster of Excellence (EXC-2082/1 – 390761711), Karlsruhe Institute of Technology (KIT), Karlsruhe, Germany

723 Single-Layer Transition Metal Dichalcogenides: Unveiling Excitonic Processes with Multimodal Microscopy

Dr Herman Duim[1], Dr Noémie Bonnet[1], Jassem Baaboura[2], Dr Florian Castioni[2], Dr Steffi Y. Woo[2], Ching-Hwa Ho[3], Kenji Watanabe[4], Takashi Taniguchi[5], Dr Luiz H.G. Tizei[2], Dr Toon Coenen[1]
[1]Delmic, Delft, The Netherlands, [2]Laboratoire de Physique des Solides, Université Paris-Saclay, Centre National de la Recherche Scientifique, Orsay, France, [3]Graduate Institute of Applied Science and Technology, National Taiwan University of Science and Technology, Taipei, Taiwan, [4]Research Center for Electronic and Optical Materials, National Institute for Material Science, Tsukuba, Japan, [5]Research Center for Materials Nanoarchitechtonics, National Institute for Material Science, Tsukuba, Japan

802 Determination of Ti3C2Tx Mxene few layers stacks architecture using valence EELS and diffraction

Dr Jerome Pacaud[1], Dr Haw-Wen Hsiao[2], Dr Renliang Yuan[2], Dr Stephane Celerier[4], Pr Jian-Min Zuo[2], Pr Vincent Mauchamp[1], Dr Thomas Bilyk[3]
[1]Institut Pprime – UPR 3346 – CNRS, Université de Poitiers, Poitiers, France, [2]Department of Materials Science and Engineering, University of Illinois at Urbana-Champaign, Urbana, USA, [3]Université Paris-Saclay, CEA, Service de recherche en Corrosion et Comportement des Matériaux, SRMP, Gif-sur-Yvette, France, [4]IC2MP – UMR 7285 – CNRS, Université de Poitiers, Poitiers, France

854 Investigating nitrogen doped nanocarbon materials as potential carbon dioxide adsorbers

Ivan Musil[1,2], Venkataprasanna Kannan Sampathkumar[1,2], Jonas Haas[1,2], Kevin Strobel[1,2], Jannik Meyer[1,2]
[1]Institute for Applied Physics, University of Tübingen, Tübingen, Germany, [2]NMI Natural and Medical Sciences Institute at the University of Tübingen, Reutlingen, Germany

858 In-Situ Manipulation of Growth Mechanisms in Ni-Seeded GaP Nanowires

Tianyi Hu[1,2], Dr. Yuanyuan Cao[1,2], Dr. Sara M. Franzén[2,3], Dr. Daniel Jacobsson[1,2,4], Dr. Michael S. Seifner[1,2], Prof. Maria E. Messing[2,3], Prof. Kimberly A. Dick[1,2,3]
[1]Centre for Analysis and Synthesis, Lund University, Lund, Sweden, [2]NanoLund, Lund University, Lund, Sweden, [3]Solid State Physics, Lund University, Lund, Sweden, [4]National Center for High Resolution Electron Microscopy, Lund University, Lund, Sweden

49 In Situ TEM Biasing and Heating of Neuromorphic Gold Nanogranular Nanofilms Showing Resistive Switching

Prof. Andrea Falqui[1], Mr. Alberto Casu[1], Mr. Paolo Milani[1], Ms. Angelica Chiodoni[2], Mr. Yurii Ivanov[3], Mr. Giorgio Divitini[3]
[1]University of Milan, Department of Physics, Milan, Italy, [2]Center for Sustainable Future Technologies @PoliTo, Istituto Italiano di Tecnologia, Turin, Italy, [3]Electron Spectroscopy and Nanoscopy, Istituto Italiano di Tecnologia, Genoa, Italy

69 Novel Insights into Atomic-Scale Interface Reconstruction during Epitaxial Growth of Metallic Delafossite Thin Films

Anna Scheid[1], Dr. Qi Song[2], Mr. Hari Pokhrel[3], Dr. Tobias Heil[1], Dr. Stephanie Ribet[4], Dr. Colin Ophus[4], Mr. Niklas Enderlein[3], Dr. Y.Eren Suyolcu[1], Prof. Dr. Philipp Hansmann[3], Prof. Dr. Darrell Schlom[2,5,6], Prof. Dr. Peter A. van Aken[1]
[1]Max Planck Institute for Solid State Research, Stuttgart, Deutschland, [2]Department of Materials Sciences and Engineering, Ithaca, USA, [3]Department of Physics, Friedrich-Alexander-Universität Erlangen-Nürnberg (FAU), Erlangen, Germany, [4]National Center for Electron Microscopy, Molecular Foundry, Lawrence Berkeley National Laboratory, Berkeley, USA, [5]Kavli Institute at Cornell for Nanoscale Science, Ithaca, USA, [6]Leibniz-Institut für Kristallzüchtung, Berlin, Germany

234 RUDDLESDEN-POPPER PLANAR DEFECTS IN METAL HALIDE PEROVSKITES: MECHANISMS OF FORMATION AND CONSEQUENCES FOR PHASE STABILITY
Irina Skvortsova[1], Mr. Tom Braeckevelt[2], Miss Nadine Schrenker[1], Mrs. Annick De Backer[1], Mr. Bapi Pradhan[3], Mr. Johan Hofkens[3], Mrs. Veronique Van Speybroeck[2], Mrs. Sandra Van Aert[1], Mrs. Sara Bals[1]
[1]EMAT, University of Antwerp, Antwerp, Belgium, [2]CMM, Ghent University, Ghent, Belgium , [3]Photomat, KU Leuven, Leuven, Belgium
412 Investigation of metal-to-metal hydride phase transformations in magnesium thin films using STEM techniques
Dr Gopi Krishnan[1]
[1]DTU Nanolab, Technical University of Denmark, Lyngby, Denmark, [2]Faculty of Applid Sciences, Delft University of Technology, Delft, The Netherlands, [3]Faculty of Applid Sciences, Delft University of Technology, Delft, The Netherlands, [4]DTU Nanolab, Technical University of Denmark, Lyngby, Denmark
529 How to better understand ZrCu Thin Films Metallic Glasses recrystallization: a TEM in situ characterization?
Pr. Philippe Steyer[1]
[1]MateIS Laboratory, SNMS Microscopy group, INSA de Lyon, Villeurbanne, France
732 Correlating atomic-resolution structure to the properties of transition metal nitride coatings
Dr. Zaoli Zhang[1], Dr. Zhuo Chen[1], Mr. Yong Huang[1]
[1]Erich Schmid Institute, Austrian Academy of Sciences, Leoben, Austria
960 Carbon nanoribbon formation by in-situ TEM manipulation of a C59N dithiolane derivative encapsulated into SWNTs
Dr Mario Pelaez-Fernandez[1,2,3], Dr Anastasios Stergiou[4], Dr Nikos Tagmatarchis[4], Dr Chris Ewels[5], Dr Raul Arenal[1,2,6]
[1]Instituto de Nanociencia y Materiales Aragón, CSIC-U. Zaragoza, Zaragoza, Spain, [2]Laboratorio de Microscopías Avanzadas, Universidad de Zaragoza, Zaragoza, Spain, [3]Unité Matériaux et Transformations (UMET UMR 8207), Univ Lille, Villeneuve d'Ascq, France, [4]Theoretical and Physical Chemistry Institute, National Hellenic Research Foundation, Athens, Greece, [5]Institut de Matériaux de Nantes Jean Rouxel, CNRS – Université de Nantes, , France, [6]ARAID Foundation, Zaragoza, Spain
1114 Structural characterization of single wall carbon nanotubes via AI assisted transmission electron microscopy
Dr. Antonin Louiset[1], Dr Daniel FÖRSTER[2], Ms. Eira MEDINA[3], Mr. Saïd TAHIR[3], Dr. Vincent JOURDAIN[3], Dr. Christophe BICHARA[4], Dr. Hanako OKUNO[1]
[1]IRIG-MEM, CEA, Université Grenoble Alpes, Grenoble, France, [2]Laboratoire d'Etude des Microstructures, ONERA-CNRS, Université Paris-Saclay, Châtillon, France, [3]Laboratoire Charles Coulomb, CNRS, Université de Montpellier, Montpellier, France, [4]CINaM, CNRS, Université Aix-Marseille, Marseille, France

Poster Presentation

3 Nanotubes and Nanostructures of VS_2, WS_2, and MoS_2: Structural Effects on the Hydrogen Evolution Reaction
Maya Bar Sadan[1]
[1]Ben-Gurion University of the Negev, Department of Chemistry, Beer Sheva, Israel
41 Thermoelectric structure-property relationship establishment in TlGaSe2
Mr Tigran Simonian[1,2], Dr. Ahin Roy[1,2], Dr. Akash Bajaj[3], Dr. Rui Dong[3], Prof. Zdenek Sofer[4], Prof. Stefano Sanvito[3], Prof. Valeria Nicolosi[1,2]
[1]Advanced Microscopy Lab, Trinity College Dublin, Dublin, Ireland, [2]School of Chemistry, Trinity College Dublin, Dublin, Ireland, [3]School of Physics, Trinity College Dublin, Dublin, Ireland,

[4]Department of Inorganic Chemistry, University of Chemistry and Technology Prague, Prague, Czech Republic

76 In-Situ TEM assessment of phase transformation in VO2-based thin films with Ho addition

Ellen Suhr[1], Dr. Aleksander Kostka[2], Prof. Dr.-Ing. Alfred Ludwig[1]
[1]Institute for Materials, Ruhr University Bochum (RUB), , Bochum, Germany, [2]ZGH, Ruhr University Bochum (RUB), , Bochum, Germany

270 Fe/Pt spintronic bilayers: Tailoring structure for enhanced THz emission

Dr. Isaak Vasileiadis[1], Dr. Laura Scheuer[2], Dr. Dimitrios Karfaridis[1], Professor George Dimitrakopulos[1], Dr. Evangelos Papaioannou[1,3], Thomas Kehagias[1]
[1]School of Physics, Aristotle University of Thessaloniki, Thessaloniki, Greece, [2]Department of Physics, Technical University of Kaiserslautern, Kaiserslautern, Germany, [3]Institute of Physics, Martin Luther University Halle-Wittenberg, Halle, Germany

278 TEM Investigations of Multi-Layer Selective Absorber thin films for concentrated solar plant: structure and composition

Nicolas Gautier[1], Dr Florian Chabanais[1], Dr Mireille Richard-Plouet[1], Dr Aissatou Diop[2,3], Dr Béatrice Plujat[2,3], Dr Angélique Bousquet[4], Dr Audrey Soum-Glaude[2], Pr Éric Tomasella[2,3], Pr Laurent Thomas[2,3], Pr Antoine Goullet[1]
[1]Nantes Université, CNRS, Institut des Matériaux de Nantes Jean Rouxel, IMN, Nantes, France, [2]PROMES-CNRS UPR 8521 (Laboratory of PROcesses, Materials, Solar Energy), Font-Romeu, France, [3]Université de Perpignan, Perpignan, France, [4]Université Clermont Auvergne, CNRS, SIGMA Clermont, ICCF, Aubière, France

280 A comprehensive (S)TEM analysis of Zn_3P_2 suitability for green energy applications

Helena Freitas[1], Mr. Thomas Hagger[2], Mr. Raphael Lemerle[2], Miss Didem Dede[2], Mrs. Anna Fontcuberta i Morral[2], Miss Brooke Jablon[3], Mrs. Maria Chiara Spadaro[1,4], Mr. Jordi Arbiol[1,5]
[1]Catalan Institute of Nanoscience and Nanotechnology (ICN2), CSIC and BIST, Campus UAB, Bellaterra, Barcelona, Spain, [2]EPFL STI IMX LMSC, MXC 317 (Bâtiment MXC), Station 12, Lausanne, Switzerland, [3]Oxford Instruments SAS, Za de Courtaboeuf, 9 Avenue du Canada, Batiment le Meridien, Les Ulis, France, [4]Physics and Astronomy Department (DFA) Catania University, Catania, Italy, [5]ICREA, Pg Lluis Companys 23, Barcelona, Spain

294 Anisotropic van der Waals Epitaxy and Sliding of CsPbBr3 Nanoplatelets on ReSe2

Noya Ruth Itzhak[1], Dr. Irit Goldian[2], Dr. Sidney Cohen[2], Dr. Olga Brontvein[2], Katya Rechav[2], Dr. Hagai Cohen[2], Prof. Ernesto Joselevich[1]
[1]Department of Molecular Chemistry and Materials Science, Weizmann Institute of Science, Rehovot, Israel, [2]Chemical Research Support, Weizmann Institute of Science, Rehovot, Israel

299 In situ electron beam irradiation of Ti3C2Tz MXenes. A STEM-EELS study

Ayoub Benmoumen[1,2], Dr. Marie-Laure David[1], Dr. Eric Gautron[2], Dr. Sophie Morisset[3], Dr. Aurélien Habrioux[3], Dr. Stéphane Célérier[3], Pr. Philippe Moreau[2], Pr. Vincent Mauchamp[1]
[1]Université de Poitiers, ISAE-ENSMA, CNRS, PPRIME, Poitiers, France, [2]Nantes Université, CNRS, IMN, Nantes, France, [3]Université de Poitiers, CNRS, IC2MP, Poitiers, France

338 Physico-chemical and biological characterization of Ag- and Cu-doped ZnO thin films coated with calcium phosphates

Ana-Marija Milisav[1], Dr. Maja Mičetić[1], Dr. Pavo Dubček[1], Lamborghini Sotelo[2,3], Cristina Cantallops Villà[4], Dr. Tommaso Fontanot[5], Dr. Ina Erceg[1,5], Dr. Krunoslav Bojanić[1], Dr. Željka Fiket[1], Dr. Maja Ivanić[1], Prof. Dr. Silke Christiansen[3,5], Assist. Prof. Dr. Edwige Meurice[4], Dr. Tihomir Car[1], Dr. Maja Dutour Sikirić[1]
[1]Ruđer Bošković Institute, Zagreb, Croatia, [2]Friedrich-Alexander Universität Erlangen-Nürnberg, Erlangen, Germany, [3]Innovations-Institut für Nanotechnologie und Korrelative Mikroskopie, Forchheim, Germany, [4]CERAMATHS, Université Polytechnique Hauts-de-France, Cambrai, France, Cambrai, France, [5]Fraunhofer Institute for Ceramic Technologies and Systems IKTS, Forchheim, Germany

339 Influence of titanium surface modifications on formation of composite calcium phosphates / silver nanoparticles coatings
Suzana Inkret[1], Dr. Ina Erceg[1,2], Prof. Dr. Silke Christiansen[2,3], Dr. Maja Dutour Sikirić[1]
[1]Department of Physical Chemistry, Ruđer Bošković Institute, Zagreb, Croatia, [2]Fraunhofer Institute for Ceramic Technologies and Systems IKTS, Forchheim, Germany, [3]Innovation Institute for Nanotechnology and Correlative Microscopy – INAM, Forchheim, Germany
341 Impact of Electron Beam Irradiation on Carbon Black Oxidation
David Wahlqvist[1], Dr Mattias Mases[2], Dr Daniel Jacobsson[1], Dr Henrik Wiinikka[3], Dr Martin Ek[1]
[1]Center for Analysis and Synthesis, Lund University, Lund, Sweden, [2]Division of Materials Science, Luleå University of Technology, Luleå, Sweden, [3]RISE Energy Technology Center, Piteå, Sweden
392 Direct observation of the interplay between stacking polytypes and self-intercalation in epitaxial Nb1+xSe2 films
Dr. Hongguang Wang[1], BS. Jiawei Zhang[1], Dr. Chen Shen[2], Dr. Chao Yang[1], Dr. Kathrin Küster[1], Dr. Julia Deuschle[1], Prof. Ulrich Starke[1], Prof. Hongbin Zhang[2], Dr. Masahiko Isobe[1], Dr. Dennis Huang[1], Prof. Peter A. van Aken[1], Prof. Hidenori Takagi[1,3,4]
[1]Max Planck Institute for Solid State Research, Heisenbergstr. 1, 70569, Stuttgart, Germany, [2]Department of Materials and Earth Sciences, Technical University of Darmstadt, Darmstadt, Germany, [3]Institute for Functional Matter and Quantum Technologies, University of Stuttgart, 70569 Stuttgart, Germany, [4]Department of Physics, University of Tokyo, 113-0033 Tokyo, Japan
484 Temperature-dependence of beam-driven dynamics in graphene-fullerene sandwiches
Kevin Strobel[1,2], Michael Schlegel[1,2], Mitisha Jain[3], Dr. Silvan Kretschmer[3], Dr. Arkady V. Krasheninnikov[3], Prof. Dr. Jannik C. Meyer[1,2]
[1]Institute of Applied Physics University of Tübingen, Tübingen, Germany, [2]NMI Natural and Medical Sciences Institute at the University of Tübingen, Reutlingen, Germany, [3]Institute of Ion Beam Physics and Materials Research, Helmholtz-Zentrum Dresden-Rossendorf, Dresden, Germany
498 Heating effects in Bi-doped Cu nanowires for spintronics: atomic resolution in-situ insights
Miss Alejandra Guedeja-Marron[1,2], Dr Matilde Saura-Muzquiz[1], Miss Ines Garcia-Manuz[3], Dr Juan I. Beltran[1], Dr Henrik L. Andersen[4], Dr Lunjie J. Zeng[5], Dr Alok Ranjan[5], Prof. Eva Olsson[5], Dr Paolo Perna[6], Prof. Lucas Perez[1,6], Prof. Maria Varela[1,2]
[1]Dept. Fisica de Materiales, Complutense University of Madrid, Madrid, Spain, [2]Instituto Pluridisciplinar, Complutense University of Madrid, Madrid, Spain, [3]Universidad Autonoma de Madrid, Madrid, Spain, [4]Instituto de Ciencia de Materiales de Madrid (ICMM) - CSIC, Madrid, Spain, [5]Chalmers University of Technology, , Sweden, [6]Instituto Madrileño de Estudios Avanzados – IMDEA Nanociencia, Madrid, Spain
515 Mechanism of WS2 nanotube formation revealed by in-situ/ex-situ imaging and cross-sectional sequences
Dr. Vojtech Kundrat[1,2], Dr. Libor Novak[2], Dr. Kristyna Bukvisova[2,3], Assoc. Prof. Miroslav Kolibal[3], Prof. Reshef Tenne[1]
[1]Weizmann Institute of Science, Rehovot, Israel, [2]Thermo Fisher Scientific, Brno, Czech Republic, [3]Brno University of Technology, Brno, Czech Republic
570 Water condensation on core-shell nanofibers studied using multiscale environmental electron microscopy
Laura Montes-Montañez[1], Dr Annie Malchère[2], Dr Lucian Roiban[2], Dr Victor Rico[1], Dr Victor Trillaud[2], Prof Philippe Trillaud[2], Prof Karine Masenelli-Varlot[2], Prof Agustín R González-Elipe[1], Dr Ana Borrás[1], Dr Carmen López-Santos[1,3]
[1]Institute of Materials Science of Seville (US-CSIC) , Seville, Spain, [2]INSA Lyon, Universite Claude Bernard Lyon 1, CNRS, MATEIS, UMR5510, Villeurbanne, France, [3]Departamento de Física Aplicada I, Escuela Politécnica Superior, Universidad de Sevilla, Seville, Spain
621 Rapid and large FOV mapping of 60° grains in epitaxial MX2 with a segmented detector
Dr. Ankit Nalin Mehta[1], Dr. Gerardo Martinez Alanis[1], Dr. Maxim Korytov[1], Dr. Henry Medina Silva[1], Dr. Paola Favia[1], Dr. Olivier Richard[1], Dr. Eva Grieten[1]

[1]imec, Leuven, Belgium

626 Nanotubes of (SmxY1-x)S-TaS2 based on Quaternary Misfit Layered Compounds (MLCs)

Mr Mohammad Furqan[1,2], Dr Simon Hettler[1,2], Dr MB Sreedhara[3], Dr Reshef Tenne[4], Dr Raul Arenal[1,2,5]

[1]Laboratorio de Microscopias Avanzadas (LMA), Universidad de Zaragoza, Zaragoza, Spain, , , [2]Instituto de Nanociencia y Materiales de Aragón (INMA), Universidad de Zaragoza, , , Spain, [3]Solid State and Structural Chemistry Unit, Indian Institute of Science, Bengaluru, India,, , , [4]Department of Molecular Chemistry and Materials Science, Weizmann Institute of Science, Rehovot, Israel, , , [5]ARAID Foundation, Zaragoza, Spain, ,

663 Characterisation of 2-D chalcogenides utilising Electron Microscopy techniques and Density Functional Theory.

Dr Danielle Douglas-Henry[1,2], Mr. Ilias Oikonomou[1,2,4], Dr. Tigran Simonian[1,2], Dr. Jonathan J. P. Peters[1,3], Dr. Thomas Brumme[4], Prof. Thomas Heine[4], Prof. Valeria Nicolosi[1,2]

[1]Advanced Microscopy Lab, Trinity College Dublin, Dublin, Ireland, [2]School of Chemistry, Trinity College Dublin, Dublin, Ireland, [3]School of Physics, Trinity College Dublin, Dublin, Ireland, [4]Chair of Theoretical Chemistry, TU Dresden, Dresden, Germany

665 Ptychography Optimization for Atomic Analysis of Bending Mode in Bilayer Transition Metal Dichalcogenide Translational Motion

Yunyeong Chang[1], Dr Jinseok Ryu[3], Prof Hyobin Yoo[2], Prof Heung Nam Han[1], Prof Miyoung Kim[1]

[1]Seoul National University, , Republic of Korea, [2]Sogang University, , Republic of Korea, [3]Diamond Light Source Ltd, , United Kingdom

671 Influence of low-pressure atmosphere in the pores formed in hexagonal boron nitride under electron irradiation

Umair Javed[1,2], Clara Kofler[1,2], Clemens Mangler[1], Jani Kotakoski[1]

[1]University of Vienna, Faculty of Physics, Vienna, Austria, [2]University of Vienna, Vienna Doctoral School in Physics, Vienna, Austria

769 Atomic-resolution investigation of 2D hematene

Phd Jana Dzibelova[1], Jan Filip[2], Jani Kotakoski[1]

[1]University of Vienna, Vienna, Austria, [2]Czech Advanced Technology and Research Institute, Palacky University, Olomouc, Czech Republic

776 Structural phase transition induced microstructure changes in V2O3 based hybrid magnetic heterostructures

Prof. Unnar Arnalds[1]

[1]University of Iceland, Reykjavik, Iceland

777 In situ closed-cell microscopy study of Ti3C2Tz MXene

Phd Student Changjie Huang[1], Asst. Prof. Leiqiang Qin[2], Prof. Johanna Rosen[2], Prof. Per O.Å Persson[1], Assoc. Prof. Justinas Palisaitis[1]

[1]Thin Film Physics Division, Department of Physics, Chemistry and Biology (IFM), Linköping University, Linköping, Sweden, [2]Material Design Division, Department of Physics, Chemistry and Biology (IFM), Linköping, Sweden

805 Nanotubes of (SmxY1-x)S-TaS2 based on Quaternary Misfit Layered Compounds (MLCs)

Mr Mohammad Furqan[1], Dr Simon Hettler[1,2], Dr MB Sreedhara[3], Dr Reshef Tenne[4], Dr Raul Arenal[1,2,5]

[1]Laboratorio de Microscopias Avanzadas (LMA), Universidad de Zaragoza, Zaragoza, Spain, , , [2]Instituto de Nanociencia y Materiales de Aragón (INMA), Universidad de Zaragoza, Zaragoza, Spain, , , [3]Solid State and Structural Chemistry Unit, Indian Institute of Science, Bengaluru, India,, , , [4]Department of Molecular Chemistry and Materials Science, Weizmann Institute of Science, Rehovot, Israel, , , [5]ARAID Foundation, Zaragoza, Spain, ,

827 Guided growth of 1D van der Waals Nanowires for Enhanced Optoelectronic Functionalities

Maayan Persky[1], Shahar Bialer[1], Noya Ruth Itzhak[1], Anna Eden Kossoy[2], Lotar Houben[2], Ernesto Joselevich[1]

[1]Department of Molecular Chemistry and Materials, Weizmann Institute of Science Science,, Rehovot, Israel, [2]Chemical Research Support, Weizmann Institute of Science, Rehovot, Israel

833 FIB-induced nanorod formation in 2D layered crystals

Dr. Julia Deuschle[1], Dr. Tobias Heil[1], Dr. Hongguang Wang Hongguang Wang[1], Prof. Dr. Peter van Aken[1]

[1]Max Planck Institute for Solid State Research, Stuttgart, Germany

863 In situ examination of oxygen vacancy dynamics in epitaxial LaCoO3 thin films

Dr. Seung Jo Yoo[1], Mrs. Ji-Hyun Lee[1], Mr. Sang-Gil Lee[1], Dr. Hyung Joong Yun[1]

[1]Korea Basic Science Institute, Deajeon, Republic of Korea

870 High-resolution structural analysis of cation-mixed (Fe,Mn,Ni)PS3 van der Waals single crystals

Dr. Tatiana Smoliarova[1], B.Sc. Moritz Küster[1], Dr. Apoorva Chaturvedi[2], Prof. Edwin-Hang-Tong Teo[2], Prof. Michael Farle[1], Dr. Anna Semisalova[1]

[1]Faculty of Physics and Center of Nanointegration (CENIDE), University of Duisburg-Essen, Duisburg, Germany, [2]Center for Programmable Materials, School of Materials Science and Engineering, Nanyang Technological University, Singapore, Singapore

907 Morphological investigation of periodic structures created by focused ion gallium beam

Márk Windisch[1,2], Dániel Selmeczi[3], Ádám Vida[2], Zoltán Dankházi[1]

[1]Eötvös Loránd University Department of Materials Physics, Budapest, Hungary, [2]Bay Zoltán Nonprofit Ltd. for Applied Research, Budapest, Hungary, [3]Semilab Semiconductor Physics Laboratory Co. Ltd., Budapest, Hungary

909 Functionalization of Single-Walled Carbon Nanotubes Analyzed by Spatially-Resolved EELS

Dr Raul Arenal[1,2,3], Dr. Laurent Alvarez[4], Prof. Jean-Louis Bantignies[4]

[1]Instituto de Nanociencia y Materiales de Aragón, CSIC-Universidad de Zaragoza, Zaragoza, Spain., Zaragoza, Spain, [2]Laboratorio de Microscopías Avanzadas (LMA), Universidad de Zaragoza. Zaragoza, Spain, Zaragoza, Spain, [3] Araid Foundation, Zaragoza, Spain , Zaragoza, Spain, [4]Laboratoire Charles Coulomb, U. Montpelier - CNRS, Montpellier, France

911 Microstructure and mechanical properties of AlCu thin films in a wide range of composition

Dániel Olasz[1,2], György Sáfrán[2], Noémi Szász[2], Tamás Kolonits[2], Nguyen Quang Chinh[1]

[1]Department of Materials Physics, Eötvös Loránd University, Budapest, Hungary, [2]Institute for Technical Physics and Materials Science, HUN-REN Centre for Energy Research, Budapest, Hungary

912 Enhanced Visible Light Photocatalytic Activity of Cu-Doped ZnO ALD Films Deposited on Porous Substrates

Assistant professor Ivna Kavre Piltaver[1,2], Robert Peter[1,2], Daria Jardas Babić[1,2], Matejka Podlogar[3], Aleš Omerzu[1,2], Krešimir Salamon[4]

[1]Faculty of Physics, University of Rijeka, Rijeka, Croatia, [2]Center for Micro- and Nanosciences and Technologies, Universitu of Rijeka, Rijeka, Croatia, [3]Jozef Stefan Institute, Ljubljana, Slovenia, [4]Ruđer Bošković Institute, Zagreb, Croatia

925 Analysis of the cause of imperfect adhesion of cataphoretic coating using SEM and EDS method

Ph.D. Zuzana Koutova[1], Ing. Marie Novotna[1]

[1]MemBrain s.r.o., Stráž pod Ralskem, Czechia

946 Investigation of earth-abundant photovoltaic material Zn3P2 nanostructures using electron microscopy

Aidas Urbonavicius[1,2], Dr. Sebastian Lehmann[2,3], Prof. Kimberly A. Dick[1,2,3], Dr. Simon Escobar Steinvall[1,2]

[1]Centre for Analysis and Synthesis, Lund University, Lund, Sweden, [2]NanoLund, Lund, Sweden, [3]Division of Solid State Physics, Lund University, Lund, Sweden

950 Atomic-scale imaging of local structure of layered Cu-Te phases

Dr. Habil. Andriy Lotnyk[1], Dr. Vladimir Roddatis[2], Nils Braun[1], Sonja Cremer[1], Dr. Hagen Bryja[1], Lennart Voss[3], Prof. Lorenz Kienle[3]

[1]Leibniz Institute of Surface Engineering (IOM), , Leipzig, Germany, [2]GFZ German Research Centre for Geosciences, Potsdam, Germany, [3]Institute for Materials Science, Faculty of Engineering, University of Kiel, Kiel , Germany

998 Contribution of residual gas and surface contaminants to contamination growth on irradiated samples

Arne Schwartz[1], Dr. Erich Müller[1], TT.-Prof. Dr.-Ing. Yolita Eggeler[1,2]
[1]Laboratory for Electron Microscopy, Karlsruhe Institute of Technology (KIT), Karlsruhe, , [2]3DMM2O - Cluster of Excellence (EXC-2082/1 – 390761711), Karlsruhe Institute of Technology (KIT), Karlsruhe,

1022 TEM investigation of AlN-Cu(O) with variable amounts of copper

PL Martin[1], PY Jouan[1], Nicolas Gautier[1], M Richard-Plouet[1], Dr Valerie Brien[1]
[1]Nantes université, CNRS, Institut des Matériaux de Nantes Jean Rouxel, IMN, F-44000 Nantes, France

1090 Fabrication and high-resolution transmission electron microscopy characterization of nanopores in silicon nitride and 2D materials

Teresa Tang[1], Marco Kögel[1], Michael Mierzejewski[1], Michael Schlegel[1,2], Peter D. Jones[1], Jannik C. Meyer[1,2]
[1]NMI Natural and Medical Sciences Institute at the University of Tübingen, Reutlingen, Germany, [2]Institute of Applied Physics, University of Tübingen, Tübingen, Germany

1097 Investigation of Lateral and Vertical Heterostructures of MoS2/WS2

Jürgen Belz[1], Dr. Oliver Maßmeyer[1], Samane Ojaghi Dogahe[1], Dr. Andreas Beyer[1], Henrik Myja[2], Tillmar Kümmell[2], Bacher Gerd[2], Michael Heuken[3], Annika Grundmann[4], Holger Kalisch[4], Andrei Vescan[4], Kerstin Volz[1]
[1]Department of Physics & Structure & Technology Research Laboratory, Marburg, Germany, [2]Werkstoffe der Elektrotechnik & CENIDE, University of Duisburg-Essen, Duisburg-Essen, Germany, [3]AIXTRON SE, Herzogenrath, Germany, [4]Compound Semiconductor Technology, RWTH Aachen University, Aachen, Germany

1100 Insights into the formation of polycrystalline seed layers for the solution growth of semiconductor nanorods

Sarka Kucerova[1,2], Dr. Jozef Veselý[2], Dr. Michal Mazur[3], Jan Macháček[1], Matěj Berešík[1], Dr. Nikola Bašinová[1], Dr. Roman Yatskiv[1], Prof. Seungbum Hong[4], Dr. Jan Grym[1], Seongwoo Cho[5]
[1]Institute of Photonics and Electronics, CAS, Chaberská 57, 18251, Praha 8, Czech Republic, [2]Faculty of Mathematics and Physics, Charles University, Ke Karlovu 3, 121 16, Praha 2, Czech Republic, [3]Faculty of Science, Charles University, Hlavova 8, 128 43, Praha 2, Czech Republic, [4]Korea Advanced Institute of Science and Technology, 291 Daehak-ro, Yuseong-gu Daejeon 34141, Republic of Korea

1110 Sample holder design for TEM in-situ straining experiments on 2D materials

Carmen Rubach[1], Dr. Xin Zhou[1], Tobias Dierke[2], Robert Kammel[1], Michael Sommerschuh[1], Prof. Janina Maultzsch[2], Prof. Erdmann Spiecker[1]
[1]Institute of Micro- and Nanostructure Research (IMN) & Center for Nanoanalysis and Electron Microscopy (CENEM), Friedrich-Alexander-University Erlangen-Nürnberg, 91058 Erlangen, Germany, [2]Institute of Condensed Matter Physics, Friedrich-Alexander-University Erlangen-Nürnberg, 91058 Erlangen, Germany

Late Poster Presentation

1240 Electrochemical sensors for detection of benzotriazole in water

Assist. Prof. Kristina Žagar Soderžnik[1,2], Neža Sodnika[1], Melanija Hadolin[3], Zoran Samardžija[1]
[1]Jožef Stefan Institute, Ljubljana, Slovenia, [2]Jožef Stefan International Postgraduate School, Ljubljana, Slovenia, [3]Faculty of Chemistry and Chemical Technology, Ljubljana, Slovenia

1274 Low energy electron microscopy and spectroscopy of 2D materials

Dr. Eliška Materna Mikmeková[1], Dr Ivo Konvalina[1], Dr. Lukáš Průcha[1], Dr. Ilona Müllerová[1], Dr Aleš Paták[1]

[1]Institute of Scientific Instruments of the CAS, v.v.i., Brno, Czech Republic

1290 Nanosized Ti-Ni composite

Miroslav Cieslar[1], Nikoleta Štaffenová[1], Elena Chochoľáková[1], Jan Fikar[2], Jan Hanuš[1], Lucia Bajtošová[1]

[1]Charles University, Faculty of Mathematics and Physics, Ke Karlovu 5, 121 16, Prague, Czech Republic, [2]2Czech Academy of Sciences, Institute of Physics of Materials, Žižkova 22, 616 00 , Brno, Czech Republic

1317 TEM-based study of the effect of precursor in thermal polymerization synthesis of graphitic carbon nitride

Dr. Rosaria Brescia[1], Paolo Negro[2], Prof. Federico Cesano[2], Prof. Domenica Scarano[2]

[1]Electron Microscopy Facility, Istituto Italiano di Tecnologia, Genoa, Italy, [2]Chemistry Department of Excellence and NIS (Nanomaterial for Industry and Sustainability) Interdepartmental Centre, University of Torino & INSTM-UdR, Turin, Italy

1339 Effect of thin 2D support layers on the catalytic properties of catalysts

Jeongwook Bae[1], Joohyun Lim[1]

[1]Department of chemistry, Kangwon National University, Chuncheon, Republic of korea

1342 Application of dual-beam microscope with TOF-SIMS in characterization of ceramic coatings deposited on filtration membranes

PhD Piotr Wiecinski[1], Professor Halina Garbacz[1], PhD Joanna Kacprzynska-Golacka[2], Profefssor Jerzy Smolik[2], Professor Andrzej Krasiński[1]

[1]Warsaw University of Technology, Warsaw, Poland, [2]Lukasiewicz Research Network – Institute for Sustainable Technologies, Radom, Poland

146

In and ex situ (S)TEM manipulation of 2D materials without air exposure

Manuel Längle, Alberto Trentino, Georg Zagler, Barbara Mayer, Clemens Mangler, Harriet Ahlgren, Kimmo Mustonen, Toma Susi, Jani Kotakoski[1]
[1]University of Vienna, Vienna, Austria

PS-01 (1), Lecture Theater 3, august 28, 2024, 10:30 - 12:30

Graphene—the one-atom-thick sheet of carbon—is the most famous of 2D materials due to its unique electronic properties and mechanical strength. However, its chemical inertness makes graphene also an excellent nearly electron-transparent support for other materials, nanostructures and even active individual atoms for example for single-atom catalysis. Similarly, the insulating counterpart of graphene, hexagonal boron nitride, has emerged as an interesting host for single-photon emitters realized as point defects. Unfortunately, since 2D materials consist solely of surface, they are easily obscured by the ubiquitous surface contamination that makes working with them challenging.

In this contribution, I will demonstrate that defect-engineering of graphene [1] enables its substitutional heteroatom doping [2] and growth of nanoclusters with a well-defined concentration and a narrow size distribution, as well as the direct correlation of its atomic structure and mechanical properties. I will further show that hBN can similarly be tailored with low-energy noble gas irradiation to create point-defects in a controlled manner. The defect manipulation is carried out in a vacuum system [3] that is directly connected to a Nion UltraSTEM 100 microscope, which allows sample cleaning, manipulation, and atomic-scale imaging and spectroscopy without air exposure. The defects are imaged via annular dark field imaging and the impurity atom identification is confirmed by electron energy loss spectroscopy.

The methodology employed here can be easily extended to other 2D materials, and is expected to lead to structures with potential applications in plasmonics, quantum information technology, sensorics and catalysis.

Keywords:

graphene, hBN, 2D materials, defect-engineering

Reference:

[1] Trentino et al., Nano Lett. 21, 5179-5185 (2021)
[2] Inani et al., J. Phys. Chem. C 123, 13136-13140 (2019); Zagler et al., 2D Mater. 9, 035009 (2022); Trentino et al., 2D Mater. 9, 025011 (2022).
[3] Mangler et al., Microsc. Microanal. 28 S1, 2940 (2022).

222

In-situ observation of rheotaxy: 2D materials‘ growth on liquid substrates

Ms Kristyna Bukvisova[2,4], Mr Radek Kalousek[1,2], Mr Marek Patocka[2], Mr Suneel Kodambaka[3], Mr Libor Novak[4], Mr Tomas Sikola[1,2], Mr. Miroslav Kolibal[1,2]
[1]CEITEC, Brno University of Technology, Brno, Czech Republic, [2]Institute of Physical Engineering, Brno University of Technology, Brno, Czech Republic, [3]Virginia Polytechnic Institute and State University, Blacksburg, United States, [4]Thermo Fisher Scientific, Brno, Czech Republic

PS-01 (1), Lecture Theater 3, august 28, 2024, 10:30 - 12:30

Background incl. aims
The isolation of graphene in 2004 raised an enormous excitement in the community, bringing to light a fundamentally new class of low-dimensional materials. Soon after, the graphene's insulating cousin – hexagonal boron nitride – was introduced, initiating a burst of papers speculating about a new electronics era. Process scalability, which is necessary for the utilization of 2D materials on a larger scale, excludes the mechanical exfoliation and significantly narrows the choice of suitable growth techniques. In this regard, the most promising approach is that of chemical vapour deposition (CVD), in which the precursors are delivered from a gas phase to the substrate, where they react and form the growing layer. However, in contrast to exfoliated layers, those prepared by CVD exhibit a significantly higher concentration of various structural defects, which are detrimental to many quantum effects and device functionalities the physicists and engineers search for. The defect family in 2D materials includes domain boundaries (GBs) and twin defects, together with many types of vacancies and anti-sites. GBs were identified to play a critical role in many aspects. The mitigation strategies include specific sample preparation techniques or the use of single-crystal substrates. Developing a more general strategy to avoid the formation of GBs within a footstep of the intended 2D-material-based device (and, preferably, at a wafer-scale) is desirable. Rheotaxy (growth on a liquid substrate) has been proposed as a viable method to achieve domain ordering and self-assembly already in 2012 for graphene [1]. However, it remains poorly explored due to a lack of in-situ experimental techniques that confirm or disprove hypotheses raised concerning the formation mechanisms [2]. Only recently, experimental studies started to pop-out [3].

Methods
We have utilized two modified microscopes for observing the graphene growth on liquid : a microReactor [4] in SEM and ultrahigh vacuum SEM. We observe graphene growth behaviour in situ, allowing to record movies of graphene flake behaviour on liquid gold and copper. We combine our electron microscopy observations with in situ atomic force microscopy (AFM) measurement of the contact angle of graphene on liquid gold, together with ex situ Raman characterization of the final graphene layer.

Results
We have been able to demonstrate some aspects of the graphene growth on liquid substrate, that have been hypothesized so far, namely movement and ordering of the graphene flakes on liquid surface (Cu and Au), via real-time movies under various reaction conditions. The flakes seem to assemble into regular patterns on liquid surface, however, this pattern is prone to disturbances, caused by e.g. hydrodynamics of the liquid (Fig. 1). Additionally, we obtained kinetic data of graphene growth, allowing us to directly compare solid and liquid growth rates. These data show significant increase of reaction constants on liquid metal. Last, we will show in situ AFM data, discussing the possible presence of meniscus between the graphene flake and the liquid metal. Altogether, we frame these observations within a simple physical model.

Fig.1 shows behavior of graphene islands on undercooled liquid gold captured by the SEM, at temperature 1040 °C and C2H4/H2 partial pressure of 40 Pa. The movement is oscillatory (a) and the islands rotate and align with respect each other, which causes the distortion of the image and appearance of "vibrations" because of the scanning beam. Coalescence happens slowly, except for cases when the islands' distances decrease below a certain value or after stimuli such as solidification (b). The scale bar is 1 µm.

Conclusion

In this contribution, we will show a quantitative analysis of in situ experimental data of graphene flakes assembly on liquid metal under growth reaction conditions. We combine in situ electron microscopy in different vacuum environments at extreme temperature with atomic force microscopy to show that the choice of the liquid metal is vital for achieving regular assembly of graphene and seamless stitching. We corroborate experimental observations with simple physical models of 2D solids floating on a liquid surface and explore weak-points of the synthesis, giving directions for further research towards scalable growth of 2D materials.

Acknowledgements

This work was supported by the project Quantum materials for applications in sustainable technologies (QM4ST), funded as project No. CZ.02.01.01/00/22_008/0004572 by OP JAK, call Excellent Research.

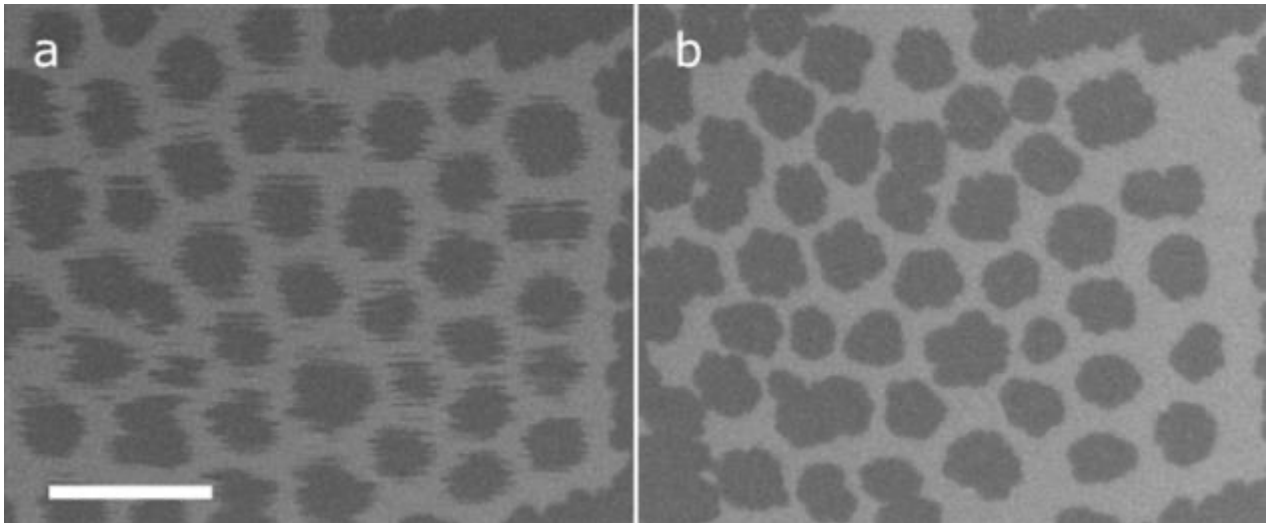

Keywords:

In-situ, liquid metals, graphene, growth

Reference:

[1] Geng, D. et al. PNAS 2012, 109, 7992-7996.
[2] Tsakonas, C.; Dimitropoulos, M.; Manikas, A. C.; Galiotis, C. Nanoscale 2021, 13, 3346-3373.
[3] Jankowski M. et al., ACS Nano 2021, 15, 9638-9648.
[4] Novák, L., Wandrol, P., Vesseur J. R. Micr.&Microanal. 2020, 26 (S2), 1144-1145.

262

Two-dimensional few-atom noble gas clusters in a graphene sandwich

Manuel Längle[1], Kenichiro Mizohata[2], Clemens Mangler[1], Alberto Trentino[1], Kimmo Mustonen[1], E. Harriet Åhlgren[1,2], Jani Kotakoski[1]
[1]Faculty of Physics, University of Vienna, Vienna, Austria, [2]Department of Physics, University of Helsinki, Helsinki, Finland

PS-01 (1), Lecture Theater 3, august 28, 2024, 10:30 - 12:30

Background incl. aims
Van der Waals atomic solids of noble gases on metals at cryogenic temperatures were the first experimental examples of two-dimensional systems [1]. Recently, such structures have also been created on surfaces under encapsulation by graphene, allowing studies at elevated temperatures through scanning tunneling microscopy [2,3]. However, for this technique, the encapsulation layer often obscures the arrangement of the noble gas atoms. When atoms are introduced into the van der Waals gap between the layers of suspended multilayer graphene the resulting structures can be directly observed at room temperature via transmission electron microscopy [4].
Methods
In this work low-energy ion irradiation has been used to irradiate suspended bilayers and double layers of graphene and hBN. Implantation parameters for noble gases from Ar to Xe were experimentally determined. Trapping occurred for Ar between 20 and 30 eV, for Kr between 25 and 60 eV, and for Xe between 15 and 65 eV. Irradiation can be carried out within the ultra-high vacuum system directly connected to a scanning transmission electron microscope [5] where the samples can be transported to a Nion UltraSTEM 100 microscope, capable of atomic-scale imaging and electron energy loss spectroscopy, without exposure to air.
Results
The atomic structure of small Kr and Xe clusters was studied via aberration-corrected scanning transmission electron microscopy [4]. We show that small crystals ($N < 9$) arrange on the basis of the simple non-directional van der Waals interaction (Fig. 1). Larger crystals show some deviations, possibly enabled by deformations in the encapsulating graphene lattice. We further discuss the dynamics of the clusters within the graphene sandwich and show that although all the Xe clusters with up to $N \approx 100$ remain solid, Kr clusters with already $N \approx 16$ turn occasionally fluid under our experimental conditions (under a pressure of ~0.3 GPa).
The figure shows the structure of small clusters. Filtered STEM-ADF images of Kr (top row) and Xe (bottom row) including all the cases where the experimentally observed structures correspond to that with the lowest energy according to the simulations for Kr (middle row) are shown.
The encapsulated clusters show dynamic behavior such as "jumps" between different positions and occasional cluster growth and shrinking. Molecular dynamics simulations were used to understand this behavior. The trapped clusters also exhibit interesting phase behavior. While all small clusters remain solid, larger clusters exhibit either solid- or liquid-like structures depending on their size, chemical element and local microscopic environment.
Conclusion
We image noble gas atoms, their cluster formation, stability and phase in two dimensions. Due to their chemical inertness, they would not condense under normal conditions, however, when trapped between two graphene sheets the atoms are forced together by the external pressure that leads to the formation of clusters [4]. This results in a simple two-dimensional van der Waals solid that can be described to a good degree simply with the Lennard Jones potential. This opens a way for the unexplored frontier of encapsulated two-dimensional van der Waals solids with exciting possibilities for fundamental condensed-matter physics research.

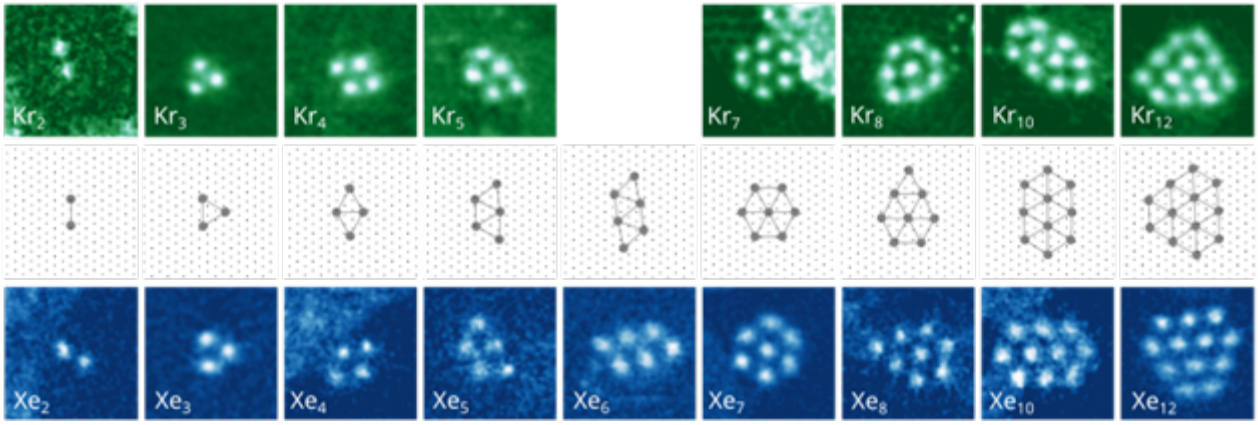

Keywords:

graphene, hBN, noble gas, irradiation

Reference:

[1] Jortner, J. et al., J. Chem. Phys. 42, 4250–4253 (1965).
[2] Herbig, C. et a., 2D Mater. 3, 025032 (2016).
[3] Valerius, P. et al., Phys. Rev. B 96, 235410 (2017).
[4] Längle, M. et al., Nat. Mater. (2024).
[5] Mangler, C. et al., Microsc. Microanal. 28(S1):2940-2942 (2022)

377

A twist to superlubric sliding in bilayer graphene uncovered by in situ TEM

Dr. Xin Zhou[1], Dr. Mingjian Wu[1], Prof. Erdmann Spiecker[1]
[1]Institute of Micro- and Nanostructure Research (IMN) & Center for Nanoanalysis and Electron Microscopy (CENEM), Friedrich-Alexander-Universität Erlangen-Nürnberg, Erlangen, Germany

PS-01 (1), Lecture Theater 3, august 28, 2024, 10:30 - 12:30

Background incl. aims
Twist in two-dimensional (2D) Van der Waals (vdW) bilayers, which results in the formation of moiré superlattice, has garnered attractive interest and can lead to unprecedented exotic physical properties including superlubricity.1 The twist angle (θt) offers not only a new and unique degree of freedom for modulating the properties, but also small and local variations in θt can result in exceptional differences in these properties.2 Indeed, it was discovered that the superlubricity in graphite is intimately dependent on the interlayer twist angle (thus incommensurability), interfacial cleanliness, and thickness. Fruitful experimental exploration on the superlubric features in artificially stacked graphite surfaces at a wide range of twist angles has been achieved and the underlying mechanism has been readily explained as the twist-related incommensurate stack between the sliding layers using a rigid-body model. 3,4 However, the scenario of the transition to superlubricity becomes more complex due to atomic scale structure relaxation and reconstruction at a small twist angle regime ($\theta t < 4^{o}$), thus normal rigid-body model fail to predict. Meanwhile, the existing experimental approaches fail to capture the details of superlubric sliding, and direct insight with high precision measurement into how the interface between two atomic layers undergoes transitions from structurally reconstructed bilayers to incommensuration to approach superlubricity is still lacking.
In this work, we report the observation of the superlubric sliding between two monolayer graphene in free-standing bilayer graphene (BLG) by the implementation of an in situ transmission electron microscopy (TEM) tensile straining setup combined with 4D scanning transmission electron microscopy (4D STEM) to probe local twist angle and strain.
Methods
We transfer bilayer graphene samples (ACS materials, 1cm×1cm) to a homemade Cu support with a small window, and then clean the Poly (methyl methacrylate) coating by acetone. Tensile straining was imposed by using a single-tilte Gatan straining holder 654 and in situ TEM experiments were carried out using a ThermoFisher Scientific Spectra 200 microscope operated at 80 kV. Dark-field TEM (DF-TEM) images, selected area electron diffraction (SAED) patterns, and ($1\bar{1}\bar{1}20$) DF-TEM image series were recorded throughout the straining process to visualize the dynamics of basal plane dislocations during straining. The mechanical loading was paused in between to carefully characterize the basal plane dislocations and to acquire 4D-STEM datasets (Fig. A). The 4D STEM experiments was carried out using micro-probe mode with a nominal convergence half-angle of 0.47 mrad and the data acquired using a Ceta-S camera running at ~300 fps. These datasets were analysed using py4DSTEM package and custom codes. A similar straining experiment and data acquisition process was succeeded for a second BLG sample. Both straining experiments were terminated until fully detachment of the monolayers.
Results
We realized the strain experiment on graphene samples with a monolayer-bilayer-monolayer (MLG-BLG-MLG) configuration (Fig. B). Before straining, basal plane dislocation with line direction parallel to the straining direction was observed (Fig. B), which is likely resulted from film buckling. After an incubation period during straining, where the width of the bilayer region decreased, we observed nucleation of new basal plane dislocation with line direction perpendicular to the straining direction, indicating initiation of twist between the monolayers. Further straining resulted in continuous

nucleation of dislocations and a dramatic increase in the density of these dislocations, thus the increase in twist angle (Fig. C and D). Using 4D STEM analysis, we quantified the twist angle within the bilayer region by measuring the angular difference of Bragg disks in the local nano-beam diffraction (NBD) patterns, which are extracted from the left-side and right-side monolayer regions. Similarly, the local elastic strain in the monolayer regions was determined by analysing the displacement of Bragg peaks throughout all datasets, referencing a free region near the edge of MLG as zero strain. The established relationship between twist angle and strain, derived from extensive measurement points in both samples, clearly disclosed a consistent tendency of decreasing in strain with increasing twist angle. Leveraging the strain-twist angle correlation, and employing the quasi-kinetic equilibrium force model alongside the elastic properties of monolayer graphene (Fig. A), we investigated frictional properties associated with twist angle in bilayer graphene. Notably, a smooth reduction in the coefficient of friction (CoF) was observed as a function of twist angle, with the CoF dropping below 0.01 for twist angle exceeding 1.5°, implying the approach of superlubricity in bilayer graphene.

Conclusions

Our study delved into the phenomenon of twist-modulated superlubric sliding between monolayer graphene by directly visualizing the dynamic transition from commensurability to incommensurability in marginally twisted bilayer graphene. These findings provide the direct experimental observation of superlubric feature between atomic graphene layers and open a new avenue to build up twist angle gradients in 2D materials for investigating their twist-related exotic properties.

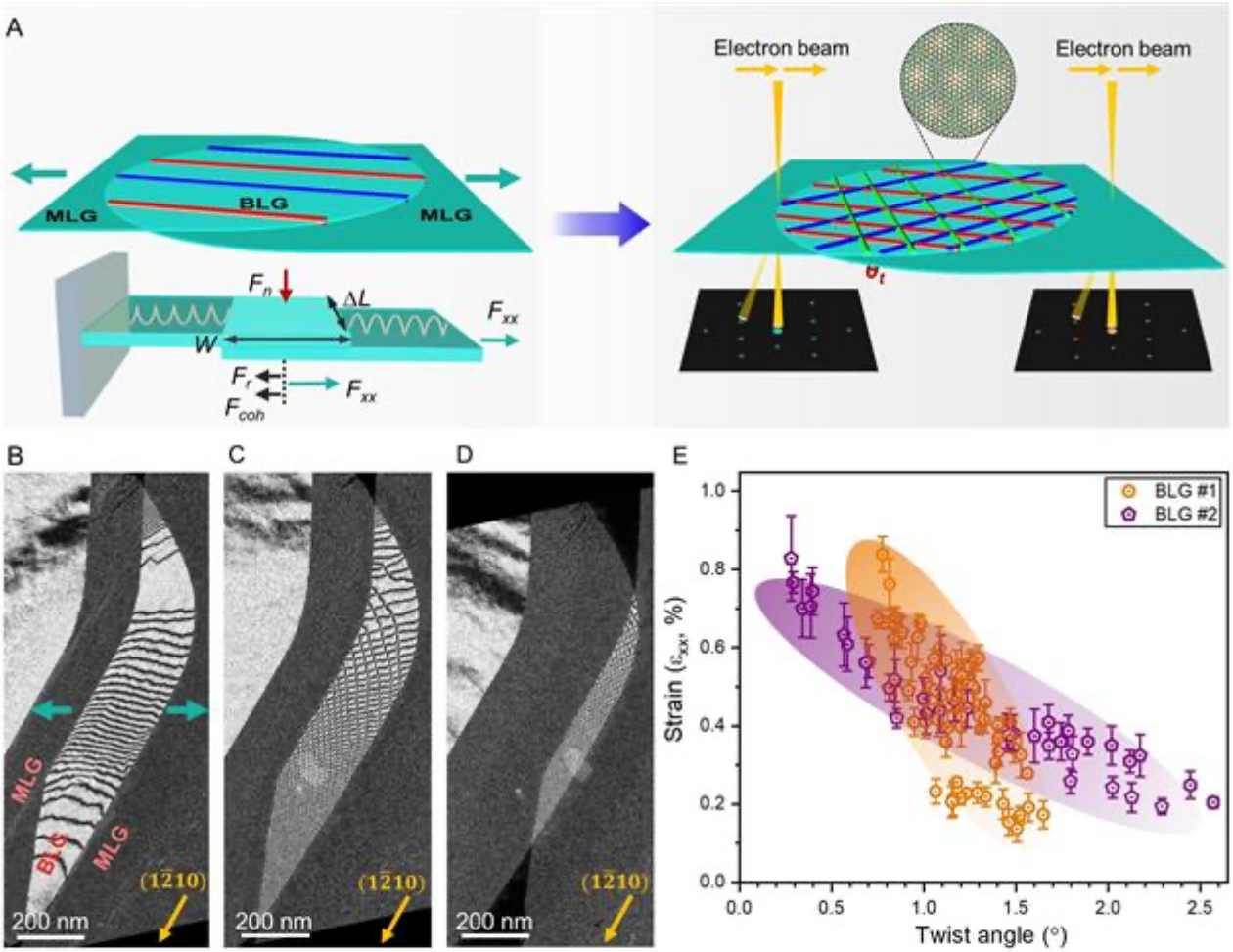

Fig. (A) Schematic representation of BLG undergoing twisting and formation of Moiré superlattice during strain-induced sliding. 4D STEM set-up for strain and twist angle evaluation as well as the quasi-kinetic sliding equilibrium force model are illustrated. (B to D) Series of DF-TEM images taken with $(1\bar{2}10)$reflection revealing the interfacial dislocation network in the BLG region at different strain steps. (E) Strain-twist angle correlation, showing a decreasing trend of strain with the increasing twist angle.

Keywords:

Graphene, twist, in-situ straining, superlubricity

Reference:

(1) J. H. Baek, et al. Nat. Mater., 2023, 22, 1463.
(2) N. P. Kazmierczak, et. al., Nat. Mater., 2021, 20 956
(3) M. Dienwiebel, et al. Phys. Rev. Lett., 2004, 92, 12.
(4) H. Z. Bai, et al. Carbon, 2002, 191, 28.
(5) X. Zhou, et al. in preparation.

409

Surface Polarity Dynamics and Strong Reconstruction in Partially Reduced Nickelate Films

Prof. Dr. Peter A. Van Aken[1], Mr. Chao Yang[1], Mrs. Rebecca Pons[1], Mr. Wilfried Sigle[1], Mr. Hongguang Wang[1], Mrs. Eva Benckiser[1], Mr. Gennady Logvenov[1], Mr. Bernhard Keimer[1]
[1]Max Planck Institute for Solid State Research, Stuttgart, Germany

PS-01 (1), Lecture Theater 3, august 28, 2024, 10:30 - 12:30

Background incl. aims
Surface polarity dynamics profoundly influence the electronic and structural properties of oxide thin films. This study aims to investigate the atomic structure and electrostatic characteristics of partially reduced nickelate films to elucidate the mechanism behind strong surface reconstruction.

Methods
Advanced STEM techniques, including annular bright field (ABF) imaging, four-dimensional scanning transmission electron microscopy (4D-STEM), and electron energy-loss spectroscopy (STEM-EELS), were employed to probe the atomic and electronic structures, along with the near-surface electrostatic charge distribution.

Results
Surface analysis revealed a polar distortion coupled with octahedral rotations in both fully oxidized and partially reduced nickelate films. A stronger polar distortion was observed in the reduced sample, indicating a relationship with oxygen vacancies generated during topochemical reduction (Fig. 1a,b). Direct evidence of homogenous Sr doping and distinct valence variations of Ni atoms near the surface were provided by 4D-STEM imaging. EELS analysis confirmed changes in Ni valence and oxygen concentration, consistent with the observed surface reconstruction.

Conclusions
This study bridges the gap in experimental examinations of surface effects in oxide thin films, providing crucial insights into the nuanced interplay between surface polarity, electronic structure, and structural transformations. The observed surface reconstructions, influenced by oxygen vacancies, impact electronic transport properties, contributing to the understanding and engineering of surface polarity at the atomic scale in functional materials [1].

Figure 1: (a) ABF-STEM image of a $Pr_{0.8}Sr_{0.2}NiO_{2}$+x film on a (110)-oriented $NdGaO_3$ substrate. (b) Enlarged ABF images of the regions marked in (a) and corresponding structure model.

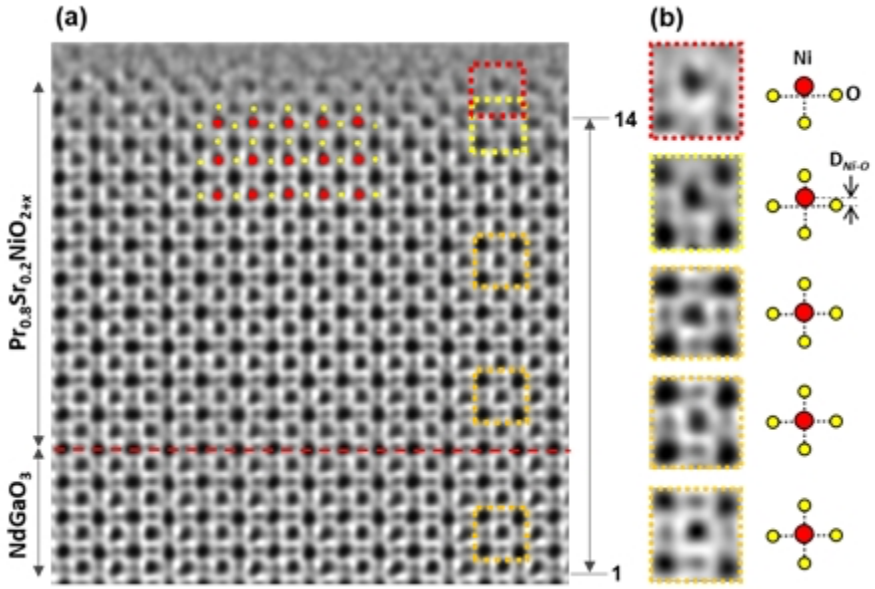

Keywords:

Surface polarity, polar distortion, nickelates

Reference:

[1] C. Yang et al., Nat. Commun. 15 (2024) 378, https://doi.org/10.1038/s41467-023-44616-x

645

Intralayer modification on Ti3C2Tz MXene Multilayer by Tailoring Surface Terminations

Mr Hari Hara Sudhan Thangavelu[1], Assoc. Prof. Fredrik Eriksson[1], Asst. Prof. Leiqiang Qin[2], Assoc. Prof. Jonas Björk[2], Prof. Johanna Rosén[2], Prof. Per Persson[1]
[1]Thin Film Physics Division, Department of Physics, Chemistry and Biology (IFM), Linköping University, SE - 58183, Sweden, [2]Materials Design Division, Department of Physics, Chemistry, and Biology (IFM), Linköping University, SE - 58183, Sweden

PS-01 (1), Lecture Theater 3, august 28, 2024, 10:30 - 12:30

Background incl. aims
MXenes are a class of two-dimensional materials whose properties can be tuned by tailoring surface terminations during the etching of the parent MAX phase precursors (1). It can be affirmed that the repetition of a MXene multilayer structure is the sum of interlayer width and intralayer thicknesses. Notably, conventional measurement techniques like X-ray diffraction (XRD) do not distinguish between these dimensions. However, it is crucial to recognize that the interlayer spacing holds particular significance in numerous applications, especially those reliant on swift diffusion of species in between MXene sheets, for example energy storage, material separation and interception. Consequently, understanding the determining variables for the interlayer spacing requires a thorough interpretation of intralayer spacing. Through theoretical simulations it has been identified that the surface terminations of Ti_3C_2Tz MXene affect the sheet thickness. As is evident from a theoretical study which is shown in the graphic below, the sheet thickness varies for different surface terminations. Therefore, the aim of this study is to experimentally verify the structural changes that occur as a function of surface termination chemistry.

Methods
Ti_3C_2Tz MXene multilayer structures with a mix of Oxygen (-O), hydroxide (-OH), and fluorine (-F) surface terminations have been used in this study. It is well known from the previous studies that F desorbs from the surface at around 500 °C and is removed completely while heating upon 700 °C (2). Double aberration corrected Scanning Transmission Electron Micrsscope (STEM) was used to observe the changes occurring within the MXene sheets at the atomic scale during in situ heating, to these temperatures. Images were obtained at ambient conditions after maintaining 15 minutes at every 100 °C up to a maximum temperature of 800 °C. Electron Energy Loss Spectroscopy (EELS) was used to explore the chemistry of the MXene.

Results
Experiments were conducted under vacuum between the temperature range of 100 °C to 800 °C. For every 100 °C increment, the structural and compositional changes in MXene multilayers were investigated. As expected F starts to leaves the surface after 500 °C, which was confirmed by EELS and accordingly changes the surface termination chemistry. From High Angle Annular Dark Field (HAADF) imaging in STEM mode the MXene intralayer corresponds to 0.482 ± 0.002 nm at 100 °C. This thickness is maintained until 500 °C after which it is reduced and reaches a spacing of 0.457 ± 0.002 nm at 700 °C arises as a result of fluorine removal from the surface. These results clearly reveal the impact of surface terminations on the sheet thickness. In addition, as the intralayer spacing decreases, the interlayer spacing increases by 0.026 nm at 700 °C (0.597 nm) in comparision to the ambient MXene conditions (0.571 nm).

Conclusions

In conclusion, it is evident that the surface terminations significantly influence the MXene sheet thickness. This variation is proposed to originate as a consequence of the strength of the interaction between the electron cloud of Titanium atoms and the surface terminations. This intralayer tuning can be widely applied in any MXene applications where intercalation plays a vital role.

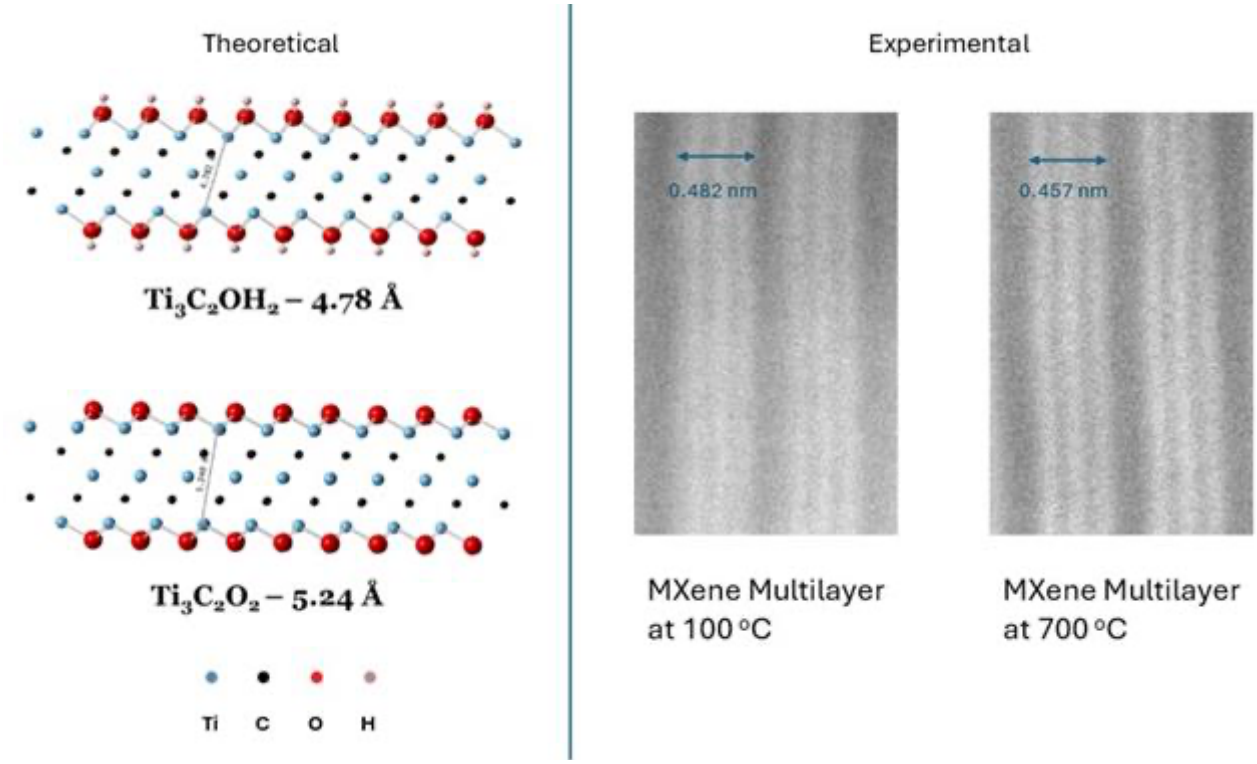

Keywords:

MXenes, Surface terminations, in-situ STEM

Reference:

(1) Naguib, M.; Kurtoglu, M.; Presser, V.; Lu, J.; Niu, J.; Heon, M.; Hultman, L.; Gogotsi, Y.; Barsoum, M. W. Two-Dimensional Nanocrystals Produced by Exfoliation of Ti_3AlC_2. Advanced Materials 2011, 23 (37), 4248–4253. https://doi.org/10.1002/adma.201102306.

(2) Persson, I.; Näslund, L.-Å.; Halim, J.; Barsoum, M. W.; Darakchieva, V.; Palisaitis, J.; Rosen, J.; Persson, P. O. Å. On the Organization and Thermal Behavior of Functional Groups on Ti_3C_2 MXene Surfaces in Vacuum. 2D Mater. 2017, 5 (1), 015002. https://doi.org/10.1088/2053-1583/aa89cd.

660

Enabling atomic resolution electron microscopy at elevated temperature and beyond pressures of a few bar

Hjalte Ambjørner[1], Anton Bjørnlund[1], Tobias Bonczyk[2], Edwin Dollekamp[2], Lau Kaas[1], Sofie Colding-Fagerholt[1], Kristian Mølhave[3], Christian Damsgaard[3], Stig Helveg[1], Peter Vesborg[1,2]
[1]Center for Visualizing Catalytic Processes (VISION), Department of Physics, Technical University of Denmark, 2800 Kgs. Lyngby, Denmark, [2]Surface Physics and Catalysis (SURFCAT), Department of Physics, Technical University of Denmark, 2800 Kgs. Lyngby, Denmark, [3]National Centre for Nano Fabrication and Characterization (Nanolab), Technical University of Denmark, 2800 Kgs. Lyngby, Denmark

PS-01 (1), Lecture Theater 3, august 28, 2024, 10:30 - 12:30

Background
Transmission electron microscopy (TEM) is an invaluable tool in knowledge-driven optimization of catalysts. Over the years, important mechanistic insights in chemical processes have been gained by combining the atomic resolution of TEM with miniaturized reactors. This type of reactors confines gas or liquid phase reaction environments to the vicinity of the catalyst between pairs of thin electron-transparent windows and has opened up for in situ and operando studies of catalysts during reactions conditions mimicking industrial catalysis. However, the electron beam has to traverse the reaction environment as well as the windows which, in turn, have to remain impermeable and mechanical stable to sustain pressure differences of up to several bars and therefore typically consist of 15-30 nm thick Si-based membranes. In practical terms, such membranes reduce signal contrast, and eventually resolution. Thus, thinner windows of similar strength and impermeability are needed to further improve imaging conditions.

The class of two-dimensional (2D) materials, and especially graphene, are interesting in this regard. It has been observed that graphene membranes sealing small volumes in a substrate can sustain pressure differences beyond 15 bars before delaminating from the substrate, and in addition, even a single layer of graphene is highly impermeable. 2D materials adhere to substrates via the Van der Waals force, and so graphene's ability to seal off a substrate, is of utmost importance, if graphene is to be employed as window material. At this stage, the performance of graphene-based seals at room temperature, i.e. leakage circumventing the graphene-based seal, exhibits large variation and allows gasses to leave sealed volumes through the interface between seal and substrate, making graphene-based windows impractical. Furthermore, the temperature dependence of the leakage have until now been unknown.

Methods
To investigate the leak from graphene-sealed volumes, we prepared electron transparent cavities and sealed them by mechanically exfoliating few-layer-graphene sheets on top. After exfoliation, the samples were cut to fit a GATAN heating holder. Prior to inserting the sample into the holder and subsequently the electron microscope, the cavities were filled with argon in a pressure chamber. Inside the vacuum of the TEM, the gradual decrease in argon content of the cavities was monitored as a function of time and temperature with Electron Energy Loss spectroscopy using a bottom-mounted Gatan Image Filter.

Results
At elevated temperature, the argon content of the cavities was found to decrease exponentially with time in accordance with what has been found at room temperature in previous studies. Furthermore, the exponential rate constant of the decay was itself exponentially dependent on the temperature,

i.e. exhibiting an Arrhenius dependency. This indicates that the diffusion from the graphene-sealed cavities is a thermally activated process in which the argon atoms are surpassing an energy barrier. This behavior was found across different samples and cavities sealed by the same flake, showing the generality of the phenomenon. Surprisingly, repeated emptying and filling of the cavities at elevated temperature drastically improved the leak tightness of the seals, and in one case, the leak rate at room temperature improved 6 orders of magnitude from an already decent origin, as compared to previously reported leak rates. Consequently, some graphene-sealed cavities could after repeated experiments sustain pressures up to approximately 10 bars at 500 °C, while exhibiting a remarkably low leakage.

Conclusion

Our investigations reveal that graphene-based windows can be used for in situ and operando high resolution electron microscopy at elevated temperature and beyond pressures of a few bar. However, thermal engineering of the graphene seal is needed to tune the graphene-based seals' performance properly.

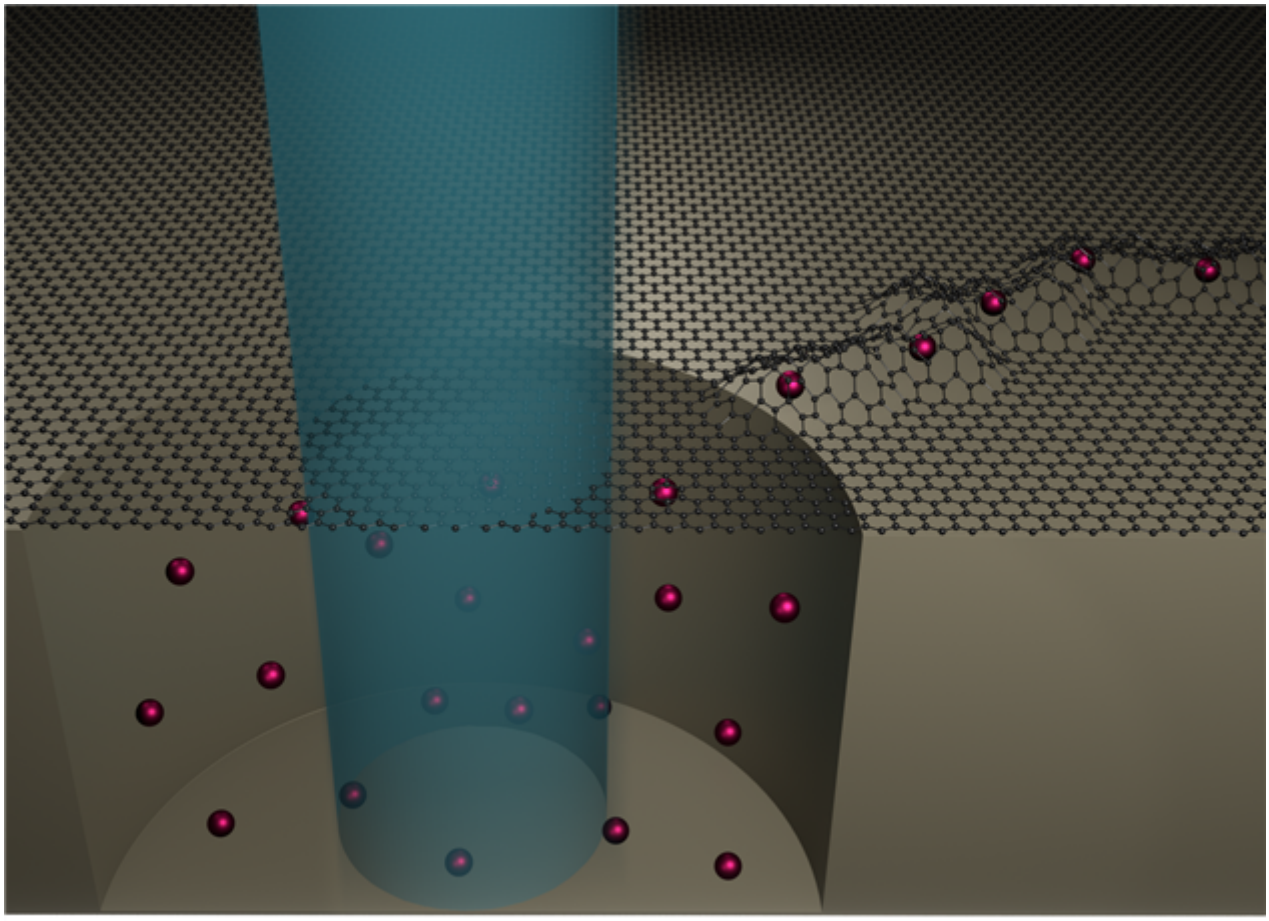

Keywords:

Graphene, Thermal, Seal, TEM, Heating

Reference:

Nature Nanotech, 2011, 6, 543–546
Nano Letters, 2019, 19, 8, 5313–5318
ACS Applied Materials and Interfaces, 2020, 12, 33, 37750–37756
Nanoscale, 2023, 15, 16896-16903

The Center for Visualizing Catalytic Processes is sponsored by the Danish National Research Foundation (DNRF146).

87

Temperature-driven in-situ TEM cation exchange at the solid state: a combined experimental and computational study

Alberto Casu[1], Mr. Claudio Melis[2], Mr. Luciano Colombo[2], Mr. Andrea Falqui[1,3]
[1]Department of Physics, University of Milan, Milan, Italia, [2]Department of Physics, University of Cagliari, Monserrato, Italy, [3]Interdisciplinary Centre for Nanostructured Materials and Interfaces (CIMaINa)- Department of Physics, University of Milan, Milan, Italy

PS-01 (2), Lecture Theater 3, august 28, 2024, 14:00 - 16:00

Background including aims
Over the past two decades, the demand for innovative nanomaterials has surged due to their remarkable adaptability across various fields such as optoelectronics, photonics, and catalysis. This has led to the development of robust synthetic techniques to produce nanocrystals (NCs) with finely tuned compositions, crystal phases, and morphologies.
Post-synthetic transformations of preformed nanostructures can be singled out among the available methods as a general approach to produce nanomaterials with features unattainable through conventional synthetic routes. Cation exchange (CE) is a prominent example this approach, because it is based on the substitution of cations within a host NC lattice, offering precise control over compositions and phases without affecting the NCs' morphology. Understanding the underlying mechanism of CE reactions is crucial for the rational design of nanostructures, but previous approaches to elucidate it relied on analyzing intermediate samples extracted during CE reactions in liquid state, and were hindered by the rapid kinetics of liquid-phase reactions and limited sampling capabilities. To overcome these limitations, solid-state observations of CE reactions were conducted using an in-situ transmission electron microscopy (TEM) approach. This technique enables continuous monitoring of CE reactions with enhanced detail over extended time frames, thanks to the slower kinetics of solid-state reactions and the rapid sampling afforded by TEM. After proving the feasibility of solid-state CE reactions, the focus was moved towards understanding CE reactions and their early stages through a combined experimental/computational approach. The experimental studies focused on in-situ TEM experiments utilizing advanced microelectronic mechanical systems (MEMS)-based heating holders for precise heating control, high-resolution scanning TEM (HRSTEM) imaging coupled with electron energy loss (EELS) and energy dispersive X-ray spectroscopy (EDS) for detailed chemical analysis, and the introduction of different crystal structures to examine variations in CE reactions. The results of these studies constituted the starting point for a comprehensive theoretical study employing classical molecular dynamics (MD) simulations, conducted to provide numerical estimations of activation energies and elucidate the factors influencing CE reaction dynamics. This combined experimental and theoretical approach offers a comprehensive framework for understanding and manipulating CE reactions, shedding light on their intricacies and potential applications in nanomaterial design.
Methods
In-situ TEM and its ancillary techniques were used for the experimental studies on CE reactions at the solid state involving Cu2Se NCs (cation donors) and CdSe nanowires (NWs) with cubic and hexagonal crystal structure (cation acceptors). The mixed populations were closely monitored against temperature using a MEMS-based in situ heating holder. HRSTEM and STEM-based chemical mapping were used to observe the initial phases of CE and analyze the local chemical compositions. MD was used for the calculations related to the atomistic CE model, which included portions of CdSe NWs initially surrounded by Cu atoms, and a suitable force-field (FF) was adopted to replicate mutual interactions occurring between Cu atoms and CdSe matrices across both crystal structures.
Results

Two parallel studies investigating CE reactions between Cu2Se nanospheres and hexagonal CdSe NWs or cubic CdSe NWs were conducted by a combination of HRSTEM, STEM-EDS mapping and STEM-EELS-based spectrum imaging, with particular attention devoted to early-stage CE. For this reason, available copper was deliberately minimized during the experimental design to slow CE reaction rates. Both studies revealed the formation of distinct CE fronts, negligible direct influence from Cu2Se nanospheres and the presence of a thin Cu layer around the NWs prior to the actual CE. However, the activation temperatures and CE rates changed drastically from one system to the other, going from 400 °C for hexagonal CdSe NWs to 125 °C for cubic CdSe NWs. Also, an unstable regime was observed for cubic CdSe NWs up to 250°C, allowing for partial reversibility of exchanged Cu2Se domains into CdSe.

An atomistic model developed via classical MD simulations provided a theoretical framework for the experimental results, aiming to pinpoint specific local mechanisms involved in CE and to quantify their respective contributions to the overall process. The CE reaction was divided into 4 sequential steps: formation of a Cu shell around a CdSe NW; penetration of Cu atoms into the CdSe NW and subsequent creation of Cu interstitial defects; diffusion of Cu interstitial defects within the CdSe matrix; Cu to Cd substitution via a kick-off event. Each step was simulated to estimate the corresponding activation energy and interatomic interactions in CdSe and Cu2Se were modeled using a combination of Lennard-Jones and Coulombic terms, adapted from the CdSe FF to describe CdSe and Cu2Se structures. MD simulations were conducted for both cubic and hexagonal CdSe structures, revealing differences in energy barriers and migration energies. Notably, cubic CdSe exhibited lower energy barriers, suggesting a more favorable CE process. The model predictions align well with experimental observations for both systems.

Conclusions

In-situ TEM studies on thermally-activated CE reactions at the solid-state between Cu2Se NCs and hexagonal or cubic CdSe NWs were carried out employing a MEMS-based heating holder to explore the early stages of CE and how the acceptor's crystal structure influences the CE process. Notably, expelled copper forms an external shell around CdSe NWs before CE starts and it was found that CE reactions exhibit different threshold temperatures (400°C for hexagonal CdSe and at 125°C for cubic CdSe) and kinetics depending on the host matrix's crystalline phase, with an unstable regime observed for cubic CdSe NWs at low temperatures.Classical molecular dynamics simulations were employed to numerically estimate activation energies and elucidate the probabilities of the entire CE process for different CdSe crystal structures, leading to a good agreement between experimental and computational results. This combined experimental and theoretical approach not only enhances our understanding of thermally activated CE but also sheds light on the mechanisms governing CE reactions with unprecedented detail, particularly in relation to the influence of nanoparticle crystal structure on reaction dynamics.

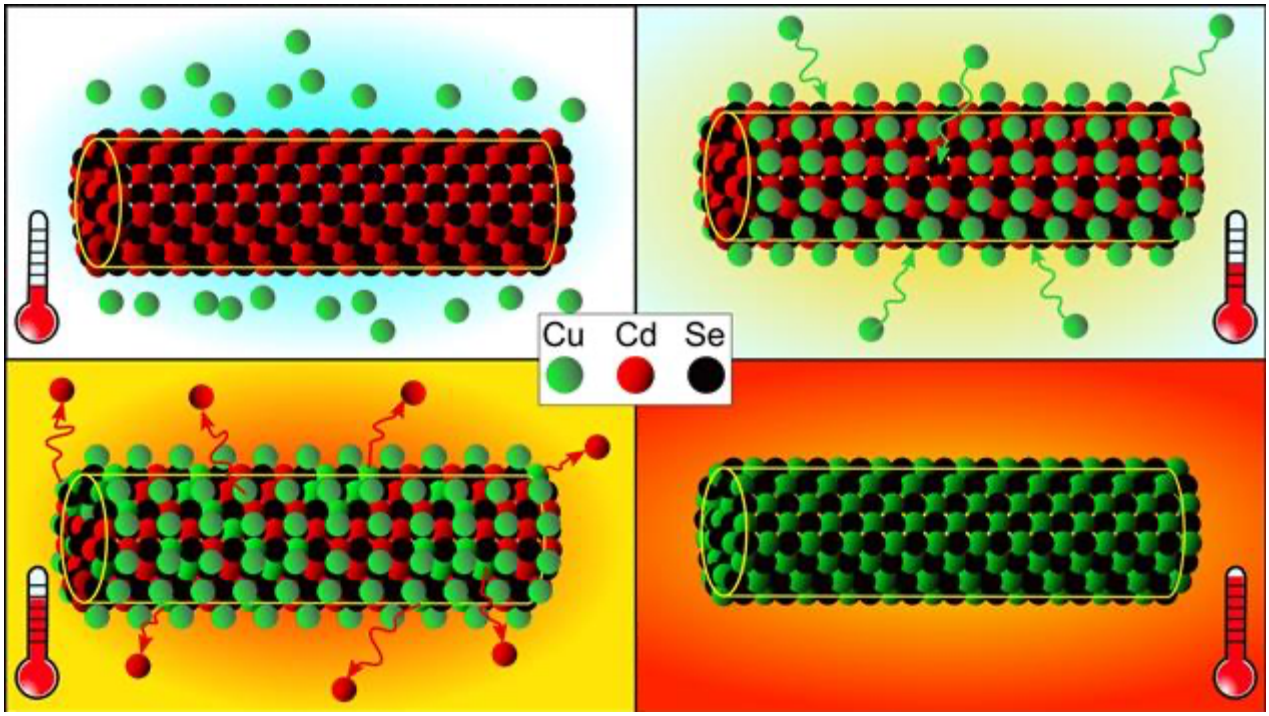

Keywords:

In-situ heating TEM cation exchange

Reference:

1)Casu, A., et al. Cu2Se and Cu Nanocrystals as Local Sources of Copper in Thermally-Activated In-Situ Cation Exchange. ACS Nano 2016, 10 (2), 2406−2414.
2)Casu, A.; et al.. Thermally-Promoted Cation Exchange at the Solid State in the Transmission Electron Microscope: How It Actually Works. ACS Nano 2023, 17, 17, 17058–17069

365

Electron-beam-induced surface diffusion of contaminants and growth of carbon contamination

Dr. Erich Müller[1], Mr. Arne Johan Schwartz[1], Mrs. Yolita M. Eggeler[1,2]
[1]Laboratory for Electron Microscopy, Karlsruhe Institute of Technology (KIT), Karlsruhe, Germany, [2]3DMM2O - Cluster of Excellence (EXC-2082/1 – 390761711), Karlsruhe Institute of Technology (KIT), Karlsruhe, Germany

PS-01 (2), Lecture Theater 3, august 28, 2024, 14:00 - 16:00

Background incl. aims
Carbonaceous contamination deposited on samples illuminated by a beam degrade the quality of images and aggravate structural and compositional analysis of the material. Contamination results from irradiation-induced polymerization of contaminants, which can be hydrocarbon molecules already present on the sample surface or molecules adsorbed from the residual gas of the instrument chamber [1]. Several authors concluded that the contribution of surface contaminants is dominant [2,3], but already earlier models consider an additional source from the residual gas in the instrument [4].
The goal of this work is to describe the flow of contaminants and their polymerization in the irradiated area with a number of parameters reduced to a minimum necessary. To analyze possible sources of contaminants, both, a surface diffusion process and the supply of contaminants from the residual gas are considered. It is hypothesized that the diffusion process is driven by the gradient of the surface density of contaminants, generated by the impact of the electron beam probe. The contribution of the residual gas atmosphere in the instrument is described by the tendency to re-establish an equilibrium surface density of contaminants.
A time-dependent reaction-diffusion model is elaborated to describe contamination growth on surfaces illuminated by an electron beam. The unknown parameters of the model are determined by comparing the theoretical predictions with experimental results. The experiments are designed such that the influence of each parameter can be unequivocally separated. Successive contamination measurements, performed at distinct time intervals allow to follow the dynamic of the process. Examination of the individual contribution of contaminants from the sample surface and from the residual gas of the instrument is facilitated by experiments with appropriate variations of these parameters.
Methods
Circular contamination patterns were grown in a FEI DualBeam Strata 400S on commercial thin (~10 nm) amorphous carbon films by illuminating the sample homogeneously with a defocused electron beam. The radius of the irradiation disk was chosen to be sufficiently large (~ 700 nm) to separate the influence of the distinct parameters on the contamination growth. Thus, the inflow of the surface contaminants by diffusion was noticed at the margin of the disk, while the residual gas contributed on the entire sample surface. The dynamical evolution of the process was followed by successive contamination measurements performed up to 20 minutes at time intervals of 5 minutes.
The local height and shape of the contamination rings were quantified by taking high-angle-annular-dark-filed (HAADF) images in scanning-transmission-electron-microscopy (STEM) mode between the irradiation cycles, and comparing their intensities with corresponding Monte-Carlo simulations. Both, irradiating and imaging, were conducted at electron beam energy of 20 keV and with a current of 120 pA.
To elucidate the supply of contaminants from the residual gas, the chamber pressure of the microscope was varied by different pumping periods and the usage of a cooling vessel trap. The initial density of the surface contaminants was altered by subjecting the sample to variable duration of in-chamber plasma cleaning.

Consideration of the main parameters of the process lead to a reaction-surface-diffusion model with an additional source term. It was supposed that the relative density of contaminants $n = N/N_o$, normalized to an initial density $N_o = N(t = 0)$, changed locally due to polymerization to amorphous carbon contamination by the illuminating beam. The occurring gradient of n generated a surface diffusion process of contaminants, characterized by the diffusion coefficient D. The reaction of the irradiating electrons with the contaminants was described by the reaction-frequency σ. An adsorption frequency η of molecules from the residual gas considered for a source term with the tendency to re-establish the initial density of the surface contaminants. With these terms, the reaction-diffusion equation was elaborated as follows:

$\partial n/\partial t = D \cdot \Delta n - \sigma \cdot n + \eta \cdot (1 - n)$,

with Δ representing the Laplace operator in cylindrical coordinates for radial symmetry.

Comparing the predictions of this model with the time evolution of the experimentally grown contamination, the parameters of the process could be determined. All results were considered with respect to reference measurements, performed prior to the experiments with parameter variation.

Results

A surface-plot in Fig.1 a) shows the HAADF-STEM image intensities of contamination grown during 20 minutes of local irradiation with a defocused electron-beam of 20 keV. The modeled thickness profiles (continuous lines) in comparison with the measured radial profiles (dashed lines) of the contamination ring are depicted for distinct time intervals in Fig.1 b). Comparing the predictions of the reaction-diffusion model with experimentally grown contaminations, the diffusion of the surface contaminants was described by $D \sim 10^3$ nm²/s and the polymerization of the contaminants by a reaction frequency $\sigma \sim 1$ Hz. Small variations of D and σ for distinct measurements could be explained by local differences of the contaminants type of the corresponding experiments.

The contribution of contaminants from the sample surface and from the residual gas were separately determined by varying accordingly the experimental conditions by plasma cleaning, respective pumping and cooling of the instrument chamber. Already short plasma cleaning durations significantly reduced contamination growth and the exponential decay in time of surface contaminant density N_o showed an effective removal of surface contaminants.

With higher chamber pressures, the residual gas supply of contaminants increased, as indicated by the raise of the adsorption frequency of contaminants. However, its value $\eta \sim 0.002$ Hz remained very low in comparison with the other parameters and contributed only with a small amount to the total contamination growth. Its direct influence in the illuminated area was relatively reduced, but became noticeable for contaminant adsorption outside the illuminated area and their subsequent diffusion into it.

Conclusion

In conclusion, it can be asserted that contaminants stem from the sample surface and diffuse into the illuminated area. This underlines the effectiveness of in situ plasma cleaning. The residual gas contributes less to direct contamination growth but should be considered for experiments of longer duration.

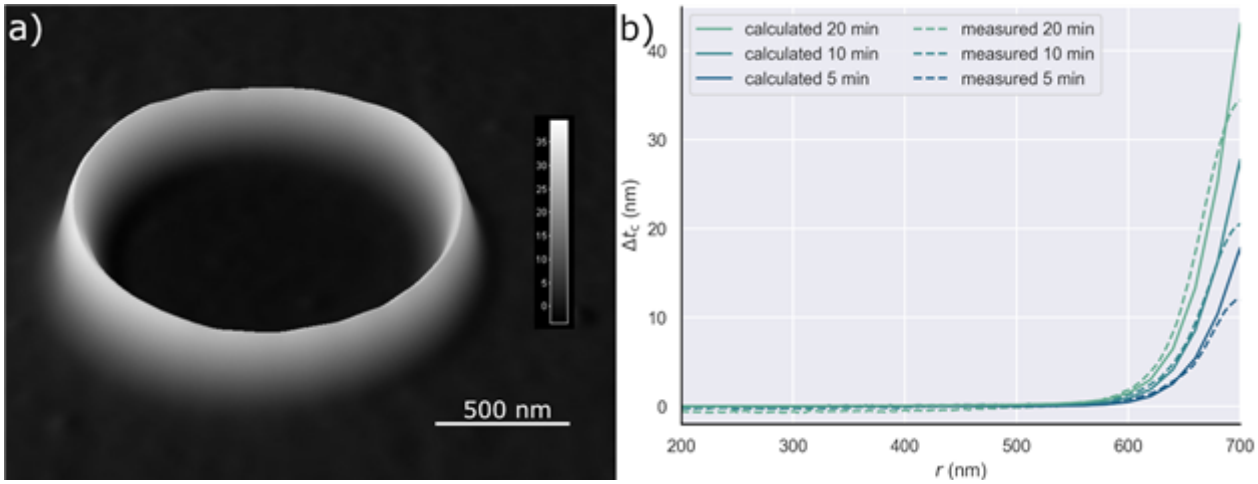

Keywords:

contamination, surface diffusion, electron microscopy

Reference:

[1] L. Reimer, Scanning Electron Microscopy, Springer (1998)
[2] K. Rykaczewski et al., J Appl Phys. 101 (2007)
[3] M. Hugenschmidt et al., Microsc. Microanal. 29 (2022)
[4] K.H. Müller, Optik 33 (1971)
[5] We acknowledge funding by the Deutsche Forschungsgemeinschaft (DFG) under Germany's Excellence Strategy – 2082/1 – 390761711 and thank the Carl Zeiss Foundation for financial support.

723

Single-Layer Transition Metal Dichalcogenides: Unveiling Excitonic Processes with Multimodal Microscopy

Dr Herman Duim[1], Dr Noémie Bonnet[1], Jassem Baaboura[2], Dr Florian Castioni[2], Dr Steffi Y. Woo[2], Ching-Hwa Ho[3], Kenji Watanabe[4], Takashi Taniguchi[5], Dr Luiz H.G. Tizei[2], Dr Toon Coenen[1]
[1]Delmic, Delft, The Netherlands, [2]Laboratoire de Physique des Solides, Université Paris-Saclay, Centre National de la Recherche Scientifique, Orsay, France, [3]Graduate Institute of Applied Science and Technology, National Taiwan University of Science and Technology, Taipei, Taiwan, [4]Research Center for Electronic and Optical Materials, National Institute for Material Science, Tsukuba, Japan, [5]Research Center for Materials Nanoarchitechtonics, National Institute for Material Science, Tsukuba, Japan

PS-01 (2), Lecture Theater 3, august 28, 2024, 14:00 - 16:00

Background
Single-layer transition metal dichalcogenides (TMDs) exhibit remarkable light-matter interaction, making them prime candidates for next-generation optoelectronic devices. When thinned down to a single monolayer, the bandgap of TMDs changes from an indirect to a direct bandgap, resulting in efficient light emission. However, harnessing their full potential requires a deep understanding of their nanoscale optical properties. Probing these properties is challenging due to the highly confined nature of excitons in TMDs [1]. Advanced techniques like cathodoluminescence (CL) and electron energy loss spectroscopy (EELS) offer powerful tools for such investigations, but successful implementation hinges on meticulous control over sample preparation. Integration with hexagonal boron nitride (hBN) encapsulation offers a promising solution, potentially leading to improved optical properties and the emergence of moiré potentials for further functionalities [2, 3].

Results
This work addresses the aforementioned challenges in studying excitonic processes within single-layer TMDs. We leverage meticulous sample preparation techniques, including polymer-assisted stamping and encapsulation in hBN flakes, to ensure well-defined interfaces and controlled heterostructure thickness [4]. This meticulous approach paves the way for reliable analysis using advanced microscopy techniques.
We employ a multimodal approach, combining Scanning Transmission Electron Microscopy (STEM)-CL and STEM-EELS for comprehensive characterization. While STEM-CL allows for precise mapping of excitonic recombination processes, STEM-EELS measurements with monochromated electron beams provide information about the absorption mechanisms within the heterostructure at a high spatial resolution. Our investigation highlights the crucial role of hBN encapsulation in enhancing the intensity of cathodoluminescence. By comparing SEM-CL and STEM-CL on the same sample across a wide range of acceleration voltages, we directly assess the effectiveness of each technique. Additionally, we explore the impact of different substrates like SiO2/Si on emission characteristics and spatial resolution, emphasizing the importance of substrate selection for optimal analysis.

Furthermore, we leverage Monte Carlo simulations to understand the relationship between energy deposition within the heterostructure, influenced by acceleration voltage and sample thickness, and the resulting CL intensity. We observe a proportional relationship between these parameters, further validating our experimental findings.
Conclusions
This study offers valuable insights into the influence of material interfaces and heterostructure thickness on the optical properties of TMD monolayers. By elucidating the role of hBN encapsulation in enhancing CL intensity, we pave the way for the development of high-performance optoelectronic

devices. Furthermore, our multimodal approach, combining STEM-CL and STEM-EELS, provides a comprehensive understanding of excitonic processes in TMD monolayers. This knowledge is crucial for the future design of complex nanostructures with tailored optical properties and the development of controlled quantum emitters. The ability to correlate CL and EELS measurements offers an unparalleled perspective on light emission processes, laying the groundwork for fundamental advancements in understanding excitons in 2D materials.

Figure caption: Results from SEM-CL and STEM-EELS. (a) Normalized SEM-CL intensity map integrated over the spectral range from 775 to 805 nm, as indicated by the dashed lines in (b). Bubbles corresponding to residues from sample preparation can be observed as dark patches in the intensity map. (b) Normalized CL spectrum extracted from the SEM-CL intensity map in (a) exhibiting a single CL peak originating from the A-exciton (XA) of the TMD monolayer. (c) Monochromated STEM-EELS spectra taken at a beam accelartion of 100 keV. The EELS spectra are displayed for different dispersion so that absorption features from both the TMD monolayer as well as the hBN encapsulation layer can be observed.

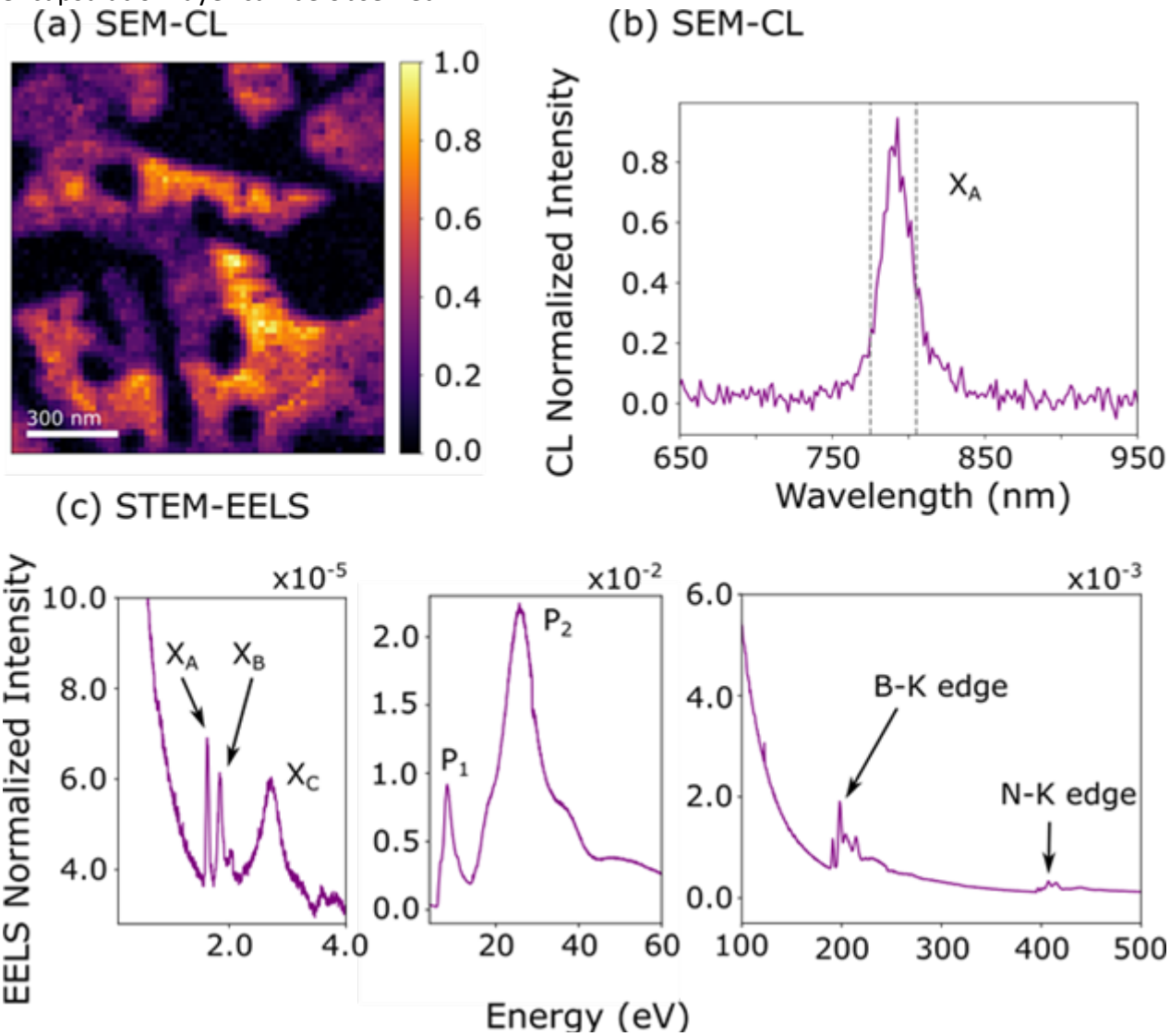

Keywords:

TMD, CL, EELS, Excitons, encapsulation

Reference:

1. N Bonnet et al., Nano Lett. 21, 10178 (2021), https://doi.org/10.1021/acs.nanolett.1c02600
2. F Shao et al., Phys. Rev. Mater. 6, 074005 (2022), https://doi.org/10.1103/PhysRevMaterials.6.074005
3. S Zheng et al., Nano Lett. 17, 6475 (2017), https://doi.org/10.1021/acs.nanolett.7b03585
4. N Bonnet et al., submitted

802

Determination of Ti3C2Tx Mxene few layers stacks architecture using valence EELS and diffraction

Dr Jerome Pacaud[1], Dr Haw-Wen Hsiao[2], Dr Renliang Yuan[2], Dr Stephane Celerier[4], Pr Jian-Min Zuo[2], Pr Vincent Mauchamp[1], Dr Thomas Bilyk[3]
[1]Institut Pprime – UPR 3346 – CNRS, Université de Poitiers, Poitiers, France, [2]Department of Materials Science and Engineering, University of Illinois at Urbana-Champaign, Urbana, USA, [3]Université Paris-Saclay, CEA, Service de recherche en Corrosion et Comportement des Matériaux, SRMP, Gif-sur-Yvette, France, [4]IC2MP – UMR 7285 – CNRS, Université de Poitiers, Poitiers, France

PS-01 (2), Lecture Theater 3, august 28, 2024, 14:00 - 16:00

The properties of two-dimensional (2D) materials generally depend on their architecture, e.g. the number of layers in a stack, the interlayer distance or the layer functionalization. Focusing on the most studied MXene compound to date, i.e. Ti3C2Tx 2D layers (where T-groups usually correspond to O, OH, F and/or Cl surface terminations inherited from the synthesis process), it has been shown that physical properties have a significant dependence on the number of layers in few-layer stacks. Beyond their thickness, MXene properties are also very sensitive to the interlayer distance which can be increased by intercalation of ions and/or molecules, or reduced by removing the interlayer intercalated water. In order to evidence the thickness/properties interplay in this rich family of 2D materials, one thus needs to precisely determine the architecture of a given MXene few-layer stack during TEM experiments. In this context, we show that valence EELS (VEELS) which corresponds to the excitation of the materials valence electrons, combined to density functional theory (DFT) simulations, provides a direct way to quantify (i) the number of layers in Ti3C2Tx few layer stacks for thicknesses up to ~10 layers, and (ii) the average inter-layer distance. [1]
Figure 1 shows a comparison between experimental VEEL spectra recorded on different Ti3C2Tx multilayers and the spectra simulated for different numbers of layers. To push the comparison quantitatively the mean squared error between experiments and simulations has been plotted, allowing to determine the exact number of layers in the thinnest samples. In addition, the position of the main peak, corresponding to the bulk plasmon, is closely correlated with the distance between sheets in the stack. Its shift can thus be used to estimate interlayer distance variations in a MXene multilayer with nanometer scale resolution
Finally, the thickness of a sample can also be obtained through diffraction measurements and intensity profiles STEM-HAADF analysis. Therefore in order to validate the thickness measurements obtained by the VEELS method, position averaged CBED (PACBED) patterns and STEM-HAADF images were recorded on the very same areas of the Ti3C2Tx MXenes. Different families of reflections exhibit different behavior of their pendellösung allowing to determine the sample thickness by comparison between experimental and simulated intensity ratios (Figure 2). PACBED and STEM-HAADF analysis confirm the outcomes of the VEEL spectra analysis.
TB, SC, VM and JP acknowledge the ANR through the MXENE-CAT project. JMZ is partially supported by DOE DE-SC0022060 and RLY was supported by Intel Corporation through an SRC project (Award #54071821)
Figure 1: (Left) Comparison between experimental VEEL spectra (black and grey curves) and DFT simulations considering thickness effects with the Kröger formula (color curves). Spectra were recorded on a FEI Themis Z microscope, equipped with a monochromator and operated at 80 kV. (Right) Mean squared error between experimental curves and simulations. It shows the very good precision on thickness determination for very thin samples.
Figure 2 : Pendellösung of the 100 and 110 reflections in the [001] zone axis and intensity ratio between the reflexions as a function of the thickness.

Figure 1:

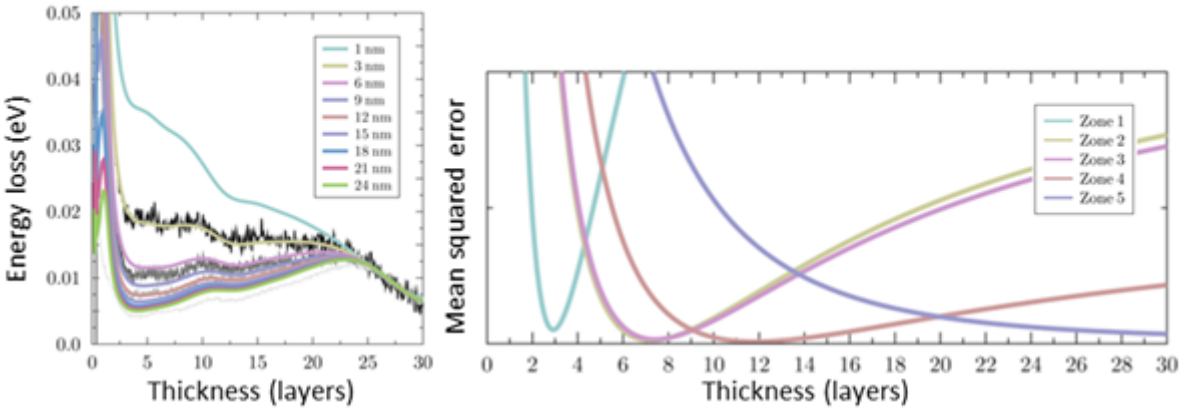

Figure 2:

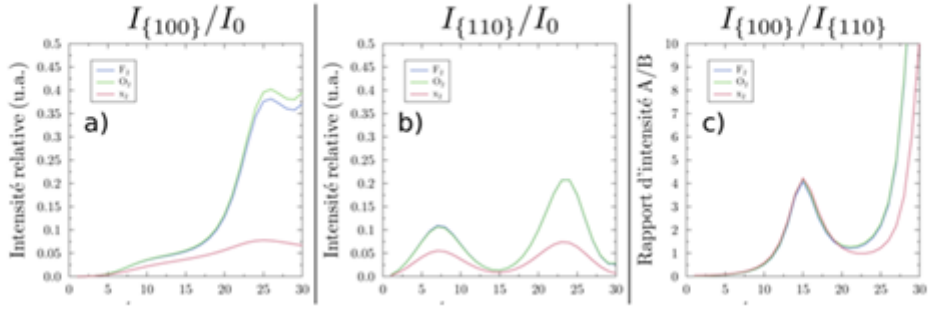

Keywords:

low-loss, thickness measurement, diffraction

Reference:

[1] T. Bilyk et al., 2D Materials, 9 (2022), p.035017

854

Investigating nitrogen doped nanocarbon materials as potential carbon dioxide adsorbers

Ivan Musil[1,2], Venkataprasanna Kannan Sampathkumar[1,2], Jonas Haas[1,2], Kevin Strobel[1,2], Jannik Meyer[1,2]
[1]Institute for Applied Physics, University of Tübingen, Tübingen, Germany, [2]NMI Natural and Medical Sciences Institute at the University of Tübingen, Reutlingen, Germany

PS-01 (2), Lecture Theater 3, august 28, 2024, 14:00 - 16:00

Background
The climate crisis, propelled by the continuous rise of carbon dioxide emissions, has spurred research to find technical solutions for this problem. One possibility is to directly capture carbon dioxide from the atmosphere and sequester it inside suitable long-term storage. Unfortunately, the success of this method strongly depends on the efficiency of the adsorber material. Here, nanocarbon materials such as graphene and carbon nanotubes could come into play, as they offer several beneficial characteristics like high surface area and stability. However, the catch is their nonreactive nature. To enable chemical adsorption one could alter the chemical structure of the nanocarbons by inserting new elements through doping. Nitrogen is a promising candidate, as it can be exchanged with the carbon atoms inside the crystal lattice of the materials. It is known to be a crucial component in other carbon dioxide fixating mechanisms, for example in plants. One goal of this research is to find novel routes for nitrogen doping of these materials and try to understand and control the process of ion implantation. Furthermore, the nitrogen doped nanocarbons are investigated as carbon dioxide adsorbers.
Methods
Nitrogen doping is realised by different methods of ion bombardment. HRTEM is used to examine the effects of doping on the atomic level. Further investigation is conducted with STEM coupled with EDX, FIB-SEM coupled with ToF-SIMS, AFM and XPS. A self-built setup is established, dedicated to measure the carbon dioxide capture performance of the materials, a scheme of it is shown in part A of the figure.
Results
Various methods of ion bombardment were successfully used to dope graphene with nitrogen. This was verified by HRTEM, observing implanted nitrogen atoms as well as defects introduced by nitrogen ion bombardment. The same treatment is conducted with carbon nanotube films. These films are produced via filtration of carbon nanotube suspension in a controlled manner and various thicknesses, which are checked by AFM. FIB-SEM with ToF-SIMS as well as XPS verify that nitrogen is present in the upper 100 nm of the films that have been bombarded with nitrogen ions. Further investigation through STEM coupled with EDX give insight into the ion dosage dependent distribution of nitrogen in thicker carbon nanotube bundles after doping, as shown in part B of the figure. Additionally, HRTEM shows the deterioration of the carbon nanotube crystal structure after excessive ion bombardment, which can be seen in part C of the figure. Carbon dioxide capture performance of various carbon nanotube films has been measured with the dedicated setup. An increase in performance was observed after treatment with nitrogen ions.
Conclusion
Different ways of ion bombardment were used to implant nitrogen into the crystal structure of graphene and carbon nanotubes. This was verified by various microscopic and spectroscopic methods. The effects of the doping procedure were investigated on atomic as well as microscopic level, giving insights in the doping mechanisms during ion bombardment. Furthermore, it was shown that nitrogen doping changes carbon nanotube films in a way, that improves their ability to sequester carbon dioxide from the atmosphere.

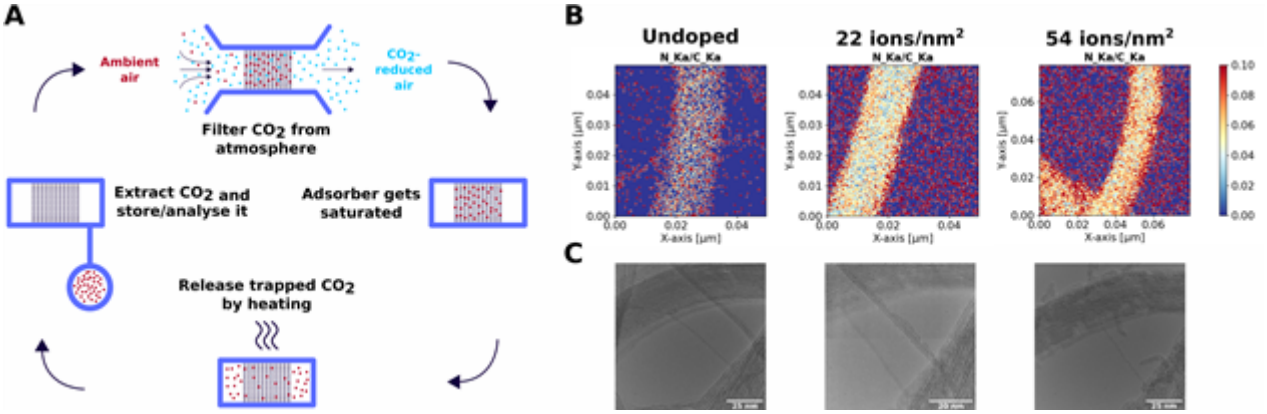

Keywords:

Nanocarbons, nitrogen doping, carbon capture

858

In-Situ Manipulation of Growth Mechanisms in Ni-Seeded GaP Nanowires

Tianyi Hu[1,2], Dr. Yuanyuan Cao[1,2], Dr. Sara M. Franzén[2,3], Dr. Daniel Jacobsson[1,2,4], Dr. Michael S. Seifner[1,2], Prof. Maria E. Messing[2,3], Prof. Kimberly A. Dick[1,2,3]
[1]Centre for Analysis and Synthesis, Lund University, Lund, Sweden, [2]NanoLund, Lund University, Lund, Sweden, [3]Solid State Physics, Lund University, Lund, Sweden, [4]National Center for High Resolution Electron Microscopy, Lund University, Lund, Sweden

PS-01 (2), Lecture Theater 3, august 28, 2024, 14:00 - 16:00

III-V semiconductor nanowires (NWs) have emerged as a promising class of materials for next-generation nanoelectronics and photonics due to their unique electronic, optical, and mechanical properties.[1] The ability to grow III-V NWs with high precision and controllability has led to the development of numerous applications in the fields of electronics, photonics, and energy conversion.[2] Thus, precise control over the growth of III-V NWs has been a major topic that enables the creation of uniform and reproducible nanostructures with tailored properties.
So far, the bottom-up approach is widely used for synthesizing the semiconductor NWs, where an intrinsic or foreign metal (called as seed particle) is often used to promote the anisotropic one-dimensional growth. There has been abundant research focusing on the influence of seed material, preparation and dynamics on NW growth.[3] However, most of such research are carried out in a post-growth condition, where the NWs are cooled and transferred from the synthesis equipment for further analysis. Thus, there is a lack of understanding on the dynamic interplay between seed particles and NWs under the growth environment, such as the real-time crystal structure and composition of the seed particles and their impact on the corresponding NWs.
This conference contribution reports a detailed investigation on the growth of gallium phosphide (GaP) NWs using Ni as seed material. An aberration-corrected environmental transmission electron microscope (ETEM) integrated with a metal-organic chemical vapor deposition (MOCVD) system was used. Ni nanoparticles were transformed into Ni_5P_4 crystals by the supply of phosphine. After adding trimethylgallium (TMGa) to the precursor supply, the nucleation of GaP NWs was observed and captured by high-resolution TEM (HRTEM) movies. The phases involved in the nucleation and NW growth process were characterized via energy-dispersive X-ray spectroscopy (EDS) and power spectra obtained from the HRTEM images.
In the investigated range of partial pressures, two types of seed particles were observed: At low V/III ratios (defined as corrected partial pressure ratio between group V and group III supplies), NWs grew from two Ni-Ga phases at a similar growth rate, namely the solid NiGa phase, as well as the Ni_2Ga_3 phase. In contrast, at high V/III ratios, NWs grew from Ni_2P particles, where interdiffusion through Ni_2P contributes to multiple nucleation and leads to a much higher growth rate. The ability to manipulate the seed particle phases offers the potential for precise control over the growth of compositionally abrupt heterostructure NWs, where group III or V elements can be individually switched. Our research results represent a significant step forward in the replacement of Au as a conventional seed particle material, as well as in the ability to locally modify the composition, doping levels, and morphology within the same NW.

Keywords:

In situ TEM, semiconductor nanowires

Reference:

1. Jia, Chuancheng, et al. "Nanowire electronics: from nanoscale to macroscale." Chemical reviews 119.15 (2019): 9074-9135.
2. Barrigón, Enrique, et al. "Synthesis and applications of III–V nanowires." Chemical reviews 119.15 (2019): 9170-9220.
3. Dick, Kimberly A., and Philippe Caroff. "Metal-seeded growth of III–V semiconductor nanowires: towards gold-free synthesis." Nanoscale 6.6 (2014): 3006-3021.

49

In Situ TEM Biasing and Heating of Neuromorphic Gold Nanogranular Nanofilms Showing Resistive Switching

Prof. Andrea Falqui[1], Mr. Alberto Casu[1], Mr. Paolo Milani[1], Ms. Angelica Chiodoni[2], Mr. Yurii Ivanov[3], Mr. Giorgio Divitini[3]
[1]University of Milan, Department of Physics, Milan, Italy, [2]Center for Sustainable Future Technologies @PoliTo, Istituto Italiano di Tecnologia, Turin, Italy, [3]Electron Spectroscopy and Nanoscopy, Istituto Italiano di Tecnologia, Genoa, Italy

PS-01 (3), Lecture Theater 3, august 30, 2024, 14:00 - 16:00

Background incl. aims
Nanogranular gold films, when prepared by supersonic cluster beam deposition with a thickness just above the electrical percolation threshold, exhibit highly branched structure with a neuromorphic behavior reminiscent of biological neural networks, including resistive switching and adaptation. Such characteristics position these materials as viable substrates for neuromorphic computing. Despite their potential, the understanding of the underlying phenomena has been limited to electrical measurements and theoretical speculation. The objective of this study was to visually elucidate the morphological transformations that occur at the micro- and nanoscale within these films during electrical stimulation and to assess how these changes correlate with neuromorphic functionality.

Methods
Gold nanogranular films were deposited at approximately 17 nm thickness to balance electrical conductivity with TEM imaging suitability. These films were then subjected to in situ biasing within a two-electrode configuration. High temporal resolution imaging was conducted using a CMOS direct detection camera, operating at a controlled low electron dose. The morphology of the entire area between electrodes was observed during sequential electrical stimulations—first across a voltage ramp and then at a constant voltage. Additionally, in situ heating TEM imaging was applied, observing the films under thermal stress at both high resolution and low magnification.

Results
Initial in situ biasing caused the localized de-percolation effect shown in figure [1], and characterized by the retraction of gold branches without mass loss, leading to the formation of isolated gold islands. This morphological adaptation was highly localized and accompanied by the development of small, dense gold structures. Upon global thermal stimulation, the films underwent a more extensive de-percolation, resulting in the creation of distinct, polycrystalline gold islands across the whole heating substrate. This behavior is akin to that observed in atom-assembled gold films. The in situ TEM imaging revealed the likely occurrence of extremely intense and localized hot spots, whose temperature and extent appear to grow with increased voltage and may induce localized melting, even possibly capable of disrupting the amorphous silicon nitride substrate when the highest voltage and temperature are reached [1].

Conclusions
The study presents a novel visual insight into the morphological dynamics of nanogranular gold films under electrical and thermal stimuli, suggesting that intense, localized hot spots may play a critical role in neuromorphic behavior. The findings highlight the need for further exploration of the local temperature within these hot spots, the role of electromigration and Joule heating, and the impact of the substrate on the film's behavior. In situ TEM imaging has proven invaluable in expanding our understanding of the physical phenomena driving the unique electrical characteristics of metal

nanogranular films, offering implications for the advancement of materials with neuromorphic properties.

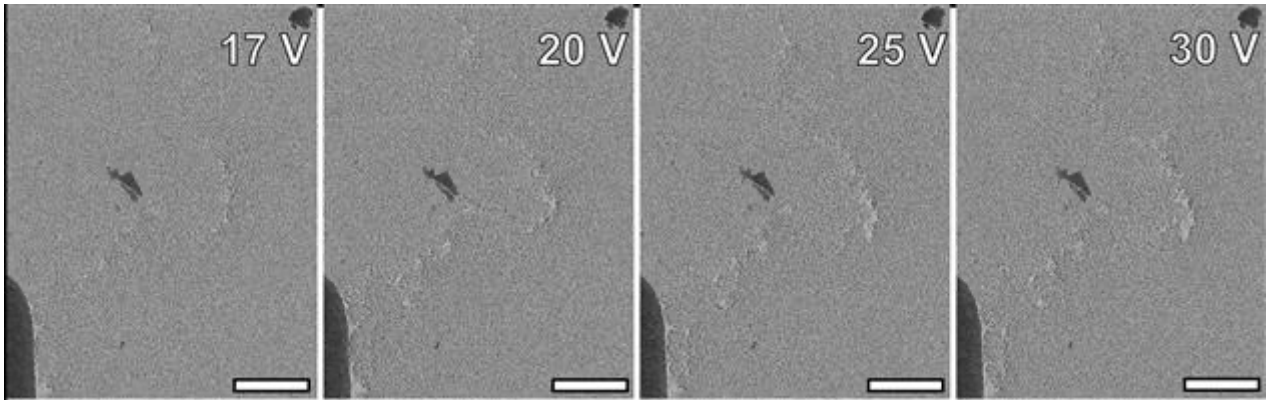

Keywords:

in-situ biasing and heating TEM

Reference:

[1] A. Casu, Angelica Chiodoni, Yurii P. Ivanov, Giorgio Divitini, Paolo Milani,* and Andrea Falqui*. In Situ TEM Investigation of Thermally Induced Modifications of Cluster-assembled Gold Films Undergoing Resistive Switching: Implications for Nanostructured Neuromorphic Devices. Accepted by ACS Applied Nano Materials, March 2024.

69

Novel Insights into Atomic-Scale Interface Reconstruction during Epitaxial Growth of Metallic Delafossite Thin Films

Anna Scheid[1], Dr. Qi Song[2], Mr. Hari Pokhrel[3], Dr. Tobias Heil[1], Dr. Stephanie Ribet[4], Dr. Colin Ophus[4], Mr. Niklas Enderlein[3], Dr. Y.Eren Suyolcu[1], Prof. Dr. Philipp Hansmann[3], Prof. Dr. Darrell Schlom[2,5,6], Prof. Dr. Peter A. van Aken[1]
[1]Max Planck Institute for Solid State Research, Stuttgart, Deutschland, [2]Department of Materials Sciences and Engineering, Ithaca, USA, [3]Department of Physics, Friedrich-Alexander-Universität Erlangen-Nürnberg (FAU), Erlangen, Germany, [4]National Center for Electron Microscopy, Molecular Foundry, Lawrence Berkeley National Laboratory, Berkeley, USA, [5]Kavli Institute at Cornell for Nanoscale Science, Ithaca, USA, [6]Leibniz-Institut für Kristallzüchtung, Berlin, Germany

PS-01 (3), Lecture Theater 3, august 30, 2024, 14:00 - 16:00

Delafossites are classified as oxides with a general chemical composition of ABO_2, containing metal ions in the formal oxidation states of A+ and B3+ [1]. Depending on the cations of choice, delafossites exhibit a wide range of interesting physical properties, including p-type or bipolar semiconductivity (when A = Cu, B = Al, Cr, Fe, Ga, Y, In), photocatalytic activity (as observed in $AgGaO_2$), and metallic conductivity ($PdCoO_2$, $PdCrO_2$, $PdRhO_2$, $PtCoO_2$, and $AgNiO_2$) [2].

The metallic delafossites crystallize in the rhombohedral 3R phase with $R\bar{3}m$ symmetry and exhibit unusually large in-plane conductivities for oxides, surpassing even most pure metals. For example, $PdCoO_2$ has a conductivity about four times that of pure Pd, approaching the level of pure Cu, Ag, and Au. Therefore, metallic delafossites such as $PdCoO_2$ are of great interest for exploring their potential in oxide heterostructures and for applications in electronics and spintronics. To account for the limited size of their single crystals, researchers have fabricated thin films of metallic delafossites using methods such as reactive sputtering, pulsed laser deposition (PLD), and molecular beam epitaxy (MBE) [2]. Delafossite thin films are typically grown along the c-axis on substrates such as Al_2O_3 (0001) and β-Ga_2O_3 (201). Despite significant lattice mismatches between metallic delafossites and substrates, e.g., a mismatch of ~6% for $PdCrO_2$ on c-Al_2O_3, high-quality c-axis oriented thin films can be successfully grown. This is possible due to an intriguing mechanism during the growth process that appears to mitigate the mismatch strain at the interface, although the exact nature of this mechanism remains unexplained. In particular, the realization of high-quality films can be attributed to the choice of CoO_2 as the first layer grown in ozone-assisted MBE [3,4].

In this study, we reveal the presence of atomic-scale reconstructions at the $PdCoO_2$ – Al_2O_3 interface by combining advanced scanning transmission electron microscopy (STEM) techniques, including electron energy loss spectroscopy (EELS) and 4D STEM phase reconstructions via electron ptychography. The reconstructed phase (Figure 1(a)) reveals the presence of atomic columns at the interface that are not consistent with the atomic model of either the film or the substrate, while EELS fine structure analyses (Figure 1(b)) indicate a Co valence reduction across the interface. Insights from the combination of spectroscopy and phase reconstruction suggest the formation of a unit-cell thick layer of CoO within the first atomic layer of the substrate. This previously undiscovered behavior has significant implications for the understanding of the mechanism of epitaxial growth of metallic delafossite thin films.

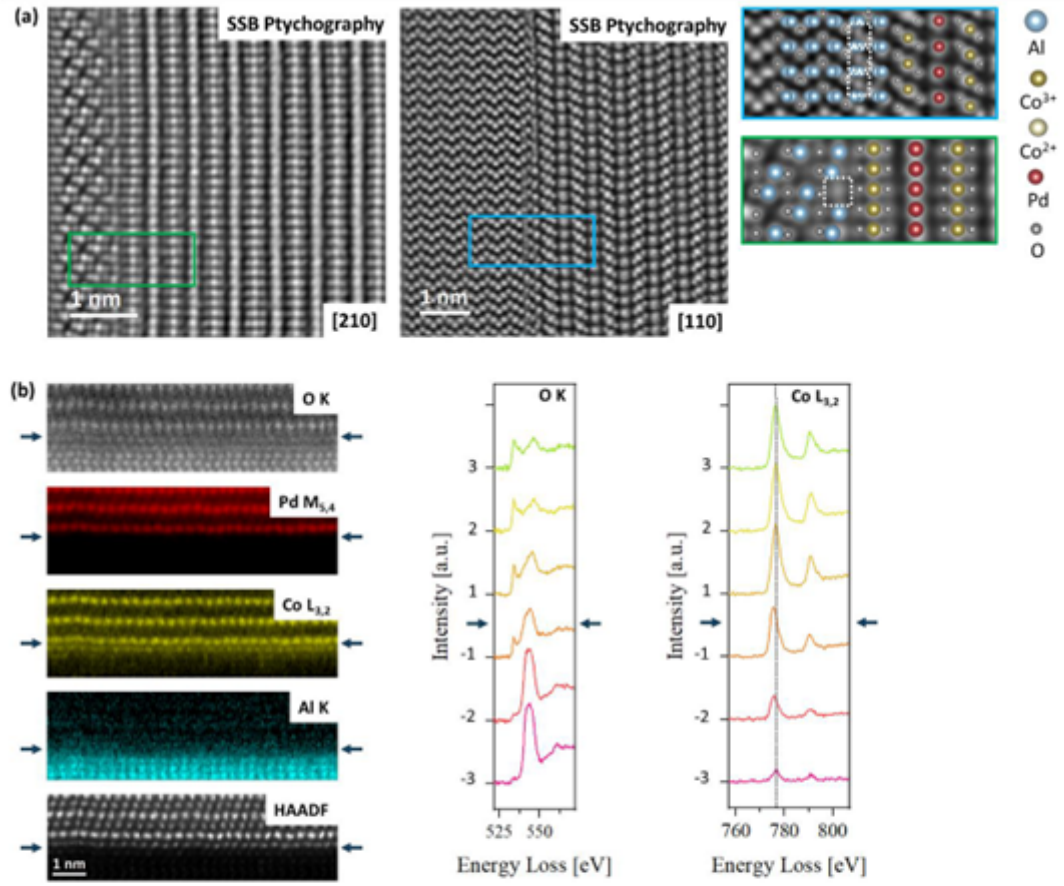

Figure 1. (a) 4D STEM phase reconstructions of $PdCoO_2$ on Al_2O_3 along the [210] (left) and [110] (middle) zone axes. The phase reconstructions provide strong contrast for all atomic species, revealing the oxygen positions in the lattice. The magnified insets (right) include the structural models for the substrate and film as an overlay, revealing unaligned atomic columns at the interface (white boxes). (b) EELS elemental mapping of the interface region along the [110] zone axis. The film consists of alternating layers of $[CoO]^-$ and Pd^+, starting with $[CoO]^-$. The pronounced Co signal in the first layer of the substrate indicates the presence of the interface reconstruction. Due to the overlap of the EELS edges, the Pd signal is superimposed on the oxygen signal. The arrows indicate the film–substrate interface. The EELS fine structure signal was extracted from atomic layers across the interface (negative numbers correspond to layers in the substrate and positive numbers correspond to the film), of the O K and Co $L_{3,2}$ edges. The Co $L_{3,2}$ white lines show a clear shift towards lower energy losses and a change in the ratio between the L_3/L_2 peaks, indicating a transition to a lower Co valence state.

Keywords:

delafossite, interface, reconstruction, 4DSTEM, ptychography

Reference:

1. A. P. Mackenzie, Rep. Prog. Phys. 80, 032501 (2017), https://doi.org/10.1088/1361-6633/aa50e5.
2. T. Harada et al., Materials Today Advances, 11, (2021), https://doi.org/10.1016/j.mtadv.2021.100146.
3. J. Sun et al., APL Mater. 7, 121112 (2019), https://doi.org/10.1063/1.5130627.
4. Q. Song et al., APL Materials, 10, 9 (2022), https://doi.org/10.1063/5.0101837.

234

RUDDLESDEN-POPPER PLANAR DEFECTS IN METAL HALIDE PEROVSKITES: MECHANISMS OF FORMATION AND CONSEQUENCES FOR PHASE STABILITY

Irina Skvortsova[1], Mr. Tom Braeckevelt[2], Miss Nadine Schrenker[1], Mrs. Annick De Backer[1], Mr. Bapi Pradhan[3], Mr. Johan Hofkens[3], Mrs. Veronique Van Speybroeck[2], Mrs. Sandra Van Aert[1], Mrs. Sara Bals[1]
[1]EMAT, University of Antwerp, Antwerp, Belgium, [2]CMM, Ghent University, Ghent, Belgium , [3]Photomat, KU Leuven, Leuven, Belgium

PS-01 (3), Lecture Theater 3, august 30, 2024, 14:00 - 16:00

Background: Metal halide perovskites (MHPs) are promising candidates for the next generation of optoelectronic and photovoltaic devices. This is mainly due to their wide-gamut emissions, high color purity (<35 nm spread) and remarkable photoluminescence quantum yield of more than 90%. However, their commercial application is still hindered by fast degradation under real conditions. The main cause of the CsPbI3 instability is its transformation from the black perovskite phase (photoactive) into the yellow non-perovskite (inactive) phase under ambient conditions, where water molecules decrease energy barriers of phase transition. Strategies towards more phase-stable CsPbI3 include interfaces, ligands as well as composition engineering. The last one is frequently associated with the formation of Ruddlesden-Popper (RP) planar defects, as shown for doped CsPbBr3. However, the underlying reasons and pathways of formation of the RP phase remain undiscovered. Therefore, the aim of this study is to understand how modification of CsPbI3 with Zn2+ and Cd2+ helps to prolong phase degradation by exploiting local techniques such as quantitative transmission electron microscopy (TEM) combined with molecular dynamics (MD) structure simulations.
Methods: In this work, we utilize different TEM techniques such as High Angle Annular Dark Field Scanning Transmission Electron Microscopy (HAADF-STEM), 4D STEM and Energy Dispersive X-ray Spectroscopy (EDX) under low-dose conditions to retrieve local structural changes which might explain stability improvement upon doping. These experimental investigations were complemented by quantitative analysis using StatSTEM software. Moreover, to demonstrate single-phase 3D structure as well as the structure of RP/perovskite interfaces, MD simulations were used along with TEM image simulations through the MULTEM software.
Results: Cd2+ and Zn2+ precursors were introduced into the reactive batch during hot-injection synthesis of CsPbI3 nanocrystals. As-prepared modified material contained ~2.1 at.% of Zn and ~2.5 at.% of Cd uniformly distributed along the nanocrystals. To understand the mechanism of nanocrystals degradation, a series of ex situ TEM experiments was performed for pristine and modified samples. It was established that the degradation pathway includes the agglomeration stage and the phase transformation. Here, both modified samples have demonstrated prolonged stability after agglomeration up to 5 days for Cd-containing and 10 days for Zn-containing CsPbI3. Ruddlesden-Popper planar defects in a specific configuration were identified for each modified sample by means of advanced electron microscopy. Using high-resolution EDX we showed that both transition metals are mainly distributed in these defects which are present along the diagonals of the square-like projection of the nanocrystals. Detailed analysis showed that Cd2+ doping results in ½ lattice shift in one direction, whereas Zn2+ doping provides ½ lattice shifts in two perpendicular directions. This difference can be ascribed to the ionic radii difference between Cd (1.09 Å) and Zn (0.88 Å). Combining these observations with molecular dynamic simulations, Zn2+ presumably occupies interstitial positions in RP regions with only changing Cs and I content slightly to balance the charges, whereas Cd substitutes Pb atoms. Moreover, the RP phases include CsI layers of different length in-between perovskite structure, providing a smooth transition from RP into the gamma-phase along [110]CsPbI3/[001]RP direction. The process of RP phase formation includes the drifting apart of neighboring [PbI6]4- octahedra as a result of strain in the lattice due to Zn and Cd

incorporation. Afterwards, additional Cs and I atoms have to enter the created void, which is followed by a shift of the two perovskite parts in one or two directions for the Cd- or Zn-modified samples, respectively. We associate an improvement in phase stability for these materials with the presence of as-described RP defects. In the α-phase of CsPbI3 a corner-sharing structure is preserved with Pb-I-Pb bond angles of 180^{o}, while in a δ-phase the structure consists of edge-sharing [PbI6]4- octahedra with the Pb-I-Pb bond angles of 90^{o}. Hence, the smaller these angles are, the lower kinetic stability is, hence, black-to-yellow transformation occurs faster. According to MD simulations, the gamma-phase most likely has Pb-I-Pb bond angles of 152.7^{o}, while for the one-shifted RP phase, observed for Cd-modified material, the value equals to 154.2^{o} and for two-shifted RP phase, observed for Zn-modified material, the angle is 155.1^{o}. The observed tendency perfectly correlates with the phase stability test, where Zn-modified material demonstrated the highest stability in comparison to Cd-containing and unmodified sample, whereas Cd-containing sample also surpassed unmodified material. At the interface between RP/perovskite phases the angles are 154.5^{o} and 156.0^{o} for Zn and Cd-modified samples respectively, which also contributes to the enhanced phase stability.

Conclusions: We applied a combined experimental/theoretical approach to unravel the influence of modification with Zn2+ and Cd2+ on phase stability of CsPbI3 nanocrystals. From an experimental point of view, we were able to observe specific types of Ruddlesden-Popper (RP) phase defects across the nanocrystals, where Cd and Zn are mainly localized. These defects were analyzed in a quantitative manner using statistical parameter estimation theory applied to the TEM results. Combination of these experimental results with MD simulations reveals how the RP planar faults are formed in a presence of transition metals, where these atoms are positioned and explains how phase stability, as shown by series of ex situ TEM results, is related to these defects. This is why our study contributes to an enhanced understanding of mechanisms underlying perovskites stabilization and may foster its commercialization for further use in devices.

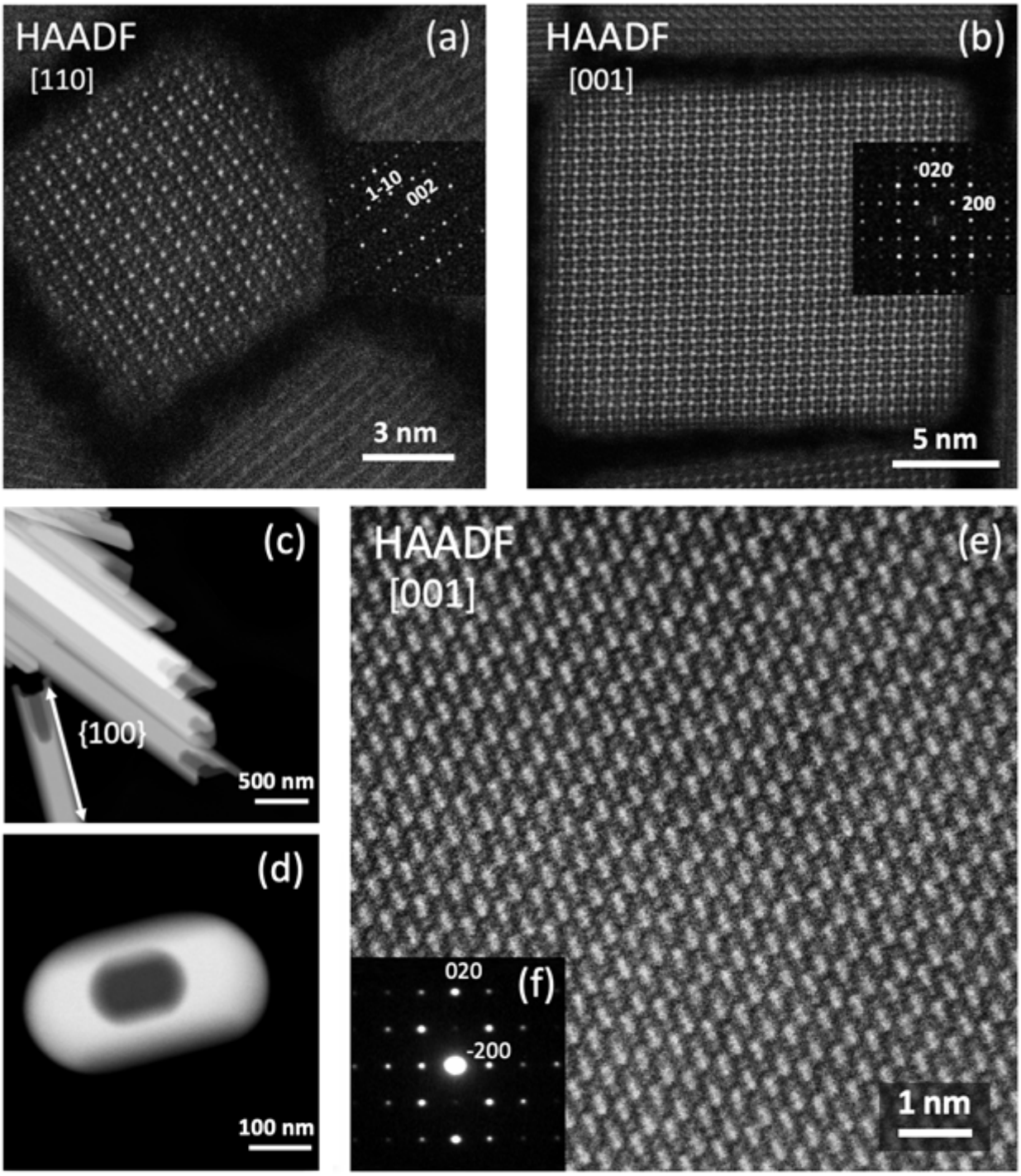

Figure 1. Low-dose HAADF-STEM images of pristine $CsPbI_3$ nanocrystals in a black-phase with corresponding FFT patterns for (a) [110] and (b) [001] orientations of orthorhombic structure (Pnma). Overview and high-resolution images of [001]-oriented $CsPbI_3$ yellow phase are shown in (c, d) and (e) accordingly. Corresponding SAED pattern (f) is indexed in the orthorhombic crystal system.

Keywords:

phase transitions, lattice shifts, defects

Reference:

Chem. Mater. 2023, 35 (6), 2321-2329

Chem. Mater. 2020, 32 (24), 10641-10652

Angew. Chem. Int. Ed. 2020, 59, 6794

Ultramicroscopy 2016, 171, 104-116

Ultramicroscopy 2015, 156, 9-17

The authors acknowledge the financial support of the Research Foundation Flanders (FWO, Belgium) SBO project 1SHA024N.

412

Investigation of metal-to-metal hydride phase transformations in magnesium thin films using STEM techniques

Dr Gopi Krishnan[1]
[1]DTU Nanolab, Technical University of Denmark, Lyngby, Denmark, [2]Faculty of Applid Sciences, Delft University of Technology, Delft, The Netherlands, [3]Faculty of Applid Sciences, Delft University of Technology, Delft, The Netherlands, [4]DTU Nanolab, Technical University of Denmark, Lyngby, Denmark

PS-01 (3), Lecture Theater 3, august 30, 2024, 14:00 - 16:00

Background incl. aims
In the pursuit of a decarbonized society and economy, hydrogen (H2) stands out for its zero-emission potential as a fuel, energy storage medium, and chemical feedstock. However, achieving compact hydrogen storage, especially in safe, solid forms such as metal hydrides, remains a significant challenge.
Enhancing storage efficiency requires a deep understanding of the nano/atomic-scale dynamics of, e.g., the metal-to-metal hydride transformation, including nucleation, growth, and the effects of stress, strain, and defects on hydrogen storage properties. Therefore, to pave the way for improved storage solutions, we must develop a deeper understanding of hydrogen sorption and desorption dynamics through the real-time observation of the transformation process in scanning/transmission electron microscopy (S/TEM).
Methods
We used magnesium (Mg) thin films as a model system to study metal-to-metal hydride phase transformation. The Mg films were grown using a DC magnetron sputtering to a thickness of 500 nm with an 8 nm adhesion layer of Titanium (Ti) and a catalyst layer of Palladium (Pd) of 100 nm. A ThermoFisher Hydra plasma-focused ion beam (PFIB, Xe, 30kV) was used to prepare the TEM lamellas. Structural investigations were performed using a ThermoFisher Spectra Ultra equipped with an X-FEG mono and a Gatan Image Filter (GIF) Continuum HR. These phase transformations were studied under both in-situ and ex-situ conditions using STEM, low-loss plasmon electron energy loss spectroscopy (EELS), and electron diffraction (ED).
Results
The hydrogen absorption/desorption process in Mg is observed using the bulk plasmon shift in EELS due to a structural change from a hexagonal closed-packed (HCP) to a tetragonal crystal structure. During absorption, TEM dark-field imaging confirms that the Mg thin film loses its initial morphology and transforms into nanocrystalline particles, which is attributed to volume expansion. Low-loss EELS further confirms that the hydride phase transformation occurs through nucleation and growth, distinguishing it from the desorption process. The desorption process starts with the formation of pores/voids at the interface between Mg and Ti, followed by crack formation that initiates Mg formation. The Complete H2 desorption in thin films results in a fully porous structure, with subsequent coalescence leading to void formation in Mg. The thin film's increasing porosity and void formation with subsequent cycling indicate a deterioration of its durability. However, initial porosity at the Mg/Ti interface promotes Mg nucleation during desorption. In order to validate our findings, we combine both in-situ and ex-situ studies at high spatial resolution in STEM, enabling us to compare our results and interpret the effect of the e-beam dose rate on the analysis.
Conclusion
We demonstrate that STEM imaging, low-loss EELS, and ED allow us to track the phase transformation from metal-to-metal hydride in Mg thin films along with its structural and morphological changes. The nucleation and growth of Mg are influenced by the stress/strain generated during the hydride transformation, distinct from the desorption process.

Keywords:

STEMEELS
Phasetransformation
Hydrogen storage
MgH2.

Reference:

Reference:
1 V. A. Yartys et al, vol. 44, (2019), p. 7809, doi:10.1016/j.ijhydene.2018.12.212.
2 T. C. Narayan, A. Baldi, A. L. Koh, R. Sinclair, and J. A. Dionne, Nat Mater, (2016), doi: 10.1038/nmat4620.
3 F. Sterl, H. Linnenbank, T. Steinle, F. Mörz, N. Strohfeldt, and H. Giessen, Nano Lett, 2018, doi: 10.1021/acs.nanolett.8b01277.
4 N. Patelli, M. Calizzi, and L. Pasquini, Inorganics, vol. 6, (2018) p. 1, doi: 10.3390/inorganics6010013.
5 J. A. Kammerer, X. Duan, F. Neubrech, R. R. Schröder, N. Liu, and M. Pfannmöller, Advanced Materials, vol. 33, (2021),doi: 10.1002/adma.202008259.

529

How to better understand ZrCu Thin Films Metallic Glasses recrystallization: a TEM in situ characterization?

Pr. Philippe Steyer[1]
[1]MateIS Laboratory, SNMS Microscopy group, INSA de Lyon, Villeurbanne, France

PS-01 (3), Lecture Theater 3, august 30, 2024, 14:00 - 16:00

Evolution of nanostructured thin films is closely related to their intrinsic small scale. Therefore, adapted characterization tools and techniques have to be developed, to highlight such relationships. The talk will focus on an advanced generation of surfaces: the thin film metallic glasses (TFMGs), obtained by magnetron sputtering. In this field, the Zr-Cu system does represent a model film, quite well-known at a meso/macro-scopic scale. In particular, its functional properties strongly depend on its crystallization dynamics, which is not clearly established, and needs to be better understood. The objective of the talk is then to demonstrate how specific research strategies involving, in particular, advanced TEM mode (in situ HT) were able to determine the evolution of the films' microstructural evolution.

Metallic glasses (MGs) have been intensively studied since the 60's, for their amorphous structure and associated properties. However, applications of MGs have stayed limited due to the fast quenching imposed to limit the crystallization process, and leading to small pieces of multicomponent materials. The condensation from the vapor phase to form a solid film in PVD process is another way to design metallic glasses. TFMGs indeed may show, for instance, particular interest in terms of physico-chemical and bactericide behaviors, coupled with an enhanced ductility [1]. Thermal stability of such amorphous metals nevertheless remains an issue. A non-conventional in situ technique, high-temperature scanning indentation (HTSI) [2], was first used to monitor the physical changes occurring in ZrCu-TFMGs during heat treatment. A complementary study was also done in parallel with the same film exposed to the same thermal conditions, at the TEM scale using specific heating chip equipped with the Wildfire sample-holder from Dens Solutions. This part will be developed within the framework of the talk. To correlate local transformation with a more global approach, all results acquired at the nanometer-scale were systematically compared with High-temperature XRD characterization, using the same thermal treatment. It was shown, for the first time, that crystallization initiates at ZrO2 nanoclusters as a transformation front, propagating throughout the film (Fig. 1). Acquired every 30 seconds, the front progression was measured, leading to thermodynamic and kinetic key-parameters as coefficients of diffusion. Behind the front, recrystallization results in the formation of bco- Zr7Cu10 intermetallics, identified by HRTEM. The transformation kinetics was also deduced from JMAK' modeling, giving rise to a well-documented new transformation mechanism [3].

From a quantitative point of view, really close crystallization kinetics were observed with our dual global-local approach, with close reaction rate (6.2·10-4 s-1 1 and 9.3·10-4 s-1, respectively) and Avrami exponents (1.9 and 2.2, respectively). Both measurements also give similar activation energies for crystallization (441 kJ.mol-1 and 445 kJ.mol-1, respectively). It suggests that crystallization mechanisms are the same for both investigated scales, despite the different sample configurations (micrometric thin film for XRD versus nanometric thin film for TEM).

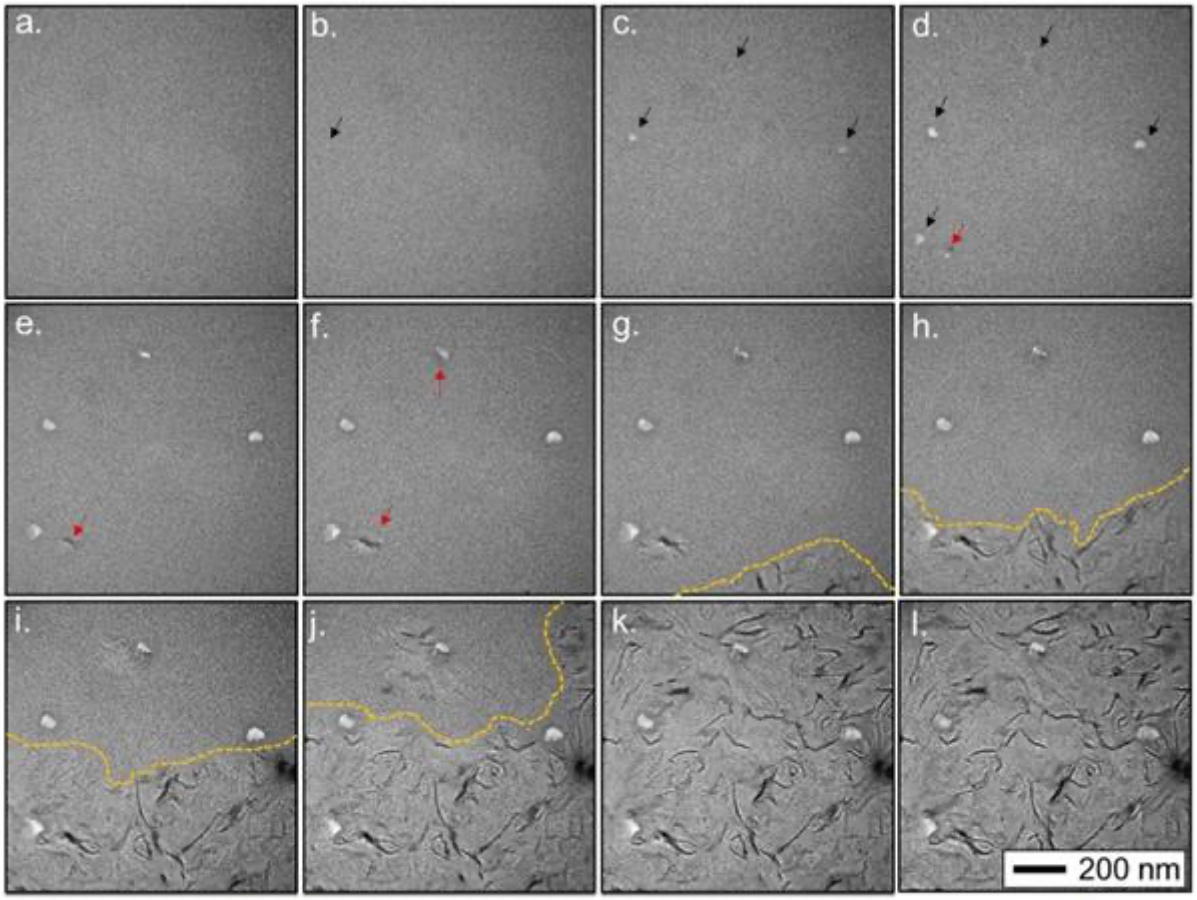

Fig. 4. TEM images of ZrCu-TFMG during 400°C heating at t = 0 min (a), t = 2 min (b), t = 9 min (c), t = 19 min (d), t = 29 min (e), t = 34 min (f), t = 39 min (g), t = 44 min (h), t = 47 min (i), t = 49 min (j), t = 54 min (k) and t = 60 min (l). The main crystallization front is highlighted in yellow. Full film in supporting information.

Keywords:

TEM, in-situ, recristallization, Metallic glass

Reference:

[1]: S. Comby-Dassonneville, T. Venot, A. Borroto, E. Longin, C. der Loughian, B. ter Ovanessian, M-A. Leroy, J-F. Pierson, P. Steyer, ZrCuAg Thin-Film Metallic Glasses: Toward Biostatic Durable Advanced Surfaces, ACS Applied Materials & Interfaces 2021 13 (14), 17062 doi:10.1021/acsami.1c01127
[2]: S. Comby-Dassonneville, G. Tiphéne, A. Borroto, G. Guillonneau, L. Roiban, G. Kermouche, J-F. Pierson, J-L. Loubet, P. Steyer, Real-time high-temperature scanning indentation: Probing physical changes in thin-film metallic glasses, Applied Materials Today 24 (2021) 101126 doi:10.1016/j.apmt.2021.101126
[3]: S. Comby-Dassonneville, L. Roiban, A. Borroto, A. Malchère, S. Cardinal, T. Douillard, C. Langlois, J-F. Pierson, J-M. Pelletier, P. Steyer, Better understand the crystallization dynamics of ZrCu TFMGs: Benefits of
combining global and local in situ approaches, Journal of Alloys and Compounds 987 (2024) 174233 doi:10.1016/j.jallcom.2024.174233

732

Correlating atomic-resolution structure to the properties of transition metal nitride coatings

Dr. Zaoli Zhang[1], Dr. Zhuo Chen[1], Mr. Yong Huang[1]
[1]Erich Schmid Institute, Austrian Academy of Sciences, Leoben, Austria

PS-01 (3), Lecture Theater 3, august 30, 2024, 14:00 - 16:00

Introduction
The industrial applications of transition metal nitrides require an in-depth understanding of the structures and their correlations to properties. This has led to numerous experimental and theoretical research [1-5]. Utilizing modern electron microscopy and spectroscopy, our understanding of nitride structure and property relations and its deformation has been significantly advanced. This presentation will briefly summarize our recent atomic-resolution studies on transition metal nitride coatings using spherical aberration-corrected transmission electron microscopy (TEM).
Methods
The film used in this study was prepared by direct current magnetron sputtering using a custom-made lab-scale magnetron sputter deposition system. The film was grown on MgO(001) or Si substrate at 700 ℃, and the potential was kept floating during the deposition. Specific deposition conditions for different films are slightly different. Nanoindentation tests were conducted on a KLA Nanoindenter G200 equipped with a diamond cube-corner indenter tip to obtain H and E by the conventional analysis first proposed by Oliver and Pharr. The tests applied the continuous stiffness measurement method with a constant indentation strain rate □ of 0.05 s−1. The cross-sectional TEM lamella of the as-deposited and indented films was machined by focused ion beam (FIB) using an FEI Helios NanoLab 660 workstation. The lamella was cut along the <110> direction of the substrate and then transferred to a Cu TEM grid. The lamella was polished using accelerating voltages from 30 to 2 kV and ion currents ranging from 20 nA to 7 pA. Some TEM specimens were also prepared using a standard approach, i.e., grinding, polishing, dimpling, and Ar ion-milling.
For high-resolution TEM (HRTEM) characterization, a JEOL 2100F and FEI Titan Themis 60-300 cubed TEM, both equipped with an image-side Cs-corrector, were adopted. The scanning TEM (STEM) images and energy-dispersive X-ray spectroscopy (EDXS) were acquired by a 300 kV field emission TEM (JEOL ARM300F) equipped with double Cs-correctors. The microscope has two windowless detectors, each with an active area of 100 mm2.
Results
The extensive high-resolution transmission electron microscopy (HRTEM) observations on TaN/TiN multilayer reveal that the dissociation of full dislocations results in the network of stacking faults (SFs) and the formation of Lomer-Cottrell lock arrays inside the TaN layer. Consequently, the high density of stacking faults dramatically strengthens the TaN/TiN multilayer [1]. Using valence electrons and inner shell electron spectroscopy, a combined experimental analysis on a multilayered structure of CrN/AlN allowed mapping of the multilayer's mechanical properties (bulk modulus) at the nanometer scale [2]. Moreover, we found that the presence of oxygen impurities causes a remarkable reduction of the bulk modulus of rs-CrN while having no significant effect on the bulk modulus of the stable wurtzite structure wz-AlN layers. The findings have been validated by theoretical calculations [2].
We observed an atomic-scale intermixing phenomenon in the nanoscale TiN/AlN multilayer by coupling the cross-sectional FIB cutting with detailed atomic resolution electron microscopy analyses. A new solid solution phase was created during nanoindentation, which could be unambiguously shown by mapping the electronic structure differences (i.e., using Ti-L2,3 edge). This also raises some concerns about understanding experimentally measured hardness values in multilayers using the nanoindentation method. By using atomic-resolution energy dispersive x-ray spectroscopy, we

further corroborated that such a homogenous solid solution zone formed upon loads [3]. We recently found a new deformation mechanism of a high vacancy-mediated WNx/TiN multilayer through quantitative electron microscopy analysis, theoretical calculations enabled by ab initio molecular dynamics, and combined with mechanical testing [5].

Conclusions

Advanced electron microscopy methods reveal the atomic and electronic structures of transition metal nitride coatings, which allows correlating the structure with properties at the atomic scale and leads to new findings. These exciting findings shed light on the design of novel multilayer coatings for applications.

Keywords:

Nitride, HRTEM/STEM, EELS, deformation

Reference:

[1] Yong Huang et al., Acta Materialia 255 (2023) 119027
[2] Zaoli Zhang et al., Acta Materialia, 194(2020) 343
[3] Zhuo Chen et al., Acta Materialia, 214(2021)117004.
[4] Zaoli Zhang et al., Materials & Design, 207(2021)109844.
[5] Zhuo Chen et al., Nature Communications, (2023)

Acknowledgment: This work is financially supported by the Austrian Science Fund (FWF P33696-N). The authors would thank Prof. Christian Mitterer, David Holec (Montanuniversität Leoben), and Paul Heinz Mayrhofer (Technische Universitaet Wien) for delivering the samples, performing DFT calculations and for very fruitful discussions.

960

Carbon nanoribbon formation by in-situ TEM manipulation of a C59N dithiolane derivative encapsulated into SWNTs

Dr Mario Pelaez-Fernandez[1,2,3], Dr Anastasios Stergiou[4], Dr Nikos Tagmatarchis[4], Dr Chris Ewels[5], Dr Raul Arenal[1,2,6]
[1]Instituto de Nanociencia y Materiales Aragón, CSIC-U. Zaragoza, Zaragoza, Spain, [2]Laboratorio de Microscopías Avanzadas, Universidad de Zaragoza, Zaragoza, Spain, [3]Unité Matériaux et Transformations (UMET UMR 8207), Univ Lille, Villeneuve d'Ascq, France, [4]Theoretical and Physical Chemistry Institute, National Hellenic Research Foundation, Athens, Greece, [5]Institut de Matériaux de Nantes Jean Rouxel, CNRS – Université de Nantes, , France, [6]ARAID Foundation, Zaragoza, Spain
PS-01 (3), Lecture Theater 3, august 30, 2024, 14:00 - 16:00

Background
The synthesis of new kinds of functionalized carbon nanostructures continues to attract a growing amount of interest within solid-state physics research, due to the wide range of potential applications that it can yield [1]. Within this field, electron irradiation within an electron microscope is a great tool for in-situ studies on these structures, being able to characterize their formation and the changes they can undergo as they are happening at the nanoscale [2].
Within the subject of carbon nanostructures, single-wall carbon nanotubes (SWCNTs) have been a cornerstone in the field, not only as a malleable material but also as a medium for the fabrication of other materials. Within this new realm of materials, carbon 'peapods' (fullerenes and fullerene-based molecules encapsulated inside of single-walled nanotubes [3]) continue to increase interest regarding the controlled formation of nanostructures. A good case of this nanostructure formation is graphene nanoribbons (GNRs) templated by encapsulated functionalized fullerenes, which form the nanoribbons upon heating or beam irradiation [4]. Additionally, doping has been one of the main preferred methods for carbon nanostructure modification, with carbon being a relatively easy-to-dope material, improving the electrical properties of 1D carbon nanomaterials.
In this sense, functionalized C59N using a dithiolane (DT) moiety containing sulfur and oxygen [5] is a very promising material that may give rise to the creation of fine GNRs within SWNTs under beam irradiation, passivated with a combination of S, O, H and maybe N, possibly with some form of doping within their structure. To study these GNRs, previous in-situ studies on similar, non-doped samples offer micrographs before and after the GNR has been formed, but no intermediate states.
This study aims to get a fuller picture of the formation of GNR by acquiring micrographs not just before and after, but throughout the whole GNR formation process, and to delve into the structure these GNRs have.

Methods
In this work, these derivatives (C59N-DT) have been introduced into SWNTs and irradiated in situ within a TEM while acquiring high-resolution TEM videos at 80 kV, to have enough control over the dose to be able to modify the C59N-DT@SWCNTs when the beam was focused while having enough control over it not to damage the sample before the in situ studies.
Additionally, to discern the edge passivation on these nanoribbons, DFT calculations have been performed to discern the energetic viability of different GNR edges, modifying the geometry of the carbon edge, the different elements passivating it, and their relative concentration. The formation enthalpy of each edge configuration has been estimated as a way to discern which are the most energetically favorable structures and, in turn, which ones are the least likely to prevail in these samples.

Results

Figure 1 shows the functionalized fullerene used for these studies (top left), an image series detailing the formation process of the nanoribbon (top right), and a formation enthalpy comparison for different mixed passivating edges (bottom).
The results of these TEM image series, as well as micrograph integrations from crucial moments in the in-situ study, point out to the formation of a first intermediate structure with the C59N-DT starting to fuse to each other and, later on, passivated, sometimes twisted GNRs.
Likewise, preliminary calculations seem to show that stoichiometrically favorable configurations, such as S-O co-passivated edges, as well as O-passivated edges are more thermodynamically stable than previously proposed S-passivated edges [3].

Conclusion
These results point to a successful way to obtain GNRs from a doped C59N-DT and show their formation in situ. DFT calculations show that the edges of these GNRs are probably made of S-O co-passivated edges.

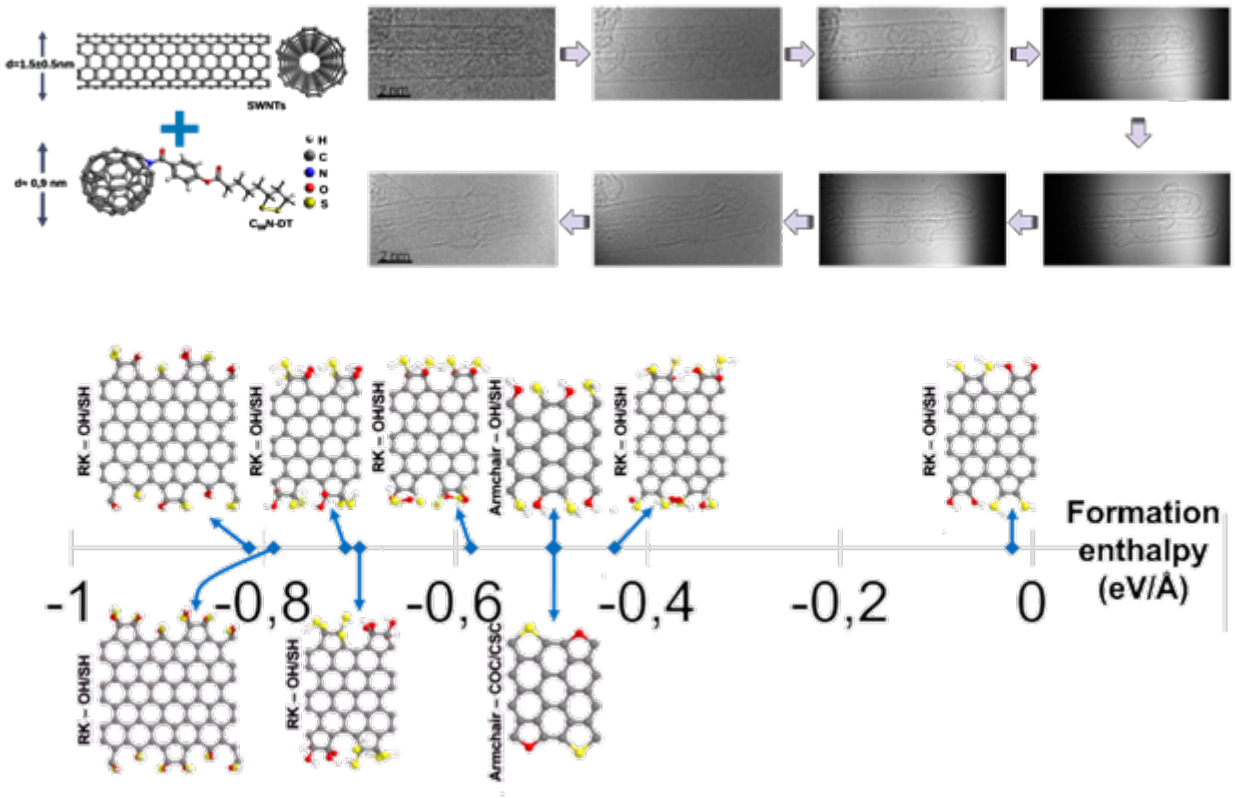

Keywords:

Graphene nanoribbons, in-situ TEM, DFT

Reference:

[1] Celis A et al. J. Phys. D. Appl. Phys. 49(14):143001, 2016
[2] Arenal, R. and Lopez-Bezanilla, ACS Nano 2014.
[3] Smith, B. W. et al, Nature 1998, 396, 323-324
[4] Chuvilin, A. et al, Nature Materials 2011, 10, 687-692.
[5] G. Rotas and N. Tagmatarchis, Chem. Eur. J. 2016, 22, 1206 – 1214

1114

Structural characterization of single wall carbon nanotubes via AI assisted transmission electron microscopy

Dr. Antonin Louiset[1], Dr Daniel FÖRSTER[2], Ms. Eira MEDINA[3], Mr. Saïd TAHIR[3], Dr. Vincent JOURDAIN[3], Dr. Christophe BICHARA[4], Dr. Hanako OKUNO[1]
[1]IRIG-MEM, CEA, Université Grenoble Alpes, Grenoble, France, [2]Laboratoire d'Etude des Microstructures, ONERA-CNRS, Université Paris-Saclay, Châtillon, France, [3]Laboratoire Charles Coulomb, CNRS, Université de Montpellier, Montpellier, France, [4]CINaM, CNRS, Université Aix-Marseille, Marseille, France

PS-01 (3), Lecture Theater 3, august 30, 2024, 14:00 - 16:00

Correlating single wall carbon nanotubes (SWCNT) structural properties with growth conditions during catalytic chemical vapor deposition (C-CVD) is the key to understand the fundamental mechanism involved during this process. However, characterization of individual SWCNTs has always been a challenge, especially under real growth conditions. Recently, homodyne polarization microscopy was able to perform in-situ observations of SWCNT growth inside a CVD reactor [1]. While this technique provides high-throughput growth kinetic measurements, it is still unable to determine the atomic configuration, i.e. chirality, of each individual tube. On the other hand, transmission electron microscopy (TEM) is the technique of choice to directly image SWCNT at the atomic scale and therefore unambiguously determine their chirality [2]. Combining both characterization on the same tubes would reveal significant information about the growth mechanism of CNT. However, TEM sample preparation often relies on random CNT dispersion onto a TEM grid preventing any individual tube identification inside the microscope. In addition, manually determine the chirality for each tube from high-resolution (HR) TEM images is a long process limiting the analysis to a small number of tubes. Here, we aim to develop a new sample preparation protocol to transfer SWCNTs from a substrate to a TEM grid while preserving their location and allowing high quality atomic scale imaging. Furthermore, our goal is also to speed up chirality determination using artificial intelligence (AI) based image analysis.

First, SWCNTs were grown on a quartz substrate inside a custom CVD reactor allowing in-situ optical microscopy imaging. After growth, Au markers were deposited by optical lithography and scanning electron microscopy of the sample was performed to locate tube positions relative to the markers. Before transferring SWCNTs onto a TEM grid, the latter was covered with a graphene monolayer using the PMMA-mediated graphene-transfer method [3]. This layer acts as a mechanical support, preventing tube breaking above grid holes, and facilitating charge evacuation during TEM imaging. Then both SWCNTs and Au markers were transferred onto the graphene coated TEM grid using a similar wet transfer method. Atomic scale images of SWCNT on graphene were then obtained using an aberration corrected TEM equipped with a field emission gun and a monochromator. Finally, fast chirality determination was performed using an open source deep learning code based on convolutional neural networks [4]. This AI code is intended to analyze only SWCNT images; hence, the graphene layer signal must be removed. We developed a new filtering method called Geometric Amplitude and Phase Interpolation (GAPI) based on Fourier transform (FT) filtering that allows us to subtract the graphene signal even when it is superimposed over the SWCNT signal in both real and reciprocal space.

SWCNTs were successfully transferred with the Au markers on the custom TEM grid coated with graphene. Nanotubes, previously observed by in-situ techniques were imaged at high resolution inside the TEM. Both AI and manual methods were used to determine the chirality of the tubes of interest. The strong agreement between the chiral indices measured by both methods highlighted

the efficiency of the AI algorithm. In comparison to other FT-based methods, the GAPI filtering method significantly improved AI chirality determination. Our protocol offers the possibility to track down defects and eventual chirality changes induced during growth. However, residual polymer contamination from the transfer processes prevented the analysis of all tubes across their entire length. Nevertheless, we were able to follow single chirality tubes across 10s of µm, providing a direct correlation between their structure and previously measured growth kinetic.

For the first time, the same individual SWCNTs were characterized by both in-situ optical and ex-situ HRTEM observations. The combination of a new image filtering method with automated atomic structure determination using AI, enabled a fast and unambiguous determination of their chirality providing a direct correlation between growth kinetics and tube structures. While the TEM characterization is still limited by polymer contamination, tubes chirality could still be measured in different areas, tens of µm apart.

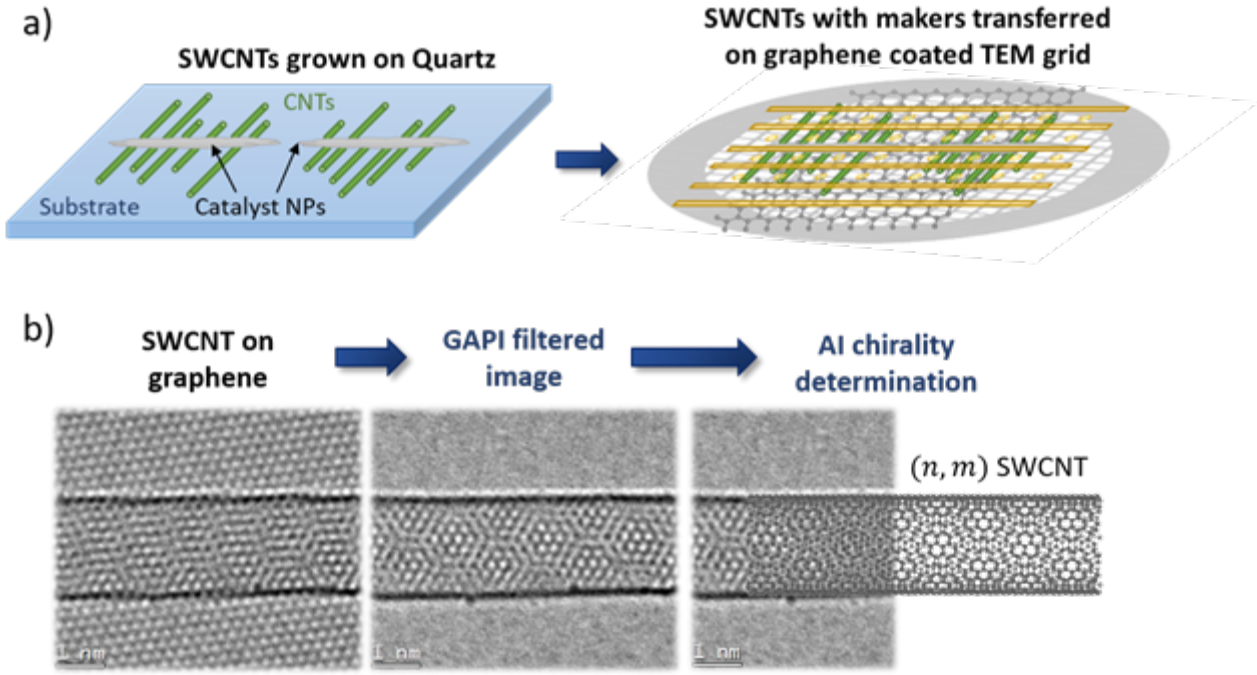

Keywords:

Carbon nanotubes, HRTEM, artificial intelligence.

Reference:

[1] Pimonov, Vladimir, et al. "Dynamic instability of individual carbon nanotube growth revealed by in situ homodyne polarization microscopy." Nano letters 21.19 (2021): 8495-8502.
[2] Yu, Yue, et al. "Determine the Complete Configuration of Single-Walled Carbon Nanotubes by One Photograph of Transmission Electron Microscopy." Advanced Science 10.15 (2023): 2206403.
[3] Li, Xuesong, et al. "Transfer of large-area graphene films for high-performance transparent conductive electrodes." Nano letters 9.12 (2009): 4359-4363.
[4] Förster, Georg Daniel, et al. "A deep learning approach for determining the chiral indices of carbon nanotubes from high-resolution transmission electron microscopy images." Carbon 169 (2020): 465-474.

3

Nanotubes and Nanostructures of VS_2, WS_2, and MoS_2: Structural Effects on the Hydrogen Evolution Reaction

Maya Bar Sadan[1]
[1]Ben-Gurion University of the Negev, Department of Chemistry, Beer Sheva, Israel

Poster Group 2

Background

Vanadium disulfide (VS_2) emerges as a remarkable functional material, boasting myriad advantages that have propelled its widespread application across various industrial sectors. Its unique electronic and optical properties render it highly desirable for utilization in electronics, optoelectronics, and catalysis. Despite these advantages, the synthesis of VS_2 in specific morphologies, particularly as nanotubes, remains a significant challenge. The complexities associated with preparing various VS_2 nanostructures stem from the intricate control required over reaction conditions, precursor selection, and the delicate balance between promoting specific morphologies and preventing unintended structural transformations. This study aims to overcome these challenges in nanotube synthesis and unlock the full potential of VS_2 in cutting-edge technologies, promising advancements in diverse fields.

Methods

This study describes the preparation of novel VS_2 nanotubes with a unique structure, offering a comparative analysis with benchmark 2D materials MoS_2 and VS_2. The unique VS_2 morphology was explored through electron tomography and compared with VS_2 nanoflowers. Catalytic activity of the various nanotubes and nanoflowers was measured, complemented by a Density Functional Theory (DFT) study to attain a fundamental understanding of the catalytic activity's origin in the materials system. Highly crystalline WS_2 nanotubes and nanotriangles, MoS_2 nanoflowers, and defect-rich MoS_2 nanotubes were synthesized and thoroughly studied for their Hydrogen Evolution Reaction (HER) activity. The synthesis of VS_2 nanostructures depended on the solvent and vanadium precursor, resulting in nanotubes and nanoflowers.

Results

Characterization techniques, including TEM, SEM, powder X-ray diffraction (XRD), and X-ray photoelectron spectroscopy (XPS), confirmed the structures' crystallinity and composition. Electron tomography provided 3D insights into the VS_2 nanoflower and nanotube structures. Electrochemical performance, evaluated through linear sweep voltammetry (LSV) and Tafel analysis, demonstrated that MoS_2 outperformed WS_2 and VS_2, maintaining the catalytic activity order in both acidic and alkaline conditions. Electrochemical impedance spectroscopy (EIS) was employed to evaluate charge transfer resistance (Rct), with MoS_2 nanostructures displaying the smallest Rct. Surface area analysis indicated that MoS_2 nanotubes had the highest electrochemically active surface area (ECSA), attributed to strain and defect-rich surfaces. DFT calculations provided insights into the thermodynamic stability of nanotubes and nanoribbons, with VS_2 nanotubes exhibiting a lower energy of bending than MoS_2 and WS_2. Additionally, DFT calculations on hydrogen adsorption free energy (ΔGH) suggested that VS_2 basal planes have potential catalytic activity, contrary to experimental observations.

Conclusions

In summary, this study presents a comprehensive investigation of various transition metal dichalcogenides (TMD) nanostructures for HER activity. MoS_2 demonstrated superior performance, and despite its metallic-like nature, VS_2 exhibited lower activity. The combination of experimental

and theoretical approaches sheds light on the factors influencing TMD catalysis, emphasizing the importance of morphology, defects, and strain in designing efficient electrocatalysts.

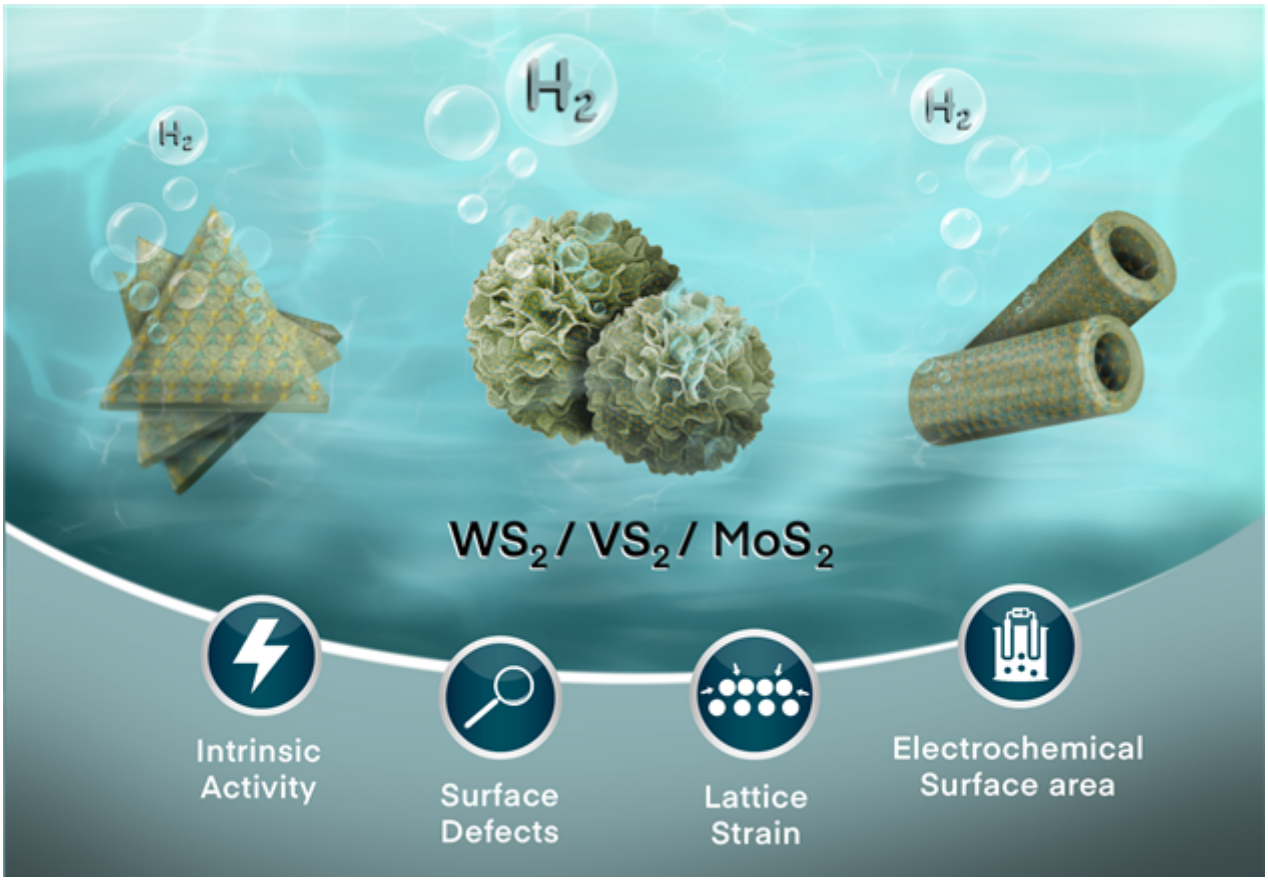

Keywords:

2D, Electrochemistry, Electron Tomography, nanotubes

41

Thermoelectric structure-property relationship establishment in TlGaSe2

Mr Tigran Simonian[1,2], Dr. Ahin Roy[1,2], Dr. Akash Bajaj[3], Dr. Rui Dong[3], Prof. Zdenek Sofer[4], Prof. Stefano Sanvito[3], Prof. Valeria Nicolosi[1,2]
[1]Advanced Microscopy Lab, Trinity College Dublin, Dublin, Ireland, [2]School of Chemistry, Trinity College Dublin, Dublin, Ireland, [3]School of Physics, Trinity College Dublin, Dublin, Ireland, [4]Department of Inorganic Chemistry, University of Chemistry and Technology Prague, Prague, Czech Republic

Poster Group 2

Background incl. aims
When devices, such as transistors, are under electrical load, the resistivity of the device often leads to unwanted heat generation. In many cases, this reduces the efficiency of the device and hence is detrimental both economically and environmentally due to excessive energy consumption. However, as devices approach the atomic scale, this wasted heat generation can lead to device failure. To overcome this, materials which have excellent electrical conductivity, but poor thermal conductivity are being investigated for their potential use in devices.
One such thermoelectric material which has potential use in optoelectronics is the layered ternary chalcogenide semiconductor $TlGaSe_2$. It has been shown to have a thermoelectric figure of merit, ZT, of approximately 0.8 [1], comparable with other heavily studied thermoelectric materials such as Bi_2Te_3 [2]. However, the material's layered nature means it is prone to stacking faults, which are often assumed to affect this value [1, 3], but to date, this has yet to be established. This is critical to understand if the material is to be used in future devices, such as near-IR sensors.
Methods
In this work, $TlGaSe_2$ is characterised via (scanning) transmission electron microscopy (STEM) and density functional theory (DFT) simulations. Streaking in selected area electron diffraction (SAED) patterns are correlated to simulations which indicate the presence of stacking faults in the growth direction [4].
Results
High resolution STEM confirms these stacking faults and indicates a lack of long-range order to the stacking. DFT calculations reveals a high preference for the system to include these faults. Electron transport simulations for structure in both stacking orders show a significant enhancement of thermoelectric power along the stacking direction when stacking faults are induced. These are further enhanced if the material is doped sufficiently. Phonon dispersion calculations show a suppression of several phonons modes when stacking faults are induced, indicating a suppression of thermal conductivity.
Conclusions
Stacking faults in $TlGaSe_2$ are shown to be prevalent throughout the material and they enhance its excellent thermoelectric properties.

Keywords:

thermoelectric, stacking faults, DFT, STEM

Reference:

[1] M. Çaydaşı, et al., Phys. status solidi, 259, 1, 2100409, 2022.
[2] J. Wei et al., J. Mater. Sci., 55, 27, 12642-12704, 2020.
[3] A. Cengiz, et al., Semicond. Sci. Technol., 33, 7, 2018.
[4] D. F. McMorrow, et al., J. Phys. Condens. Matter, 2, 16, 3699–3712, 1990.

76

In-Situ TEM assessment of phase transformation in VO2-based thin films with Ho addition

Ellen Suhr[1], Dr. Aleksander Kostka[2], Prof. Dr.-Ing. Alfred Ludwig[1]
[1]Institute for Materials, Ruhr University Bochum (RUB), , Bochum, Germany, [2]ZGH, Ruhr University Bochum (RUB), , Bochum, Germany

Poster Group 2

Background incl. aims
We present the fabrication and characterization of VO2-based thin films with Ho addition. The thin films were prepared as so-called materials libraries by reactive co-sputtering from two targets (V, Ho) to achieve a composition gradient. The effect of Ho on the phase transformation and its functional properties, like the thermochromic effect, has not been studied yet, and the materials libraries enable a screening of a large composition spread in relatively short time. The materials libraries were characterized in a high-throughput approach regarding their chemical composition, crystallinity, and electrical resistance at different temperatures to study the phase transformation. TEM investigations were carried out on two types of samples, both selected from specific composition region of the materials library: (i) focused ion beam (FIB) prepared TEM lamella, for analysis of the present Ho-rich precipitates, and (ii) sputtered on SiN Wildfire (DENSsolution) chips for in-situ TEM heating experiments to assess the phase transformation – to avoid Ga-ion contamination and its effects on the phase transformation.[1]
Methods
The thin films were prepared by reactive co-sputtering on 4-inch Si wafer and the Wildfire chips from two targets: V and Ho2O3. The positioning of the targets results in two gradients across the thin film library (see Figure 1) the composition gradient along the diagonal from lower right to upper left with decreasing Ho-content, and a thickness gradient along the other diagonal. The substrates were heated to 500 °C and the oxygen flow was controlled using plasma emission monitoring.[2] The thin film thickness was controlled by the deposition time: 30 min (approx. 150 to 350 nm) for the materials library on Si (SEM, EDS, XRD, resistance measurements) and 5 min for the depositions on the Wildfire chips (approx. 40 nm).
Results
The materials library was first characterized regarding its chemical composition (EDS), crystallinity (XRD, Figure 2) and electrical resistance (in the range of 20 to 120 °C, Figure 4) getting the first overview of the thin films properties using high-throughput automated measurements.[3]
The preliminary investigations of the library suggested a single-phase solid solution with a monoclinic VO2 phase. The temperature-dependent resistance measurements reveal a slight shift of the transformation temperature towards lower temperatures with increasing Ho content (Figure 4).
TEM analysis of the selected composition region revealed the presence of small Ho-rich precipitates and larger VO2 crystals. The in-situ heating experiments showed that the phase transformation starts at 54 °C and it is completed at about 60 °C. The transformation is well visible in the electron diffraction but does not result in microstructural changes; grain size and morphology remain unchanged.
Future work shall focus on the investigation of the thin films functional properties and their possible applications in nanoactuators or in thermochromic coatings for windows.

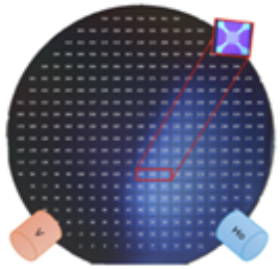

Figure 1: Deposition set-up showing the target positions during fabrication of the materials library. The tiny numbers are showing the measurement areas for the high throughput measurements (EDS, XRD, electrical resistance measurements). Marked in red are the areas, where the Wildfire chips were placed for deposition.

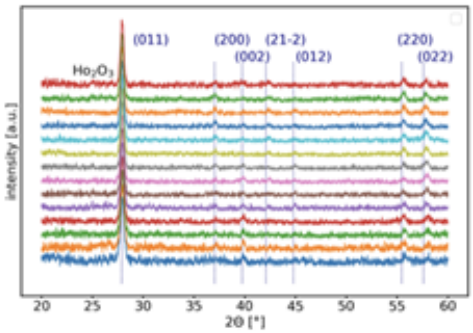

Figure 2: XRD results along the diagonal from the Ho-rich side to the other side of the library. All peaks could be indicated using only a VO_2 powder pattern as reference.

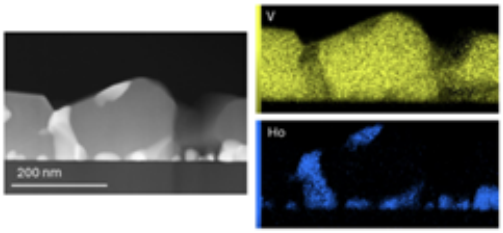

Figure 3: TEM analysis from a more Ho-rich area. ADF STEM image above and V- and Ho-maps below. TEM images resolved that Ho-rich precipitates are formed. The latter is pure monoclinic VO_2.

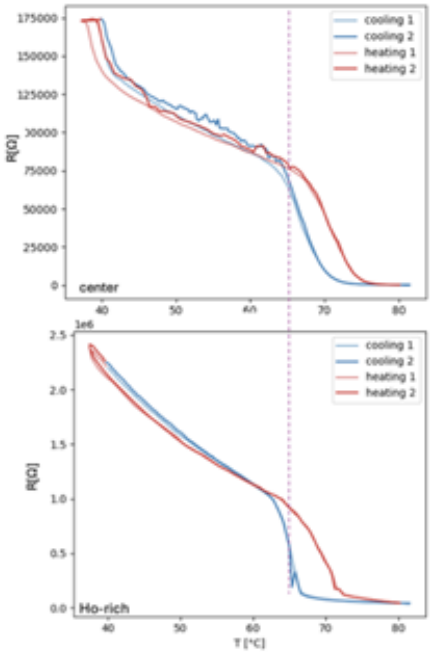

Figure 4: Temperature dependent electrical resistance measurements on different locations of the library. It is evident that VO_2 transforms, and the transformation temperature decreases with increasing Ho-content.

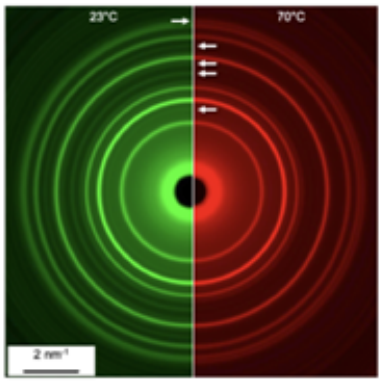

Figure 5: Results of In-situ heating TEM experiments. The TEM image on the left shows no change morphology, only a slight shift in contrast, which is related to thermal drift and focus change. On the right side the electron diffraction as rotational averaged pattern. Changes are marked with arrows.

Keywords:

In-situ TEM, vanadium-dioxide, high-throughput characterisation

Reference:

[1] W. Brückner et al., Phys. Stat. Sol. (a) 42, 295 (1977)
[2] X. Wang, E. Suhr et al., ACS Appl. Electron. Mater. 2, 1176 (2020)
[3] R. Zarnetta et al., Adv. Funct. Mater. 20, 1917 (2010)

270

Fe/Pt spintronic bilayers: Tailoring structure for enhanced THz emission

Dr. Isaak Vasileiadis[1], Dr. Laura Scheuer[2], Dr. Dimitrios Karfaridis[1], Professor George Dimitrakopulos[1], Dr. Evangelos Papaioannou[1,3], Thomas Kehagias[1]
[1]School of Physics, Aristotle University of Thessaloniki, Thessaloniki, Greece, [2]Department of Physics, Technical University of Kaiserslautern, Kaiserslautern, Germany, [3]Institute of Physics, Martin Luther University Halle-Wittenberg, Halle, Germany

Poster Group 2

Background incl. aims
Driven by potential applications in spintronics, layered ferromagnetic/non-magnetic (FM/NM) nanostructures have attracted significant interest, particularly due to efficient spin transport across epitaxial interfaces in Fe/Pt bilayers [1,2]. This renders Fe/Pt bilayers as a promising candidate material system for THz spintronic devices [3]. However, the crucial role of interface quality in these bilayers cannot be disregarded, as it significantly affects spin current transmission. Optimization of the FM/NM interfacial structure and defect density is thus a potential approach for manipulating the performance of spintronic THz emitters [4]. Here, we explore this concept by investigating structural modifications of the Fe/Pt interface, obtained by tuning growth and annealing temperatures of the bilayers. The structural properties of the resulting configurations with modified interfaces were then characterized to establish a correlation between interfacial features and the emitted THz signal.
Methods
Fe/Pt bilayers with a nominal thickness of Fe(12nm)/Pt(6nm) were deposited on MgO(100) substrates using electron beam evaporation. To maintain a constant total thickness across all samples, only the Pt layer's growth temperature was varied, to induce modifications in the Fe/Pt interface. At first, a 12 nm thick Fe film was deposited on the MgO substrate at 300°C, followed by annealing at the same temperature for 30 minutes, in all samples. Subsequently, 6 nm of Pt were deposited on top of the Fe layer at various growth temperatures, namely 300°C, 450°C and 600°C. After Pt layer deposition, an annealing process similar to the Fe layer was performed at the corresponding growth temperature of each sample. The terahertz (THz) emission properties of the resulting heterostructures were characterized using a standard THz time-domain spectrometer (THz-TDS). Initial structural investigations were conducted using X-ray diffraction (XRD). Nanoscale structural and chemical analysis was then performed using a combination of transmission and scanning transmission electron microscopy (TEM/STEM), energy-dispersive X-ray spectroscopy (EDXS), high-resolution TEM (HRTEM), and Z-contrast high-resolution STEM (HRSTEM) imaging, along with Z-contrast HRSTEM image simulations.
Results
The largest THz emission, nearly double the amplitude observed for the Fe/Pt(300°C) sample, originated from the Fe/Pt(450°C) sample, while the Fe/Pt(600°C) sample displayed negligible signal [5]. XRD analysis revealed an almost strain-free Fe/Pt configuration for the 300°C sample. In contrast, the presence of an additional $L1_0$-FePt peak in the 450°C sample suggested interfacial modifications. Furthermore, the disappearance of Fe and Pt peaks and the emergence of new peaks corresponding to the face-centered-tetragonal (fct) lattice of $L1_0$-FePt in the 600°C sample, suggested a complete transformation of the bilayer into the ordered alloy.
TEM observations confirmed distinct Fe and Pt layers with nominal thicknesses for the 300°C sample, exhibiting epitaxial growth on the MgO(100) substrate following the Bain orientation. In the 450°C sample, HRTEM analysis revealed the formation of a 2 nm thick interlayer (IL) at the Fe/Pt interface (graphic). This IL displayed a characteristic periodic intensity modulation, indicative of a superlattice structure with high chemical ordering. Further HRTEM imaging confirmed the IL's tetragonal symmetry and identified the ordered $L1_0$-FePt structure. Moreover, the interplanar spacings of

resolved lattice planes in MgO/Pt and Fe nearly matched the corresponding values of their bulk structures, implying a strain-free configuration and an epitaxial growth of the IL on the Fe layer. Z-contrast HRSTEM observations and simulations confirmed the IL's chemical ordering, with the observed intensity modulation matching a periodic arrangement of single-element Fe and Pt atomic layers in the $L1_o$-FePt structure. STEM-EDXS analysis further corroborated this, revealing interdiffusion of Fe and Pt elements confined solely at the Fe/Pt interface. For the 600°C sample, TEM observations showed complete interdiffusion and merging of the Fe/Pt layers into a single layer comprising large grains slightly misoriented to each other. The latter finding can be attributed to the presence of uneven atomic size steps and terraces on the MgO surface. HRTEM imaging revealed a periodic intensity modulation along the growth axis, indicating the formation of a chemically ordered FexPt(1-x) alloy throughout the entire layer. STEM-EDXS analysis confirmed Fe and Pt intermixing across the entire FexPt(1-x) layer, with the Pt composition decreasing from the top of the film towards the MgO/FePt interface. Notably, the $L1_o$ structure with fct symmetry was preserved regardless of the non-uniform stoichiometry.

In summary, the significantly enhanced THz emission concurred with the modified Fe/$L1_o$-FePt(2nm)/Pt interface in the Fe/Pt(450°C) sample compared to the Fe/Pt(300°C) bilayer. Conversely, the absence of the non-magnetic Pt capping layer at the Fe/Pt(600°C) sample, and despite the $L1_o$ ordered alloy formation, resulted in the suppression of the THz signal.

Conclusion

The interplay between Pt growth temperature, structural features, and THz emission in Fe/Pt spintronic bilayers on MgO substrates was investigated. High-quality Fe/Pt bilayers were achieved at 300°C. Distinct structural modifications were observed at elevated Pt growth and subsequent annealing temperatures, which were used to engineer the Fe/Pt interface, namely a 2 nm thick $L1_o$-FePt IL formed at 450°C, while a fully intermixed FexPt(1-x) alloy with ordered fct structure and alternating pure Fe and Pt-rich atomic layers superseded the individual Fe and Pt layers at 600°C. The presence of the ordered IL in the Fe/Pt(450°C) sample significantly enhanced THz emission by facilitating interface transmission. Conversely, complete intermixing and the absence of the non-magnetic Pt capping layer in the Fe/Pt(600°C) sample suppressed the THz signal. The observed enhancement in the Fe/$L1_o$-FePt/Pt trilayer configuration opens exciting possibilities for spintronic THz emitters. Furthermore, the ability to control (FM/NM) interface properties through engineered interlayers offers significant flexibility for designing future spintronic devices.

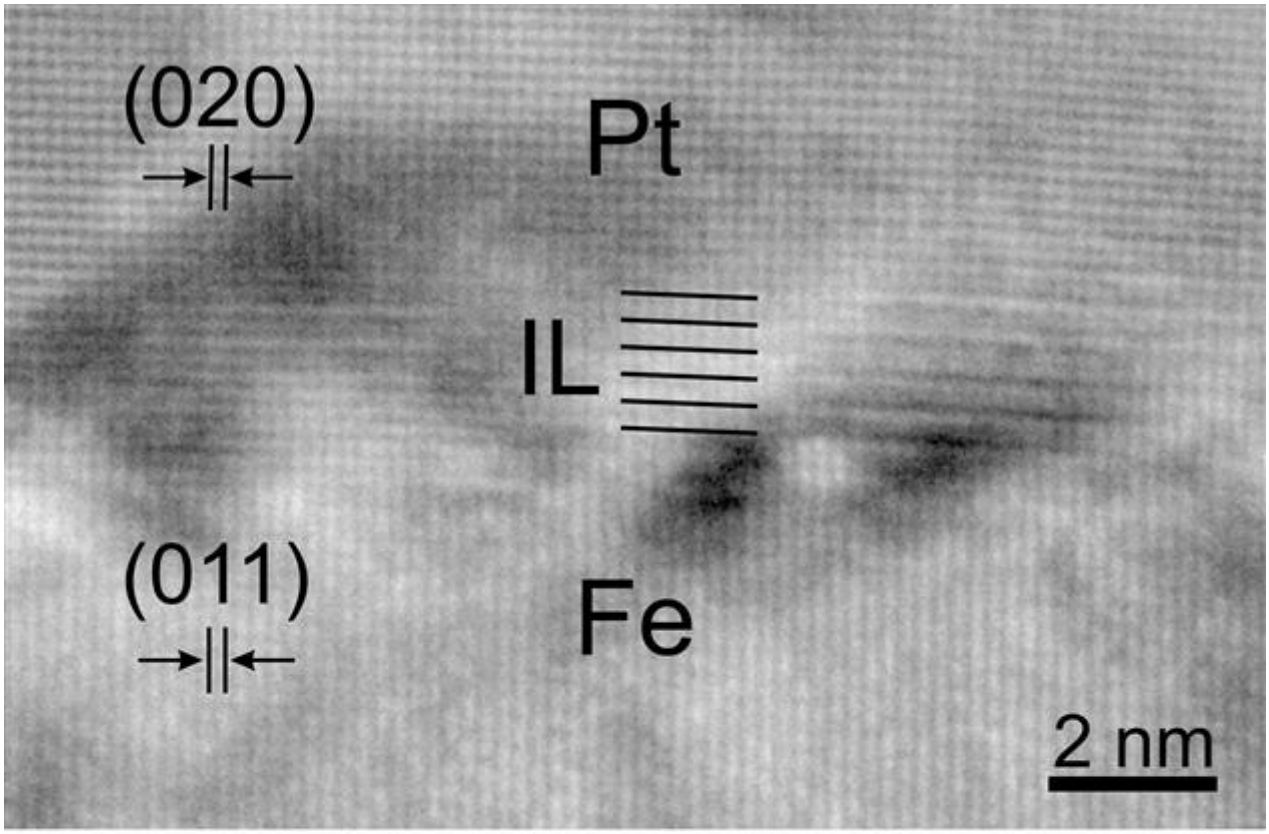

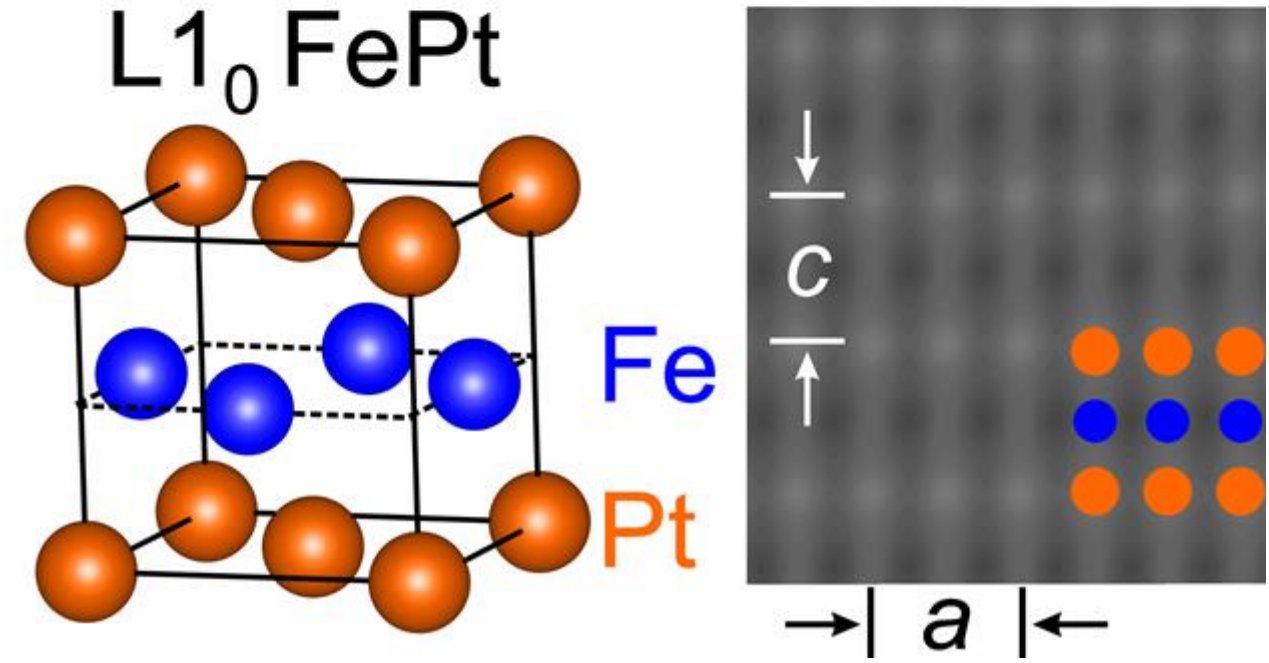

Keywords:

Fe-Pt heteroepitaxy, TEM-STEM-EDXS, $L1_o$-ordering, THz-emission

Reference:

[1] A. Conca et al., Phys. Rev. B 93, 134405 (2016).
[2] L. Mihalceanu et al., Appl. Phys. Lett. 110, 252406 (2017)
[3] E. T. Papaioannou et al., Nanophotonics 10, 1243 (2021).
[4] D. M. Nenno et al., Sci. Rep. 9, 13348 (2019).
[5] L. Scheuer et al., iScience 25,104319 (2022).

278

TEM Investigations of Multi-Layer Selective Absorber thin films for concentrated solar plant: structure and composition

Nicolas Gautier[1], Dr Florian Chabanais[1], Dr Mireille Richard-Plouet[1], Dr Aissatou Diop[2,3], Dr Béatrice Plujat[2,3], Dr Angélique Bousquet[4], Dr Audrey Soum-Glaude[2], Pr Éric Tomasella[2,3], Pr Laurent Thomas[2,3], Pr Antoine Goullet[1]
[1]Nantes Université, CNRS, Institut des Matériaux de Nantes Jean Rouxel, IMN, Nantes, France, [2]PROMES-CNRS UPR 8521 (Laboratory of PROcesses, Materials, Solar Energy), Font-Romeu, France, [3]Université de Perpignan, Perpignan, France, [4]Université Clermont Auvergne, CNRS, SIGMA Clermont, ICCF, Aubière, France

Poster Group 2

Background and Method
The solar energy resource is still relatively under-exploited although it could cover most of our energy needs. Beyond the development of photovoltaics, there is a worldwide challenge to deploy large-scale concentrated solar thermal power plants. To address this issue, materials with high absorption in the visible range, low emissivity and good temperature resistance are required. To this end, multi-layered optical thin films produced by plasma processes are developed in the NANOPLAST project (nanoplast-project.cnrs.fr, ANR-19-CE08-0019). The stack encompasses an anti-reflective top-layer based on tantalum oxide or oxynitride, a selective absorber in the W-Si-C ternary system and a tungsten Infra-red reflective layer, denoted [Ta-O-N]/[W-Si-C]/[W]. These films are deposited by plasma-assisted technique: first Direct Current sputtering from a W target for the IR reflector, second dual reactive magnetron sputtering and Plasma Enhanced Chemical Vapour deposition, from a W target combined with different amounts (5% to 28%) of TMS-Si(CH3)4 diluted in Ar and finally reactive magnetron sputtering by adjusting O2 and N2 for Ta-O-N top layer[1].

Results
TEM characterisations were carried out to get insight into the structure and composition of the absorber, the anti-reflective top films and then the annealing of the complete system. Particular attention was paid to the influence of sample preparation. FIB (Focused Ion Beam) and ultramicrotomy were carried to get insight in the homogeneity along the growth direction of the multi-layer. In this work, we want to highlight the complementarity of both sample preparations for TEM. Actually if FIB is now well-established and allows to precisely select the region to be analysed, in the present case due to the non-equilibrium deposition conditions, FIB could also induce artefacts due to differential sputtering and/or re-deposition of elements (such as Ga) that may lead to misinterpretations. Hence by observing cross-sections prepared by ultramicrotomy, we were able to dismiss possible impacts of FIB on the observations thanks to the adhesion of the whole stack. Therefore, for the absorber, depending on the tetramethylsilane (TMS-Si(CH3)4) fraction in the Ar discharge, the quantity of Si introduced in the W-SiC:H material can be tuned with the objective to explore the possibility to prepare nanocomposite thin film composed of W nanoparticles dispersed in a dielectric SiC:H matrix. In dedicated conditions (5 and 8% TMS), FIB preparation and ultramicrotomy confirmed that W nano-crystallites incorporating C atoms could actually be identified by coupling STEM-HAADF (Figure 1.a) (Scanning Transmission Electron Microscopy - High-Angle Annular Dark Field) images, EDS mapping (Figure 1.b) and High Resolution imaging. In other conditions (20 and 28% TMS), amorphous layers are observed.
Next, the annealing of the layers was studied, first the absorber alone and then on the complete multilayer device (Figure 1.c multilayer before annealing). We thus highlighted the influence of the annealing mode (air or vacuum) and its duration on the structure, composition and therefore properties of the thin film.

Conclusion

These STEM analyses provided crucial information on the structure of the active layer and on the evolution of all layers after thermal annealing. Such information is crucial for optimizing the deposition process, especially concerning its intended application. In addition, this study illustrates the complementarity between sample preparation by FIB and ultramicrotomy. Selecting regions of interest for the FIB preparations can bring more interesting results compared to random slicing by ultramicrotomy whereas the latter allows ascertaining results observed on FIB cross-section thanks to its less damaging conditions.

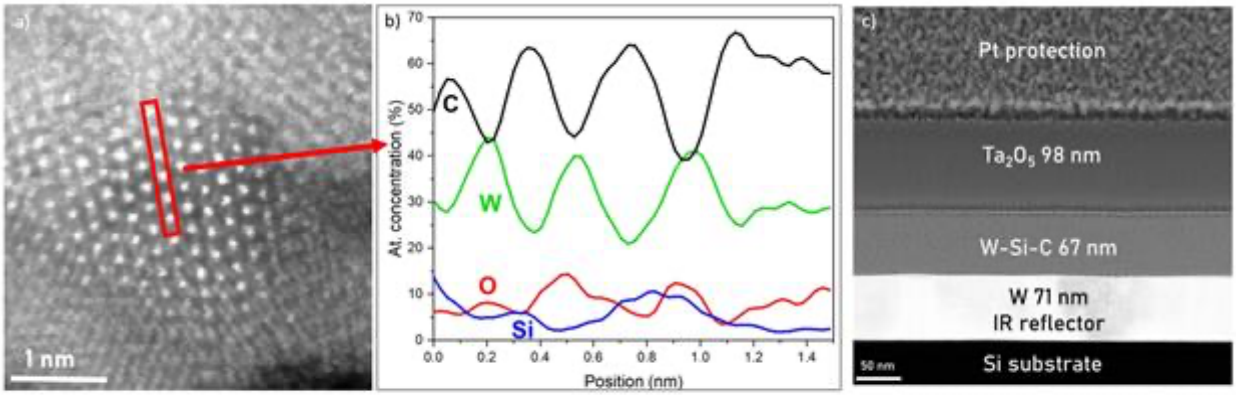

Figure 1 : a) STEM-HAADF images of nano-crystalites (ultramicrotomy preparation) and b) its corresponding EDX profiles; c) STEM-HAADF image of the complete stack before annealing (FIB preparation)

Keywords:

STEM-HAADF, Multilayer coating, FIB, Ultramicrotomy

Reference:

[1] A. Diop et al., 'Comprehensive study of WSiC:H coatings synthesized by microwave-assisted RF reactive sputtering', Surf. Coat. Technol., vol. 459, p. 129408, Apr. 2023

280

A comprehensive (S)TEM analysis of Zn_3P_2 suitability for green energy applications

Helena Freitas[1], Mr. Thomas Hagger[2], Mr. Raphael Lemerle[2], Miss Didem Dede[2], Mrs. Anna Fontcuberta i Morral[2], Miss Brooke Jablon[3], Mrs. Maria Chiara Spadaro[1,4], Mr. Jordi Arbiol[1,5]
[1]Catalan Institute of Nanoscience and Nanotechnology (ICN2), CSIC and BIST, Campus UAB, Bellaterra, Barcelona, Spain, [2]EPFL STI IMX LMSC, MXC 317 (Bâtiment MXC), Station 12, Lausanne, Switzerland, [3]Oxford Instruments SAS, Za de Courtaboeuf, 9 Avenue du Canada, Batiment le Meridien, Les Ulis, France, [4]Physics and Astronomy Department (DFA) Catania University, Catania, Italy, [5]ICREA, Pg Lluis Companys 23, Barcelona, Spain

Poster Group 2

There has been an increasing demand for the development of innovative and sustainable energy conversion devices, aiming to replace conventional and often non-renewable or intermittent energy sources. The motivation for this drive lies in the quest for sophisticated devices, propelling efforts to discover innovative nanostructured materials pivotal in enhancing performance and safeguarding the environment. Understanding a material's compositional and structural traits at the nano and atomic levels, including the configuration of active atoms, crystalline phases, and defects, is paramount in establishing the structure-performance relationship crucial for designing new materials and enhancing existing ones. Transmission electron microscopy (TEM) is a valuable technique employed in characterizing functional nanomaterials, offering insights into crystal structures at a local scale. When combined with techniques like Electron Energy Loss Spectroscopy (EELS) and Energy-dispersive X-ray spectroscopy (EDS) it provides a comprehensive map of elemental information and atomic arrangements, facilitating insights into various promising applications. This work provides an overview of the benefits of utilizing these characterization tools for mapping layer growth, thickness, morphology, and defects of nanostructured Zinc Phosphide (Zn_3P_2) thin films and nanoislands grown by Molecular Beam Epitaxy (MBE) on substrates such as InP and 6H SiC/graphene, with a focus on solar energy applications. Atomic resolution HAADF STEM images of Zn_3P_2 thin films on InP substrates present homogeneous growth and epitaxial relationship between substrate and layer. GPA analysis displays misfit dislocations and rotated domains, and STEM EELS and XRD results indicate composition varying from 60-70% of Zn, in contrast to 30-40% of P. In the case of Zn_3P_2 nanoislands grown on 6H SiC/graphene, atomic resolution HAADF STEM images and GPA analysis reveal that some of the Zn_3P_2 grains are randomly oriented with respect to the 6H SiC/graphene substrate and also, between each other. Rotation maps reveal that, in some areas, there is a rotation of up to 1.6° of the Zn_3P_2 layer with respect to the substrate, which can be justified by the Van der Waals epitaxy between the Zn_3P_2 and graphene. These findings are corroborated by EBSD results, that indicate a most prominent orientation of the grains, and a potential small population of islands with different orientations. Rotated domains are observed, and STEM EDS attest the stoichiometry of the Zn_3P_2 grains. Samples of Zn_3P_2 on different substrates have been analysed to determine the ideal growth conditions for an effective final device. Atomic resolution STEM images have given powerful information on the crystallinity defects present on the samples. These results give the key for growth Zn_3P_2 in an optimal way and go beyond the state-of-the-art in the field of solar cells.

Keywords:

Solar cells;Zinc Phosphide(Zn3P2);HAADF STEM;Electron Microscopy.

Reference:

Stutz, E. Z. et al (2022). Faraday Discuss., 239,202-218

Spadaro, M. C. et al (2021). Nanoscale, 13,18441-18450
Escobar Steinvall, S (2021). NanoscaleAdvances, 3(2), 326–332

294

Anisotropic van der Waals Epitaxy and Sliding of CsPbBr3 Nanoplatelets on ReSe2

Noya Ruth Itzhak[1], Dr. Irit Goldian[2], Dr. Sidney Cohen[2], Dr. Olga Brontvein[2], Katya Rechav[2], Dr. Hagai Cohen[2], Prof. Ernesto Joselevich[1]
[1]Department of Molecular Chemistry and Materials Science, Weizmann Institute of Science, Rehovot, Israel, [2]Chemical Research Support, Weizmann Institute of Science, Rehovot, Israel

Poster Group 2

Background
Dimensionality and size profoundly influence material properties, driving diverse functionalities and applications. Current nanomaterials research focuses on specific dimensionalities like fullerene (0D), carbon nanotube (1D), graphene (2D), and graphite (bulk 2D), each offering distinct traits. Combining materials with different dimensionalities can unlock new functionalities, leading to "mixed-dimensional heterostructures." The crucial role of interfaces in these structures often lacks precise control.
We aim to utilize two-dimensional layered materials as substrates for growing nanostructures through van der Waals (vdW) epitaxy. This approach targets mitigating strain and stress issues inherent in conventional covalent epitaxy.[1] By creating well-defined mixed-dimensional heterostructures, we aim to enhance the heterostructure functionalities.[2] Here, we present the study of the growth of $CsPbBr_3$ perovskite nanoplatelets on low symmetry layered $ReSe_2$.
Methods
The mixed dimensional heterostructure of $CsPbBr_3$ on two-dimensional $ReSe_2$ was synthesized in a home built chemical-vapor-deposition system composed of a three-zone tube furnace. The structural and chemical characterization of the heterostructure was done by scanning and high-resolution electron microscope (Sigma 500 SEM, Zeiss and HRTEM-Themis Z, respectively). Band alignment characterization was done by X-ray photoelectron spectroscopy. Nanotribology studies were performed using AFM and in-situ combined AFM-SEM system.
Results
Mixed dimensional heterostructure of $CsPbBr_3$ platelets on $ReSe_2$ shows the growth of well-aligned and elongated $CsPbBr_3$ nanoplatelets. The optoelectronic properties the mix-dimensional were characterized, revealing type-I band alignment. In addition, tribological studies[3] were conducted by monitoring the force required to push the nanoplatelets along the surface. This revealed an anisotropic sliding effect when pushing rectangular platelets along their long and short axis. This effect is correlated with the commensurability of the two lattice structures in each direction, as revealed by HRTEM analysis. Sliding along the surface can also be hindered by atomic steps and defects, which are easily detected by scanning electron microscope. Therefore, sliding experiments were performed in situ in a combined AFM-SEM system and were compared to an ambient AFM system. These comprehensive experiments enabled a detailed view of the surface and $CsPbBr_3$ platelets before and after sliding, providing a rapid overview of the sample.
Conclusions
The mixed dimensional heterostructure of $CsPbBr_3$ platelets on $ReSe_2$ shows well-defined epitaxial relations. The heterostructure interface was probed to study the charge transfer mechanism and the epitaxial relations. The anisotropic growth of the platelets manifested itself in both TEM characterization and tribology experiments, revealing an anisotropic sliding effect of the $CsPbBr_3$ over the $ReSe_2$. Overall, this work presents a route for guided growth of mixed-dimensional heterostructures using vdW epitaxy and characterizes the vdW bonding nature within the heterostructure.

Keywords:

Mixed-dimensional hererostructures, vdW epitaxy, nanotribology

Reference:

(1) Oksenberg, E.; Merdasa, A.; Houben, L.; Kaplan-Ashiri, I.; Rothman, A.; Scheblykin, I. G.; Unger, E. L.; Joselevich, E. Large Lattice Distortions and Size-Dependent Bandgap Modulation in Epitaxial Halide Perovskite Nanowires. Nature Communications 2020 11:1 2020, 11 (1), 1–11.
(2) Novoselov, K. S.; Mishchenko, A.; Carvalho, A.; Castro Neto, A. H. 2D Materials and van Der Waals Heterostructures. Science (1979) 2016, 353 (6298).
(3) Paul E. Sheehan, C. M. L. Nanotribology and Nanofabrication of MoO3 Structures by Atomic Force Microscopy. Science (1979) 1996, 272

299

In situ electron beam irradiation of Ti3C2Tz MXenes. A STEM-EELS study

Ayoub Benmoumen[1,2], Dr. Marie-Laure David[1], Dr. Eric Gautron[2], Dr. Sophie Morisset[3], Dr. Aurélien Habrioux[3], Dr. Stéphane Célérier[3], Pr. Philippe Moreau[2], Pr. Vincent Mauchamp[1]
[1]Université de Poitiers, ISAE-ENSMA, CNRS, PPRIME, Poitiers, France, [2]Nantes Université, CNRS, IMN, Nantes, France, [3]Université de Poitiers, CNRS, IC2MP, Poitiers, France

Poster Group 2

Background incl. aims
MXenes are a family of 2D transition metal carbide or nitride layers obtained from the exfoliation of nanolaminated ceramics called MAX phases [1]. Their chemical formula is Mn+1XnTz (n = 1, 2 or 3), with M a transition metal, X being C and/or N, and T are surface terminations (e.g. O(H), F, Cl) inherited from the exfoliation process. They present very good electrical conductivity, as well as high hydrophilicity, making them very promising materials for various applications, including transparent conductive electrodes or energy storage devices [2]. Our previous study [3] showed the strong influence of ion irradiation induced defects on the structural and physical properties of Ti3C2Tz MXenes, resulting in a reduced hydration potential, an increase in the charger carrier density as well as a modification of their optical properties. In the meanwhile, a large conductivity is preserved. Electron beams have also been shown to be a valuable tool for the structural engineering of MXenes on the nanometer scale [4]. Here, we present a new experimental protocol, which aims towards localized defect engineering in MXenes, using electron beam irradiation in situ in a transmission electron microscope (TEM), performed in cryogenic conditions.
Methods
This is achieved by adjusting the exposure time, the beam current and the number of frames in STEM-EELS (electron energy-loss spectroscopy) measurements, to reach an electron dose that allows for the introduction of defects into the sample. The study was performed on pristine Ti3C2Tz, exfoliated from its MAX phase precursors following the protocol detailed in [5], the powder was then dispersed in water to delaminate the MXenes sheets and dropped on a TEM lacey carbon grid. The TEM grid was placed on a cryo sample-holder and measurements were performed at liquid nitrogen temperature.
Results
At low temperature, irradiation conditions can be controlled precisely, by the creation of either punctual depressions, roughly the size of the electron beam, or bigger “crater-like” dips spanning over hundreds of nm² (Figure), depending on the irradiation conditions. The evolution of the structure and chemistry of the sample is monitored as a function of the electron dose using core-loss spectra acquired both during and after irradiation.
Conclusion
This study gives a valuable insight into the defect formation mechanisms at play in electron beam irradiation of MXenes, by observing the behavior of the surface functional groups, as well as the core atoms in regards to the incoming high-energy electrons. This innovative approach can potentially be generalized to other MXenes and 2D materials, as well as up scaled to thin films using other electron irradiation techniques such as SEM.

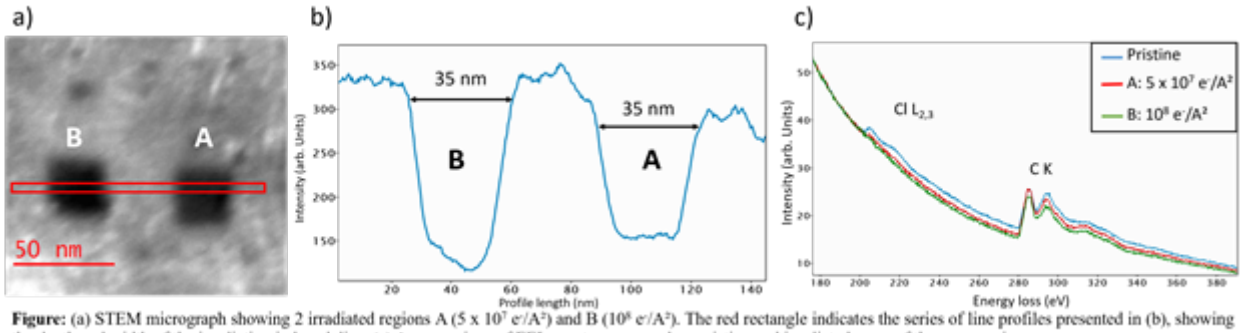

Figure: (a) STEM micrograph showing 2 irradiated regions A (5 x 10^7 e^-/A^2) and B (10^8 e^-/A^2). The red rectangle indicates the series of line profiles presented in (b), showing the depth and width of the irradiation induced dips. (c) A comparison of EEL spectra measured on pristine and irradiated areas of the same region.

Keywords:

MXenes, STEM-EELS, irradiation, defects, quantification

Reference:

[1] M. Naguib et al., Adv. Mater., 2011, 23, 4248-4253.
[2] S. Abdolhosseinzadeh et al., Materials Today, 2021, 48, 214
[3] A. Benmoumen et al., Applied Surface Science, 2024, 652, 159206
[4] X. Sang et al., Nature Communications, 2018, 9, 2266
[5] M. Benchakar et al., Applied Surface Science, 2020, 530, 147209

338

Physico-chemical and biological characterization of Ag- and Cu-doped ZnO thin films coated with calcium phosphates

Ana-Marija Milisav[1], Dr. Maja Mičetić[1], Dr. Pavo Dubček[1], Lamborghini Sotelo[2,3], Cristina Cantallops Villà[4], Dr. Tommaso Fontanot[5], Dr. Ina Erceg[1,5], Dr. Krunoslav Bojanić[1], Dr. Željka Fiket[1], Dr. Maja Ivanić[1], Prof. Dr. Silke Christiansen[3,5], Assist. Prof. Dr. Edwige Meurice[4], Dr. Tihomir Car[1], Dr. Maja Dutour Sikirić[1]
[1]Ruđer Bošković Institute, Zagreb, Croatia, [2]Friedrich-Alexander Universität Erlangen-Nürnberg, Erlangen, Germany, [3]Innovations-Institut für Nanotechnologie und Korrelative Mikroskopie, Forchheim, Germany, [4]CERAMATHS, Université Polytechnique Hauts-de-France, Cambrai, France, Cambrai, France, [5]Fraunhofer Institute for Ceramic Technologies and Systems IKTS, Forchheim, Germany

Poster Group 2

Background incl. aims
Bacterial contamination of biomedical surfaces is a serious threat that can lead to nosocomial infections, with a prevalence reported up to 10 %.1 Treatment of such infections is complicated by emerging antimicrobial resistance.2 Potential solution lies in the development of novel antibacterial surfaces that prevent the initial bacterial adhesion. In this sense, magnetron sputtered ZnO thin films are attracting attention as the properties, including biological, of the thin films can be regulated by changing the sputtering conditions. In addition, doping ZnO with elements from group I and IB (e.g. Ag and Cu) can influence the structural and morphological properties of the thin films. However, a major disadvantage for the biomedical application of this material is the lack of porosity.3 The aim of this research was to evaluate the differences between Ag and Cu doping of ZnO and to determine whether changes in surface morphology due to the coating with calcium phosphate can influence the biological responses of the material.
Methods
Ag- and Cu-doped ZnO thin films were prepared by magnetron sputtering, followed by biomimetic deposition of calcium phosphate to potentially improve bioactivity. Characterization focused on microscopy techniques including scanning electron microscopy (SEM), helium ion microscopy (HIM) and atomic force microscopy (AFM) to investigate microstructural changes. Additional characterization of structure and composition included grazing incidence small-angle X-ray scattering (GISAXS), energy dispersive spectroscopy (SEM/EDX), and X-ray diffraction (XRD). Wettability and surface free energy were assessed, and ion release was measured using inductively coupled plasma mass spectrometry (ICP-MS). Biological characterization included cell viability assays with MG-63 cells and biofilm formation assays with Staphylococcus aureus and Pseudomonas aeruginosa.
Results
Microscopic analysis revealed that the thin films have irregular granular structures in all cases, with Ag or Cu doping influencing the size and shape of grains. Increased Ag or Cu content had opposite effects on the grain size of the nanostructured thin film. Further SEM/EDX and XRD analyzes indicated that Ag or Cu were incorporated into the ZnO crystal structure. Calcium phosphates were successfully deposited as individual crystals or aggregates. The deposition of calcium phosphates slightly improved cell viability, with the effect being greater for Ag-doped ZnO. The addition of calcium phosphates also showed better prevention of biofilm formation.
Conclusion
Ag- and Cu-doped ZnO thin films with calcium phosphates were investigated as antibacterial surfaces for biomedical applications. The doping allowed control over the morphology of the nanoparticles, while the deposition of calcium phosphates showed the potential to improve cell viability and inhibit

biofilm formation. These results are promising for the development of effective coatings to prevent nosocomial infections and for a variety of other antimicrobial applications.

Keywords:

Magnetron sputtering, calcium phosphates, biofilms

Reference:

1. Cloutier, M. et al. Trends Biotechnol. 33, 637–652 (2015).
2. Gupta, A. et al. Chem. Soc. Rev. 48, 415–427 (2019).
3. Samiee, M. et al. Ceram. Int. 47, 6179–6186 (2021).

339

Influence of titanium surface modifications on formation of composite calcium phosphates / silver nanoparticles coatings

Suzana Inkret[1], Dr. Ina Erceg[1,2], Prof. Dr. Silke Christiansen[2,3], Dr. Maja Dutour Sikirić[1]
[1]Department of Physical Chemistry, Ruđer Bošković Institute, Zagreb, Croatia, [2]Fraunhofer Institute for Ceramic Technologies and Systems IKTS, Forchheim, Germany, [3]Innovation Institute for Nanotechnology and Correlative Microscopy – INAM, Forchheim, Germany

Poster Group 2

Background incl. aims
Due to their chemical and mechanical stability, as well as biocompatibility titanium and its alloys are among most frequently used materials for hard tissue implant materials [1]. However, they are biologically inert, a problem which is usually surpassed by coating them with bioactive calcium phosphates, which results in improved adhesion of coating material and cells [2]. As major problem in orthopaedic surgery are implant associated infections, the coatings should in addition have antimicrobial properties. One way of achieving this is incorporation of antimicrobial components in calcium phosphate coatings. In this sense, silver nanoparticles attract attention due to the fact that silver exhibits a broad spectrum of antimicrobial activity and is unlikely to cause bacterial resistance [3].

Methods
The titanium surface was chemically modified using two different methods using strong acids, namely hydrochloric acid previously described by Lu et.al. [4] and using a mixture of hydrochloric and sulfuric acid previously described by Wang et.al. [5]. After modification of the titanium surface, composites of silver nanoparticles and calcium phosphates were coated by wet chemistry method. The influence of the different surface modifications on the formation of the composites was investigated by scanning electron microscopy (SEM), energy dispersive X-ray spectroscopy (EDS), Raman spectroscopy and atomic force microscopy (AFM).

Results
The modification of titanium surfaces changes surface properties such as roughness and wettability, as shown by AFM and contact angle measurements. Composites of calcium phosphates and silver nanoparticles formed on treated, but also on untreated titanium surfaces. SEM and EDS measurements showed that the morphology and uniformity of the coatings change depending on the surface modification.

Conclusion
Surface modification of titanium is an important step in a process for coating titanium with functional materials such as composites of calcium phosphates and silver nanoparticles, as it modifies surface properties and thus influences the deposition of coatings. The results obtained can contribute to the development of an ideal procedure for the preparation of antimicrobial coatings on titanium surfaces.

Keywords:

composites, titanium implants, surface modification

Reference:

[1] X. Lu, Z. Wu, K. Xu, X. Wang, S. Wang, H. Qiu, X. Li, J. Chen, Front. Bioeng. Biotechnol. 9 (2021) 783816.
[2] J. Barberi, S. Spriano. Mater. 14 (2021) 1590.
[3] S.L. Percival, P.G. Bowler, D. Russell. JHI 60 (2005) 1–7.
[4] X. Lu, Z. Zhao, Y. Leng, Mater. Sci. Eng. C 27 (2007) 700–708.
[5] D. Wang, G. He, Y. Tian, N. Ren, W. Liu, X. Zhang. J. Biomed. Mater. Res. 108 (2020) 2386–2395.

341

Impact of Electron Beam Irradiation on Carbon Black Oxidation

David Wahlqvist[1], Dr Mattias Mases[2], Dr Daniel Jacobsson[1], Dr Henrik Wiinikka[3], Dr Martin Ek[1]
[1]Center for Analysis and Synthesis, Lund University, Lund, Sweden, [2]Division of Materials Science, Luleå University of Technology, Luleå, Sweden, [3]RISE Energy Technology Center, Piteå, Sweden

Poster Group 2

Background
The use of environmental transmission electron microscopy (ETEM) in oxidation studies of nanocarbons, such as carbon black (CB), has revealed new, and confirmed previously suggested, oxidation mechanisms [1]. However, connecting ETEM studies to technical processes (occurring at very different conditions) is not necessarily straightforward. Primarily, the influence of the electron beam can present a large issue that is not easily resolved. For nanocarbon oxidation, there is a clear increase in oxidation rate depending on the dose rate, however, there are few studies reporting any quantification of this effect [2].
To better understand the origin of the beam-enhanced oxidation rate, we note that CB reacts with oxygen gas only at active sites, imperfections in the graphitic shell. These active sites are inherent to CB but can also be generated through interactions with the electron beam through 3 distinct mechanisms. Firstly, ionized oxygen species can react directly with the graphitic shell of CB, these species can be produced through ionization interactions with either primary electrons (PE) or secondary electrons (SE). Additionally, active sites can be generated through atomic displacements in CB by PE. These three mechanisms; ionization of O2 by PE [3], ionization of O2 by SE [4], and atomic displacements by PE; have different underlying mechanisms and respond differently to variation of reaction and imaging conditions.
Methods
In our study, we have observed the oxidation of CB at varying electron dose rates and electron energies in two ETEM setups. Data were collected using electron energy loss (EEL) spectroscopy time-series for determination of an average oxidation rate over agglomerates, as calculated from the time-dependent decrease in the C-K signal. This data were complemented with data high-resolution time resolved image series to investigate the local effect on individual particles and to validate the EEL spectroscopy results.
Results
Our experiments show that in situ beam-enhanced CB oxidation is localized to the irradiated area, that the oxidation rate is not significantly affected by changes to the electron energy, and that the in situ beam enhancement is non-linear in nature. Additionally, the reaction only occurs in the presence of an oxidizing gas, i.e. not in inert gases like N2. These findings contradict that ionization by PE is the driving force behind the increase in oxidation rate in TEM, as the ionized species are expected to spread out over an area larger than the illuminated, and the rate at which ionized oxygen species is expected to approximately double as the electron energy is reduced from 300 keV to 100 keV. Similarly, oxygen ionization by SE, is also expected to increase when the electron energy is decreased, however, this mechanism may have a minor impact if the CB sample is located on a support, in which case an excess of SEs is generated. Rather, the results are consistent with atomic displacement as the main driving force; given that the electron energy required to knock an atom out of its lattice position is exceeded, the probability of displacement does not change to a large extent over the relevant electron energy scale. Additionally, atomic displacements can only occur where the electron beam has been located, and no damage is observed outside of the irradiated area.
Conclusion
We have shown that CB oxidation is mainly affected by elastic high-energy electron-sample interactions, with a smaller contribution from inelastic electron-gas processes from secondary

electrons emitted from the sample and sample support. While this process suggests that there are no safe conditions, the beam effect can be made vanishingly small compared to the intrinsic oxidation. We show how EELS can link processes seen at individual particles to whole agglomerates. This further illustrates the importance of comparing results obtained in the ETEM with results obtained via other methods such as TGA or its like.

Graphic

Figure: Summary of methods and primary results of study. a) EEL spectroscopy time-series (blue) of the C-K signal and linear fit (orange) to the linear region of the time-series. The inset illustrates selected average spectra from times s. b) The linear oxidation rate as calculated from the linear fit in time-series as in a) illustrating no significant difference between 80 keV and 300 keV. c) Results from an image time-series with insets showing a CB particle at various stages of oxidation. d) Aggregate results of image time-series, the green region represents an “inherent” oxidation rate with intermittent imaging.

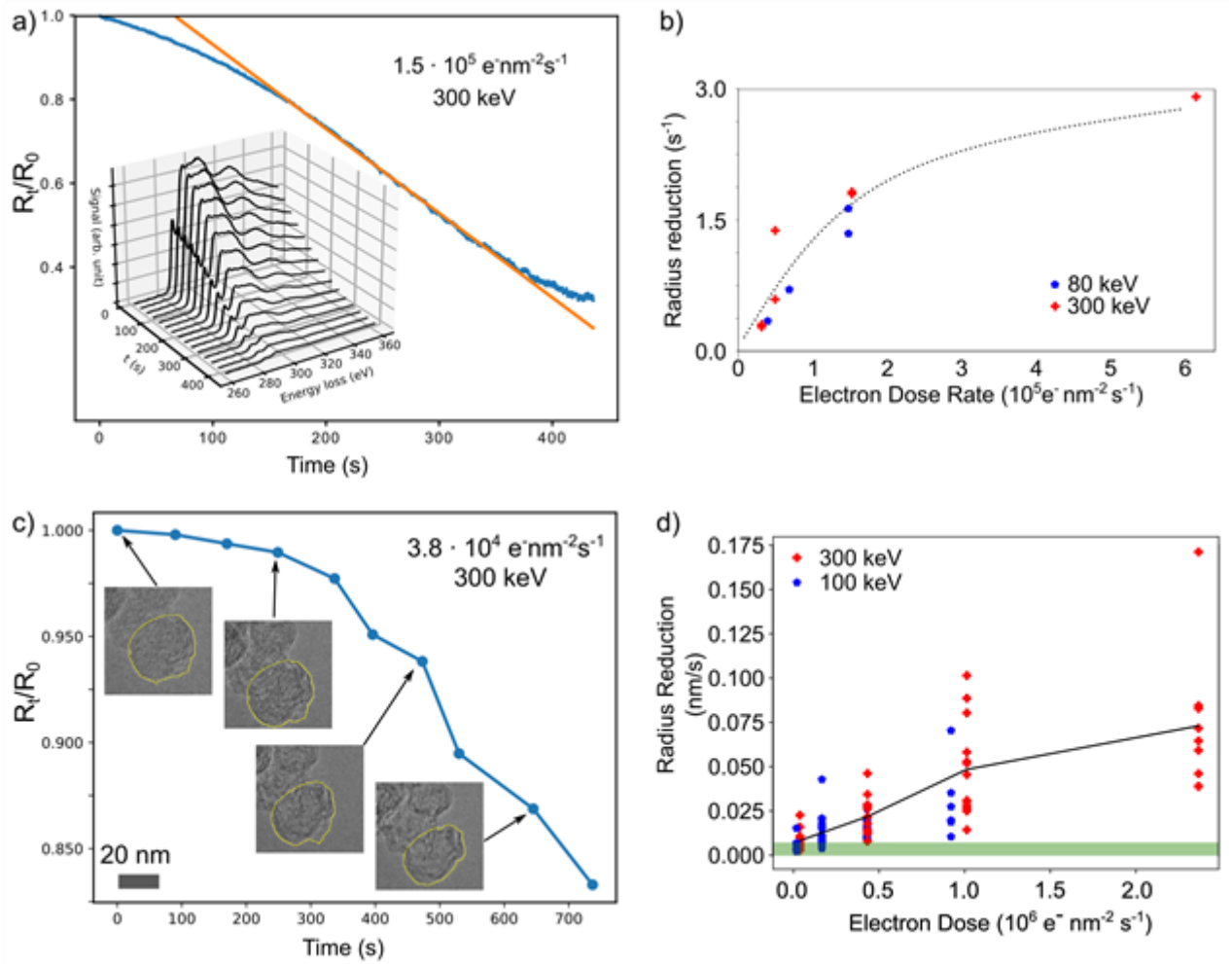

Keywords:

Electron beam nanocarbon oxidation ETEM

Reference:

[1] H. Wiinikka et al. Carbon 2019, DOI: 10.1016/j.carbon.2019.01.007
[2] D. Wahlqvist et al. Carbon 2024, DOI: 10.1016/j.carbon.2023.118686
[3] A. L. Koh et al. Ultramicroscopy 2017, DOI: 10.1016/j.ultramic.2016.12.009
[4] H. Yoshida et al. Nanotechnology 2017, DOI: 10.1088/1361-6528/aa6a4c

392

Direct observation of the interplay between stacking polytypes and self-intercalation in epitaxial Nb1+xSe2 films

Dr. Hongguang Wang[1], BS. Jiawei Zhang[1], Dr. Chen Shen[2], Dr. Chao Yang[1], Dr. Kathrin Küster[1], Dr. Julia Deuschle[1], Prof. Ulrich Starke[1], Prof. Hongbin Zhang[2], Dr. Masahiko Isobe[1], Dr. Dennis Huang[1], Prof. Peter A. van Aken[1], Prof. Hidenori Takagi[1,3,4]
[1]Max Planck Institute for Solid State Research, Heisenbergstr. 1, 70569, Stuttgart, Germany, [2]Department of Materials and Earth Sciences, Technical University of Darmstadt, Darmstadt, Germany, [3]Institute for Functional Matter and Quantum Technologies, University of Stuttgart, 70569 Stuttgart, Germany, [4]Department of Physics, University of Tokyo, 113-0033 Tokyo, Japan

Poster Group 2

Background
Stacking and intercalation are crucial for modifying and engineering the properties of two-dimensional (2D) van der Waals (vdW) materials [1, 2]. Stacking, as a control parameter, involves varying the lateral registry or twist angle between adjacent layers to realize, for example, exotic electronic phases in a moiré superlattice [3]. Intercalation refers to the insertion of atoms or molecules into the vdW gap between two layers [4]. This can be achieved by synthetic routes or electrochemistry, potentially leading to emergent superconducting or magnetic states. While the individual potentials of stacking and intercalation have yet to be fully explored, a natural progression is to investigate the synergistic combinations of these two tuning parameters. Understanding the interplay between stacking and self-intercalation is therefore important. However, current knowledge of the interplay between stacking polytypes and intercalation is often based on macroscopically averaged probes, which fail to accurately identify the exact atomic position and chemical state of the intercalants in real space. Atomic-scale observation of the cross section of vdW materials is essential for further clarification.

Methods
In this work, utilizing atomic-resolution electron energy-loss spectroscopy (EELS) in a scanning transmission electron microscope, we systematically investigate the atomic and electronic structures and local chemistry in epitaxial transition-metal dichalcogenide Nb1+xSe2 films grown by "hybrid" pulsed laser deposition and Nb1+xSe2 crystals grown via chemical vapor transport techniques. Density functional theory calculations were performed to evaluate the roles of thermodynamics and kinetics in these observations.

Results
Using high spatial resolution scanning transmission electron microscopy (STEM), we observe that thin films with an average x ~ 0.29 comprise a nanoscale phase mixture of NbSe2 layers stacked with both 180° and 0° in-plane rotations. The 180°-stacked layers exhibit significant self-intercalation with Nb at the octahedral interstitial sites, likely reaching several tens of percent occupancy, whereas the 0°-stacked layers contain few detectable intercalants at their octahedral interstitial sites. Our findings extend beyond merely imaging intercalants or different stacking structures to establishing a correlative relationship between the two. Density functional theory (DFT) confirms that the energetically favored stacking orientation transitions from 0° to 180° when the self-intercalation exceeds a threshold of approximately x ~ 0.25. However, achieving this threshold appears to necessitate kinetic pathways distinct from those in the thin films. Efforts to replicate these observations with Nb1+xSe2 crystals grown via chemical vapor transport (CVT) yield a homogeneous phase of intercalated, 0°-stacked layers with an average x of at most ~0.20. The presence of Nb intercalants reduces the size of the Fermi hole pockets and suppresses superconductivity in NbSe2,

and these altered properties may provide a foundation for fabricating junctions and nanostructures with more precise control over stacking and self-intercalation.

Conclusion

Using STEM and EELS, we have directly visualized a stacking-selective self-intercalation phenomenon in epitaxial Nb1+xSe2 films. Our results offer not only renewed mechanistic insights into stacking and intercalation, but also open up prospects for engineering the functionality of TMDCs via stacking-selective self-intercalation. [5]

Fig. 1 stacking-selective self-intercalation phenomenon in epitaxial Nb1+xSe2 films

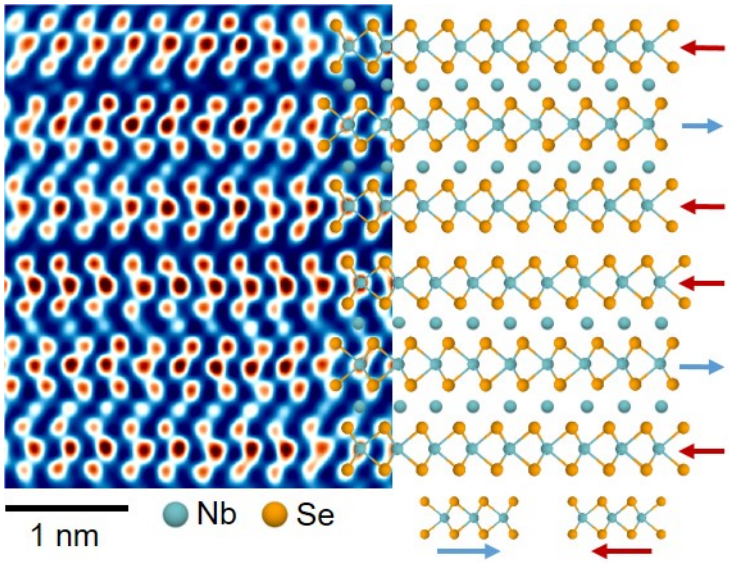

Keywords:

STEM, NbSe2, staking polytypes, self-intercalation

Reference:

1. P. Ajayan et al. Phys. Today 69 (2016), 39-44.
2. K. S. Novoselov et al. Science 353 (2016), aac9439.
3. R. Huisman et al. J. Less-Common Met. 21 (1970), 187-193.
4. Y. Wu et al. Nat. Commun. 13 (2022), 3008.
5. H. Wang et al. Nat. Commun. 15(2024), 2541.

484

Temperature-dependence of beam-driven dynamics in graphene-fullerene sandwiches

Kevin Strobel[1,2], Michael Schlegel[1,2], Mitisha Jain[3], Dr. Silvan Kretschmer[3], Dr. Arkady V. Krasheninnikov[3], Prof. Dr. Jannik C. Meyer[1,2]
[1]Institute of Applied Physics University of Tübingen, Tübingen, Germany, [2]NMI Natural and Medical Sciences Institute at the University of Tübingen, Reutlingen, Germany, [3]Institute of Ion Beam Physics and Materials Research, Helmholtz-Zentrum Dresden-Rossendorf, Dresden, Germany

Poster Group 2

Aberration-corrected high-resolution transmission electron microscopy was used to investigate C60 fullerenes encapsulated between graphene sheets at different temperatures (ca. 93K, 293K, and 773 K), along with molecular dynamics simulations. Cryogenic and heated conditions were reached using a custom in situ MEMS heating system. The study focused on the beam-induced dynamics of the C60 fullerenes and the encapsulating graphene, measuring the critical doses for the initial damage to the fullerenes and following the beam-induced polymerization. We observe that the doses for the initial damage are not significantly affected by temperature. However, the clusters formed by subsequent polymerization exhibit more tubular shapes at lower temperatures, while sheet-like structures are generated at higher temperatures.
These experimental findings are supported by the results of first-principles and analytical potential molecular dynamics simulations. The merging of curved carbon sheets is promoted at higher temperatures and occurs rapidly over segments of only a few nanometers.

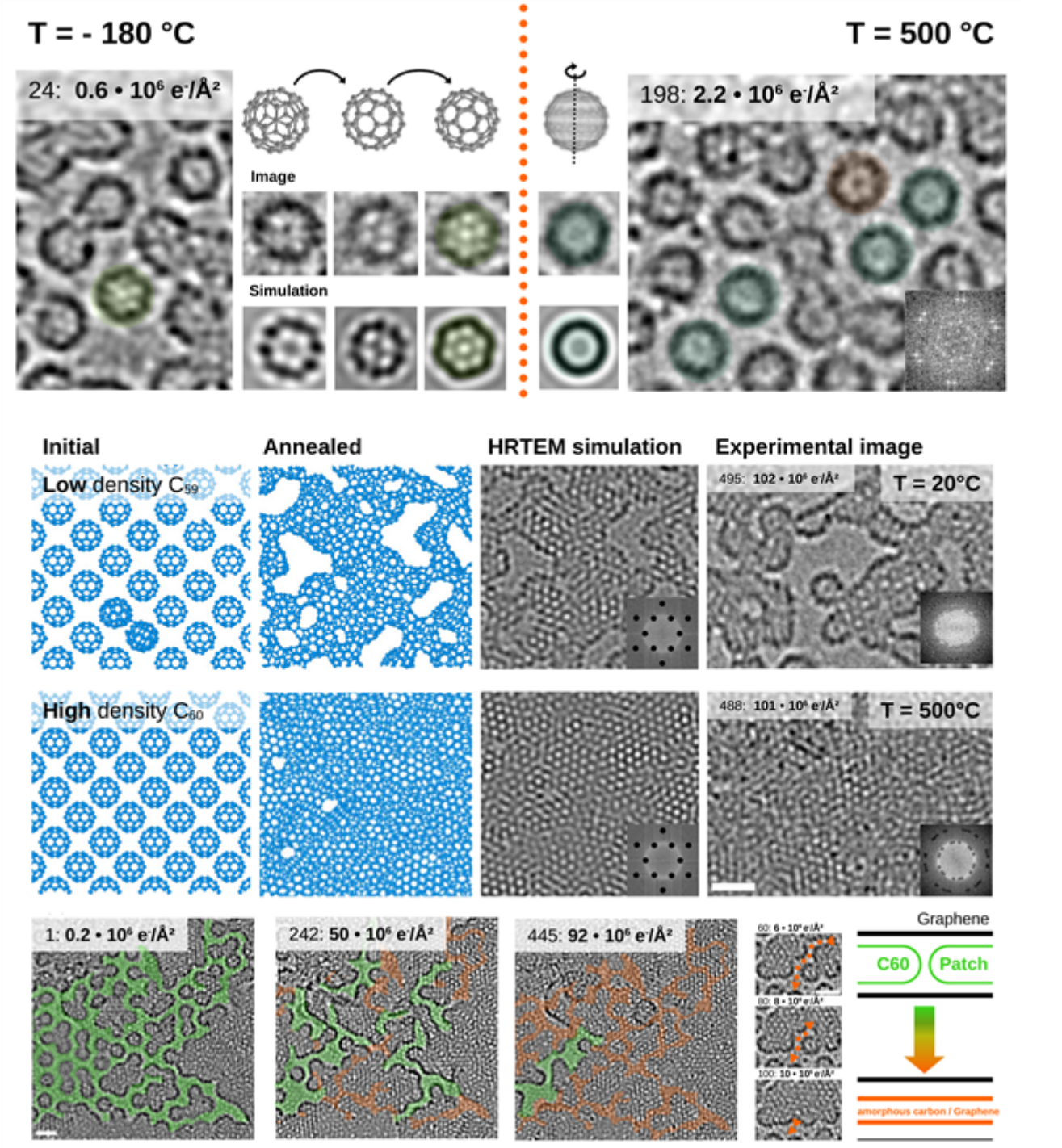

Keywords:

C60 Graphene 2D HRTEM MEMS

Reference:

1. Madsen, J., & Susi, T. (2021). The abTEM code: transmission electron microscopy from first principles. Open Research Europe, 1, 24. https://doi.org/10.12688/openreseurope.13015.1
2. Mirzayev, R., Mustonen, K., Monazam, M. R. A., Mittelberger, A., Pennycook, T. J., Mangler, C., Susi, T., Kotakoski, J., & Meyer, J. C. (2017). Buckyball sandwiches. Science Advances, 3(6), e1700176. https://doi.org/10.1126/sciadv.1700176
3. Skowron, S. T., Roberts, S. L., Khlobystov, A. N., & Besley, E. (2019). The effects of encapsulation on damage to molecules by electron radiation. Micron, 120(January), 96–103. https://doi.org/10.1016/j.micron.2019.02.007

498

Heating effects in Bi-doped Cu nanowires for spintronics: atomic resolution in-situ insights

Miss Alejandra Guedeja-Marron[1,2], Dr Matilde Saura-Muzquiz[1], Miss Ines Garcia-Manuz[3], Dr Juan I. Beltran[1], Dr Henrik L. Andersen[4], Dr Lunjie J. Zeng[5], Dr Alok Ranjan[5], Prof. Eva Olsson[5], Dr Paolo Perna[6], Prof. Lucas Perez[1,6], Prof. Maria Varela[1,2]
[1]Dept. Fisica de Materiales, Complutense University of Madrid, Madrid, Spain, [2]Instituto Pluridisciplinar, Complutense University of Madrid, Madrid, Spain, [3]Universidad Autonoma de Madrid, Madrid, Spain, [4]Instituto de Ciencia de Materiales de Madrid (ICMM) - CSIC, Madrid, Spain, [5]Chalmers University of Technology, , Sweden, [6]Instituto Madrileño de Estudios Avanzados – IMDEA Nanociencia, Madrid, Spain

Poster Group 2

Background incl. aims
CuBi alloys are predicted to exhibit a giant spin Hall effect (SHE), making them promising materials for developing spintronic devices. This prediction was supported by the direct observation of SHE in Cu95Bi5 films by X-ray spectroscopy. However, the material composition and structure, e.g. crystallinity, crystallite size, effective Bi insertion into the Cu lattice or formation of metallic clusters of Bi, can affect the spin Hall angle, which is related to the efficiency of the spin-to-charge current conversion. This efficiency becomes more and more critical in the case of reduced dimensionality systems, where some dimensions may become smaller than the spin diffusion length. Changes taking place during device operation, such as those related to Joule heating, may also affect the system performance.

Methods
Here, we present a detailed structural characterization of Bi-doped Cu nanowires (NWs) with a high Bi doping level (up to 7% Bi) and different degrees of crystallinity, grown by template-assisted electrochemical deposition. The combination of in-situ atomic resolution scanning transmission electron microscopy (STEM), diffraction, electron energy-loss spectroscopy (EELS) and high-resolution synchrotron powder X-ray diffraction (PXRD), allows studying in detail the atomic structure of the NWs, which is critical for optimization of the spin transport related properties.

Results
Nanodiffraction (4DSTEM) measurements were used to analyze the crystallite size and orientation of the nanowires (see Figure 1(a,b)), allowing to harness the growth procedures in order to achieve a controlled distribution of grain boundaries, with average crystal sizes ranging from tens of nm to the micron scale. In-situ heating experiments, using both STEM and PXRD techniques, were carried out to reproduce operando conditions subject to Joule heating effects. After heating for an interval of several minutes at 400°C, in-situ PXRD measurements show that a temperature induced structural transition takes place. For an initial Bi doping of 6%, diffraction peaks typical of pure Bi appear after heating, pointing to the presence of significant Bi diffusion (Figure 1(c)). EELS chemical quantification reveals that the NWs average doping decreases to 1 at. % of Bi after heating. A decrease in the unit cell lattice parameter can be detected both by PXRD analysis and STEM images, suggesting that Bi is coming out of solution in a thermally activated process. In fact, a pure Bi phase is detected after the annealing, associated with Bi nucleation on external surfaces and also at grain boundaries. Indeed, high angle annular dark field (HAADF) images show the early stages of Bi nucleation, coming out of solution from the Cu cubic matrix along the edges of the NWs, indicating preferred orientations for Bi segregation during heating (Figure 1(d)). Density-functional theory will be used to explain these

processes, which must be taken into account when trying to understand the behavior of these nanosystems under working conditions in future devices exploiting SHE.

Conclusions

Our study explores Bi-doped Cu nanowires grown via electrochemical deposition. Synchrotron and Advanced microscopy techniques reveal structural details critical for spin transport optimization. In-situ heating experiments expose a temperature-induced Bi diffusion, leading to nucleation of a pure Bi phase. This suggests a thermally activated process affecting NW doping and lattice parameters. Understanding these phenomena is crucial for developing efficient spintronic devices driven by the spin Hall effect.

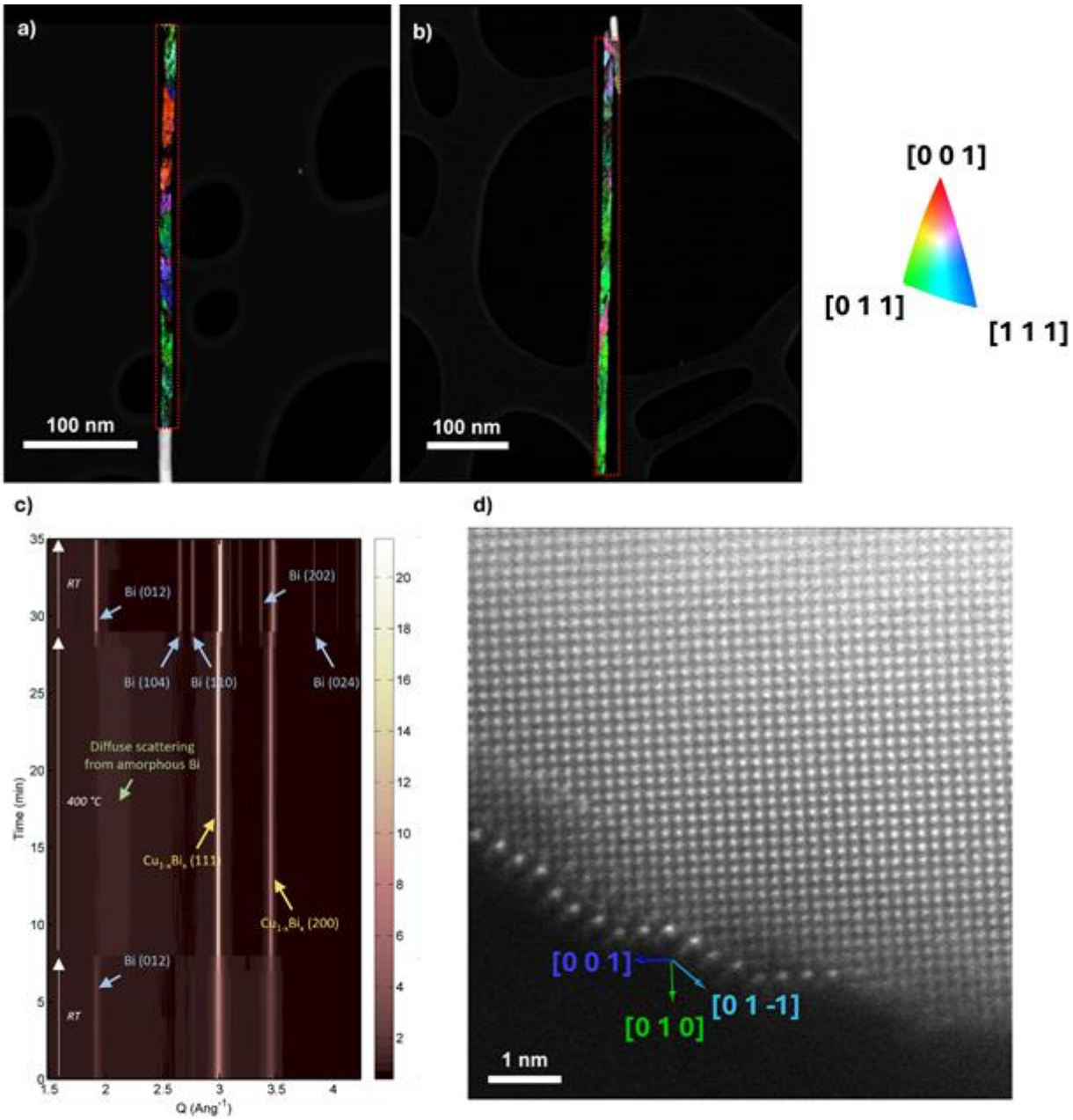

Figure 1: HAADF images and 4DSTEM out-of-plain orientation maps with a false color stereographic projection of the [001], [011] and [111] directions. (a) Small grain-like and (b) large grain-like NWs with grain sizes of around 200 nm and 1 µm, respectively. (c) Contour plot of low Q-range of time-resolved synchrotron PXRD data collected on a $Cu_{1-x}Bi_x$ (x=0.06) NW before, during and after heating to 400 °C. (d) High resolution HAADF-STEM image of the surface of a NW showing Bi segregation after heating and recrystallisation.

Keywords:

HR-STEM, EELS, in-situ, nanowires, spintronics

Reference:

T. Jungwirth et al., Nature. 11 (2012) 5

Y. Niimi et al., Phys. Rev. Lett. 109 (2012)

J. Sinova et al., Rev. Mod. Phys. 87 (2015) 1213. 15

S. Ruiz-Gomez et al., Phys. Rev. X. 12 (2022) 3

S. Ruiz-Gomez et al., J. Magn. Magn. Mater. 545 (2022) 168645

515

Mechanism of WS2 nanotube formation revealed by in-situ/ex-situ imaging and cross-sectional sequences

Dr. Vojtech Kundrat[1,2], Dr. Libor Novak[2], Dr. Kristyna Bukvisova[2,3], Assoc. Prof. Miroslav Kolibal[3], Prof. Reshef Tenne[1]
[1]Weizmann Institute of Science, Rehovot, Israel, [2]Thermo Fisher Scientific, Brno, Czech Republic, [3]Brno University of Technology, Brno, Czech Republic

Poster Group 2

Multiwall WS_2 nanotubes have been synthesized from $W_{18}O_{49}$ nanowhiskers in substantial amounts for over a decade [1]. The established growth model is based on the “surface-inwards” mechanism, whereby the high-temperature reaction with H_2S starts on the nanowhisker surface, and the oxide-to-sulfide conversion progresses inwards until hollow-core multiwall WS_2 nanotubes are obtained [2]. In the present work, an upgraded in-situ SEM µReactor [3] with an H_2S source has been conceived to study the growth mechanism in detail. Ex-situ TEM technique was developed to gain structural insight to the reaction at selected times. Further inspection was done by cross-sectional ex-situ TEM sequences where preselected long $W_{18}O_{49}$ nanowhisker was observed from the (010) direction during the sulfidation reaction as a series of lamellae. Based on these techniques, a hitherto undescribed growth mechanism, named “receding oxide core”, which complements the “surface-inwards” model, is observed and kinetically evaluated. Initially, the nanowhisker is passivated by several WS_2 layers via the surface-inwards reaction. At this point, the diffusion of H_2S through the already existing outer layers becomes exceedingly sluggish, and the surface-inwards reaction is slowed down appreciably. Subsequently, the tungsten suboxide core is anisotropically volatilized within the core close to its tips. The oxide vapors within the core lead to its partial out-diffuse out, partially, forming a cavity that expands with reaction time. Additionally, the oxide vapors react with the internalized H_2S gas, forming fresh WS_2 layers in the cavity of the nascent nanotube. The rate of the receding oxide core mode increases with temperatures above 900 °C. The growth of nanotubes in the atmospheric pressure flow reactor is carried out, as well, showing that the proposed growth model (receding oxide core) is also relevant under regular reaction parameters. The current study comprehensively explains the WS_2 nanotube growth mechanism, combining the known model with contemporary insight.

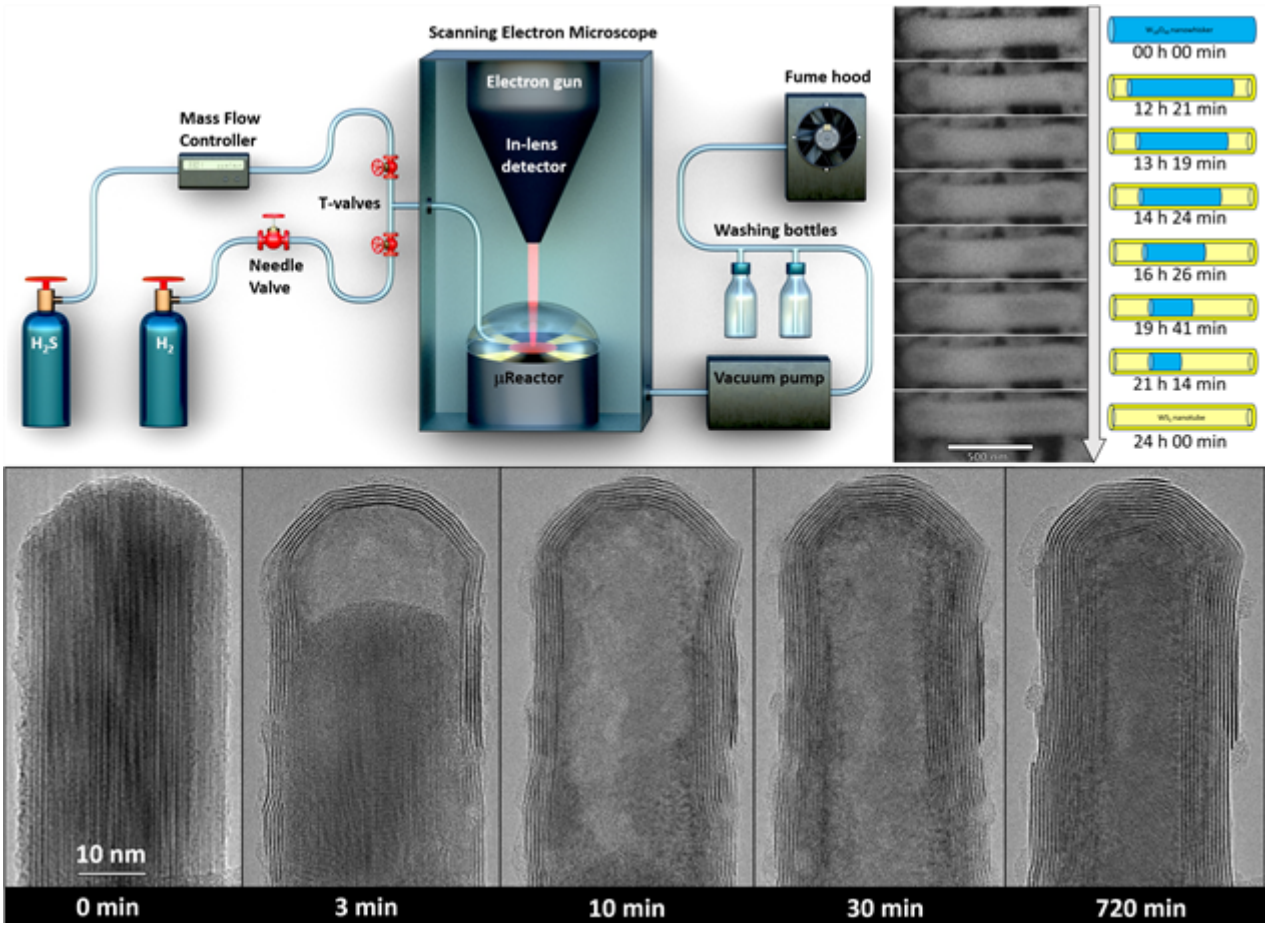

Keywords:

WS2-nanotube, in-situ, ex-situ, SEM, TEM

Reference:

[1] Tenne, R.; Margulis, L.; Genut, M.; Hodes, G. Polyhedral and Cylindrical Structures of Tungsten Disulphide. Nature 1992, 360 (6403), 444–446. https://doi.org/10.1038/360444a0.
[2] Rothschild, A.; Sloan, J.; Tenne, R. Growth of WS2 Nanotubes Phases. J. Am. Chem. Soc. 2000, 122 (21), 5169–5179. https://doi.org/10.1021/ja994118v.
[3] Kundrat, V.; Bukvisova, K.; Novak, L.; Prucha, L.; Houben, L.; Zalesak, J.; Vukusic, A.; Holec, D.; Tenne, R.; Pinkas, J. W18O49 Nanowhiskers Decorating SiO2 Nanofibers: Lessons from In Situ SEM/TEM Growth to Large Scale Synthesis and Fundamental Structural Understanding. Crystal Growth & Design 2023, acs.cgd.3c01094. https://doi.org/10.1021/acs.cgd.3c01094.

570

Water condensation on core-shell nanofibers studied using multiscale environmental electron microscopy

Laura Montes-Montañez[1], Dr Annie Malchère[2], Dr Lucian Roiban[2], Dr Victor Rico[1], Dr Victor Trillaud[2], Prof Philippe Trillaud[2], Prof Karine Masenelli-Varlot[2], Prof Agustín R González-Elipe[1], Dr Ana Borrás[1], Dr Carmen López-Santos[1,3]
[1]Institute of Materials Science of Seville (US-CSIC) , Seville, Spain, [2]INSA Lyon, Universite Claude Bernard Lyon 1, CNRS, MATEIS, UMR5510, Villeurbanne, France, [3]Departamento de Física Aplicada I, Escuela Politécnica Superior, Universidad de Sevilla, Seville, Spain

Poster Group 2

Background incl. aims
Superhydrophobic, omniphobic, icephobic and self-cleaning mean advanced properties of a surface when precise control of the roughness combining different levels of topography, from micro- to-nanostructures for the called hierarchical surface [1-4]. Particularly one-dimensional nanostructured matrix allows the integration of nanowires with dimensions around several micrometers with the nanofiber surface roughness at the nanoscale. We study here hierarchical photoactive core-shell nanostructured surfaces, which wetting behaviour can be easily tuned. Understanding the mechanism of water condensation on such nanofibers at the nanoscale is crucial to design efficient systems. In this presentation, we identify their hydrophobic/hydrophilic behaviour and discuss the water condensation mechanisms using multiscale environmental electron microscopy.
Methods
Liquid-phase electron microscopy can be carried out with different systems. We used a dedicated environmental scanning electron microscope (ESEM) and an environmental transmission electron microscope (ETEM), in which different hydration states can be reached by controlling the sample temperature and the water vapor pressure.
TiO_2 core-shell nanowires were fabricated by vacuum and plasma assisted deposition techniques according to the soft template method [5]. In order to obtain the water repellent character, surface functionalization by fluorine-based grafting of the oxide surface has been employed [1]. Hydrophobic nanowires were collected by scratching the substrate and were dry-deposited onto a grid with a holey carbon membrane. The fibers were either analyzed as such, or plasma-treated to become hydrophilic. During the experiments, care was taken to minimize irradiation damage and preserve the hydrophilic/hydrophobic nature. An image processing method was developed to highlight the changes brought about by water condensation.
Results
Experiments in ESEM were performed in the STEM mode (see Figures 1a and d). Under similar conditions, where water condensates on the holey carbon membrane, the hydrophilic nature of the plasma-treated nanowires can clearly be evidenced: they are systematically surrounded by water. On the contrary, water droplets are visible on the carbon membrane but not on hydrophobic nanostructures. The presence of water onto hydrophilic surfaces but not on hydrophobic ones could be confirmed at the nanoscale using similar thermodynamic conditions in ETEM (see Figures 1b and e). The experiments were continued until water was visible around both types of nanowires (see Figures 1c and f).
Conclusion
ESEM images, obtained on a large number of core-shell nanowires, enable us to assess the reproducibility of results obtained at nanometric scale in ETEM on isolated fibers. Irradiation of the nanostructures with the electron beam during the experiments did not modify their hydrophilic/hydrophobic character. In fact, clear differences in behavior towards water condensation

are revealed at the nanometric scale. These differences will be discussed as a function of nanostructure and chemistry.

Acknowledgements

The authors acknowledge financial support from the CNRS -CEA ‘‘METSA’’ French network (FR CNRS 3507) for the liquid-phase experiments at CLYM (www.clym.fr), which is also acknowledged for access to the environmental microscopes.

Figure caption

water condensation on core-shell TiO2 fibers. a, b, c) hydrophilic fibers. d, e, f) hydrophobic fibers. a, d) BF-STEM images in ESEM. b, e) BF-TEM images in ETEM at the initial state. c, f) BF-TEM images in ETEM on hydrated fibers.

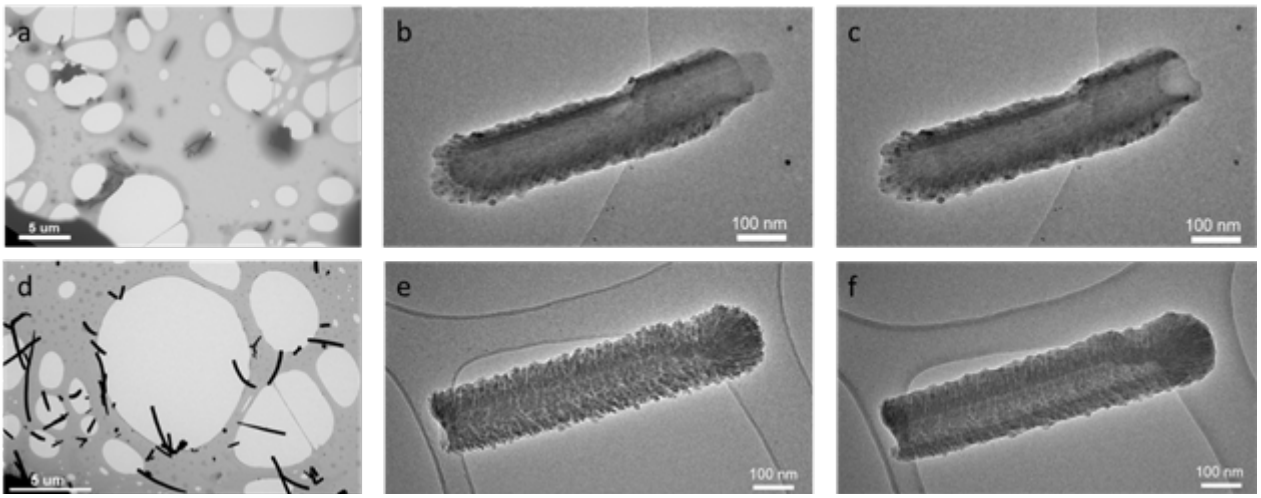

Keywords:

ESEM, ETEM, liquid, in-situ, nanowire

Reference:

[1] L. Montes et al., Adv Mater Interfaces, 2021, 8, 2100767.
[2] V. Rico et al., Appl Mater Today, 2020, 21, 100815.
[3] M. Macías-Montero et al., Langmuir, 2017, 33, 6449.
[4] M. Alcaire et al., Nanoscale, 2011,3,4554.
[5] A.N. Filippin et al., Sci. Rep. 2016, 6, 20637.

621

Rapid and large FOV mapping of 60° grains in epitaxial MX2 with a segmented detector

Dr. Ankit Nalin Mehta[1], Dr. Gerardo Martinez Alanis[1], Dr. Maxim Korytov[1], Dr. Henry Medina Silva[1], Dr. Paola Favia[1], Dr. Olivier Richard[1], Dr. Eva Grieten[1]
[1]imec, Leuven, Belgium

Poster Group 2

Owing to the rapid development in growth of synthetic MX_2 (where M is the metal and X is the chalcogenide) materials in recent years, their average grain sizes are fast approaching several tens to hundreds of micrometers [1]. Epitaxial growth on a single crystalline template is the favored approach to achieve wafer-scale and industrially compatible growth of high-quality single crystalline MX_2 monolayers. Despite the control over orientation provided by templated approaches, selective growth of domains with a single orientation while avoiding the anti-parallel orientation (or 60^o rotated domains) has proven to be challenging [2]. Inclusion of such anti-parallel domains inevitably leads to the formation of 60^o grain boundaries which are detrimental to electron mobility due to the presence of mid-gap states [3]. It is therefore necessary to develop methods to enable rapid and large field of view (FOV) mapping of the anti-parallel domains in epitaxial MX_2. We present a novel approach using segmented detector geometry to rapidly map the 60^o grain boundaries over a large FOV in epitaxially grown MX_2. This relies on the asymmetry of diffraction peak intensities which split into two families Ka and Kb due to reduced symmetry from 6-fold to 3-fold in a monolayer of MX_2 [4]. The specimens are prepared by transferring the MoS_2 from sapphire to a carbon coated TEM grid using a tape assisted method described elsewhere in detail [3]. The conventional dark-field TEM (DF-TEM) is carried out on a Thermofisher Metrios 80-200 TEM operating at 200 kV by placing the smallest objective aperture on any first order diffraction spot. A large number of images with a certain overlap are automatically acquired in a grid pattern, preprocessed, and stitched together to form a montage with significantly larger FOV. This process is repeated for the opposite diffraction spot to obtain the complementary image. The novel segmented detector approach is carried out in a Helios5 FX dual beam operated in a “STEM in SEM” setup at 2kV and equipped with a segmented annular detector. The six segments of the detector are operated such that only 3 of the 6 segments are active for the acquisition and transmitted beam is centered as shown in schematic Fig.1 a. In this mode, as the three segments are separated from each other by 120^o, the detector segments selectively collect the intensities from either the Ka or the Kb spots depending on the orientation of the grains resulting in a contrast which helps differentiate between 60^o grains in monolayer MX_2. The segmented detector approach is first tested on a small grain sample with high density of 60° twins. Fig.1(b) shows a color overlay of the two complementary images wherein the contrast in a monolayer is reversed between the two images making the layer appear either more green (0°) or more red (60^o). The boundary separating these two regions can be either a β or γ grain boundary [3]. The images are segmented using a gaussian mixture model and assigned classes to obtain statistics on 60° twin inclusion in monolayer as well as various stacking orders in bilayer MoS_2 (Fig.1(c)). The method is then applied on large grain samples and compared with the more conventional montage DF-TEM approach used so far. Fig.1(d) shows a similar color overlay obtained by montaging several DF-TEM images acquired at 200kV. The contrast between the main orientation and 60^o rotated domains is rather weak and images are noisier compared to those obtained with a segmented detector at 2kV shown in Fig. 1(e). Moreover, the stacking in bilayer cannot be uniquely identified with the conventional DF-TEM due to influence of unintended specimen tilt [4] which in case of the segmented detectors is overcome by design through radial integration. A drawback, however, is that 2kV electrons don’t have enough energy to see through the carbon support.

The segmented detector in SEM provides superior results from a large FOV in a fraction of the time it takes for montage acquisition and processing, i.e., few minutes compared to several hours or days. In addition. in bilayer, the stacking order can be easily assigned and not influenced by sample mistilt.

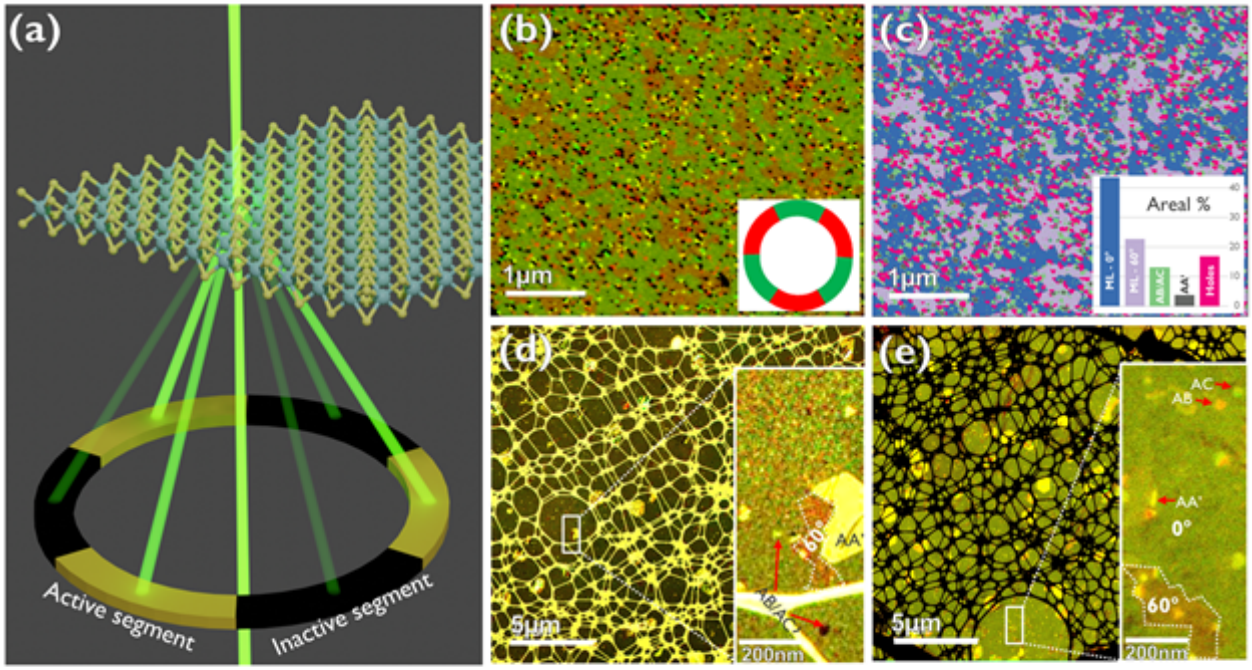

Figure 1: *(a) Schematic of six segmented annular detector on monolayer MoS_2 (b) Color overlay of the two complementary images obtained from the two modes of operation on a small grain sample. The inset shows the detector segments color coded with the same color as used in the color overlay. (c) Segmented image after clustering where the inset shows the areal percentage of various classes. Comparison between montage DF-TEM acquired on Metrios @ 200kV (d) and segmented detector STEM on Helios5@ 2kV (e) on different parts of the same large grain sample. Insets are magnified regions.*

Keywords:

Segmented, Grains, Epitaxial, MX_2, Stacking.

Reference:

1. Chen, J. et al. Advanced Science 3, (2016).
2. Dumcenco, D. et al. ACS Nano 9, 4611–4620 (2015).
3. Nalin Mehta, A. et al. The Journal of Physical Chemistry C 124, 6472–6478 (2020).
4. Nalin Mehta, A. et al. Nanotechnology 31, 445702 (2020).

626

Nanotubes of (SmxY1-x)S-TaS2 based on Quaternary Misfit Layered Compounds (MLCs)

Mr Mohammad Furqan[1,2], Dr Simon Hettler[1,2], Dr MB Sreedhara[3], Dr Reshef Tenne[4], Dr Raul Arenal[1,2,5]
[1]Laboratorio de Microscopias Avanzadas (LMA), Universidad de Zaragoza, Zaragoza, Spain, , , [2]Instituto de Nanociencia y Materiales de Aragón (INMA), Universidad de Zaragoza, , , Spain, [3]Solid State and Structural Chemistry Unit, Indian Institute of Science, Bengaluru, India,, , , [4]Department of Molecular Chemistry and Materials Science, Weizmann Institute of Science, Rehovot, Israel, , , [5]ARAID Foundation, Zaragoza, Spain, ,

Poster Group 2

Background including aims.
Misfit layered compounds (MLCs) have garnered considerable attention due to their fascinating chemistry and properties [1]. MLCs consist of two different layered oxides or chalcogenides that are stacked alternately along their c direction. The MLC stack is composed of metal chalcogenide (MX) which possesses a distorted rock salt structure and a transition metal dichalcogenide (TX2) which crystallizes in a hexagonal structure [1,2]. The properties of MLCs are determined by the chemical and structural interplay between MX and TX2. MLC-nanotubes (NTs) synthesized via the chemical vapor technique (CVT) offer potential applications in thermoelectrics due to the complementary properties of the two layered compounds [1]. Recently, a modified synthesis method of MLC-NTs has permitted the introduction of additional elements to form a quaternary compound starting from LaS-TaS2 [3,4]. Here, we present an in-depth electron microscopy analysis of the novel family of (SmxY1-x)S-TaS2 nanostructures [5]. In this novel family, the partial exchange of Sm(S) by Y(S) provides a pathway for the fine control of the MLC structure and its properties.

Methods
MLC-NTs made of (SmxY1-x)S-TaS2 were synthesized via the CVT technique [1-3] by varying the precursor proportions of Sm vs Y between x=0 to x=1. The samples will be designated by the Sm percentage, Sm20 corresponds to (Sm0.2Y0.8)S-TaS2 and similarly. To analyze these NTs, different TEM techniques (high-resolution (scanning)TEM (HR(S)TEM) imaging, selected area electron diffraction (SAED), electron energy loss spectroscopy (EELS) and energy-dispersive X-ray spectroscopy (EDS)) were performed. These TEM studies were developed using two aberration corrected Thermo Fisher Scientific Titan microscopes. Raman spectroscopy has also been employed to study these NTs.

Results
The detailed analysis of the NTs by electron microscopy and different spectroscopies verifies the partial substitution of Sm by Y in the (Sm,Y)S subsystem and also reveals the structural changes when compared to the pure SmS- or YS-TaS2 MLC-NTs. These structural changes can be linked to the slight difference in the lattice parameters of SmS and YS. Figure (a) corresponds to the SAED pattern of Sm40 (Sm0.4Y0.6)S-TaS2 sample where the reflections marked by the green dotted circles represent the reflections from (Sm,Y)S and reflections marked by red dotted circles represent the TaS2 subsystems, respectively. The c-axis periodicity (1.13 nm) is indicated by yellow arrows. The c-axis is perpendicular to the tube axis, which is given by the purple double arrow. A high-angle annular dark-field STEM image of a Sm80 NT is shown in Figure (b) and illustrates the repetitive layer stacking of (Sm,Y)S and TaS2. The inset of (b) shows a low-magnification TEM image of the Sm80 NT. Figure (c) depicts a Raman spectrum acquired from an individual Sm80 NT, which was fitted using a set of Lorentz functions. In a vibrational spectroscopy such as Raman, a Lorentz line shape is used to model pure vibrational modes, which only undergo homogeneous line broadening. Raman spectroscopy

measurements of the whole set of samples reveal the tunability of the vibrational properties of these NTs. The study of the elemental composition of these NTs by EDS is shown exemplary for a NT of the Sm80 sample in Fig 1(d), which reveals an average atomic weight percentage of around 17 at. % Ta, 24 at. % Sm+Y, and 59 at. % S. The EDS results obtained from all the samples show that the substitution of Sm by Y is homogeneous and in-phase with structural changes in the lattice parameter. Further low-loss EELS studies and electric properties of these samples are in progress. These investigations will also provide a more complete understanding of these systems including their electronic/optoelectronic properties.

Conclusion

In summary, through comprehensive electron microscopy and spectroscopy analysis, we have shown the successful synthesis of an unexplored group of quaternary MLC-nanotubes. The MLC structure is observed in all samples and the compositional analysis shows a homogeneous substitution of Sm by Y.

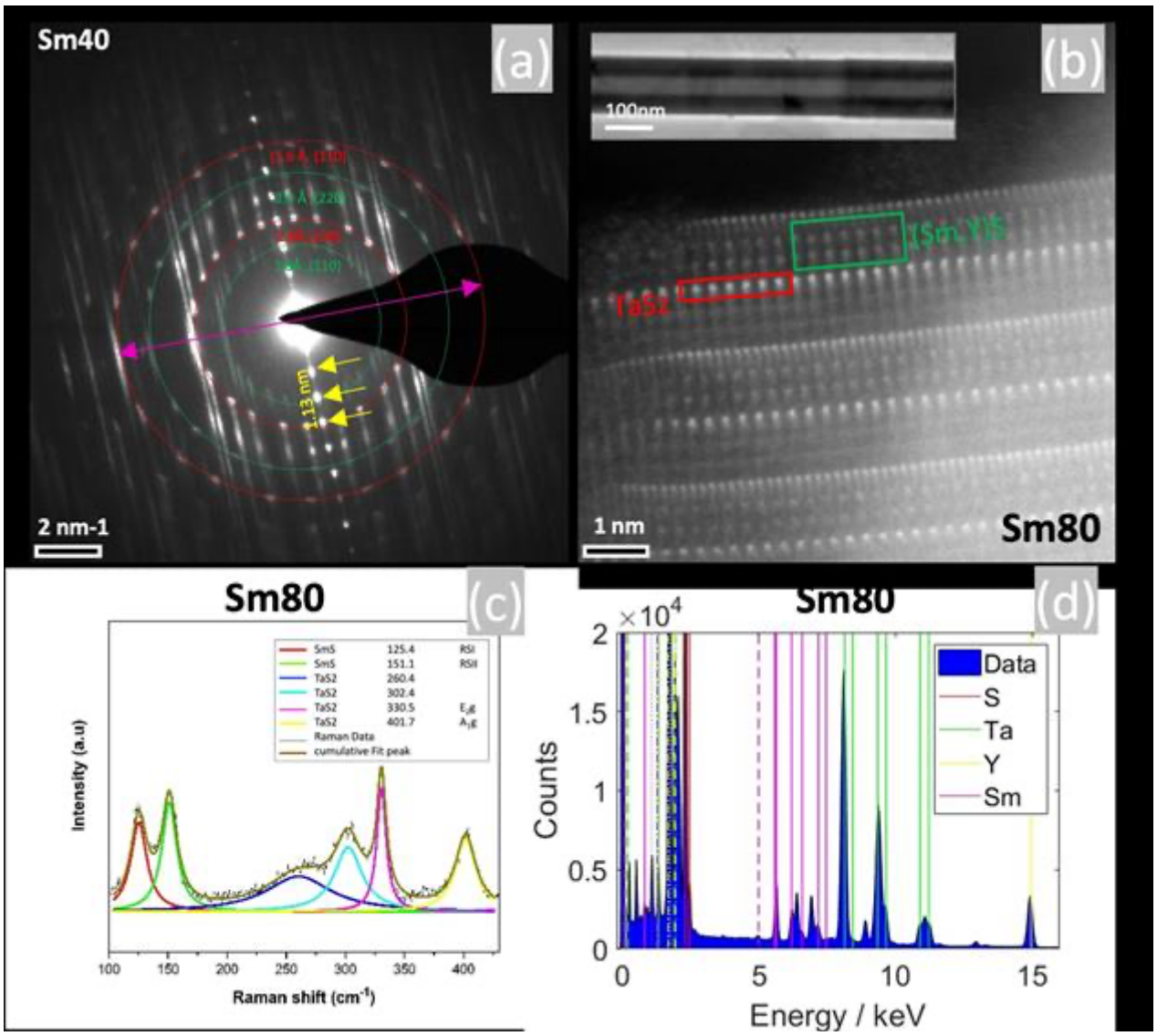

Keywords:

Inorganic-nanotubes, misfit-layered compounds-(MLC), Structural Analysis

Reference:

References

1 - M. Serra, R. Arenal, R. Tenne, (2019). Nanoscale 11, 8073-8090. https://doi.org/10.1039/C9NR01880H

2 – M.B Sreedhara et al. Chemistry of Materials 2022 34 (4), 1838-1853. https://doi.org/10.1021/acs.chemmater.1c04106
4 - S. Hettler et al. (2020), ACS Nano 14, 5, 5445–5458. https://doi.org/10.1021/acsnano.9b09284
3 - G. Radovsky et al. (2016). J Mater Chem C 4, 89–98. 10.1039/C5TC02983J
5- M. Furqan, S. Hettler, MB Sreedhara, R. Tenne, R. Arenal. To be submitted.
Funding: Research supported by the Spanish MICIU (PID2019-104739GB-100/AEI/10.13039/501100011033) and the Government of Aragon (DGA) through the project E13_23R.

663

Characterisation of 2-D chalcogenides utilising Electron Microscopy techniques and Density Functional Theory.

Dr Danielle Douglas-Henry[1,2], Mr. Ilias Oikonomou[1,2,4], Dr. Tigran Simonian[1,2], Dr. Jonathan J. P. Peters[1,3], Dr. Thomas Brumme[4], Prof. Thomas Heine[4], Prof. Valeria Nicolosi[1,2]
[1]Advanced Microscopy Lab, Trinity College Dublin, Dublin, Ireland, [2]School of Chemistry, Trinity College Dublin, Dublin, Ireland, [3]School of Physics, Trinity College Dublin, Dublin, Ireland, [4]Chair of Theoretical Chemistry, TU Dresden, Dresden, Germany

Poster Group 2

Two-dimensional material systems have garnered much attention since the first isolation of graphene[1]. Due to their low dimensionality, these materials exhibit interesting properties such as thickness dependent bandgaps [2] and magic twist-angle superconductivity [3], making them attractive for both experimentalists and theorists alike with much promise for industry application. In this study we focus on the utilization of electron microscopy techniques to experimentally characterise various chalcogen based 2D systems with the intent to compare it to Density Functional Theory (DFT) simulations.

Of particular interest for this study is the effect of various structural changes that influence the electronic structure. Firstly, a twist-angle induced Rashba splitting at the VBM in van der Waals heterostructures and secondly, the influence of various point defect complexes and their effect on the electronic band structure.

Herein, the angular dependence of GaS/GaSe heterostructures are theoretically studied via DFT calculations and compared to preliminary experimental studies. Electronic band structure calculations were performed on a series of twisted GaS/GaSe heterostructures with and without spin-orbit coupling (SOC) to investigate the effect of band splitting. The mobility of point defects in exfoliated PtSe2 was correlated using the climbing image Nudged Elastic Band method incorporated in the FHI-aims all-electron code. The atomistic models observed experimentally were geometrically optimized using FHI-vibes.

Bulk GaS and GaSe crystals (2D Semiconductors, Inc.) were exfoliated using the typical scotch-tape method. Flakes were carefully stacked and transferred using an all-dry viscoelastic stamping technique. In the study of point defect analysis and mobility, PtSe2 (HQ Graphene) was exfoliated through mechanical exfoliation to achieve few layer flakes. Scanning Transmission Electron Microscopy (STEM) imaging was performed using a FEI Titan 80-300 at 300 kV and a Nion UltraSTEM at 60 kV and 200 kV. STEM images were recorded with a high angle annular dark-field (HAADF) detector on a Nion UltraSTEM. Multi-frame imaging was utilised to reduced beam damage, while custom scan patterns minimised beam induced defect motion.

Results from first-principles calculations predict that GaS/GaSe heterostructures demonstrate the presence of Rashba spin splitting effects and an angular dependent band-gap shift. Rashba splitting was found to be asymmetric along different high symmetry paths. Heterostructures were fabricated at various twist angles and imaged using HAADF STEM with thickness measurements being performed via PACBED simulation. Low voltage HAADF-STEM was further utilised to investigate point defects inherent in exfoliated PtSe2. Many examples of Se/Pt vacancies and antisites were present along with various combinations of the two. Mobile defects were observed in few layer regions. Fast frame image series were utilized to study the hopping nature of the defects to determine energetically favorable pathways.

The collaborative use of theoretical modeling via DFT and experimental characterisation through TEM was used to characterise novel 2D material systems.

Keywords:

2-D Materials, Heterostructures, STEM, DFT

Reference:

[1] K. S. Novoselov et al., “Electric Field Effect in Atomically Thin Carbon Films”. Science, 306, 666-669 (2004).
[2] Chaves, A. et al., “Bandgap engineering of two-dimensional semiconductor materials.”, npj 2D Mater Appl, 4, 29 (2020).
[3] Cao, Y. et al., “Unconventional superconductivity in magic-angle graphene superlattices.”, Nature, 556, 43–50 (2018).

665

Ptychography Optimization for Atomic Analysis of Bending Mode in Bilayer Transition Metal Dichalcogenide Translational Motion

Yunyeong Chang[1], Dr Jinseok Ryu[3], Prof Hyobin Yoo[2], Prof Heung Nam Han[1], Prof Miyoung Kim[1]
[1]Seoul National University, , Republic of Korea, [2]Sogang University, , Republic of Korea, [3]Diamond Light Source Ltd, , United Kingdom

Poster Group 2

Background incl. aims
Twisted two-dimensional transition metal dichalcogenides, have exhibited a variety of interlayer coupling phenomena and novel structural reconstructions, leading to modifications in electronic properties. However, the atomic-scale transitions within these reconstructed structures could be observed only on scales of a few nanometers, with transitional motions requiring differentiation at sub-nanometer scales. Thus, atomic scanning transmission electron microscopy-based methods are indispensable. However, due to the beam sensitivity and instability of structures, acquiring noise-free images has posed a challenge. In this study, we utilized ptychography as a fitting experimental methodology to investigate these twisted structures.
Methods
In our study, we employed suspended homobilayer WSe2 as the substrate for sample preparation. The fabrication process involved a tear and stack method, utilizing monolayers derived via the Scotch tape technique. For the analysis, we utilized ptychographic algorithms available in the abTEM and Py4DSTEM software packages. Both multislice and single-slice calculations were performed to analyze the data. This methodology allowed for a comprehensive examination of the atomic transitions within the suspended twisted 2D structures of the WSe2 samples.
Results
By adjusting various parameters for ptychography, we have identified the most stable conditions for examining suspended bilayer bending mode samples. The optimization of ptychographic conditions, including dose, focus, scan size, and other experimental parameters, has been pursued to secure the most effective imaging results. Under these optimal conditions, an atomistic analysis of the suspended bending mode twisted samples was conducted. Remarkably, the rippling domain boundaries, which had been theoretically anticipated for the bending mode, were directly observed through ptychography under low dose conditions, facilitating stable image acquisition. Furthermore, we have delineated the transition from the vertex AA core to the saddle point across varying angles, a phenomenon previously unobserved in High-Angle Annular Dark-Field (HAADF) imaging.
Conclusions
In conclusion, this study has leveraged ptychography to unveil novel insights into the atomic-scale transition of twisted two-dimensional transition metal dichalcogenides, achieving imaging clarity under optimized conditions. Our methodical approach in adjusting ptychographic parameters has enabled the direct observation of rippling domain boundaries and the intricate transition from the vertex AA core to the saddle point. These findings not only overcome previous limitations posed by beam sensitivity and structural instability but also significantly enhance our understanding of the structural and electronic properties of these complex materials, paving the way for future explorations and applications.

Keywords:

Ptychography, Twisted 2D materials, 4DSTEM

Reference:

1.Weston, Astrid, et al. "Atomic reconstruction in twisted bilayers of transition metal dichalcogenides." Nature nanotechnology 15.7 (2020): 592-597.
2. Savitzky, Benjamin H., et al. "py4DSTEM: A software package for four-dimensional scanning transmission electron microscopy data analysis." Microscopy and Microanalysis 27.4 (2021): 712-743.
3. Madsen, Jacob, and Toma Susi. "The abTEM code: transmission electron microscopy from first principles." Open Research Europe 1 (2021).

671

Influence of low-pressure atmosphere in the pores formed in hexagonal boron nitride under electron irradiation

Umair Javed[1,2], Clara Kofler[1,2], Clemens Mangler[1], Jani Kotakoski[1]
[1]University of Vienna, Faculty of Physics, Vienna, Austria, [2]University of Vienna, Vienna Doctoral School in Physics, Vienna, Austria

Poster Group 2

Background incl. aims
During (scanning) transmission electron microscopy ((S)TEM), the energetic electrons used for imaging can lead to damage in the sample. Electron knock-on damage caused by elastically scattered electrons is the best known of such damaging mechanisms, and has been studied extensively also for 2D materials. In contrast, less is known about the damage mechanisms in insulating materials, such as hexagonal boron nitride (hBN) . In early studies, it was shown that extended irradiation leads predominantly to the formation of triangular nanopores. These pores and their triangular shape were suggested to arise from direct interaction between the electrons and the material, and it was shown that the dominated zig-zag edges were nitrogen terminated.
Methods
The Nion UltraSTEM 100 microscope integrated into our experimental setup at the University of Vienna allows experiments at low pressure atmosphere between ultra-high-vacuum (UHV) ~ 1x10-10 mbar and 4x10-6 mbar by carefully leaking the desired gas into the column. Measurements at varying pressures have already shown that the partial pressure of different gases can have an influence in the damage observed in graphene. Specifically, it was shown that different graphene edges dominate under an oxygen atmosphere and in UHV.
Results
Here hBN was imaged at UHV and up to an oxygen pressure of around 2x10-8 mbar. The most prominent finding was that the shape of pores that appeared under electron irradiation depends on the oxygen partial pressure. As an example, medium angle annular dark field (MAADF) images are shown in figure. In UHV the pore shape is round with no preference of either boron or nitrogen termination, whereas triangular pores emerge with rising oxygen partial pressure, with edges dominated by nitrogen atoms. The rate of pore growth also increases with increase in oxygen partial pressure in microscope column, and no any pore growth was observed when the sample was exposed to air without electron irradiation.
Conclusion
The results suggest that the shape of the pores observed in the earlier studies was determined by the composition of the microscope vacuum. The pores grow only under electron irradiation and their shape depends on the vacuum conditions.

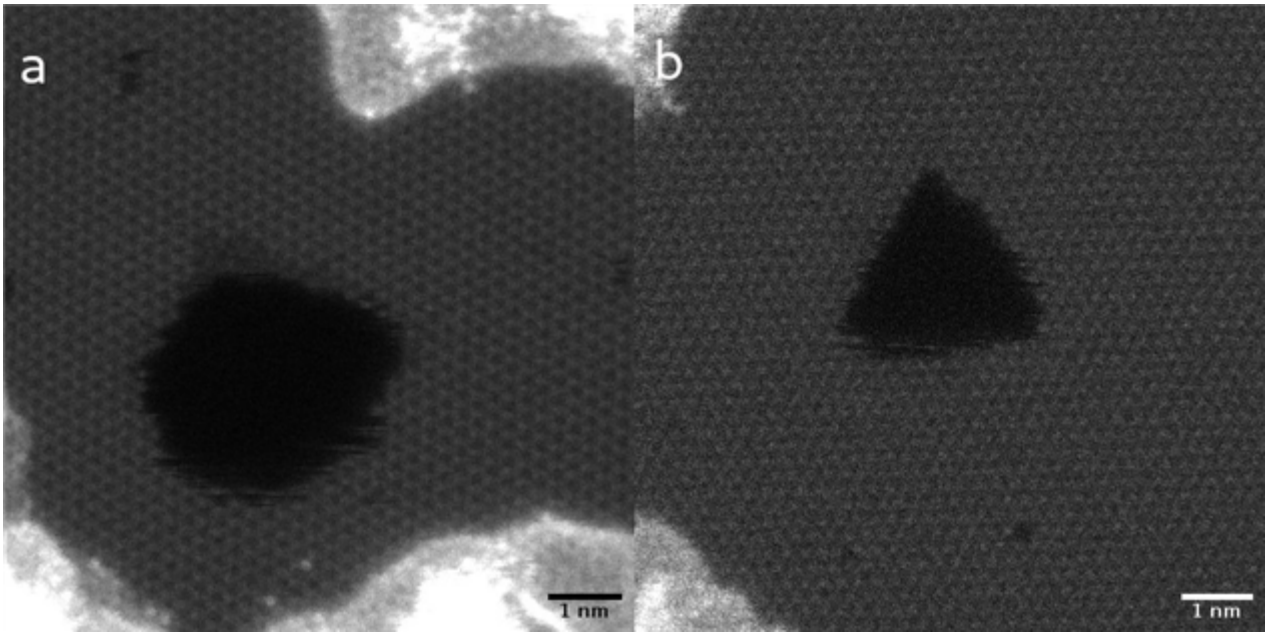

Keywords:

hBN, in-situ STEM, 2D Materials

Reference:

[1] Susi et al, Nature Reviews Physics 1, 397 (2019)
[2] Bui et al, Small 2301926 (2023)
[3] Kotakoski et al, Physical Reviews B 82, 113404 (2010)
[4] Jin et al, Physical review letters 102, 195505 (2009)
[5] Mangler et al, Microscopy and Microanalysis 28, 2904 (2022)

769

Atomic-resolution investigation of 2D hematene

Phd Jana Dzibelova[1], Jan Filip[2], Jani Kotakoski[1]
[1]University of Vienna, Vienna, Austria, [2]Czech Advanced Technology and Research Institute, Palacky University, Olomouc, Czech Republic

Poster Group 2

2D materials have attracted scientific research for decades, since they posses distinct physico-chemical properties compared to their 3D counterparts due to quantum confinement. These atomically thin structures such as graphene, hBN, etc. are typically based on so-called van der Waals systems. These 3D counterparts are defined by strong bonds oriented in-plane and solely weak bonding interaction between the layers.

However, 2D materials can also be created from a parent material with strong bonding interactions in all three directions. For these, it is significantly more complicated to cleave them into individual layers. After cleavage into atomically thin layer, the non-van der Waals 2D materials could offer a playground to explore the changes in properties induced by dimensionality restriction. Recently, a new member of these non-van der Waals 2D materials has been introduced: hematene, the 2D form of α-Fe_2O_3 [1].

The dimensional confinement of hematene structure is expected to introduce intrinsic strain to the lattice. This distortion of interatomic positions affects electronic configuration and therefore the magnetic, electronic and optical behavior of the system [2]. Here, we employ transmission electron microscopy and selected area electron diffraction to investigate the atomic structure and distortions of the lattice in thin hematene sheets with the aim to quantify the intrinsic strain to facilitate the physical description of the material.

Keywords:

Hematene, Iron oxides, 2D

Reference:

1] A. Puthirath Balan, S. Radhakrishnan, C. F. Woellner, S. K. Sinha, L. Deng, C. Reyes, B. M. Rao, M. Paulose, R. Neupane, A. Apte, V. Kochat, R. Vajtai, A. R. Harutyun- yan, C.-W. Chu, G. Costin, D. S. Galvao, A. A. MartÃ-, P. A. Aken, O. K. Varghese, C. S. Tiwary, A. Malie Madom Ramaswamy Iyer, and P. M. Ajayan, Nat. Nanotechnol. 13 (2018) 602.
[2] S. Maiti, K. Maiti, M. T. Curnan, K. Kim, K.-J. Noh, and J. Woo Ha, Energy Environ. Sci. 14 (2021) 3717.

776

Structural phase transition induced microstructure changes in V2O3 based hybrid magnetic heterostructures

Prof. Unnar Arnalds[1]
[1]University of Iceland, Reykjavik, Iceland

Poster Group 2

Vanadiumsesquioxide (V_2O_3) stands out in the realm of transition metal oxides for its distinctive and multifaceted phase transitions, offering a rich ground for exploration in the context of structural, electrical and magnetic properties [1, 2]. At room temperature, V_2O_3 is in a rhombohedral phase, exhibiting metallic properties and upon cooling to below ~150 K it undergoes a structural phase transition to an insulating monoclinic phase. Through the transition the material also changes from a paramagnetic state to a low temperature antiferromagnetic state and has been observed to induce an exchange bias into overlying magnetic layers [3].

In this work we present an investigation on the interplay between the microstructure of V_2O_3 thin films, deposited using reactive dc magnetron sputtering, and their structural properties during the phase transition. Specifically, we examine the changes in the microstructure during the phase coexistence region of the V_2O_3 layer and how these changes correlate with alterations in the magnetic properties of overlying magnetic layers in V_2O_3/Ni heterostructures [4].

Using scanning transmission electron microscopy (STEM) using high-angle annular dark-field (HAADF-STEM) imaging, energy dispersive x-ray analysis (STEM-EDX) and electron energy loss spectroscopy (EELS) we investigate the stoichiometric composition of the films and confirm their crystalline quality at the sub-nm lateral scale and observe an atomically flat interface between the Al_2O_3 substrate and the V_2O_3 layer, as well as a sharp interface between V_2O_3 and the overlying magnetic Ni layer.

The simultaneous presence of two phases in V_2O_3 during its structural phase transition was identified with temperature dependent high resolution x-ray diffraction measurements performed at the BM28 (XMaS) beamline at the European Synchrotron Radiation Facility (ESRF) in Grenoble, France. The measurements reveal an increase in surface roughness during the transition which is attributed to the coexistence of the two phases in different regions of the film. During the phase coexistence region we observe a concomitant increase in the coercivity of the magnetic layer correlated with the increased roughness of the V_2O_3 surface.

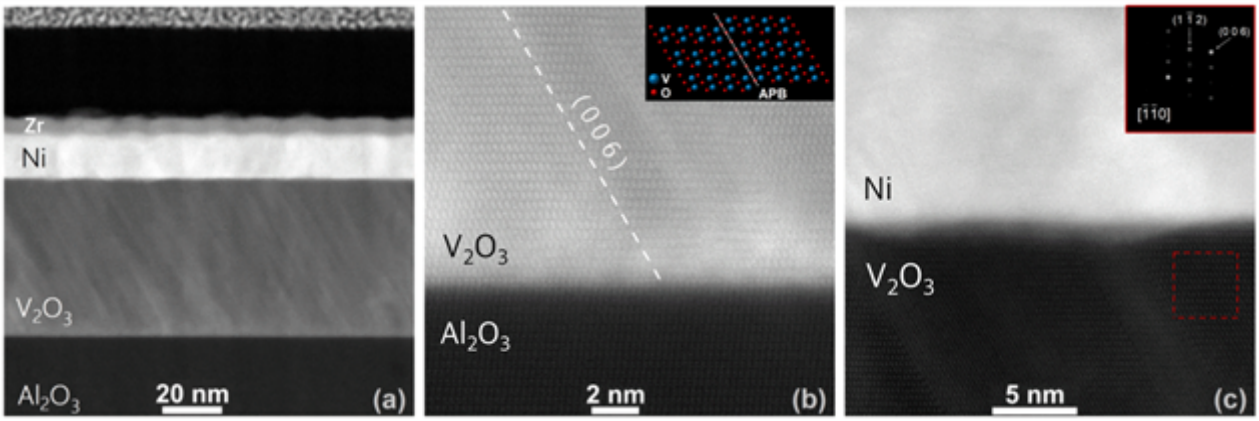

Keywords:

Phase transitions, STEM, Magnetism, Heterostructures

Reference:

[1] Controlling metal–insulator transitions in reactively sputtered vanadium sesquioxide thin films through structure and stoichiometry. E.B. Thorsteinsson, S. Shayestehaminzadeh, A.S. Ingason, F. Magnus, and U.B. Arnalds. Scientific Reports 11, 6273 (2021).
[2] Tuning metal-insulator transitions in epitaxial V_2O_3 thin films. E.B. Thorsteinsson, S. Shayestehaminzadeh, and U.B. Arnalds. Applied Physics Letters, 112, 161902 (2018).
[3] Reversible exchange bias in epitaxial V_2O_3/Ni hybrid magnetic heterostructures. K. Ignatova, E.B. Thorsteinsson, B.A. Jósteinsson, N. Strandqvist, C. Vantaraki, V. Kapaklis, A. Devishvili, G.K. Pálsson, an U.B. Arnalds. Journal of Physics: Condensed Matter 34, 495001 (2022).
[4] Phase coexistence induced surface roughness in V_2O_3/Ni magnetic heterostructures. K. Ignatova, E. Vlasov, S. D. Seddon, N. Gauquelin, S. Bals, T. P. A. Hase, and U. B. Arnalds. APL Materials 12 (2024). doi: 10.1063/5.0195961

777

In situ closed-cell microscopy study of Ti3C2Tz MXene

Phd Student Changjie Huang[1], Asst. Prof. Leiqiang Qin[2], Prof. Johanna Rosen[2], Prof. Per O.Å Persson[1], Assoc. Prof. Justinas Palisaitis[1]
[1]Thin Film Physics Division, Department of Physics, Chemistry and Biology (IFM), Linköping University, Linköping, Sweden, [2]Material Design Division, Department of Physics, Chemistry and Biology (IFM), Linköping, Sweden

Poster Group 2

Background incl. aims
MXenes are referred to as 2D transition metal carbides, nitrides, or carbonitrides and first reported in 2011. They are described by the general Mn+1XnTz (n=1,2 or 3) formula, where M is a transition metal, X stands for C or/and N and Tz represents the surface terminating species [1]. Owning to their structural and chemical diversity, MXenes enable the wide variety of properties, which makes them competitive in a wide range of applications including catalysis, energy storage, supercapacitors, sensors, spintronics, thermoelectrics and beyond [2].
Despite the immense progress in the field of MXene, a number of unresolved challenges remains, including a fundamental understanding of post synthesis stability and processing of MXenes at application relevant environments. In particularly, the detailed knowledge of the degradation mechanisms, in the environment(s) containing presence of water, is highly debated in the literature.
Previously, transmission electron microscopy (TEM) studies provided atomic level insights into the Ti3C2Tz structure and surfaces [3]. In situ TEM was applied to study Ti3C2Tz surface termination alternations [4]. Post synthesis in situ gas heating treatments of Ti3C2Tz was successfully demonstrated via environmental TEM studies [5].
The introduction of environmental closed-cell holders brings unique opportunities for the study of MXenes under real-world conditions closer to practical processing and/or application environments inside TEM.
In this study, we employed in situ closed-cell TEM to study the role of water on thermal stability of Ti3C2Tz MXene sheets during annealing in Ar or N2 atmospheres.

Methods
Ti3C2Tz MXene sheets were synthesized by the previously reported MILD method in which selective extraction of Al from Ti3AlC2 MAX phase and delamination of the layers were achieved using hydrochloric acid and lithium fluoride.
In situ experiments were performed in the Linköping double Cs corrected FEI Titan3 60-300, using a closed-cell gas heating system (Protochips, Atmosphere). During pretreatment, holder was pumped and purge with Ar to remove residual gasses from the holder tip. This was followed by continues Ar flow while annealing at 300°C for 60 min. In situ heating of Ti3C2Tz was accomplished by increasing the temperature from 600 °C to 1000 °C in steps of 100 °C and holding for 15 min at each step while continuously flowing Ar (inert) or N2 (no affinity for Ti3C2Tz) gasses at 760 torr.
After each heating step the temperature was lowered to 300 °C for acquisition of images and spectra. The structural and chemical evolution of Ti3C2Tz was tracked using high angle annular dark field STEM (HAADF-STEM) imaging and electron energy loss spectroscopy (EELS). A residual gas analyser (RGA) was used to monitor the status of the experimental and residual gases in the system.

Results
To explore the effect of water on thermal stability at atmospheric pressures, Ti3C2Tz was annealed to high temperatures while been kept at flowing Ar (99,9999% purity) or N2 (99,9999% purity) gasses at 760 torr.

The graph shows a series of HAADF-STEM images recorded during in situ heating of Ti3C2Tz during exposure to flowing N2 at 760 Torr. The morphology of Ti3C2Tz sheets remained largely unaffected up to 800 °C as observed by imaging and tracking Ti-L2,3 fine edge structure evolution. At 900 °C the morphology of the Ti3C2Tz changed entirely as it decomposed to titanium oxide nano particles. At 1000 °C the titanium oxide particles coarsened while the amorphous SiN window undergone the crystallization.
Independent of the applied atmosphere (Ar or N2), the decomposition of Ti3C2Tz resulted in the formation to titanium oxide nanoparticles at high temperatures. Water pressure decrease, achieved via extensive baking of the system, from ~3x10-7 torr to ~6x10-9 torr delayed titanium oxide particle formation and coarsening by more than 100 °C. The lower water level also suppressed SiN window crystallization at 1000 °C. Thus, the oxidation is suggested to occur from the residual water present in the system while the thermal activation offset for oxidation could be directly linked to the water pressure level.

Conclusions
The study uncovered the effect of water on thermal behaviour of Ti3C2Tz during annealing at Ar or N2 atmospheres. Residual water has the detrimental effect on the offset of the observed oxidation phenomena. Consequently, obtained results increase understanding of factors and conditions responsible for Ti3C2Tz environmental stability. As important, study highlights the importance of water level control for MXene gas reaction experiments using in situ closed-cell TEM and beyond.

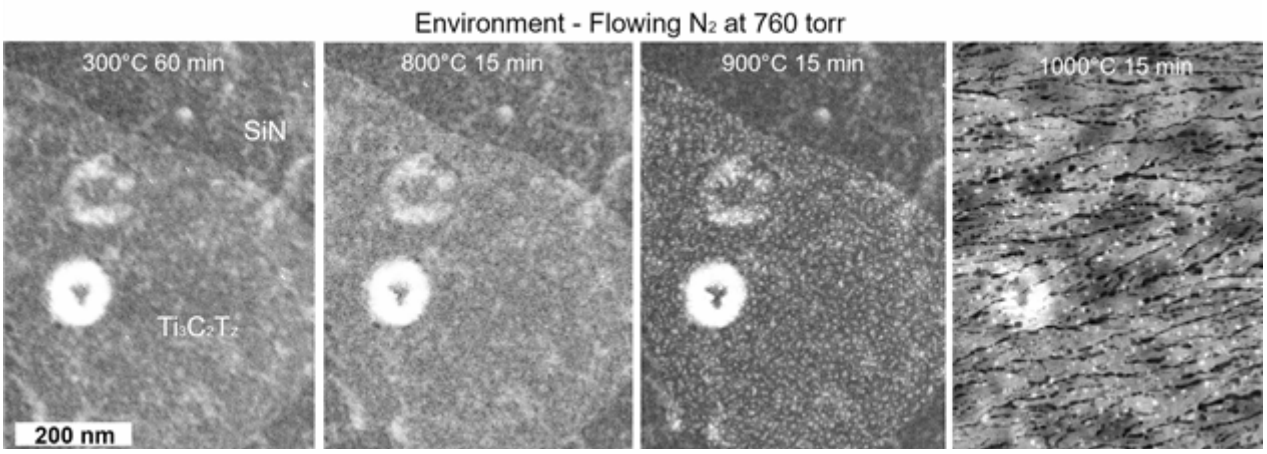

Keywords:

MXene, insitu closed-cell, thermal stability

Reference:

[1] M. Naguib et al., Advanced Materials 23, 4248 (2011).
[2] Y. Gogotsi and B. Anasori, ACS Nano 13, 8491 (2019).
[3] L. H. Karlsson et al., Nano Letters 15, 4955 (2015).
[4] I. Persson et al., 2D Materials 5, 015002 (2017).
[5] I. Persson, et al., Advanced Functional Materials 30, 1909005 (2020).

805

Nanotubes of (SmxY1-x)S-TaS2 based on Quaternary Misfit Layered Compounds (MLCs)

Mr Mohammad Furqan[1], Dr Simon Hettler[1,2], Dr MB Sreedhara[3], Dr Reshef Tenne[4], Dr Raul Arenal[1,2,5]
[1]Laboratorio de Microscopias Avanzadas (LMA), Universidad de Zaragoza, Zaragoza, Spain, , ,
[2]Instituto de Nanociencia y Materiales de Aragón (INMA), Universidad de Zaragoza, Zaragoza, Spain, , , [3]Solid State and Structural Chemistry Unit, Indian Institute of Science, Bengaluru, India,, , ,
[4]Department of Molecular Chemistry and Materials Science, Weizmann Institute of Science, Rehovot, Israel, , , [5]ARAID Foundation, Zaragoza, Spain, ,

Poster Group 2

Background including aims.
Misfit layered compounds (MLCs) have garnered considerable attention due to their fascinating chemistry and properties [1]. MLCs consist of two different layered oxides or chalcogenides that are stacked alternately along their c direction. The MLC stack is composed of metal chalcogenide (MX) which possesses a distorted rock salt structure and a transition metal dichalcogenide (TX2) which crystallizes in a hexagonal structure [1,2]. The properties of MLCs are determined by the chemical and structural interplay between MX and TX2. MLC-nanotubes (NTs) synthesized via the chemical vapor technique (CVT) offer potential applications in thermoelectrics due to the complementary properties of the two layered compounds [1]. Recently, a modified synthesis method of MLC-NTs has permitted the introduction of additional elements to form a quaternary compound starting from LaS-TaS2 [3,4]. Here, we present an in-depth electron microscopy analysis of the novel family of (SmxY1-x)S-TaS2 nanostructures [5]. In this novel family, the partial exchange of Sm(S) by Y(S) provides a pathway for the fine control of the MLC structure and its properties.

Methods
MLC-NTs made of (SmxY1-x)S-TaS2 were synthesized via the CVT technique [1-3] by varying the precursor proportions of Sm vs Y between x=0 to x=1. The samples will be designated by the Sm percentage, Sm20 corresponds to (Sm0.2Y0.8)S-TaS2 and similarly. To analyze these NTs, different TEM techniques (high-resolution (scanning)TEM (HR(S)TEM) imaging, selected area electron diffraction (SAED), electron energy loss spectroscopy (EELS) and energy-dispersive X-ray spectroscopy (EDS)) were performed. These TEM studies were developed using two aberration corrected Thermo Fisher Scientific Titan microscopes. Raman spectroscopy has also been employed to study these NTs.

Results
The detailed analysis of the NTs by electron microscopy and different spectroscopies verifies the partial substitution of Sm by Y in the (Sm,Y)S subsystem and also reveals the structural changes when compared to the pure SmS- or YS-TaS2 MLC-NTs. These structural changes can be linked to the slight difference in the lattice parameters of SmS and YS. Figure (a) corresponds to the SAED pattern of Sm40 (Sm0.4Y0.6)S-TaS2 sample where the reflections marked by the green dotted circles represent the reflections from (Sm,Y)S and reflections marked by red dotted circles represent the TaS2 subsystems, respectively. The c-axis periodicity (1.13 nm) is indicated by yellow arrows. The c-axis is perpendicular to the tube axis, which is given by the purple double arrow. A high-angle annular dark-field STEM image of a Sm80 NT is shown in Figure (b) and illustrates the repetitive layer stacking of (Sm,Y)S and TaS2. The inset of (b) shows a low-magnification TEM image of the Sm80 NT. Figure (c) depicts a Raman spectrum acquired from an individual Sm80 NT, which was fitted using a set of Lorentz functions. In a vibrational spectroscopy such as Raman, a Lorentz line shape is used to model pure vibrational modes, which only undergo homogeneous line broadening. Raman spectroscopy measurements of the whole set of samples reveal the tunability of the vibrational properties of these

NTs. The study of the elemental composition of these NTs by EDS is shown exemplary for a NT of the Sm80 sample in Fig 1(d), which reveals an average atomic weight percentage of around 17 at. % Ta, 24 at. % Sm+Y, and 59 at. % S. The EDS results obtained from all the samples show that the substitution of Sm by Y is homogeneous and in-phase with structural changes in the lattice parameter. Further low-loss EELS studies and electric properties of these samples are in progress. These investigations will also provide a more complete understanding of these systems including their electronic/optoelectronic properties.

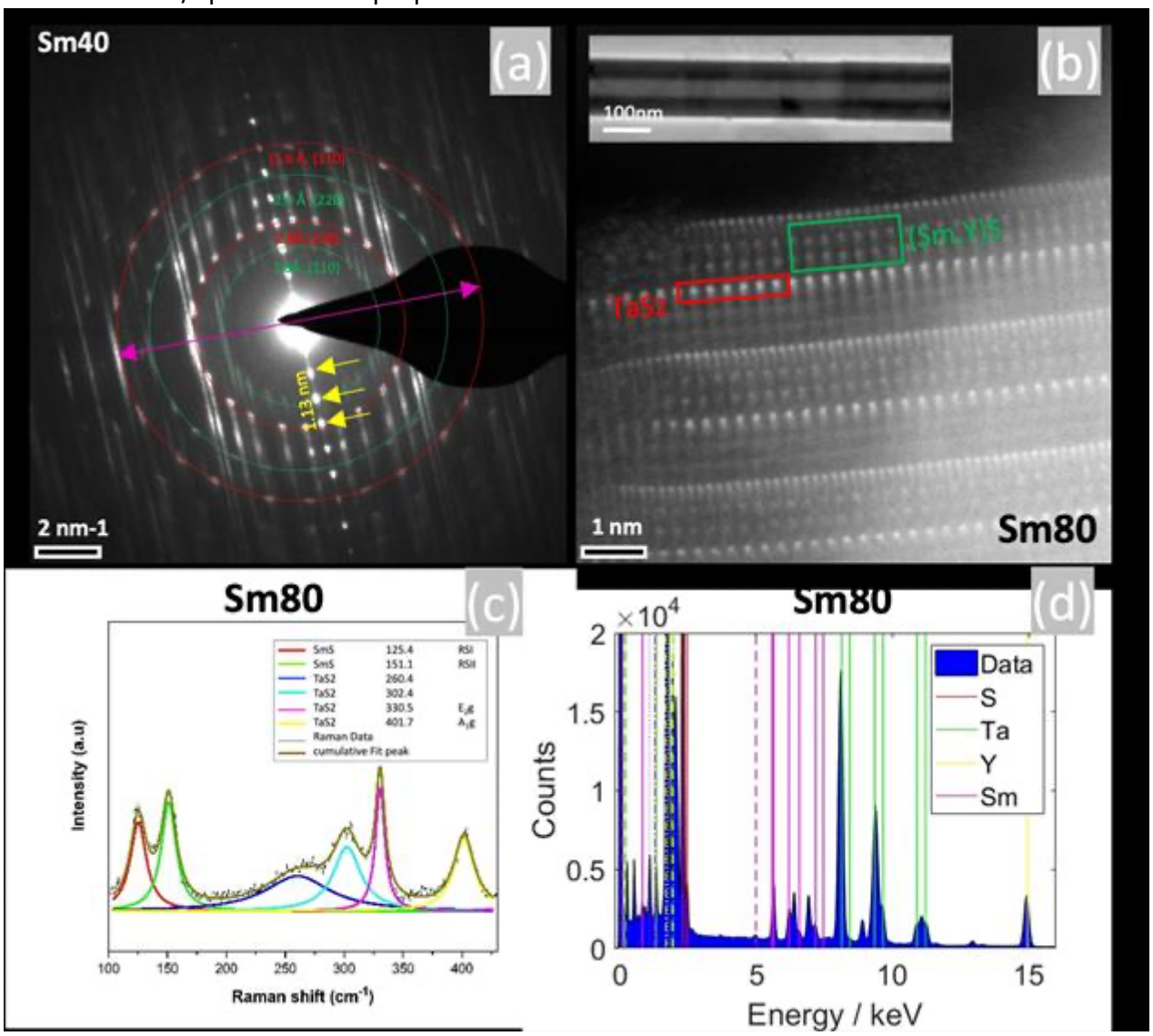

Keywords:

Inorganic-nanotubes, misfit-layered compounds-(MLC), structural analysis

Reference:

1 - M. Serra, R. Arenal, R. Tenne, (2019). Nanoscale 11, 8073-8090. https://doi.org/10.1039/C9NR01880H
2 – M.B Sreedhara et al. Chemistry of Materials 2022 34 (4), 1838-1853. https://doi.org/10.1021/acs.chemmater.1c04106
4 - S. Hettler et al. (2020), ACS Nano 14, 5, 5445–5458. https://doi.org/10.1021/acsnano.9b09284
3 - G. Radovsky et al. (2016). J Mater Chem C 4, 89–98. 10.1039/C5TC02983J
5- M. Furqan, S. Hettler, MB Sreedhara, R. Tenne, R. Arenal. To be submitted.
Funding: Research supported by the Spanish MICIU (PID2019-104739GB-100/AEI/10.13039/501100011033) and the Government of Aragon (DGA) through the project E13_23R.

827

Guided growth of 1D van der Waals Nanowires for Enhanced Optoelectronic Functionalities

Maayan Persky[1], Shahar Bialer[1], Noya Ruth Itzhak[1], Anna Eden Kossoy[2], Lotar Houben[2], Ernesto Joselevich[1]
[1]Department of Molecular Chemistry and Materials, Weizmann Institute of Science Science,, Rehovot, Israel, [2]Chemical Research Support, Weizmann Institute of Science, Rehovot, Israel

Poster Group 2

Background:
Nanomaterials, particularly those with anisotropic characteristics, have attracted significant interest in materials research due to their vast potential applications in diverse fields like optoelectronics, photocatalysis, solar cells, energy storage, sensors, and electronic devices. To unlock these possibilities, precise control over the structure, geometry, and surface arrangement is crucial. Our research group addresses this challenge by developing innovative techniques for "guided growth" of materials on surfaces.
1D van der Waals (vdW) materials, characterized by their chain-like structures connected by weak vdW forces, have emerged as promising candidates for various applications owing to their inherent anisotropic nature and intrinsic 1D dimensionality. We aim to leverage these unique properties, combined with our expertise in guided growth, to fabricate well-aligned nanowires of 1D vdW materials with superior electronic and optoelectronic functionalities. In this work, we present the successful growth of well-aligned Sb_2Se_3 and Sb_2S_3 nanowires on various substrates, including both covalent epitaxy substrates like sapphire and vdW epitaxy substrates like $ReSe_2$.

Method:
The nanowires were synthesized in our group's custom-built chemical vapor deposition (CVD) system. The structure and morphology of the nanowires were characterized using scanning electron microscopy (SEM). Compositional analysis was performed using energy-dispersive X-ray spectroscopy (EDS) and Raman spectroscopy. High-resolution transmission electron microscopy (HR-TEM) is planned to determine the crystal orientation and atomic structure. Additionally, the optical and electronic properties of the wires will be investigated through photoluminescence (PL) spectroscopy. Finally, photodetectors will be fabricated, and their optoelectronic properties will be characterized.

Results:
We successfully synthesized well-aligned nanowires of Sb_2S_3 and Sb_2Se_3 on C-plane sapphire substrates. SEM analysis confirmed the nanowire structure and revealed their oriented directions. EDS confirmed the chemical composition of the nanowires. Focused Ion Beam (FIB) milling is planned in the coming weeks to prepare cross-sectional lamellae for HR-TEM analysis, which will elucidate the epitaxial relationships and growth plane orientation. Following this, a photodetector will be fabricated to characterize the optoelectronic properties.
Furthermore, promising initial results have been obtained for guided growth of Sb_2Se_3 nanowires on $ReSe_2$ flakes, demonstrating successful vdW epitaxy. This mixed-dimensional heterostructure was characterized using Raman and PL spectroscopy. Similar to the previous case, a cross-sectional lamella will be prepared for characterization of the epitaxial relationships within this mixed-dimensional heterostructure using HR-TEM.

Conclusion:
This work demonstrates the successful synthesis of well-aligned Sb_2Se_3 and Sb_2S_3 nanowires on various substrates using our guided growth methods. Further analysis using HR-TEM and fabrication

of photodetectors are planned to fully characterize their properties. Additionally, initial results on Sb_2Se_3 nanowires grown on $ReSe_2$ flakes via vdW epitaxy are encouraging, signifying the potential for exploring novel mixed-dimensional heterostructures. This research paves the way for engineering next-generation optoelectronic devices utilizing precisely aligned 1D vdW nanowires

Keywords:

1D, guided growth, anisotropic

833

FIB-induced nanorod formation in 2D layered crystals

Dr. Julia Deuschle[1], Dr. Tobias Heil[1], Dr. Hongguang Wang Hongguang Wang[1], Prof. Dr. Peter van Aken[1]
[1]Max Planck Institute for Solid State Research, Stuttgart, Germany

Poster Group 2

In this study, we present our findings of very unusual behavior shown by bulk crystals of 2D layered materials, such as transition-metal diselenides, when subjected to focused ion beam (FIB)-milling. During FIB preparation of lamellae for transmission electron microscopy (TEM) analysis, we encountered a very pronounced curtaining effect for this type of materials. This initially leads to thickness variations in the TEM lamella, and upon further FIB milling, to the formation of wire- or rod-like structures. The curtaining is observed on different length scales from the micro- to the nanometer range. Examples of such structures can be seen in figure 1.
Interestingly, the rod-like structures form, when the milling direction is perpendicular to the 2D layers. However, the formation of rods only occurs for some crystal orientations, whereas an in-plane rotation of the bulk crystal can lead to a homogeneous milling behavior without curtaining. Furthermore, the choice of the ion beam milling parameters seems to have an influence on the resulting structures.
We present further investigations of these wire- or rod-like structures for several 2D materials with different compositions. The goal is to expand our knowledge of the conditions that either lead to or prevent the formation of the nanorods and to gain a deeper understanding of the effect that causes these structures to form.

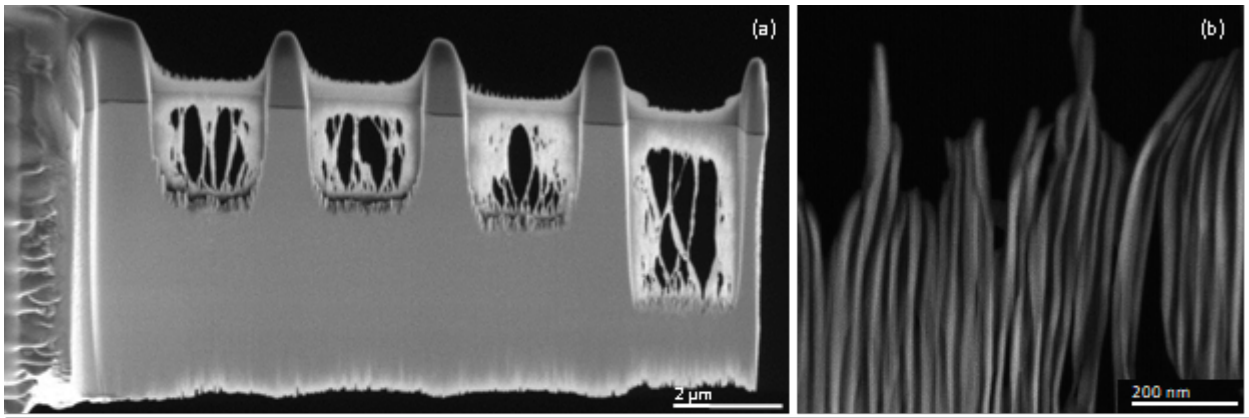

Figure1: (a) Nanowires with a length of several hundreds of nanometers in a final TEM- lamella
(b) HAADF-STEM image of nanorods.

Keywords:

Focused ion beam
2D materials

863

In situ examination of oxygen vacancy dynamics in epitaxial LaCoO3 thin films

Dr. Seung Jo Yoo[1], Mrs. Ji-Hyun Lee[1], Mr. Sang-Gil Lee[1], Dr. Hyung Joong Yun[1]
[1]Korea Basic Science Institute, Deajeon, Republic of Korea

Poster Group 2

Background incl. aims
Understanding the coupling effect between lattice strain and the energy required to create oxygen vacancies is crucial for the rational optimization of the catalytic performance of thin film perovskite electrocatalysts. However, contradictory results have been reported regarding the impact of lattice strain on both the oxygen vacancy content and formation energy, differing in terms of extent, direction, and mechanism. Theoretical studies have indicated that oxygen vacancy defects may either increase or decrease with increasing tensile strain. Additionally, the formation energy of oxygen vacancies has been observed to follow either a curved or nearly linear trend as the strain state transitions from compression to tension. These theoretical findings suggest that the energetics of oxygen vacancy formation could be highly complex and material dependent. Therefore, our study aimed to experimentally investigate the concentration and distribution of oxygen vacancies in epitaxial thin films of LaCoO3 (LCO), a highly active perovskite oxide material, for both the oxygen reduction reaction and the oxygen evolution reaction. We observed the formation behavior of oxygen vacancies at the atomic level in real time using in situ transmission electron microscopy (TEM) with an electron beam exposure function. This technique allowed us to study the dynamic behavior of oxygen vacancies under compressive and tensile lattice strains. Additionally, we utilized high angle annular dark field (HAADF) scanning transmission electron microscopy (STEM) images to directly analyze the local mapping and visualization of oxygen vacancies at the unit cell level in the LCO thin films.

Methods
On (001) LaAlO3 (LAO) and SrTiO3 (STO) substrates, LCO thin films were synthesized using the sol-gel technique. Cross-sectional TEM specimens were prepared using a focused ion beam (Quanta 3D FEG, FEI), and HAADF STEM images were acquired using TEM (Mono ARM 200F, JEOL) operating at 200 kV. The beam convergence semi-angle was set to 23.81 mrad, and the collection semi-angles ranged from 68 to 280 mrad. A consistent electron dose rate was maintained during electron beam irradiation. Wiener filtering, implemented via the HREM-Filters software package (HREM Research), was utilized to enhance image clarity.

Results
Atomic-scale HAADF STEM images depicting the initial conditions of the LCO thin films on the LAO and STO substrates are presented in Figs. 1 (a) and (f), respectively. A 15 × 15 nm region within the LCO thin film was monitored for changes in lattice parameters, encompassing 1,444 unit cells. HAADF STEM images were obtained from identical pristine regions of the LCO thin film at various time intervals as the electron beam irradiation time was increased. Figs. 1 (b–e) and (g–j) exhibit high-resolution HAADF STEM images selected at 20-minute intervals in the LCO thin film on the LAO and STO substrates, respectively. The time series of the HAADF STEM images for both LCO thin films revealed the appearance of dark strip patterns over time. The modulated contrast patterns observed in the HAADF STEM images of the LCO thin films are attributed to the ordering of oxygen vacancies, leading to localized lattice expansion and the formation of modulated dark stripe patterns. The onset time of the first dark-strip pattern differed between the two LCO thin films. Specifically, the first dark strip pattern emerged after approximately 60 minutes of continuous electron beam exposure in the

LCO thin film on the LAO substrate and after 20 minutes in the LCO thin film on the STO substrate. The red arrows indicate the first dark-strip pattern in Figs. 1 (d) and (g). Subsequently, dark-strip patterns emerged at various positions and continued to grow in the out-of-plane direction. The maximum growth of dark strip patterns in the two LCO thin films occurred after 80 minutes. Furthermore, the distribution of dark strip patterns was observed more frequently in the LCO thin films on STO substrates.

Conclusions

HAADF STEM images confirm uniform thickness and initial conditions of LCO thin films on LAO and STO substrates. With increasing electron beam irradiation time, distinctive dark strip patterns emerge, indicating oxygen vacancy ordering. Variations in pattern appearance and behavior are noted between substrates, with higher tensile strain accelerating pattern onset and distribution frequency. Quantitative analysis of lattice parameter changes corroborates these observations, confirming expanded unit cells associated with oxygen vacancies. Notably, films under higher tensile strain exhibit more uniformly distributed enlarged unit cells and significantly higher oxygen vacancy concentration. These findings support previous studies suggesting reduced formation energy of oxygen vacancies under tensile strain. Overall, this research provides valuable experimental insights into oxygen vacancy formation and distribution mechanisms in LCO thin films under strain, advancing our understanding and informing tailored material design for electrochemical applications.

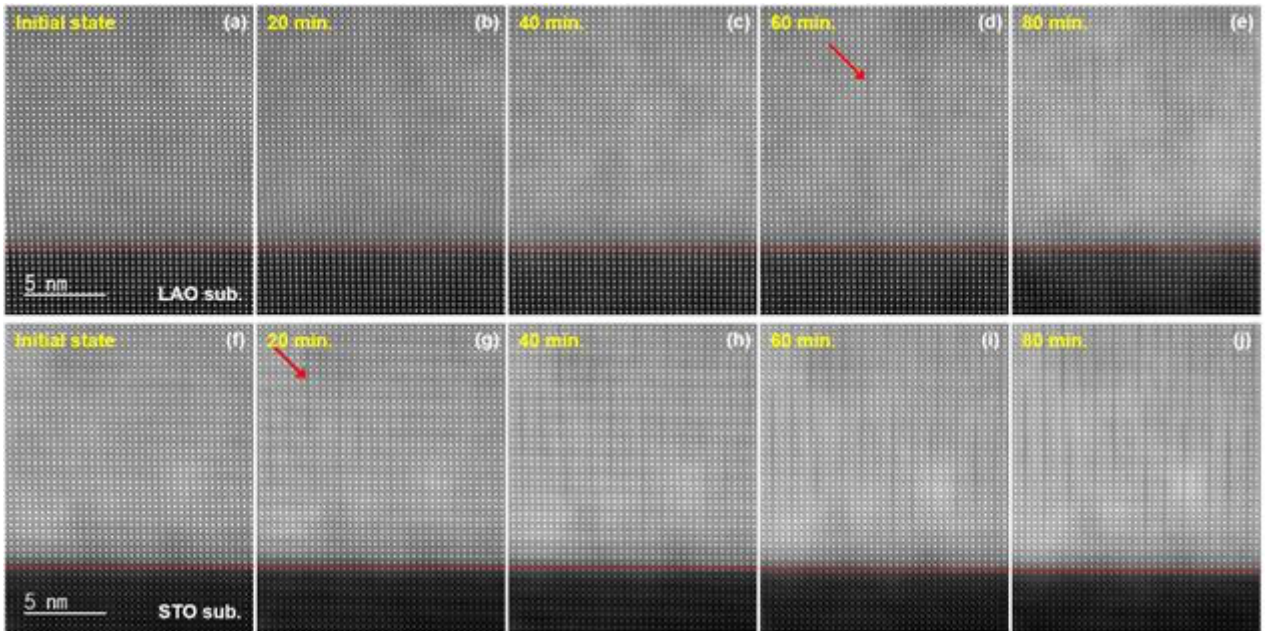

Keywords:

Oxygen vacancies, Strain states

Reference:

[1] Akhade, S.A., Kitchin, J.R., Effects of strain, d-band filling, and oxidation state on the surface electronic structure and reactivity of 3d perovskite surfaces. J. Chem. Phys. 137, 084703 (2012).
[2] Donner, W., Chen, C., Liu, M., Jacobson, A.J., Lee, Y.-L., Gadre, M., Morgan, D.: Epitaxial Strain-Induced Chemical Ordering in La0.5Sr0.5CoO3−δ Films on SrTiO3. Chem. Mater. 23, 984–988 (2011).
[3] Tahini, H.A., Tan, X., Schwingenschlögl, U., Smith, S.C.: Formation and migration of oxygen vacancies in SrCoO3 and their effect on oxygen evolution reactions. ACS Catal. 6, 5565–5570 (2016).

870

High-resolution structural analysis of cation-mixed (Fe,Mn,Ni)PS3 van der Waals single crystals

Dr. Tatiana Smoliarova[1], B.Sc. Moritz Küster[1], Dr. Apoorva Chaturvedi[2], Prof. Edwin-Hang-Tong Teo[2], Prof. Michael Farle[1], Dr. Anna Semisalova[1]
[1]Faculty of Physics and Center of Nanointegration (CENIDE), University of Duisburg-Essen, Duisburg, Germany, [2]Center for Programmable Materials, School of Materials Science and Engineering, Nanyang Technological University, Singapore, Singapore

Poster Group 2

Transition-metal (TM)-based van der Waals (vdW) materials (“2D – materials”) recently received particular attention due to their tunable magnetic properties arising from unpaired magnetic moments due to the partially filled d-shells of the TM ions. The subclass of TM phosphorous trisulfides (TMPS3) has attracted significant interest due to its wide range of TM elements, resulting in diverse properties [1]. The structure of TMPS3 is defined by its vdW nature. Layers exhibit the monoclinic crystal structure, space group 3 C2/m, and are only bound by weak vdW forces [2], which allows for easy exfoliation and leads to 2D-like properties being observable in 3D crystals.
In this study, transmission electron microscopy (TEM), energy dispersive X-ray spectroscopy (EDX), electron energy loss spectroscopy (EELS), and continuous rotation electron diffraction (cRED) have been combined to study the cation-mixed (Fe,Mn,Ni)PS3 van der Waals single crystals with different Fe, Mn, and Ni concentrations produced in a bulk state by chemical vapor transport (CVT) [3].
The high-resolution (HR) TEM image (a) shows the cross-section of a (Fe,Mn,Ni)PS3 single crystalline sample, prepared by Cryo-Ultramicrotome. An amorphous oxide layer formed on the edge of the sample is highlighted with a yellow dashed line. It has a thickness of 5 nm. The magnified HRTEM image (b) shows the layered structure with a layer distance of 0.65 ± 0.02 nm. Bright spots (atomic columns) correspond to S and P. The darker lines are the planes of TM ions. Ultrasonically exfoliated layers are shown on TEM image (c) on which selected area electron diffraction (SAED) (d) and EDX mapping (e) have been performed. The lattice parameters a = 0.647 nm, b = 1.072 nm, c = 0.698 nm, $\alpha = \gamma = 90°$ and $\beta = 111.22°$ were estimated from the SAED pattern and slightly deviate from earlier reported FePS3, MnPS3 and NiPS3 mono-compounds [4,5].
Work is funded by the Deutsche Forschungsgemeinschaft (DFG, German Research Foundation) – Project-ID 405553726 – TRR 270, Z02“

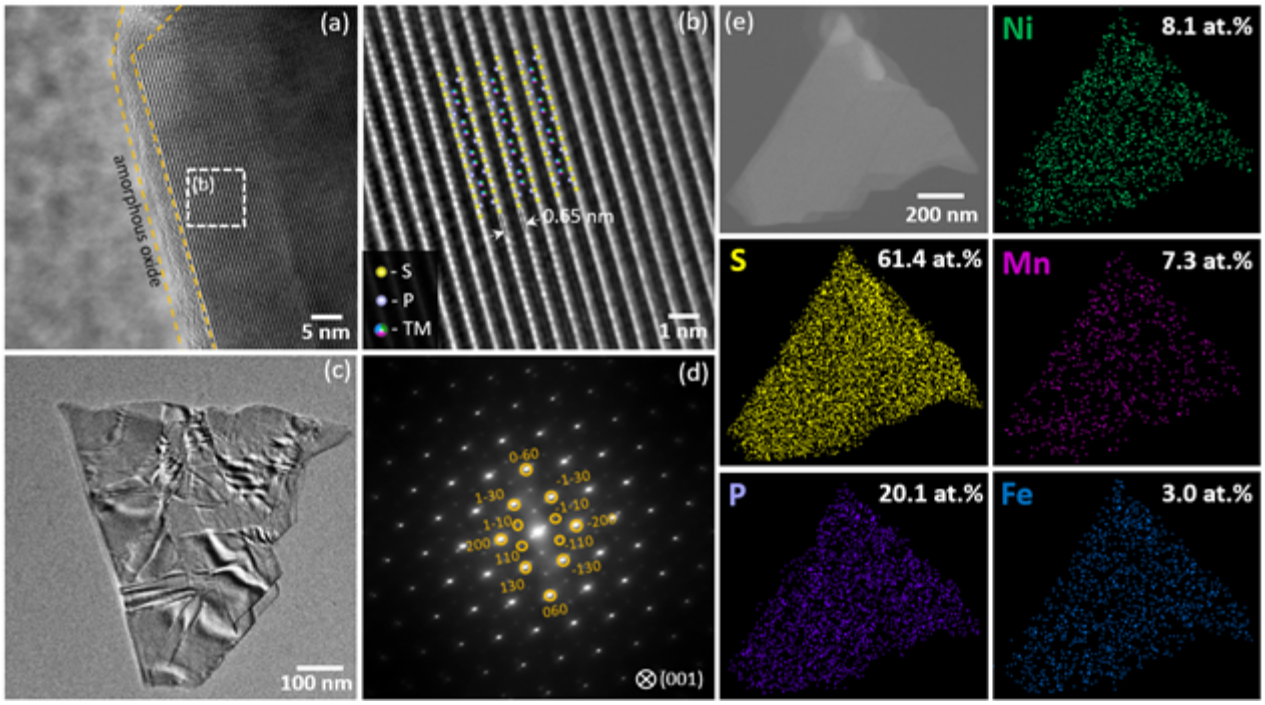

Keywords:

3D ED, cRED, 2D-materials, TMPS3

Reference:

[1] Burch, K. S., Mandrus, D., & Park, J. G. "Magnetism in two-dimensional van der Waals materials." Nature, vol. 563, no. 7729, 2018, pp. 47–52.

[2] Mayorga-Martinez, C. C., et al. "Layered Metal Thiophosphite Materials: Magnetic, Electrochemical, and Electronic Properties." ACS Applied Materials & Interfaces, vol. 9, no. 14, 2017, pp. 12563–12573.

[3] Samal, Rutuparna, et al. “Two-dimensional transition metal phosphorous trichalcogenides (MPX3): a review on emerging trends, current state and future perspectives”. In: Journal of Materials Chemistry A, vol. 9, no. 5, 2021, pp. 2560–2591.

[4] Ouvrard, G., Brec, R., & Rouxel, J. “Structural determination of some MPS3 layered phases (M = Mn, Fe, Co, Ni and Cd)”. In: Materials Research Bulletin, vol. 20, no. 10, 1985, pp. 1181–1189. ISSN: 0025-5408.

[5] Saito, Shozo, Ko Kurosawa, & Yasuo Yamaguchi. “Neutron Diffraction Study on MnPS3 and FePS3”. In: Journal of the Physical Society of Japan, 1985, pp. 3919–3926.

907

Morphological investigation of periodic structures created by focused ion gallium beam

Márk Windisch[1,2], Dániel Selmeczi[3], Ádám Vida[2], Zoltán Dankházi[1]
[1]Eötvös Loránd University Department of Materials Physics, Budapest, Hungary, [2]Bay Zoltán Nonprofit Ltd. for Applied Research, Budapest, Hungary, [3]Semilab Semiconductor Physics Laboratory Co. Ltd., Budapest, Hungary

Poster Group 2

Background incl. aims
Surface periodic structures on solids by ion-beam irradiation were first observed in the early second half of the 20th century. The initial observation, in parallel with the investigation of ion techniques, was followed by several other experimental works and theoretical descriptions based on ion-material interaction. Some developed models in this field can predict the morphological properties of the periodic structures as a function of some parameters of the ionic irradiation. In our experimental work, periodic structures were created on silicon surface by a low-energy focused ion beam at different incidence angles. The created morphology of periodic structures was compared to the predictions of the most cited Bradley-Harper (BH) model. Based on the experimental work, one of our goals is to explain the deviation from the BH model. In addition, the material structural and optical properties of the periodic patterns were also investigated by some spectroscopic measurement techniques. These measurements were used to determine the amorphization of the structured surface layer. Moreover, the reflectances of the structured surfaces were determined as a function of the applied ion incidence angle. Another goal of our work was to achieve a controlled modification of the reflection on Si surfaces by low-energy ion irradiation.

Methods
Ion irradiation was performed on polished Si (111) by focused 2 keV gallium ion beam (FIB) at incident angles between 60° and 80°. The morphology of the irradiated Si surfaces was investigated by scanning electron microscopy (SEM) and atomic force microscopy (AFM). To determine the wavelength of the structured periodic patterns, the power spectral density (PSD) function calculated from a 2-dimensional Fast Fourier Transformation was used. The position of the first peak of the PSD function was used to determine the characteristic periodicity of the structured surface. Spectroscopic elllipsometer (SE) and reflectometer were used to study the material structure of the structured Si layers.

Results
Regular ripple formation was created at ion incident angles between 60° and 72.5°. The wavelength of the ripple patterns was measured between 38 nm and 60 nm. The trend of the measured wavelengths showed exponential growth in the mentioned range. The regular periodic structure broke up above 72.5° ion incidence angle and turned into a smooth surface up to 80°. The wave vector of the ripple formation was parallel to the incident ion beam. The rotation of ripples did not appear in the range of 60° and 80° ion incidence. This observation is not consistent with the predictions of the BH model. The amorphised layer thicknesses of the strutured surface were determined between 3.8 and 7.9 nm in the range of 60° and 80° ion incidence by SE. Furthermore, the reflectances of structured surface was measured in the range of 300 nm and 900 nm wavelength of light. According to the measured results, a linear connection was observed between the reflectance and ion incident angle for 460 nm wavelength of light.

Conclusion

Periodic structures were created by low-energy focused ion beam on Si (111) in the range of given angles. The characteristic sizes of the formed structures could be controlled within a few of tens of nm by changing the ion incident angles. Based on the meaured morphology results, explaination was given for deviation from the prediction of the BH modell. The amorphization of irradiated surfaces was modified with different ion incidence angles. Furthermore, the reflectances of Si surfaces was fine-tuned in 460 nm wavelength of light by low-energy ion irraidation.

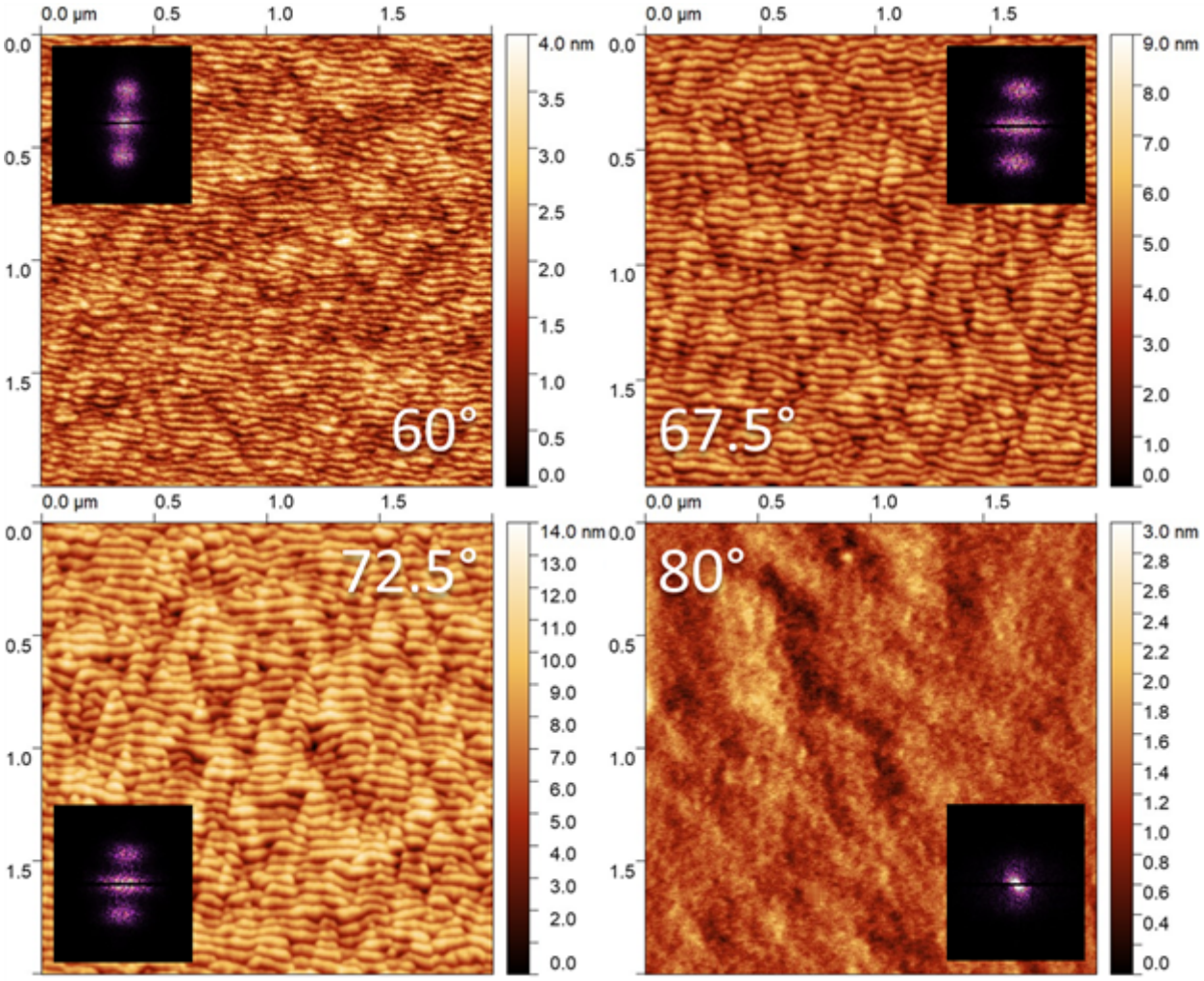

Keywords:

ripple formation, ion bombardment, silicon

Reference:

Navez, M., Chaperot, D., & Sella, C. (1962). Microscopie electronique-etude de lattaque du verre par bombardement ionique. Comptes Rendus Hebdomadaires Des Seances De L Academie Des Sciences, 254(2), 240.
Bradley, R. M., & Harper, J. M. (1988). Theory of ripple topography induced by ion bombardment. Journal of Vacuum Science & Technology A: Vacuum, Surfaces, and Films, 6(4), 2390-2395.
Keller, A., & Facsko, S. (2010). Ion-induced nanoscale ripple patterns on Si surfaces: theory and experiment. Materials, 3(10), 4811-4841.

909

Functionalization of Single-Walled Carbon Nanotubes Analyzed by Spatially-Resolved EELS

Dr Raul Arenal[1,2,3], Dr. Laurent Alvarez[4], Prof. Jean-Louis Bantignies[4]
[1]Instituto de Nanociencia y Materiales de Aragón, CSIC-Universidad de Zaragoza, Zaragoza, Spain., Zaragoza, Spain, [2]Laboratorio de Microscopías Avanzadas (LMA), Universidad de Zaragoza. Zaragoza, Spain, Zaragoza, Spain, [3] Araid Foundation, Zaragoza, Spain , Zaragoza, Spain, [4]Laboratoire Charles Coulomb, U. Montpelier - CNRS, Montpellier, France

Poster Group 2

Background incl. aims
Surface functionalization of 1D and 2D nanomaterials is a perfect way for controlling their properties [1-5]. Very detailed structural and chemical composition analyses, at the atomic scale, of such surface modifications are required in order to determine their impact on the electronic/optoelectronic properties. Transmission electron microscopy (TEM) and in particular, spatially-resolved electron energy loss spectroscopy (SR-EELS) developed in an aberration-corrected TEM, is the most powerful technique to get this information. Indeed, having access to a close to 1 angstrom electron probe, the atomic configuration and concentration of the different species of these functionalized nanomaterials can be obtained [1-5]. In this contribution, we report an in-depth study of the atomic configuration of covalent and non-covalent functionalized (pi-stacked and endohedral) single-walled (SW) C-NTs via SR-EELS [5].

Methods
These studies have been developed via spatially-resolved EELS performed using a liquid-nitrogen holder (−170 °C) and Thermo Fisher Scientific Titan Low-Base microscope, working at 80 kV. This microscope is equipped with a Cs probe corrector, a monochromator and an ultra-bright XFEG electron source. The HRTEM studies have been carried out in a Thermo Fisher Scientific Titan Cubed microscope (equipped with a Cs image corrector), under the same cryogenic conditions (−170 °C) and at 80kV.

Results
We have investigated different systems of functionalized NTs (covalent and non-covalent (endohedral and pi-stacked)), for getting local information about these different hybrid configurations, studying the chemical environment and bonding of the NTs and the organic moieties [2-5]. Figure 1 illustrates some of these results, in particular the case of endohedral functionalization: iron-phthalocyanine (Fe-Pc) moieties in single-walled nanotubes [5]. Figure 1 (a) corresponds to a HRTEM image of one of these individual filled single-walled C-NTs. Figure 1 (b) displays an atomic-sketch, showing the supramolecular order of the Fe-Pc within a SWNT and Fig. 1 (c) shows an atomic-sketch of one of these Fe-Pc molecules (a Fe atom is surrounded by 4 pyrrolic-like subunits). As it is well known, these NTs tend to be organized in bundles. Figures 1 (d) and (e), which correspond to of STEM (BF and HAADF) micrographs, show one these bundles of SW-CNTs. A 24x12 EELS spectrum-image (SPIM) has been recorded in the green marked area on one of these NT. (f) EEL spectra extracted from the squared regions marked in Fig. 1(e). They correspond to four EEL spectra each of them. C-K, N-K and Fe-$L_{2,3}$ edges are clearly seen. From these spectra, nitrogen and iron elemental maps can be obtained, see Fig. 1 (g) and (h). These studies reveal the supramolecular organization of the organic moieties (in this present case showed in this figure, iron-phthalocyanines) used for the functionalization of the NTs [5].

Conclusion

In summary, these works provide very rich information about these hybrid and complex nanomaterials, opening fascinating perspectives for optoelectronic applications of such nano-systems. All these aspects will be discussed in this contribution.

Graphic - Figure: (a) HRTEM micrograph of a SW-CNT filled with iron-phthalocyanine (Fe-Pc) moieties. (b) Atomic-sketch showing the supramolecular order of these Fe-Pc entities within a SW-NT. (c) Atomic-sketch of a Fe-Pc (a Fe atom is surrounded by 4 pyrrolic-like subunits. (d)-(e) BF- and HAADF-STEM images of a bundle of filled SWNT. A SPIM-EELS has been recorded in the green marked area. (f) EEL spectra extracted from the squared regions marked in Fig. 1(e). They correspond to 4 EEL spectra each of them. C-K, N-K and Fe-L2,3 edges are clearly seen. (g)-(h) N and Fe elemental maps. [5]

Funding:
Research supported by the Spanish MICIU (PID2019-104739GB-100/AEI/10.13039/501100011033), the Government of Aragon (DGA) through the project E13_23R and the MICIU with funding from European Union NextGenerationEU (PRTR-C17.I1) promoted by the Government of Aragon.

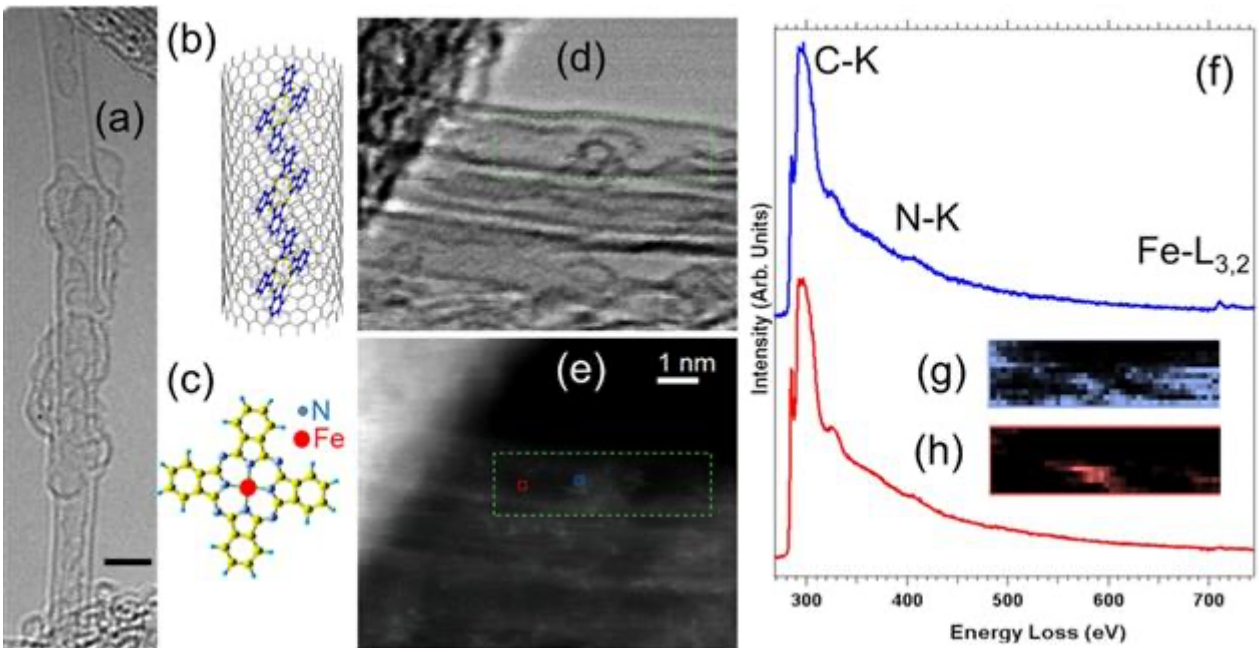

Keywords:

Functionalization, Nanotubes, Cryo-TEM, STEM-EELS, HR(S)TEM

Reference:

[1] R. Canton-Vitoria, T. Scharl, A. Stergiou, A. Cadranel, R. Arenal, D.M. Guldi, N. Tagmatarchis, Angewandte Chemie Int. 3976-3981 (2020).
[2] A. Setaro, M. Adeli, M. Glaeske, D. Przyrembel, T. Bisswanger, G. Gordeev, M. Weinelt, R. Arenal, R. Haag, S. Reich, Nature Comm. 8, 14281 (2017).
[3] F. Ernst, Z. Gao, R. Arenal, T. Heek, A. Setaro, R. Fernandez-Pacheco, R. Haag, L. Cognet, S. Reich, J. Phys. Chem. C 121, 18887–18891 (2017).
[4] L. Alvarez, et al., J. Phys. Chem. C 119, 5203–5210 (2015).
[5] R. Arenal, L. Alvarez, J.-L. Bantignies, Submitted.

911

Microstructure and mechanical properties of AlCu thin films in a wide range of composition

Dániel Olasz[1,2], György Sáfrán[2], Noémi Szász[2], Tamás Kolonits[2], Nguyen Quang Chinh[1]
[1]Department of Materials Physics, Eötvös Loránd University, Budapest, Hungary, [2]Institute for Technical Physics and Materials Science, HUN-REN Centre for Energy Research, Budapest, Hungary

Poster Group 2

Background incl. aims
Copper is a common additive in bulk aluminum alloys, where its effect on phase composition and strength of the alloys is well documented. Thin films, however, often contain non-equilibrium phases, which may change significantly the mechanical properties of the material. AlCu thin films in a wide range of composition have been less discussed in the literature, as the existing papers are mainly concentrating on the cases of small alloying concentration. In this work, we aimed to study systematically the microstructure and mechanical properties, as well as to understand their correlations in the case of AlCu thin films having compositions widely changing.

Methods
Thin films were deposited by dual DC magnetron sputtering of Al and Cu targets. Applying the micro-combinatorial technique [1] 15 Al1-xCux films with different compositions ($0 \leq x \leq 1$) were deposited within a single experiment (under the same vacuum conditions) on a single Si substrate. Depth sensing indentation (DSI) measurements were conducted to reveal the hardness and the deformation mechanism of the layers. Cross-sectional lamellas were prepared from each layer by the focused ion beam (FIB) technique, and then investigated by transmission electron microscopy (TEM) techniques, including: bright field, dark field and HRTEM imaging, selected area electron diffraction (SAED), TEM energy dispersive spectroscopy (EDS), scanning TEM (STEM).

Results
Layers near to the equiatomic compositions (Al59Cu41, Al48Cu52, Al39Cu61) are built up from crystalline columns of ~30-40 nm in diameter. At these compositions the SAED measurements show the presence of the Al4Cu9 crystalline phase, which differs from that predicted by the equilibrium phase diagram. Lamellas prepared from the indentation imprints also indicate the presence of deformation bands, suggesting an amorphous like deformation behavior. This is coupled with an exceptional hardness of ~ 16 GPa [2] and a step-like indentation curve during the loading stage of the indentation.
The pure Al and Cu layers also possess small grain-size (~300-400 nm) structure, coupled with an increased hardness compared to their bulk counterparts. Furthermore, indentation process taken on these ultrafine-grained thin film do not show the size effect often observed in the case of bulk materials. The absence of the indentation size effect may be the consequence of the deformation mechanism as intensive grain boundary sliding (GBS) is revealed in these layers by both surface SEM and cross-sectional TEM images.

Conclusion
Composition-dependent mechanical and structural properties of AlCu alloy thin films were determined over the entire alloying concentration range. The decreasing grain size and the appearance of non-equilibrium phases are in good agreement with the increasing alloying concentration - increasing hardness trend. The presence of GBS suggests a mitigation of the classical dislocation-driven plastic deformation mechanism, which is compatible with the absence of an indentation size effect.

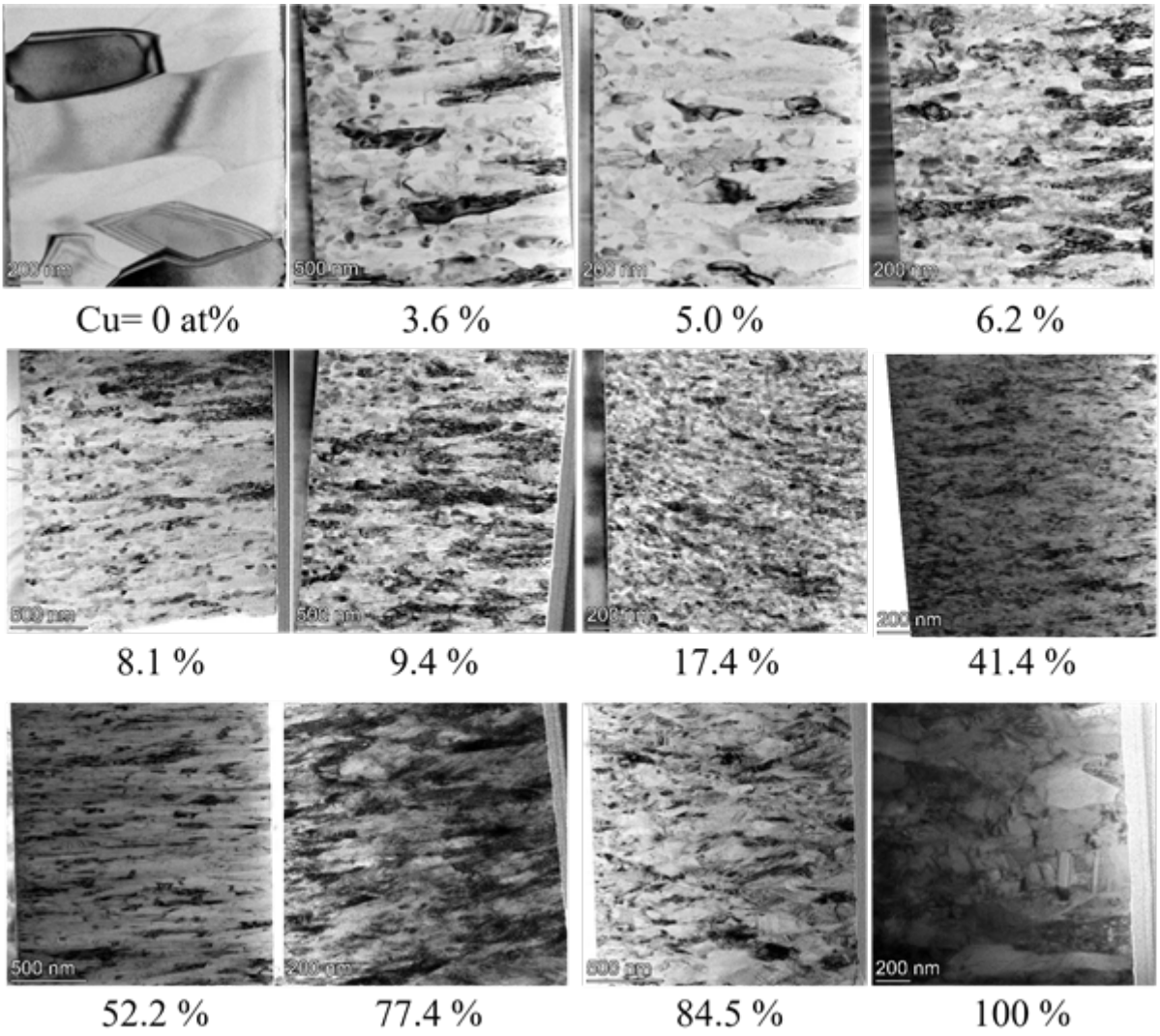

Keywords:

AlCu thin films, TEM, nanoindentation

Reference:

[1] G. Sáfrán et al.: Review on High-Throughput Micro-Combinatorial Characterization of Binary and Ternary Layers towards Databases. Materials 2023, 16, 3005.
[2] D. Olasz et al.: Indentation size effect in exceptionally hard AlCu thin films. Mater. Lett. 2023, 330, 133409.

912

Enhanced Visible Light Photocatalytic Activity of Cu-Doped ZnO ALD Films Deposited on Porous Substrates

Assistant professor Ivna Kavre Piltaver[1,2], Robert Peter[1,2], Daria Jardas Babić[1,2], Matejka Podlogar[3], Aleš Omerzu[1,2], Krešimir Salamon[4]
[1]Faculty of Physics, University of Rijeka, Rijeka, Croatia, [2]Center for Micro- and Nanosciences and Technologies, Universitu of Rijeka, Rijeka, Croatia, [3]Jozef Stefan Institute, Ljubljana, Slovenia, [4]Ruđer Bošković Institute, Zagreb, Croatia

Poster Group 2

Background incl. aims
Industrial development contributes significantly to environmental pollution, especially from organic pollutants, which underlines the urgent need for global wastewater recycling. Over the last two decades, extensive research has been conducted on the photocatalytic degradation of pollutants in wastewater [1]. This process begins with the absorption of light in the semiconductor. This generates free electrons and holes that react with oxygen and water on the semiconductor surface to produce chemically reactive products capable of degrading pollutant molecules into less harmful compounds [2].
ZnO, a wide bandgap semiconductor photocatalyst, facilitates photocatalysis under UV light exposure. Current research focuses on tailoring the energy bandgap and improving visible light absorption, which is often achieved by doping the semiconductor with transition metal atoms [3]. Copper is a promising candidate for doping ZnO as it is able to replace Zn in the matrix, creating native point defects such as oxygen vacancies, which significantly affect the material properties [4]. The effectiveness of photocatalysis is closely linked to the active surface area of the catalyst, which has led to a strong interest in the use of powders or colloidal suspensions of nanoparticles. This interest stems from their remarkable surface area-to-volume ratio, which enhances the availability of surface states that serve as reaction sites. However, the separation of nanoparticles from solution poses a major challenge. The development of highly efficient photocatalytic materials for water treatment must therefore be optimized to achieve practical benefits.
Both high surface area and high optical efficiency are essential to achieve increased photocatalytic activity in metal oxide films. Polycrystalline thin films deposited on porous substrates are promising candidates in this context, as they serve as effective photocatalysts without the need for post-treatment. They also facilitate complete recovery after the experiments. In order to take advantage of Cu-doped thin ZnO films for visible-light photocatalysis, different fabrication techniques have been used. In addition, atomic layer deposition (ALD) proves to be a promising technique for the growth of semiconductors or insulating thin films as it allows precise control over the film thickness and deposition on different substrates. [5].
Our goal is to find a photocatalyst that exhibits enhanced photocatalytic activity under UV and simulated sunlight irradiation. We achieve this by manipulating two parameters: the band gap of the ZnO films by doping with Cu atoms and the active surface area of the sample.

Methods
In this study, we have used the ALD technique to synthesize thin ZnO films and Cu-doped ZnO films on flat or porous silicon wafers. All pure ZnO samples were grown in a Beneq TSF 200 system at 180 °C using diethylzinc (DEZ, $Zn(C_2H_5)_2$) and distilled water (H_2O) as zinc and oxygen precursors, respectively. The source of copper in the ALD-grown ZnO samples doped with Cu was copper (II) acetate ($Cu(OAc)_2$), evaporated at 180 °C from a hot source into the reaction chamber with nitrogen as carrier gas. The influence of the Cu dopants on the surface morphology and topology of the samples was investigated by scanning electron microscopy (SEM), the penetration depth of the ALD

films into the pores was determined with focused ion beam (FIB), the crystallinity was investigated by grazing incidence x-ray diffraction (GIXRD). In addition, x-ray photoelectron spectroscopy (XPS) was used to analyze the chemical state of the Cu atoms and secondary ion mass spectrometry (SIMS) to determine the distribution of Cu atoms in the films. Finally, the photocatalytic activity was investigated by measuring the degradation rate of methylene blue (MB) in an aqueous solution under a UV and simulated sunlight irradiation.

Results

The ALD synthesis of ZnO, in which diethylzinc (DEZ) and water (H_2O) are used as precursors, usually leads to polycrystalline films. Size, shape and crystal orientation of the ZnO grains are influenced by deposition parameters such as temperature, pulsing and purging times of the precursors and substrate type. Our analysis starts with microscopic SEM images of undoped and Cu-doped ZnO samples on flat and porous substrates. The different surface morphologies observed in our samples correspond to variations in grain orientations within the films, as shown by the XRD patterns of the ALD-grown films. The penetration depth of pure ZnO and Cu-doped ZnO films on porous substrates was determined by examining the cross-section of the film profile within the pores using FIB.
The oxidation state of the copper was determined by XPS analysis around the Cu 2p core levels. The XPS analysis revealed two sharp and symmetrical peaks without satellite lines, demonstrating the presence of Cu+ states in the Cu-doped sample. In addition, the SIMS measurements determine the in-depth distribution of Cu dopants. The concentrations of Zn and Cu appear to be consistent throughout the film, with a sharp drop at the interface between the ZnO film and the Si substrate.
Finally, we investigated the photocatalytic activity of pure and Cu-doped ZnO films grown on flat and porous substrates under UV light and simulated sunlight. For this purpose, we immersed the samples in an aqueous solution of methylene blue (MB) and monitored the degradation rate of MB. First, we investigated the photocatalytic activity of pure ZnO films grown on both flat and porous substrates under UV light. The porous sample showed many times higher photocatalytic activity than the flat sample. We then investigated the photocatalytic activity of Cu-doped ZnO films on flat and porous substrates under simulated sunlight irradiation. The increased surface-to-volume ratio improves the availability of surface sites, which significantly enhances the photocatalytic activity of the porous sample.

Conclusion

In summary, we have investigated the structural and photocatalytic properties of flat and porous ZnO films doped in situ with Cu during the ALD process. Our results shows that ZnO films synthesized on porous substrates exhibit better photocatalytic performance under UV light than those grown on flat substrates. In addition, the Cu-doped compared to the Cu-doped films on flat substrates. By doping the ZnO ALD films with Cu atoms, we successfully shifted the photocatalytic activity from UV to visible light. In addition, by increasing the surface-to-volume ratio, we have significantly increased the photocatalytic activity.

Keywords:

ZnO, thin films, photocatalysis, ALD

Reference:

[1] H. Ding, J.S. Wei, N. Zhong, Q.Y. Gao, H.M. Xiong, Langmuir 33 (2017) 12635-12642.
[2] I. Ahmad, Y. Zou, J. Yan, Y. Liu, S. Shukrullah, M.Y. Naz, H. Hussain, W.Q.Khan, N.R. Khalid, Advances in Colloid and Interface Science 311 (2023) 102830.
[3] R. Peter, A. Omerzu, I. Kavre Piltaver, R. Speranza, K. Salamon, M. Podlogar, K. Velican, M. Percic, M. Petravic, Ceram. Int. 49 (2023) 35229-35238.
[4] G. Liang, L. Hu, W. Feng, G. Li, A. Jing, Appl. Surf. Sci. 296 (2014) 158–162.
[5] M. Knez, K. Nielsch, L. Niinisto, Adv. Mater. 19 (2007) 3425–3438.

925

Analysis of the cause of imperfect adhesion of cataphoretic coating using SEM and EDS method

Ph.D. Zuzana Koutova[1], Ing. Marie Novotna[1]
[1]MemBrain s.r.o., Stráž pod Ralskem, Czechia

Poster Group 2

The automotive industry is one of the most overloaded and stressed in the point of view materials selection, characterization, application and their corrosion prevention and surface protection. Cataphoretic coating is one of the used and technologically most advanced method of anticorrosive surface treatment processes and it is usually used as surface treatment of metal products. The process itself is a set of several steps of pre-treatment, paint application and curing and although each sub-process is rigorously controlled (including production of parts and their storage), it can occur that the final product of the cataphoretic coating process are parts with a defective coating. Consequently, the anti-corrosion protection can be reduced even due to relatively small defects and thereby increasing, among other things, the safety risk. In this contribution, case study of the cause analysis of a non-conforming cross-cut test of cataphoretic coating surface on metal part is shown, where it is necessary to use the methods of scanning electron microscopy (SEM) and scanning electron microscopy with energy dispersed X-ray spectroscopy (EDS).

The metal part with a non-conforming cross-cut test of cataphoretic coating surface were examined by the SEM and EDS method. SEM analyses were taken with scanning electron microscope Quanta FEG 250 (FEI) at the regime pressure of the low vacuum mode and high vacuum mode. Further, EDS analysis were measured with TEAM™ Software Suite, coupled with the Octane Plus System, as well at the regime pressure of the low vacuum mode and high vacuum mode.

A metal part with a cataphoretic coating on the surface was examined in a place with a non-conforming cross-cut test. In this place (of the peeled coating on the metal part), elements that may originate from the zinc-phosphate layer were locally detected. Therefore, the peeled off coating from its underside was further analysed. Differently sized crystals were found here, and their composition may correspond to the zinc-phosphate layer.

Analyzing a metal part with a cataphoretic coating on the surface with with a non-conforming cross-cut test by using SEM and EDS methods, it was proven that the zinc-phosphate layer in the pre-treatment was applied, but did not adhere to the surface of the part as it should have. It is necessary to further focus on the individual steps of pre-treatment. There may have been insufficient degreasing at the beginning of the pre-treatment process. Or the cause is the poor quality of the zinc-phosphate solution.

Keywords:

Cataphoretic coating, EDS, SEM

Reference:

Brüggemann M. et al.: Electrocoat: Formulation and Technology (2020), Vincentz Network GmbH & Co. KG ISBN: 978-3-7486-0105-0.
Weldon D. G.: Failure Analysis of Paints and Coatings, Revised Edition (2009), John Wiley & Sons, Ltd. ISBN: 978-0-470-69753-5.
Streitberger H.-J. et al.: Automotive Paints and Coatings, Second, Completely Revised and Extended Edition (2008), Wiley-VCH Verlag GmbH & Co. KGaA ISBN: 978-3-5273-0971-9.

946

Investigation of earth-abundant photovoltaic material Zn3P2 nanostructures using electron microscopy

Aidas Urbonavicius[1,2], Dr. Sebastian Lehmann[2,3], Prof. Kimberly A. Dick[1,2,3], Dr. Simon Escobar Steinvall[1,2]
[1]Centre for Analysis and Synthesis, Lund University, Lund, Sweden, [2]NanoLund, Lund, Sweden, [3]Division of Solid State Physics, Lund University, Lund, Sweden

Poster Group 2

Background incl. aims
Earth-abundant semiconductor material Zn_3P_2 is a promising alternative for photovoltaic applications. Unfortunately, there are not many suitable substrates for Zn_3P_2 nanostructure growth as it is difficult to find a lattice parameter and thermal expansion coefficient matching material. Therefore, growth of defect-free Zn_3P_2 nanostructures has been proven to be challenging as it tends to form defects during growth which results in poor crystal quality thus is detrimental for photovoltaic applications.[1][2] To minimize the number of defects, a new method of Zn_3P_2 growth is needed. Selected Area Epitaxy (SAE) and Vapour-Liquid-Solid (VLS) have been shown to be effective techniques in producing different morphologies of Zn_3P_2: nanowires, nanopyramids and thin films.[3] Both techniques reduce the interfacial area which is key in limiting defect formation. In both VLS and SAE indium has been utilized as a seed particle or the substrate (InP). By exchanging In for more earth-abundant Sn seed particles for VLS and InP substrate for Si, it would be possible to completely remove In from the growth process. It is also important to investigate high throughput methods of producing Zn_3P_2 nanostructures for possible future industrial scalability.
Methods
Metal organic vapour phase epitaxy (MOVPE) is an appealing method for growth of SAE and VLS Zn_3P_2. MOVPE is an epitaxy method that has a high through-put and is widely used in industry for manufacturing compound semiconductor devices. InP substrates have been used in our experiments with a silicon oxide (SiO_2) mask that was patterned by EBL to try and identify preliminary growth parameters for SAE growth. Growth times, temperature and precursor flows have been varied to try and find optimal conditions for Zn_3P_2 growth with minimal parasitic nucleation on the SiO_2 mask. For SAE patterning, displacement Talbot lithography (DTL) which is a lithography technique that uses collimated monochromatic light to create a periodic pattern on the substrate, was used. Moving away from EBL to DTL is a key step for scalability of Zn_3P_2 growth, as DTL can pattern much larger areas quicker. Si substrates were used for DTL dose and pattern testing. Sn seed particles on InP substrate for VLS growth were used. Scanning electron microscopy (SEM) and transmission electron microscopy (TEM) were used to image and investigate the morphology and growth selectivity of the resulting Zn_3P_2 structures. Scanning TEM (STEM) together with x-ray energy dispersive spectroscopy (XEDS) was used to image and acquire compositional data of the nanowires.

Results
SAE Zn_3P_2 pyramidal structures by MOVPE on InP substrate were successfully grown (Fig.1a). By optimizing the precursor flows and temperature we were able to minimize most of the parasitic nucleation on the SiO_2 mask layer. DTL was used to pattern hexagonal pattern of holes on SiO_2 on Si substrates, which have diameter of 180nm-200nm and pitch of 500nm (Figure 1b). Sn seeded Zn_3P_2 nanowires were grown and then transferred to a TEM copper grid (Fig. 1 c-d). Additional compositional analysis of the nanowires was performed using XEDS coupled with STEM.

Conclusion

We have shown that growth of SAE Zn_3P_2 on InP substrate is possible using MOVPE. By optimizing the growth conditions parasitic growth is minimized on the mask. Si substrates were patterned by using DTL and desired size and pitch of the nanoholes was achieved. Nanowires were successfully grown by using Sn instead of In seed particles. We hope to exchange InP for Si thus removing any scarce elements from the production and enabling full scalability of Zn_3P_2 nanostructures. Future experiments will focus on realizing SAE Zn_3P_2 growth on the patterned Si substrates and exploring Si substrates for Sn seeded VLS nanowire growth.

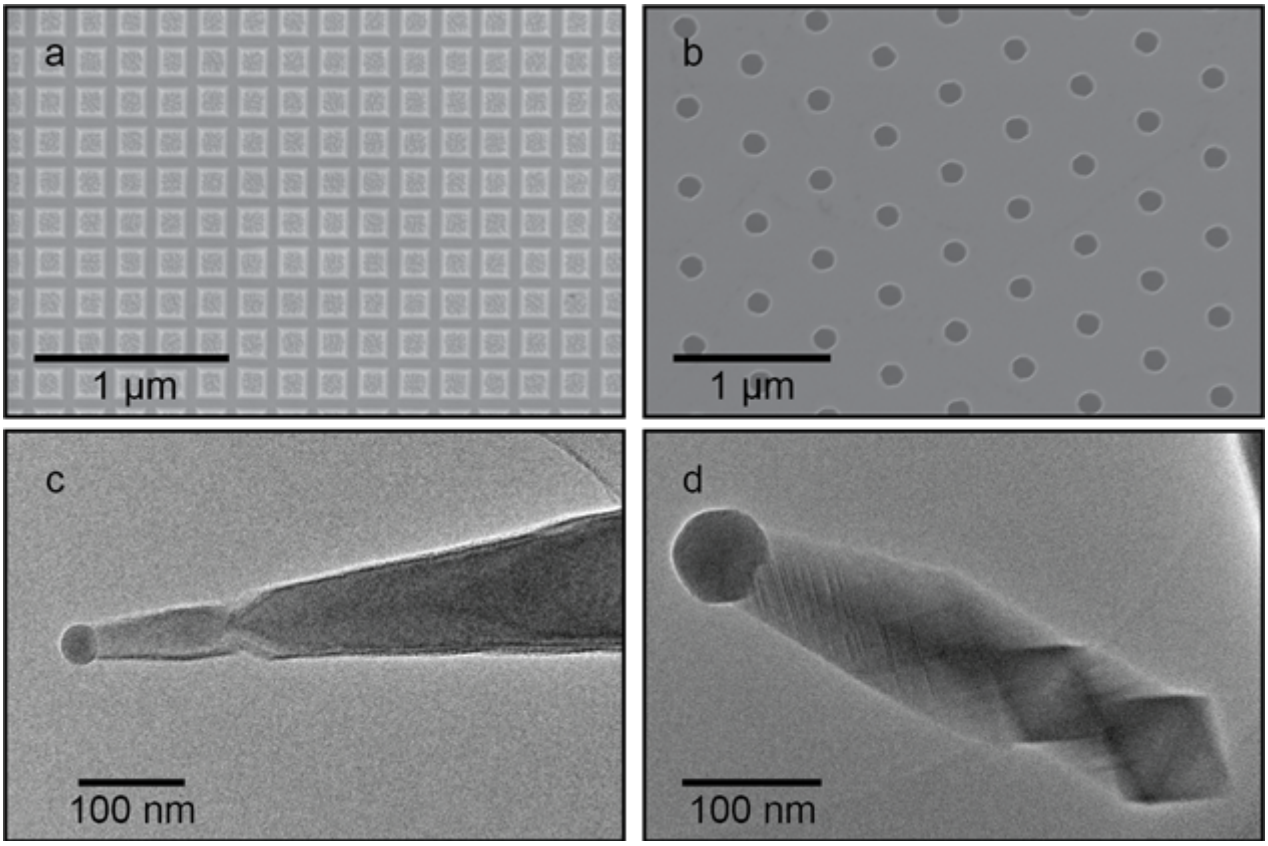

Keywords:

Zn3P2 Earth-Abundant SAE VLS SEM

Reference:

1. A. Catalano & R. B. Hall, J. Phys. Chem. Solids, 41(6), 635-640, 1980.
2. J. P. Bosco et al., J. Cryst. Growth, 363, 205-210, 2013.
3. S. Escobar Steinvall et al., ACS Appl. Energ. Mater., 5, 5298-5306, 2022.

950

Atomic-scale imaging of local structure of layered Cu-Te phases

Dr. Habil. Andriy Lotnyk[1], Dr. Vladimir Roddatis[2], Nils Braun[1], Sonja Cremer[1], Dr. Hagen Bryja[1], Lennart Voss[3], Prof. Lorenz Kienle[3]
[1]Leibniz Institute of Surface Engineering (IOM), , Leipzig, Germany, [2]GFZ German Research Centre for Geosciences, Potsdam, Germany, [3]Institute for Materials Science, Faculty of Engineering, University of Kiel, Kiel , Germany

Poster Group 2

Background incl. aims
Copper-based chalcogenide materials exhibit distinct properties, making them promising candidates for a range of applications [1]. Among these materials, Cu-Te compounds have attracted significant interest due to their versatility in fields like thermoelectricity, memory technology, photothermal therapy, photovoltaics, and batteries. The properties of these alloys are closely linked to their local structure, making accurate description essential for optimizing device performance and advancing material development. The local structure of Cu-Te compounds remains a topic of ongoing discussion [2], especially concerning materials in their low-dimensional form, such as thin films.

This study addresses the controversial aspects of the local structure of Cu-Te phases prepared by thin-film solid-state reaction. Using Cs-corrected scanning transmission electron microscopy (STEM) and atomic-resolution electron energy loss spectroscopy (EELS), the atomic positions of metal and chalcogen atoms in Cu-Te structures are directly visualized. In addition, the investigation revealed the formation of new Cu-Te phase. A crystal structure model for this phase was proposed based on atomic-scale images.

Methods
Atomic-scale investigations are carried out via direct imaging in real space utilizing iDPC, ABF, HAADF and EELS methods. Cu-Te structures are synthesized from metal Cu layer and Sb_2Te_3 epitaxial thin films by thermal heating.

Results
The microstructural investigation of the Cu/Sb2Te3 system unveiled a reaction between the Cu layer and Sb2Te3 upon heating. This reaction led to the formation of van der Waals bonded layered Cu-Te structures, comprising double and triple layers of Te, as depicted in Fig 1. Contrary to existing literature, a detailed analysis of the atomic positions of Cu and quantification of interatomic distances revealed the crystallization of a Cu-rich trigonal Cu1.75Te phase (P-3m1) as the predominant double-layered Cu-Te structure.

Furthermore, a new metastable Cu-rich trigonal phase of Cu1.75Te (P3m1) was found, for which a structural model has been proposed. The phase features a triple-layered structure, resembling the Cu1.75Te double-layered phase. Notably, this metastable phase exhibits vacancies on Cu sites. A detailed analysis of the transition regions suggests that the triple-layered Cu1.75Te structure can easily transformed into the double-layer phase through rearrangements of Cu atoms. Crystal defects, including stacking faults and dislocations, were also observed within the crystal structures. Due to its resemblance to layered Sb_2Te_3 structure, a triple-layered structure was also fabricated as a thin film through solid-state epitaxy of Cu and Sb_2Te_3 layers, using magnetron sputtering at room temperature.

Conclusion

The findings from this study offer valuable insights into the local structure and preferred phases of Cu-Te, which can be relevant during the cycling of Cu-based bulk thermoelectric materials [3]. This knowledge lays the groundwork for theoretical investigations into their properties and facilitates the design of novel layered materials.

We acknowledge A. Mill, T. Pröhl and P. Hertel for their technical support and German Research Foundation (DFG, projects 448667535 and 445693080) for financial support of this work.

Fig. 1. (a) Atomic-resolution ABF-STEM image showing van der Waals bonded layered Cu1.75Te structures consisting of double (2Te) and triple layers (3Te) of Te. (b) High-resolution HAADF-STEM image and (c) corresponding atomic-resolution EELS maps of Cu (red colour) and Te (green colour).

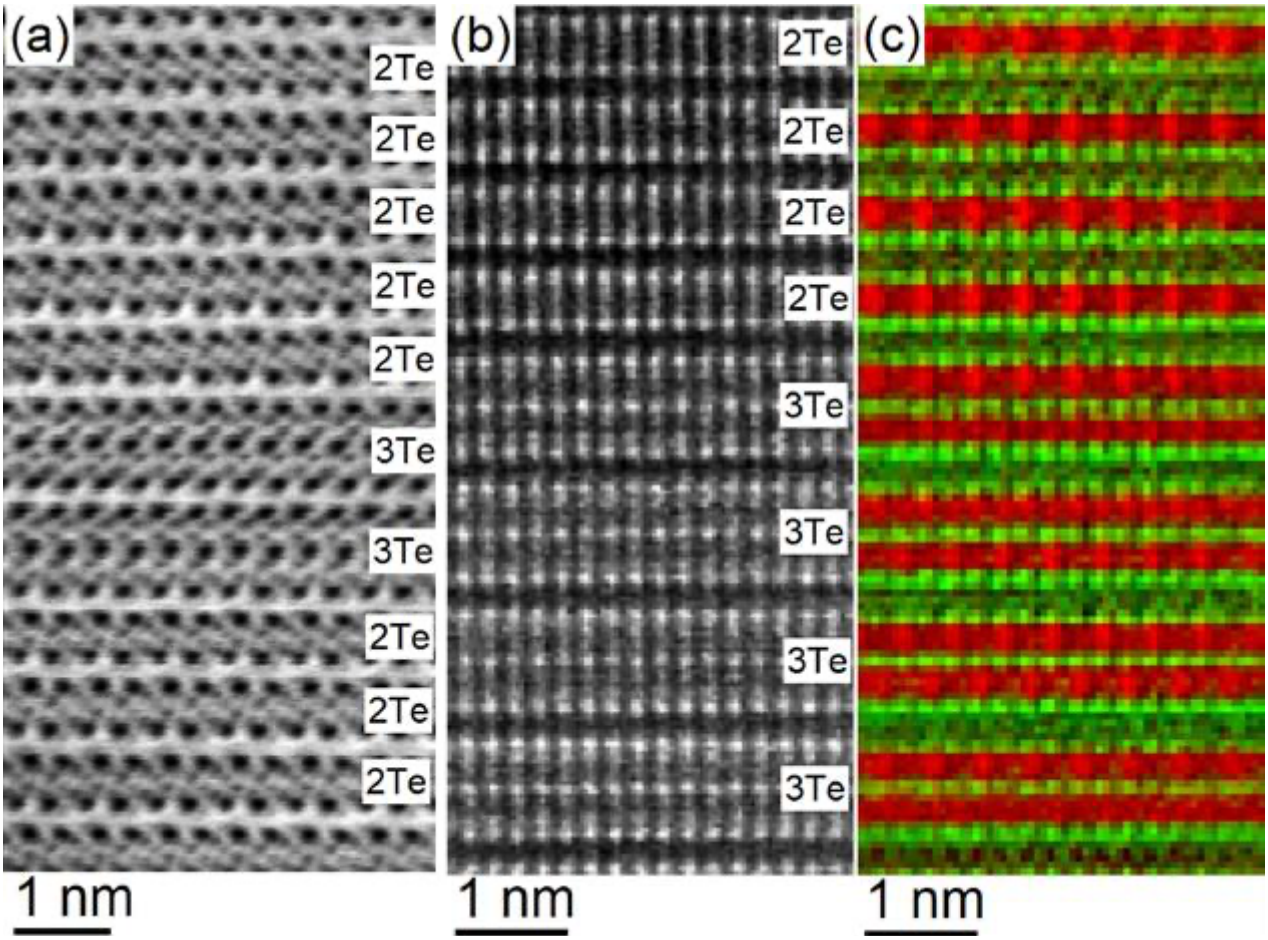

Keywords:

Thin films, Nanoscale analysis, structure

Reference:

[1] X. Chen, J. Yang, T. Wu, L. Li, W. Luo, W. Jiang, L. Wang, Nanoscale 10 (2018) 15130–15163
[2] L. Yu, K.Luo, S. Chen, C.-G. Duan, CrystEngComm 17 (2015) 2878–2885
[3] Y. Kawami, X.Q. Tran, et al., Small 18 (2022) 2204225

998

Contribution of residual gas and surface contaminants to contamination growth on irradiated samples

Arne Schwartz[1], Dr. Erich Müller[1], TT.-Prof. Dr.-Ing. Yolita Eggeler[1,2]
[1]Laboratory for Electron Microscopy, Karlsruhe Institute of Technology (KIT), Karlsruhe, , [2]3DMM2O - Cluster of Excellence (EXC-2082/1 – 390761711), Karlsruhe Institute of Technology (KIT), Karlsruhe,

Poster Group 2

Background incl. aims

Exposing a sample to an electron beam leads to growth of amorphous carbon contamination [1] deposited due to beam induced polymerization of hydrocarbons. This contamination is a challenge in electron microscopy because it can obscure fine details of the specimen, distort the signal obtained in elemental analysis and artificially modify surface reactions during reactive in situ experiments.
The sources of hydrocarbons are the residual gas in the instrument chamber and the sample surface itself, where the latter is often assumed to have the bigger impact on contamination growth [1].
This work is designed to quantify the contribution of these sources of hydrocarbons on the contamination growth using a suitable model [2] and is based on measurements from dedicated experiments. Similarly to other works [3], the contamination process is assumed to be a time-dependent reaction diffusion process driven by the electron beam. A source and a sink term are introduced to describe the supply of hydrocarbons from the residual gas in the microscope chamber and the removal of mobile hydrocarbons through polymerization by the electron beam. The contamination formation predicted by the model is compared with experimental results to determine the differently contributing parameter of the process.
This study analyzes the direct contribution of contaminants from the residual gas to polymerization by the electron beam and the indirect contribution by reestablishing an equilibrium density of surface contaminants. In addition, the contribution of surface contaminants to contamination growth by diffusion into the irradiated area is analyzed. It is intended to find from the specific process parameters not only insights regarding the supply of contaminants, their type and size, but also methods to reduce the contamination growth on illuminated sample surfaces.

Methods

To quantify the contamination growth, a thin amorphous carbon substrate (thickness < 10 nm) is illuminated homogeneously with a defocused electron beam in a FEI DualBeam Strata 400S. This is done for distinct time steps up to 20 min resulting in the growth of contamination rings.
The thickness and shape of the contamination rings is obtained through comparison of MC simulations with high-angle-annular-dark-field (HAADF) images taken in between 5 minutes of illumination. Both, irradiating and imaging are performed at primary electron energy of 20 keV and a current of 120 pA. The illuminated area is chosen to be sufficiently large (radius ~ 700 nm) to separate the individual parameters describing the contamination process.
The theoretical model used describes the change of the relative surface density of contaminants $n = N/N_0$, where $N_0 = N(t=0)$ is the density of contaminants prior to illumination [2].
The diffusion into the irradiated area is described by a diffusion constant D while the contribution of the residual gas in the microscope chamber is modeled by an adsorption frequency η that tends to reestablish the equilibrium surface density of contaminants. The removal of contaminants through polymerization into immobile contamination is described by a reaction cross section σ.
To obtain the dependency of these parameters on the residual gas condition, contamination growth experiments at different pressures are performed while evacuating the microscope chamber and also by using a cold trap. Mass spectrometer measurements are conducted to analyze the components of the residual gas in the microscope chamber, which could contribute to the supply of contaminants.

Furthermore, contamination growth measurements are performed after removing contaminants from the sample surface by in situ plasma cleaning.

Results

The parameters of the model are obtained by fitting the simulated contamination shape and thickness to the experimental data.

The reaction cross section σ = 2.22e-20 m² and the diffusion constant D = 1.15e-15 m²/s don't change significantly between measurements with different residual gas pressures of the microscope chamber. The initial density of contaminants on the sample surface slightly increases from N_0 = 1.25e20 1/m² to N_0 = 1.60e20 1/m² with higher pressure indicating the adsorption of hydrocarbons from the ambient gas to the sample surface.

Figure 1 a) shows the concentration of small hydrocarbons in the residual gas of the microscope chamber as a function of the evacuation time. It can be seen that the partial pressure of these components decreases with a similar rate as the total pressure in the vacuum chamber. Figure 1 b) shows the adsorption frequency of the contaminants onto the sample surface with respect to the pressure inside the instrument chamber. Thus, lower pressure leads to a decrease of the adsorption frequency and a lower buildup of carbon contamination on the sample surface. Anyway, the value of η smaller than 0.001 Hz is very low compared with the other frequencies governing this process.

Experiments with in-chamber plasma cleaning of the sample indicate a substantially reduced contamination growth. Measurements before and after cleaning for 100 s show a decrease in the initial density of contaminants from 7e19 1/m² to 2.2e19 1/m² pointing out the effective removal of contaminants from the sample surface. Simultaneously, the diffusion constant D increases by 28%, while the reaction cross section decreases by 83%.

Conclusion

Comparing the adsorption frequency η to the other parameters leads to the conclusion that even though the residual gas has a perceivable impact on the contamination growth, its contribution remains low in comparison to that of the contaminants present on the sample surface prior to illumination. Besides the direct add to the irradiated area, the supply of contaminants from the residual gas to the whole sample surface to an equilibrium density must be considered for longer experimental durations. However, these contributions can be reduced by lowering the chamber pressure.

The alterations in the diffusion constant and reaction cross section after plasma cleaning imply the presence of more mobile and smaller contaminants [4]. This suggests that contaminants adsorbed from residual gas might be smaller than those removed from the sample surface, being probable for the molecules shown in Figure a).

The effectiveness of in situ plasma cleaning to remove several of the present mobile contaminants is shown by a lower carbon contamination.

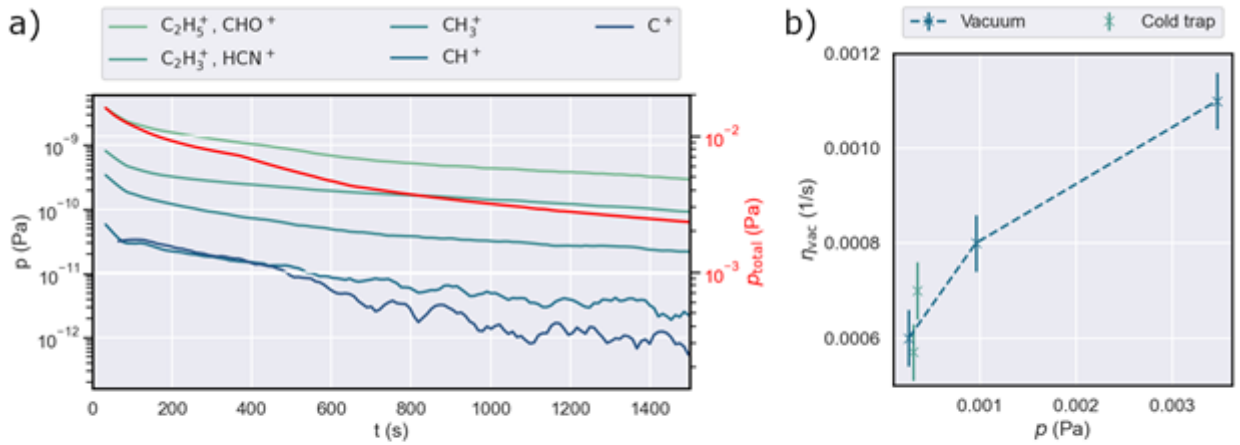

Figure 1: a) Evolution of the partial pressure of small hydrocarbons and total chamber pressure during evacuation of the microscope chamber recorded with a mass spectrometer. b) Contaminant adsorption frequency from residual gas against chamber pressure, with vacuum variation (blue) and utilization of a cold trap (green).

Keywords:

Contamination,surface diffusion,electron microscopy

Reference:

[1] M. Hugenschmidt et al., Microsc. Microanal. 29 (2022)
[2] E. Müller, Ultramicroscopy, submitted 2023
[3] K.H. Müller, Optik 33 (1971)
[4] D.A. Alman, Physics of plasmas 7 (2000)
[5] Acknowledgment: Y.M.E., E.M., A.S., acknowledge funding from 3DMM2O - Cluster of Excellence (EXC-2082/1 – 390761711), Karlsruhe Institute of Technology (KIT), and funding from TrackAct (SFB1441, Project-ID 426888090)

1022

TEM investigation of AlN-Cu(O) with variable amounts of copper

PL Martin[1], PY Jouan[1], Nicolas Gautier[1], M Richard-Plouet[1], Dr Valerie Brien[1]
[1]Nantes université, CNRS, Institut des Matériaux de Nantes Jean Rouxel, IMN, F-44000 Nantes, France

Poster Group 2

Some nitrides can have a good potential for photocatalytic applications, notably for antibacterial applications. AlN combined with copper could be one of those. The action of photocatalytic materials being conditioned by the value and electrochemical positions of electronic bands, it is necessary to start by specifying precisely the nature of composing phases of the nitrides after their synthesis.

Although recent theoretical calculations [1] (using ab initio DFT –Density Funtion Theory- and thermodynamics) can predict the stable and metastable routes of bi-metal nitrides on high ranges of composition, nothing can replace the microscopic observation of materials experimentally synthesized by an out of balance technique such as reactive magnetron sputtering.

AlN-Cu(O) material was prepared under the shape of thin films by D.C. -Direct Current- reactive magnetron sputtering under synthesis conditions chosen for facilitating film nanostructuration. The progressive addition of a third element to the binary nitride AlN could either lead to solid solution AlCuN or to a material composed of AlN and Cu rich phases. Whereas, XRD –X-ray Diffraction- was systematically performed for preliminary checking, TEM-Transmission Electron Microscopy-investigation is an essential and ideal step to discriminate the actual microstructure of the films and to position the experimental synthesis route towards the limit of solubility of copper in the nitride. Electron diffraction patterns exploited through collection of rotational signals allowed the use of EVA software classically used by X-ray Diffraction experimentators to confront diffraction data to ICDD - International Center for diffraction Data- database. This work lead to the identification of phases. Chemical localization of copper could be detected by chemical mapping (STEM-EDS: 4DSTEM-ScanningTEM-), and crystallized zones could be tracked by diffraction and subsequent filtering (dynamical dark fields or numerical ones thanks to FFT –Fast Fourier Transform- of HR-High Resolution-TEM images).
The modification of the microstructure (change of nature of phases, their chemistry, crystalline structure, changes of morphology…) will be given as a function of the amount of copper used to elaborate the samples.

Keywords:

Nanostructure, morphology, AlN, copper, cermet

Reference:

[1] W. Sun, C.J. Bartel, E. Arca, S.R. Bauers, B. Matthews, B. Orvañanos, B.-R. Chen, M.F. Toney, L.T. Schelhas, W. Tumas, J. Tate, A. Zakutayev, S. Lany, A.M. Holder, G. Ceder, A map of the inorganic ternary metal nitrides, Nat. Mater. 18 (2019) 732–739. https://doi.org/10.1038/s41563-019-0396-2.

1090

Fabrication and high-resolution transmission electron microscopy characterization of nanopores in silicon nitride and 2D materials

Teresa Tang[1], Marco Kögel[1], Michael Mierzejewski[1], Michael Schlegel[1,2], Peter D. Jones[1], Jannik C. Meyer[1,2]
[1]NMI Natural and Medical Sciences Institute at the University of Tübingen, Reutlingen, Germany,
[2]Institute of Applied Physics, University of Tübingen, Tübingen, Germany

Poster Group 2

Background
Solid-state nanopores are an emerging technology for single molecule sensing of biomolecules including DNA, RNA, and proteins [1]. They provide a more resilient alternative to tradition biological nanopores, which are sensitive to temperature, pH, and other environmental factors. Specifically for solid-state nanopores, 2D materials provide a good foundation that is easy to modify, robust, and reusable [2,3]. 2D materials have unique properties that only appear when bulk materials are reduced to the nanoscale. Specific attributes can be generated in the 2D material and alter the dynamics of molecules travelling through the nanopores. Materials of interest include graphene, hexagonal boron nitride (h-BN), and transition metal dichalcogenides (TMDCs).
Methods
Different techniques for manufacturing solid state nanopores are investigated. These include transmission electron microscopy (TEM), scanning transmission electron microscopy (STEM), and helium ion microscopy (HIM). From these microscopy methods, nanopores are created in SiNx membranes as well as in 2D materials.
Results
Pores in the range of tens of nanometres are milled into SiNx using the HIM. Single nanopores as well as arrays of nanopores were created to investigate various milling parameters (Figure 1. A, B). DNA translocations were observed by ionic current measurements, validating the presence and function of the nanopore. For 2D materials, a scaffold of SiNx must be used to create freestanding 2D materials. Graphene and h-BN are transferred onto HIM milled or gallium focused ion beam (FIB) milled holes in SiNx membranes. The resulting membranes are imaged with high resolution TEM (Figure 1.C).
Conclusion
Electron microscopy and ion beam milling are promising techniques for the production of solid-state nanopores. Various pore geometries will continue to be explored and methods will be developed to create novel nanopores in 2D materials. The combination of 2D materials results in unique properties in nanopore structures which would otherwise be difficult to achieve without the use of electron microscopy and nanostructuring.

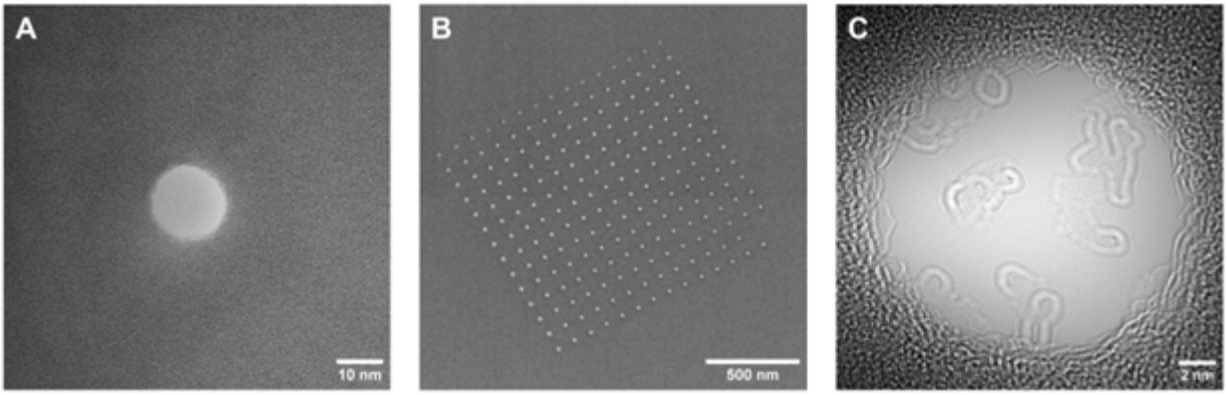

Figure 1: (HR)-TEM images of various nanopores milled into SiN_x membranes using HIM. A) A single nanopore of 15 nm diameter in SiN_x. B) An array of 225 nanopores (15×15), used to compare dose and dwell time parameters. C) Monolayer graphene transferred onto a HIM-milled nanopore of 15 nm diameter. The lattice of the graphene can be seen, as well as traces of carbon contamination.

Keywords:

Nanopores, 2D materials

Reference:

[1] Xue L et al. Nat. Rev. Mater 5, 931–51 (2020).
[2] Danda G, Drndić M. Curr. Opin. Biotechnol., 55, 124–33 (2019).
[3] M. Thakur et al., npj 2D Materials and Applications 7, Art.no. 11 (2023)
[4] This work has received funding from the Federal Ministry of Education and Research (BMBF), under project Nanodiag, 03ZU1208BG and from the State Ministry of Baden-Wuerttemberg for Economic Affairs, Labour and Tourism.

1097

Investigation of Lateral and Vertical Heterostructures of MoS2/WS2

Jürgen Belz[1], Dr. Oliver Maßmeyer[1], Samane Ojaghi Dogahe[1], Dr. Andreas Beyer[1], Henrik Myja[2], Tillmar Kümmell[2], Bacher Gerd[2], Michael Heuken[3], Annika Grundmann[4], Holger Kalisch[4], Andrei Vescan[4], Kerstin Volz[1]
[1]Department of Physics & Structure & Technology Research Laboratory, Marburg, Germany, [2]Werkstoffe der Elektrotechnik & CENIDE, University of Duisburg-Essen, Duisburg-Essen, Germany, [3]AIXTRON SE, Herzogenrath, Germany, [4]Compound Semiconductor Technology, RWTH Aachen University, Aachen, Germany

Poster Group 2

Background

Two-dimensional (2D) materials have the potential to transform semiconductor technology. Their rich compositional and stacking diversity, especially when deposited as heterostructures, allows tailoring of material properties to enable a wide range of device applications [1]. A prominent class of these 2D materials are the transition metal dichalcogenides (TMDs). With improved synthesis and fabrication capabilities, heterostructure concepts have been developed that show promising material properties for ultrathin optoelectronic devices. While these heterostructures can be fabricated by mechanical pattern transfer for small areas with high precision, these approaches are difficult to scale up. Therefore, alternative approaches such as metal organic chemical vapor deposition (MOCVD) have been developed to fabricate 2D materials and their heterostructures. Depending on the process parameters, several growth modes can dominate and thus a variety of structure combinations can be created. Since optical and electronic properties typically depend on the orientation, high-resolution measurements of the number of layers and feature sizes of each material can help to understand macroscopic optical measurements and guide the optimization of growth processes towards desired layer structures.

Methods

The MOCVD grown WS2/MoS2 heterostructures were transferred using a PMMA transfer process with successive cleaning and baking steps. Scanning transmission electron microscopy (STEM) measurements were performed using a JEOL JEM-2200FS. By tuning the convergence angle to less than 2 mrad, we obtained scanning diffraction data leading to nanoscale resolved alignment information. In addition to these diffraction measurements, we use energy dispersive X-ray spectroscopy (EDX) to resolve the chemical composition of the few-layer heterostructures. The structure is further resolved by conventional quantitative annular darkfield STEM image simulations and 4D-STEM measurements.

Results

We find evidence for both vertical and lateral heterostructures of MoS2/WS2 and a homogeneous but complex 2D film with few layers and pronounced island growth. The number of layers can be deduced by quantitative EDX mapping supported by image contrast simulations (Figure 1a). We find a nearly coalesced WS2 monolayer with additional multilayer island growth. The MoS2 layer grown on top can be shown to form either from facets of the multilayer WS2 (Figure 1b) or from nucleation without facets on top of the tungsten TMD. Figure 1c shows an example of a presumably vertically stacked MoS2/WS2 heterointerface. It can be seen that the contrast is dominated by the tungsten columns of the underlying film, which highlights the need for quantitative image simulations.

Conclusion

We can show the microscopic orientations of the TMD heterostructures in the case of MoS2 and WS2 grown by MOCVD. The combination of analytical techniques such as EDX and quantitative image simulations helps to unambiguously identify the complex layer structure of this few layer material system. We are also exploring the possibility of identifying relevant material domains by large area scanning nanobeam diffraction using 4D STEM imaging.

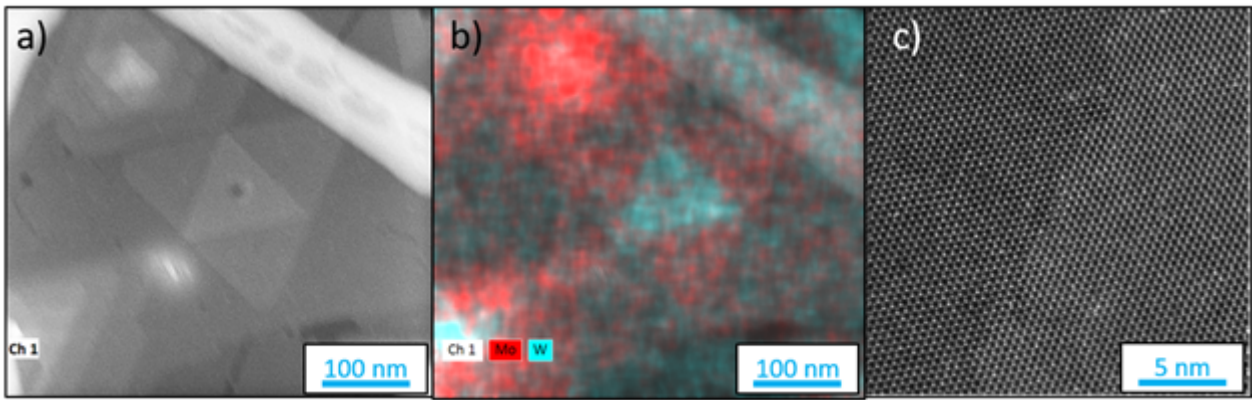

Keywords:

2D Materials, STEM, Heterostructures, TMDs,

Reference:

[1] K. S. Novoselov, et al.: Science, 2016, 353, 6298

1100

Insights into the formation of polycrystalline seed layers for the solution growth of semiconductor nanorods

Sarka Kucerova[1,2], Dr. Jozef Veselý[2], Dr. Michal Mazur[3], Jan Macháček[1], Matěj Berešík[1], Dr. Nikola Bašinová[1], Dr. Roman Yatskiv[1], Prof. Seungbum Hong[4], Dr. Jan Grym[1], Seongwoo Cho[5]
[1]Institute of Photonics and Electronics, CAS, Chaberská 57, 18251, Praha 8, Czech Republic, [2]Faculty of Mathematics and Physics, Charles University, Ke Karlovu 3, 121 16, Praha 2, Czech Republic, [3]Faculty of Science, Charles University, Hlavova 8, 128 43, Praha 2, Czech Republic, [4]Korea Advanced Institute of Science and Technology, 291 Daehak-ro, Yuseong-gu Daejeon 34141, Republic of Korea

Poster Group 2

Background incl. aims

ZnO, and Ga2O3 nanostructures are the subject of interest in many research groups. In particular, ZnO and Ga2O3 nanorods (NRs) have considerable potential for applications in gas sensors, piezoelectric nanogenerators, photovoltaic devices, and pressure sensors. Most applications require position-controlled ordered arrays of physically identical nanorods (NRs). Position-controlled nanorod arrays can be obtained by selective-area epitaxy (SAE) on a suitable seed layer (SL) [1].
The size, shape, and preferential orientation along the c-axis, as well as the in-plane orientation of the crystallites within the SLs, are crucial for successful nucleation, good alignment, and crystallinity of the NRs. Crystallographic, morphological, also optical, and electrical properties of the crystallites and nanocrystals can be influenced and enhanced by heat treatment [2, 3].
The impact of the SL on the orientation of the NRs is even more significant and visible during the SAE, where the NRs do not nucleate and grow in close proximity, and the geometrical selection is suppressed. Every deviation from the preferential orientation of crystallites along the c-axis causes a visible misalignment of the grown NRs.
Another property of wurtzite ZnO crystals, which not only influences the optical and electronic properties but also affects the nucleation and growth of ZnO and NRs, is the polarity of the crystals. Spontaneous polarization in the ZnO and GaN wurtzite structures is present because of the missing center of symmetry; therefore, the [0001] direction and [000-1] direction are not equivalent.
We provide novel insights into the formation and investigation of the properties and quality of SLs used for the growth of ZnO and Ga2O3. We utilize SAE-grown arrays of single NRs to scrutinize the misalignment of crystallites within SLs prepared under different conditions without the influence of geometrical selection. By enhancing the crystal quality, controlling the Ga2O3 phase, and understanding of the ZnO polarity, we are moving the ZnO and Ga2O3 nanostructures closer to the applications.

Methods

ZnO and Ga2O3 arrays were prepared by chemical bath deposition (CBD) on sol-gel-deposited SLs patterned by EBL. The SEM provided the first morphological characterization of the nanostructures. With the assistance of machine learning during SEM image processing, dimensional changes were evaluated in nanostructures prepared under different growth conditions.
The crystallographic structures of ZnO and Ga2O3 were further investigated using TEM and HRTEM. Plane and line defects, which significantly influence the electronic and optical properties of the nanostructures, were examined using HRTEM, DF, and WBDF.
The epitaxial relationship between the NRs and SLs was investigated in more detail by automated crystal orientation mapping in TEM (ACOM/TEM-ASTAR), where a high spatial resolution map of the crystallite lattice orientation was obtained [2]. The interfaces between the NWs and SLs were investigated not only crystallographically but also chemically using EDX in the TEM.

Piezo-force microscopy (PFM) was used to examine the polarity of the crystallites within the ZnO SL. PFM is an AFM mode that can map the piezoelectric and ferroelectric properties of a material. The polarity of ZnO polar wurtzite NRs was investigated using convergent beam electron diffraction (CBED) and annular bright field (ABF) measurements.
In situ TEM heating experiments were performed on polycrystalline ZnO SL (Fig. 1) and Ga_2O_3 NRs to provide insight into the phenomena that occur at elevated temperatures.

Results
The SAE-grown arrays of NRs showed the expected behaviour. When the NRs showed significant misalignment on the non-patterned SL, the NRs in the arrays exhibited the same behaviour. In addition, the NRs showing good alignment on non-patterned SL sometimes grew well aligned in the arrays. However, a discrepancy was observed on a significant number of ZnO SLs, where the alignment of NRs from patterned and non-patterned SLs was not in agreement. This discrepancy was caused by geometrical selection during nonpatterned growth on SLs with a low texture.
Generally, the alignment of crystallites within ZnO SLs improves with elevated temperatures at the expense of reproducibility. The results of the ZnO SL sintering experiments in different atmospheres and on various substrates indicated the simultaneous occurrence of oxygen and zinc diffusion and preferential alignment. Depending on the conditions, this phenomenon occurs at different temperatures. Surprisingly, preferential alignment was also observed in the in-situ TEM heating experiment, where the substrate was not present. Furthermore, PFM investigation of the crystallite polarity evolution during the heat treatment of the ZnO SL suggests the unification of ZnO crystalline polarity at Zn-polar at elevated temperatures.
To move towards applications and achieve monocrystalline SAE-grown ZnO NRs on ZnO SL, the correlation between the size of an opening in the patterning mask and the size of crystallites in the SL was crucial. If the size of the opening was equal to or smaller than the average size of the crystallites in the SL, the probability of nucleation and growth of monocrystalline NR from a single crystallite increased significantly. The requirements for SL were still a good crystalline preferential orientation along the c-axis, maximum crystallite size, and minimized dispersion of crystallite sizes within the SL. Investigation of the crystal polarity dependence between the ZnO SL/ZnO NR indicated a hereditary relationship between the ZnO SL/ZnO NR polarities.
Although Ga_2O_3 has several polymorphs, the monoclinic β-Ga_2O_3 phase was mostly observed in the Ga_2O_3 nanostructures. SAE of β-Ga_2O_3 NRs on SnO SL showed no preferential alignment and uncovered a significant role of the geometrical selection. Furthermore, no epitaxial relationship was observed between the SnO SL and the β-Ga_2O_3 NRs during the in situ TEM heating experiment.

Conclusion
Using microscopy techniques and SAE, we delved into the behaviour of ZnO SLs during heat treatment. We break the common belief that vertical orientation of NRs on polycrystalline SLs can be directly linked to the quality and preferential orientation of the SL. With the help of SAE, we showed that this conclusion can be made only on arrays where the distances between the NRs are high and geometrical selection affecting the growth is not involved. We further demonstrated that the development of the preferential orientation of the crystallites in the SL during heat treatment is not related to the presence of the substrate.

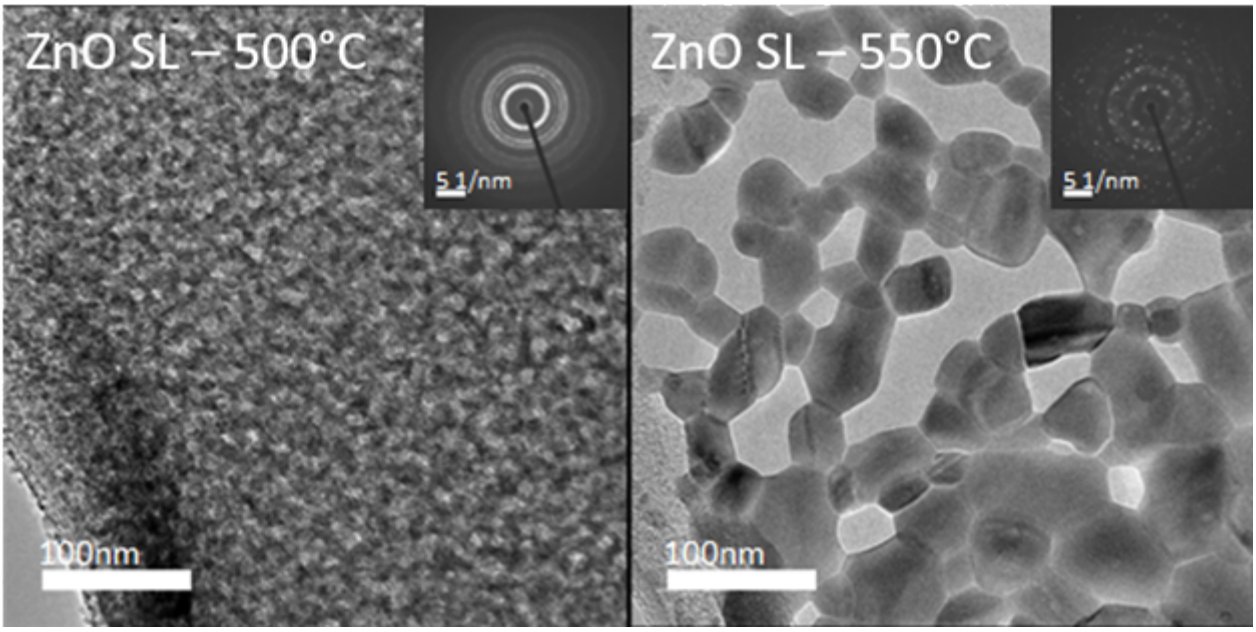

Keywords:

Nanorods, semiconductors, ZnO, polar crystals

Reference:

[1] O. Černohorský, J. Grym, H. Faitová, N. Bašinová, Š. Kučerová, R. Yatskiv, J. Veselý, Crystal Growth & Design 20(5) (2020), p. 3347–3357.
[2] R Yatskiv, J Grym, Š Kučerová, S Tiagulskyi, O Černohorský, N Bašinová and J Veselý, Journal of Sol-Gel Science and Technology 102(2) (2022), p. 447–453
[3] N Bašinová, O Černohorský, J Grym, Š Kučerová, H Faitová, R Yatskiv, … J Maixner, Crystals 9(11) (2019), p. 566

1110

Sample holder design for TEM in-situ straining experiments on 2D materials

Carmen Rubach[1], Dr. Xin Zhou[1], Tobias Dierke[2], Robert Kammel[1], Michael Sommerschuh[1], Prof. Janina Maultzsch[2], Prof. Erdmann Spiecker[1]
[1]Institute of Micro- and Nanostructure Research (IMN) & Center for Nanoanalysis and Electron Microscopy (CENEM), Friedrich-Alexander-University Erlangen-Nürnberg, 91058 Erlangen, Germany, [2]Institute of Condensed Matter Physics, Friedrich-Alexander-University Erlangen-Nürnberg, 91058 Erlangen, Germany

Poster Group 2

Background incl. aims
Two-dimensional (2D) materials consisting of single- or few-layer atoms such as graphene, transition metal dichalcogenides (TMDs, e.g. MoS2, MoSe2, WS2, WSe2) and hexagonal boron nitride (h-BN) show unique physical, chemical and mechanical properties owing to their planar atomic and band structures making them promising candidates for future device applications. For the fabrication of stable and reliable nanodevices such as for example energy storage and memory storage devices, optical switches, nanofilm displays and superconducting devices, it is crucial to understand the deformation behavior of the 2D materials used as building block of the respective device. In situ TEM tensile testing can give insights into the mechanisms of nanomechanical deformation, cleavage and sliding of the strained 2D material at the atomic level. [1]
For uniaxial in situ TEM tensile testing of freestanding 2D materials, either commercially available push-to-pull devices or custom-designed straining holders are needed. The custom fabrication of straining holders allow for the flexible adaptation of the utilized design to the needs of the transferred 2D material and/or the employed TEM techniques.
2D flakes mechanically cleaved from the bulk material are typically very small in size, but the exposed sample surface is very clean. To preserve this clean sample surface, a transfer process not involving stabilizing polymer layers (for example polymethyl methacrylate (PMMA) or polyvinyl alcohol (PVA)) should be used. For the Polydimethylsiloxane (PDMS) mediated dry stamping transfer of mechanically cleaved 2D materials a sample holder with a small central “viewing window” is required because the transfer small flakes is facilitated if they span over the whole central window. Furthermore the material surrounding the central window must be sturdy enough to withstand the slight pressure applied during the stamping transfer.
For the transfer of PMMA stabilized CVD grown 2D materials it can beneficial to have a longer viewing window (length about 20 µm) allowing the determination of the layer number of the 2D material by tilting the flake in Darkfield-TEM [2].
In this work, we report the design and fabrication of Cu support, which was used as substrate for the transfer of both mechanically exfoliated MoS2 and CVD grown bilayer graphene in situ TEM straining combined with 4D scanning transmission electron microscopy (4D STEM) were carried out to study the mechanical properties of 2D materials.

Methods
As substrate material for in-situ TEM tensile tests on 2D materials using a single-tilt Gatan straining holder 50 µm thick copper foil (Karl Schlenk AG) was chosen. As the transfer of 2D materials on the substrate requires a very smooth surface, the Cu-foil was polished to a surface roughness of 0,25 µm using diamond paste. After polishing, custom-designed dog bone shaped sample holders were sculpted from the Cu-foil, tailored to fit the Gatan straining holder 654, using a microPREP PRO laser ablation system (3D micromac). The sample holder design, measuring 12,0 mm in length, 2,4 mm in width and 1,0 mm width in the center, was generated using AutoCAD software (Autodesk). A small window with a length of 5 µm or 20 µm (depending on the transferred material) was cut into the

middle of the dog bone-shaped Cu-holder for the transfer of desired 2D flake. Two longer lateral slits (length 300 µm) were added to the design close to the central window to prevent exceeding the force limit of the Gatan straining holder 654 during tensile testing. To eliminate residual debris from the rim of the laser ablated central windows and to adjust the shape of the windows, the central area of the Cu support underwent precise ion beam refinement using a FEI Helios NanoLab 660 instrument (scanning electron microscope-focus ion beam, SEM-FIB). [3]
If the Cu-holder was used for straining molybdenum disulfide (MoS2) the polished copper surface was coated with a thin gold film (thickness 30 nm) to facilitate PDMS mediated dry transfer. The MoS2 flake to be transferred was first exfoliated to a PDMS stamp attached to a glass slide using wafer tape. The glass slide was then mounted into a micromanipulator which was used to align the flake under a stereomicroscope with the central windows of the sample holder and then to bring it in contact with its surface. To prevent slipping and deformation of the Cu-holder during the transfer process, the holder was attached on both ends with 2 strips of thermal release tape (RA-95LS(N), Rephalpha, release temperature 100-105 °C) to a glass slide prior to transfer. Once the MoS2 flake was in contact with the rim of one of the central small windows of the Cu-holder, the PDMS stamp was gently peeled off and the glass slide was placed on a hot plate at 100°C for several minutes to detach the thermal release tape.
CVD grown bilayer graphene (ACS materials, Trivial Transfer Graphene) was directly transferred to the customized Cu support by a “fishing” method. The PMMA coated CVD graphene was first immersed in deionized (DI) water, collected on a piece of filter paper and sectioned into tiny rectangles. One of these rectangular PMMA/ graphene films was then detached from the filter paper by once again immersing the filter paper in DI water and was fished out covering one of the central windows of the custom-designed Cu-holders. After drying for one hour, the PMMA was removed using acetone. [3]

Results & Conclusion

We designed straining holders tailor made for both the PDMS mediated transfer of mechanically exfoliated MoS2 as well as the polymer-assisted transfer of CVD grown bilayer graphene. After successful transfer, in situ straining experiments combined with 4D STEM were performed on both materials giving insights into the mechanisms of nanomechanical deformation at atomic level (for more details on this straining experiment on bilayer graphene see Zhou et al.- A twist to superlubric sliding in bilayer graphene uncovered by in situ TEM) .

Graphic:

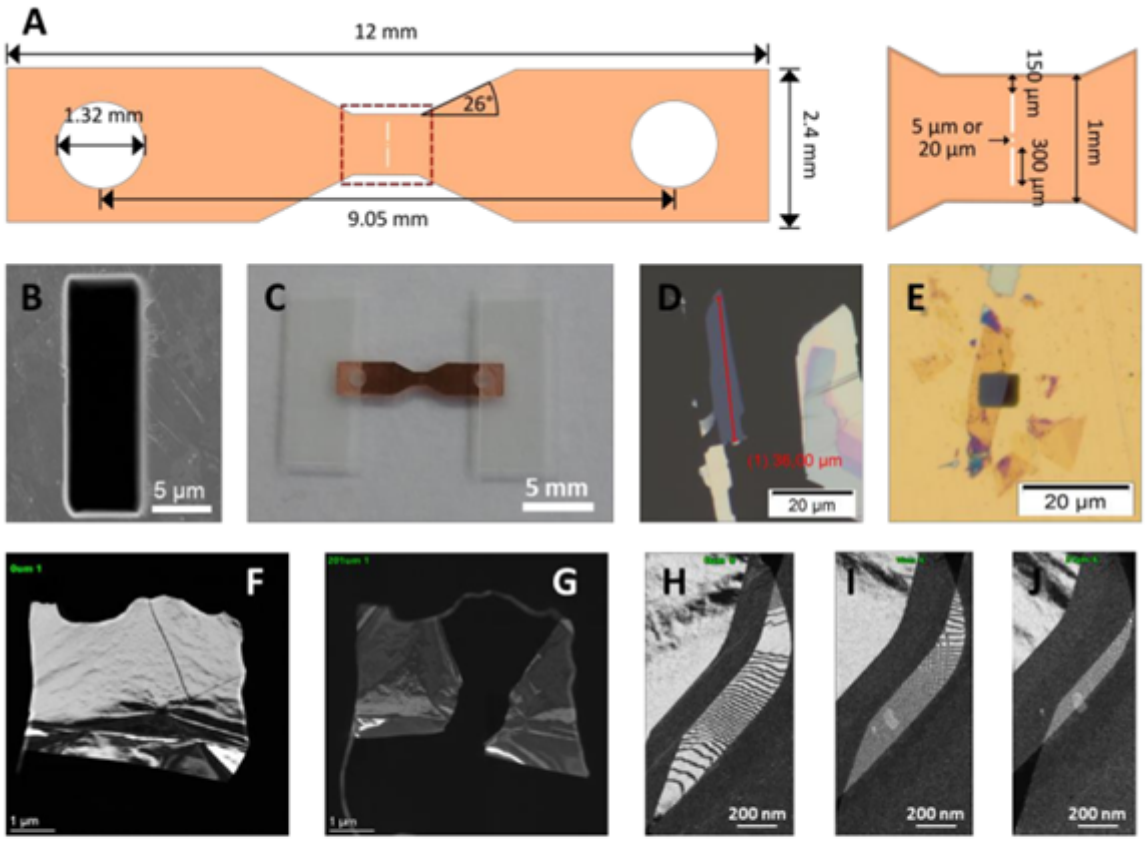

Fig. (A) Schemtic drawing of the custom-designed straining holder (B) SEM image of the central window after edge and shape refinement using a SEM-FIB (C) Lightmicroscopic image of the gold coated straining holder attached to a glass support using thermal release tape prior to PDS mediated stamping transfer (D & E) Lightmicroscopic images of a 3 layer thick MoS_2 flake on a Si/SiO_2 substrate prior to transfer and after transfer covering part of the central window of the straining holder (F & G) DF-TEM images of the flake shown in (D & E) after insertion in the TEM and after rupture of the strained flake (H to J) DF-TEM images of bilayer graphene taken at different straining step showing the change in the dislocation network

Keywords:

in-situ straining, MoS2, graphene

Reference:

[1] P. Li et al. (2021) Mater. Today 51, 247-272
[2] B. Butz et al. (2014)
[3] X. Zhou et al. in preparation

1240

Electrochemical sensors for detection of benzotriazole in water

Assist. Prof. Kristina Žagar Soderžnik[1,2], Neža Sodnika[1], Melanija Hadolin[3], Zoran Samardžija[1]
[1]Jožef Stefan Institute, Ljubljana, Slovenia, [2]Jožef Stefan International Postgraduate School, Ljubljana, Slovenia, [3]Faculty of Chemistry and Chemical Technology, Ljubljana, Slovenia

Poster Group 1

Background incl. aims

Benzotriazole (BTA) and its derivatives are extensively utilized in various industries for their properties as corrosion inhibitors, UV radiation filters, and plastic stabilizers. BTA is, therefore, found in food packaging, dishwashing detergents, textiles, lubricants, antifreeze, aircraft de-icing fluids, and other commercial and industrial products. [1,2]
Due to its solubility in water and resistance to biodegradation, BTA can persist in the environment. The inclusion of BTA as an additive in dishwashing detergents and tablets leads to its direct discharge into wastewater treatment plants, where it is only partially removed during the treatment process. As a result, BTA is prevalent in natural waters at nanomolar concentrations. While these concentrations may not pose an immediate threat to human health, the persistent nature and potential bioavailability of BTA can lead to long-term environmental consequences, which have yet to be sufficiently investigated. [1,2]
Currently, the primary methods for analyzing BTA in environmental samples involve solid-phase extraction followed by gas chromatography-mass spectrometry or liquid chromatography-mass spectrometry. However, there is a need for cost-effective, fast, reliable, in-situ detection of BTA for real-time monitoring of environmental samples. Given that BTA and some of its derivatives can be electrochemically reduced at low potentials, electrochemical detection on screen-printed electrodes (SPE) emerges as a promising approach. SPEs offer a more cost-effective, portable alternative to traditional electrochemical setups, which use conventional electrodes such as glassy carbon and mercury drop electrodes. In this work, a sensor based on carbon nanotube-Nafion-modified SPE is proposed for the detection of BTA. The modification of SPE was fully characterized via electrochemical and electron microscopy techniques.

Methods

1 mg/mL dispersions of carboxyl-functionalized single-walled or multi-walled carbon nanotubes (SWCNT, MWCNT) were prepared in a 1:1 (v/v) mixture of DMF and water containing 1 wt.% Nafion. The sensor was fabricated by drop-casting 4 µL of the CNT suspension on the working electrode of the SPE (DRP-150, Dropsens, Metrohm) and allowing it to dry at room temperature overnight.
BTA solutions were prepared in Britton-Robinson buffer (pH 2.4) and analyzed using cyclic voltammetry (CV) and square wave voltammetry (SWV). The electrochemical measurements were carried out by the PalmSens4 potentiostat.
The surface morphologies of the commercial SPE-C and modified SPE-SWCNT and SPE-MWCNT electrodes were investigated by using scanning electron microscopy (SEM) and transmission electron microscopy (TEM). The samples for SEM were embedded in metallic sample holders using conductive, carbon adhesive tape and observed at various magnifications in a field-emission-gun scanning electron microscope (FEG-SEM Verios G4 HP, Thermo Fisher Scientific, USA). Preliminary examinations of the samples showed that they were sufficiently electrically conductive for the SEM analysis. The experimental conditions for imaging were set to an accelerating voltage of 4 kV, a beam current between 20 pA and 50 pA, and a working distance of 3 mm. The electron micrographs were recorded with two detectors: (i) a through-the-lens detector (TLD) for secondary electrons (SE) and (ii) a mirror detector (MD) for backscattered electrons (BSE) positioned within the objective lens. To observe the SWCNT and MWCNT structure and size, transmission electron microscopy (TEM) with

energy-dispersive X-ray spectroscopy (EDS) was used (JEOL JEM-2100, Jeol Ltd., Tokyo, Japan). The samples for TEM observations were prepared by dispersing the nanoparticles after ultrasonic deagglomeration in water onto lacey carbon-coated Cu grids.

Results

The sensors' receptor element was based on modified commercial screen-printed electrodes (SPE). The drop-casted material's coverage of the working electrode (SWCNT or MWCNT) was assessed using electron microscopy to observe the morphology, composition, and conductivity of the material. As seen in Fig. 1a, the SWCNTs are anchored to the working electrode by a Nafion membrane, resulting in satisfactory surface coverage and conductivity. The MWCNT showed similar results with a grass-like structure and Nafion presence.

At the next step, the electrochemical behavior of BTA on the SPE-C/SWCNT was evaluated via CV. BTA exhibited a single reduction peak around –1,4 V with no observable oxidation peak during the reverse scan. The SPE-C/SWCNT exhibited significant adsorption capacity for BTA. As a result, SWV analysis was performed after a 60 s preconcentration period at –1 V. With this approach, a limit of quantification (LOQ) was determined, and the limit of detection (LOD) was calculated from the calibration curve (Fig 1b). The LOQ was 10 2 µM and LOD of 2 µM. This LOD is comparable to that obtained for BTA detection using commercially available SPE with a SWCNT working electrode [2], indicating that homemade modified SPEs offer a versatile alternative to commercial counterparts. Furthermore, by adjusting the composition, it may be possible to achieve an even lower LOD, comparable to those achieved using modified glassy carbon electrodes [3], making the proposed sensor suitable for real sample monitoring.

Figure 1. a) SEM image of the working electrode surface modified with SWCNT and Nafion and b) Calibration curve of the reduction peak current recorded on SPE-C/SWCNT.

Conclusion

Benzotriazole and its derivatives are ubiquitous in industries due to their diverse applications, yet their persistence in the environment poses ecological concerns. This study proposes a carbon nanotube-Nafion-modified screen-printed electrode for electrochemical BTA detection, addressing the need for cost-effective and rapid monitoring methods. Electrochemical analysis revealed a single reduction peak, leading to an LOD of 2 µM with square wave voltammetry. This approach offers a comparable alternative to commercial electrodes, underscoring its potential for environmental monitoring.

Acknowledgement:

The authors acknowledge the funding of our research activities by the ARRS through projects J2-3051, of which this investigation forms a part.

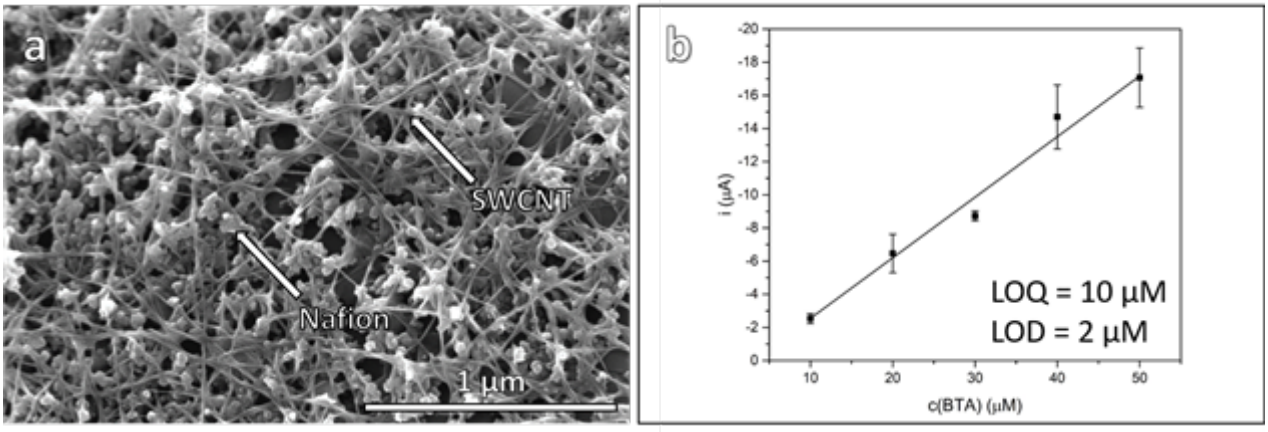

Keywords:

Benzotriazole, electrochemical sensor, SWCNTs, microscopy

Reference:

[1] A. Muschietti, N. Serrano, C. Ariño, M.S. Díaz-Cruz, J.M. Díaz-Cruz, Screen-printed electrodes for the voltammetric sensing of benzotriazoles in water, Sensors (Switzerland) 20 (2020). https://doi.org/10.3390/s20071839.
[2] Y. Zheng, F. Yang, J. Zhang, W. Pu, C. Yang, Voltammetric behaviors of an emerging pollutant benzotriazole on multiwall carbon nanotubes (MWNTs)—Nafion modified electrode in various pH mediums, Ionics (Kiel) 22 (2016) 2059–2066. https://doi.org/10.1007/s11581-016-1738-6.

1274

Low energy electron microscopy and spectroscopy of 2D materials

Dr. Eliška Materna Mikmeková[1], Dr Ivo Konvalina[1], Dr. Lukáš Průcha[1], Dr. Ilona Müllerová[1], Dr Aleš Paták[1]
[1]Institute of Scientific Instruments of the CAS, v.v.i., Brno, Czech Republic

Poster Group 1

Carbon, as the element of many different forms, is in the center of attention of many physicists for quite some time. In the last decade, carbon science and technology have enlarged its scope thanks to the discovery of 1D and 2D carbon forms (nanotubes and graphene), and the newest 2D materials – MXenes. Numerous technological applications are rising and will still arise in the foreseeable future, from these newly discovered carbon forms. Indeed, the development of these new materials and nanostructures requires the emergence of new surface-sensitive techniques for their characterization. As regards the surface sensitivity, the ultra-low-energy electron microscopy/spectroscopy can become a very powerful tool for the true examination of these atom-thin materials, capable of confirming physical phenomena predicted to occur on their surfaces. The advantage of modern commercial scanning electron microscopes is the possibility to enable imaging and analysis by low-energy electrons even at very high magnification.

Nevertheless, the real surface studies of 1D and 2D nanomaterials in microscopes equipped with selected spectroscopic techniques are not common so far, which is due to significant problems associated with the sample contamination under the electron beam. Since the specimen contamination increases with increasing of the electron dose and decreasing landing energy, specimen cleanness is a critical factor in obtaining meaningful data by low-voltage SEM/STEM. A range of various surface cleaning methods can be applied to selected samples. Typical cleaning methods, such as solvent rinsing, heating, bombarding with ions, and plasma etching have their limitations. Even a small amount of hydrocarbon contamination can severely impact the results obtained with low-energy electrons. During the scanning of surfaces by electrons, the image usually darkens because a carbonaceous layer gradually deposits on the top from adsorbed hydrocarbon precursors. This effect is called electron stimulated deposition. The surface diffusion of hydrocarbon molecules around the irradiated area serves as a source of additional precursors responsible for an even darker frame of the contaminated field of view. On the other hand, the effect of electron stimulated desorption occurs at the same time, especially at low energies. So, the fundamental question arises, whether the deposition of desorption will dominate, which depends on parameters settings in SEMs. We are using the slow electrons to electron-induced in-situ cleaning, which is gentle, experimentally convenient, and very effective for a wide range of specimens.

Detailed knowledge of mechanisms of electron scattering and its practical consequences for very low energies are of prime importance for not only measurement techniques but also development of new
materials for next-generation electronic devices. Determining inelastic mean free path (IMFP) of electrons in bulk materials is an ongoing topic in spectroscopy. Information on IMFP for very low electron energies, $E \leq 100$ eV, is not satisfactory and it is often missing in case of 2D materials, which are promising in the semiconductor industry. Low thickness of 2D crystalline materials motivated us to develop the unique UHV device analyzing samples via transmitted electrons in a standard microscopic regime (energy range 0 – 5 keV), and also via time-of-flight (ToF) method (focusing on energy range $E \leq 300$ eV). [1]

Graphene is one of the most well-known 2D materials, it is lightweight and strong, and its other unique
properties such as excellent electrical and thermal conductivity and transparency make it an ideal candidate for study at very low energies in the transmission mode of our device. We performed experiments with multilayered graphene to obtain electron energy loss spectra (EELS). Both plasmon peaks (π and π+σ) are present in the measured spectra for 2 layer and 3-5 layers graphene samples (Figure 1). The position of the plasmon peaks increases with both the number of layers of 2D samples and the momentum transfer value [2, 3]. The experimental EELS data are used to derive IMFP values. The measured data are supported by simulated momentum-resolved EELS spectra using many-body perturbation theory (Yambo code), on top of density-functional theory (DFT), Quantum Espresso [4].

We are focusing on the precise characterization of advanced 1D and 2D carbon-based nanomaterials (mainly graphene) and comparing the obtained data with theoretical DFT simulations. Moreover, we also examine possible surface damage by low-energy electron irradiation, which is a very important parameter in the electron analysis. We are using the low- and ultra-low-energy electrons for in-situ cleaning and even for already observed possible structure recovery. The influence of electron irradiation on sample quality (recovery/damage) is studied by Raman spectroscopy in detail.

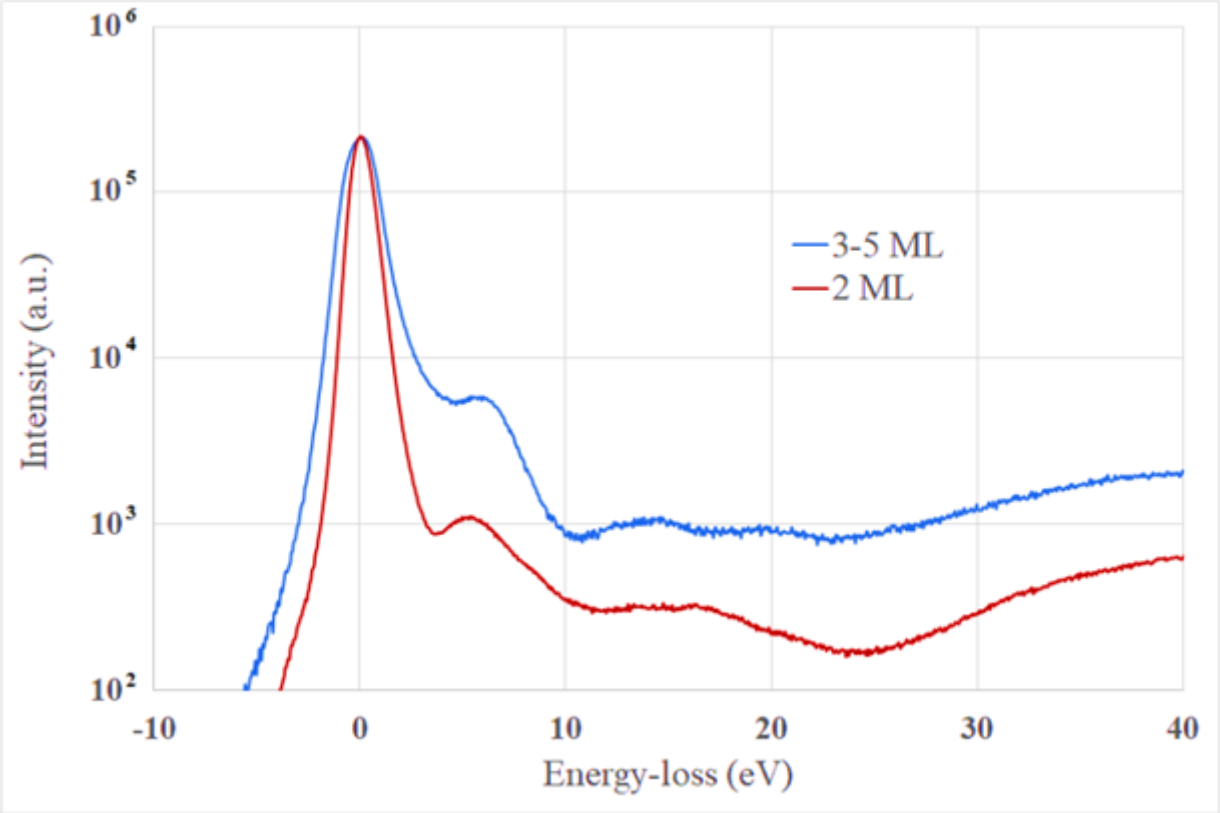

Keywords:

LVS(T)EM, ToF spectroscopy, graphene, DFT

Reference:

[1]I. Konvalina et al., Nanomaterials 11, (2021), 2435. https://doi.org/10.3390/nano11092435
[2]M. P. Seah and W. A. Dench, Surf. Interface Anal. 1 (1979), p. 2. https://doi.org/10.1002/sia.740010103
[3]P. Wachsmuth et al., Phys. Rev. B 90, (2014), 235434.https://doi.org/10.1103/PhysRevB.90.235434
[4]P Giannozzi et al., J. Phys. Condens. Matter 21 (2009), 395502. http://dx.doi.org/10.1088/0953-8984/21/39/395502

Acknowledgement:
The authors acknowledge funding from the Czech Science Foundation, GAČR- grant number GA22-34286S and the Technology Agency of the Czech Republic, grant number TN02000020.

1290

Nanosized Ti-Ni composite

Miroslav Cieslar[1], Nikoleta Štaffenová[1], Elena Chochoľáková[1], Jan Fikar[2], Jan Hanuš[1], Lucia Bajtošová[1]
[1]Charles University, Faculty of Mathematics and Physics, Ke Karlovu 5, 121 16, Prague, Czech Republic, [2]2Czech Academy of Sciences, Institute of Physics of Materials, Žižkova 22, 616 00 , Brno, Czech Republic

Poster Group 1

Background incl. aims
Self-propagating High-temperature Synthesis (SHS) is a relatively novel and straightforward method for producing advanced ceramics, composites, and intermetallic compounds [1]. The foundation of SHS lies in the ability of highly exothermic reactions to sustain themselves through a reaction (combustion) wave. SHS reactions have also been observed in Ni-Ti multilayer films [2], possessing great potential as an external heat source in various applications, including joining, ignitors, and intermetallic synthesis on the nanoscale. A novel approach proposes to use nanoparticles to achieve similar self-propagating reactions. This concept is particularly promising due to the ease of application of nanoparticles on various surfaces. Core-shell nanoparticles, especially those with a titanium (Ti) core and a nickel (Ni) shell, are of significant interest. This configuration ensures a stable Ni to Ti ratio while the Ni shell protects the Ti core from oxidation. This study presents basic configurations of Ti and Ni nanoparticles and their composite produced by gas aggregation source (GAS) under different conditions.

Methods
DC magnetron sputtering with two planar magnetrons was used to prepare Ti-Ni core-shell nanoparticles and a mixture of Ni and Ti nanoparticles. The sputtering system consisted of a primary gas aggregation cluster source (GAS) for creating Ti nanoparticles (NPs) and a secondary chamber for coating them with a Ni film, producing Ni nanoparticles, or depositing Ni nanoparticles on Ti ones. Ar gas with 99.996% purity was used as the working gas with a pressure of 35 Pa in the Ni and 11 Pa in the Ti chamber. A current of 400 mA on Ni magnetron and a current varying between 100 and 900 mA on Ti magnetron were used. Further details about the experimental setup are available in the work by Hanus et al. [3].
The nanoparticles were deposited onto a glass substrate. The samples for TEM analysis were prepared by depositing the nanoparticles, suspended in methanol, onto a grid with a SiN or lacey-carbon support film. A Jeol 2200FS transmission electron microscope operated at 200 kV was employed in STEM mode. Chemical mapping was done using energy dispersive spectroscopy (EDS).

Results
Pure Ti nanoparticles were prepared in the aggregation chamber (current of 400 mA). Their size is about 40 nm. Their surface is covered by a 3-5 nm thick TiO2 amorphous film, which probably forms during the exposition of nanoparticles to air. Pure nickel nanoparticles form in the secondary chamber (current of 400 mA). Their size ranges between 8-10 nm. A very thin oxide layer also forms on their surface after longer exposure to atmospheric oxide. However, its thickness is significantly smaller (less than 1 nm).
The composite nanoparticles were formed with a current of 100 mA in the GAS chamber for the Ti particle formation and 400 mA on the Ni coating magnetron. They are composed of a 30-40 nm Ti core encapsulated in a 5-10 nm thick Ni shell.

Conclusion

Titanium and nickel nanoparticles for SHS were successfully synthesized using a DC magnetron sputtering technique, which produced particles with a core-shell structure characterized by a metallic core and an oxidized shell. A thick oxide layer forms immediately on Ti nanoparticles, preventing their reactive properties. The oxide layer on Ni nanoparticles forms after longer exposure to atmospheric air, and its thickness is significantly lower. Composite nanoparticles consisting of Ti-core and Ni-shell could be prepared in the GAS with a simple engineering of the Ni/Ti ratio and used for the SHS synthesis.

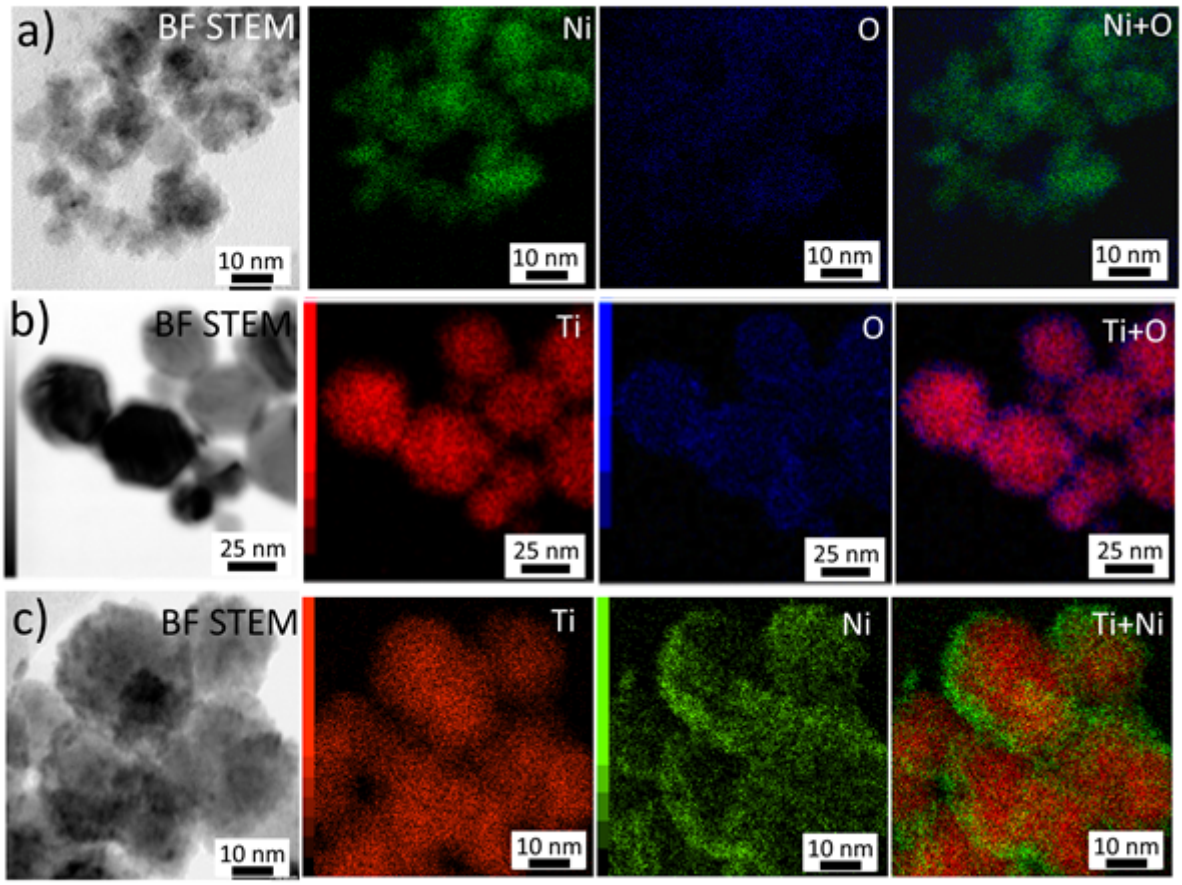

Keywords:

Nanoparticles, Ti-Ni core-shell nanocomposite

Reference:

[1] VIDYUK, T.M., KORCHAGIN, M.A., DUDINA, D.V. et al. Synthesis of Ceramic and Composite Materials Using a Combination of Self-Propagating High-Temperature Synthesis and Spark Plasma Sintering (Review). Combustion, Explosion, and Shock Waves, 2021, vol. 57, pp. 385–397.

[2] SEN, S.et al. Al-based binary reactive multilayer films: Large area freestanding film synthesis and self-propagating reaction analysis. Applied Surface Science, 2019, vol. 474, pp. 243-249.

[3] SOLAŘ, P. et al. Fabrication of Ni@Ti core-shell nanoparticles by modified gas aggregation source. J. Phys. D: Appl. Phys., 2017, vol. 50, article 475307.

1317

TEM-based study of the effect of precursor in thermal polymerization synthesis of graphitic carbon nitride

Dr. Rosaria Brescia[1], Paolo Negro[2], Prof. Federico Cesano[2], Prof. Domenica Scarano[2]
[1]Electron Microscopy Facility, Istituto Italiano di Tecnologia, Genoa, Italy, [2]Chemistry Department of Excellence and NIS (Nanomaterial for Industry and Sustainability) Interdepartmental Centre, University of Torino & INSTM-UdR, Turin, Italy

Poster Group 1

In the last years, graphitic carbon nitride (g-C_3N_4) emerged as an attractive alternative to carbon materials, especially for photocatalysis. Several synthesis strategies were shown to lead to a plethora of partially polymerized allotropes, while the fully polymerized form of g-C_3N_4 is hardly obtained. The 3D structure of g-C_3N_4 obtained by thermal polymerization of N-rich precursors is usually well described as consisting of tri-s-triazine building blocks arranged in layers bound by Van der Waals forces, more or less hydrogenated [1,2]. Among possible precursors, melamine (M) and urea (U) have been tested in thermal polymerization methods [3]. The mixture of these two precursors can lead to a tunable combination of high reaction yield and high specific surface area. This contribution provides a study at nanometer scale of the material obtained using M and U precursors and mixtures of them, which is key for understanding the variations in catalytic functionalities.
The material investigated has been synthesized via thermal polymerization in air at 550°C starting from powder precursors, using pure melamine (sample M100), pure urea (sample U100) and mixtures of them (U/M (mass)= 80/20 and 50/50, resulting in samples U80 and U50, respectively) [4]. The obtained powders, after grinding in a mortar, have been suspended in ethanol, sonicated and drop-cast onto holey-carbon-coated TEM grids. BF-TEM and SAED analyses (using a SA aperture of 5.8 µm) were carried out by a Tecnai F20. For HRTEM analyses, an image-Cs-corrected JEM-2200FS with a direct electron detection camera (Gatan K2 Summit) was used, which allowed to obtain large field-of-view images at minimized electron-dose-rate thus beam-induced damage, expected for this material [5]. HRTEM images were obtained at an electron dose rate of about 30 e-/(Å²·s) and a total dose of about 330 e-/Å².
Similar to what reported earlier, morphological analysis shows that, while M100 material consists of thicker and bulkier flakes, U100 is characterized by crinkled, thinner and porous flakes (BF-TEM in panels a, e). SAED analysis shows polycrystalline flakes in both samples, but a higher crystallinity characterizes M100, which exhibits a higher number of sharp diffraction rings compared to U100 (panels b, f). For both samples, SAED patterns match with an orthorhombic phase, hydrogenated ($C_{24}N_{30}(NH_2)_6$, ICSD 194747) reported for g-C_3N_4 obtained by thermal polycondensation of melamine [1]. The bulkier flakes in M100 are formed by nanometer-size crystalline domains, which give rise to sharp diffraction rings corresponding to the (hk0) planes of the structure, generated by the in-plane stacking arrangement of tri-s-triazine units. The dominant diffraction feature in SAED patterns for U100 is instead the (002), corresponding to the distance between stacked graphitic planes, while (hk0)-related features are much less visible: this stands for a much weaker in-plane order and higher defectivity in the material. FFT analyses of HRTEM images, obtained from smaller areas, show a hexagonal-symmetry pattern for M100, with rings that however show an in-plane-rotation of the crystallites forming the flake (panels c, d). HRTEM analysis of U100 confirms the totally random orientation of crystallites and the presence of (002) planes due to rolled-up flakes (panels g, h). Increasing electron doses show faster amorphization and final degradation in U100, due to the knock-on of hydrogen atoms, probably present at a higher content due to incomplete polymerization of the urea precursor [5]. From the comparison between SAED and HRTEM results, the comparably well-defined (hk0) peaks for M100 signify long-range order within the extended layers. Intermediate compositions lead to intermediate characteristics in the nanometer-scale structure, as expected.

In summary, overall the material obtained by thermal polymerization of U/M powders is characterized by a lack of long-range order. However, significant differences occur between the outcomes of different U/M precursor ratios, which can be explained in terms of nanostructure organization of crystalline domains. This tunable structure allows to control the material properties with the aim of optimizing their employ in application.

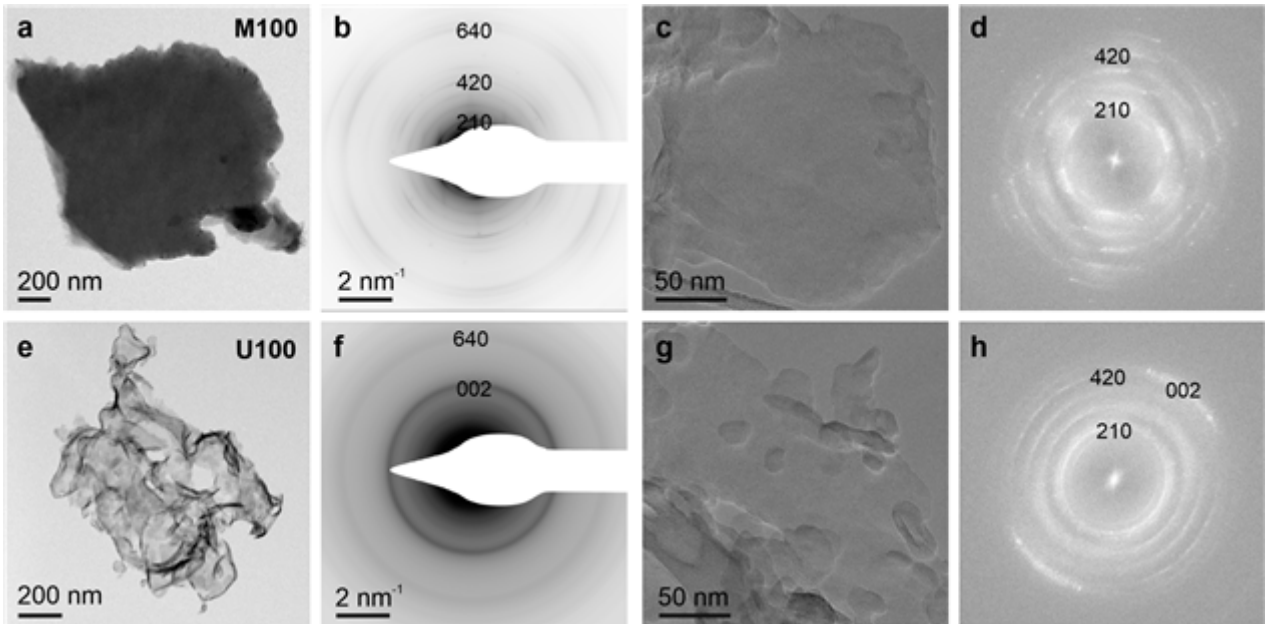

Keywords:

graphitic carbon nitride, thermal polymerization

Reference:

[1] F. Fina et al., Chem. Mater. 27 (2015) 2612
[2] P. Negro et al., Materials 16 (2023) 3644
[3] S. Martha et al., J. Mater. Chem. A 1 (2013) 7816
[4] P. Negro et al., J. Alloys Compounds 1002 (2024) 175053
[5] D. M. Haiber et al., ACS Nano 12 (2018) 5463

1339

Effect of thin 2D support layers on the catalytic properties of catalysts

Jeongwook Bae[1], Joohyun Lim[1]
[1]Department of chemistry, Kangwon National University, Chuncheon, Republic of korea

Poster Group 1

Background incl. aims
Electrochemical catalysts composed of metals used as active materials and supports for dispersion of active materials have advantages on both activity and stability. Carbon nanomaterials are widely used as conductive supporting materials. The coverage of support materials, even by a very thin layer of graphene, has been regarded as harmful for electrochemical reactions due to the physical blockage of active sites. However, recent research reported that the catalytic performance could be optimized depending on whether the active metal surface is covered with a monolayer of graphene, which alters the adsorption and desorption energies of reactants1 Considering diverse structures from the composites of metal nanoparticles and 2D support materials, controlling their structures and investigating structure-property relationships are important for developing novel catalysts. In this work, we used Pt nanoparticles as an active catalyst, and 2D MnO2 as support to prepare Pt-exposed and Pt-covered models for structure-relationship study.
Methods
Pt nanoparticles were synthesized using polyvinylpyrrolidone as a surfactant and ethylene glycol as a reductant. 2D MnO2 nanosheets were synthesized through oxidation of Mn2+ by H2O2 in the presence of tetramethylammonium hydroxide. To obtain Pt/MnO2 composites, the electrostatic self-assembly strategy was conducted. By changing the self-assembly process, two composite models were prepared. One is Pt nanoparticles covered with 2D MnO2 nanosheets (Pt-covered), and the other is Pt nanoparticles placed on the surface of 2D MnO2 nanosheets (Pt-exposed). The local structures and relative ratio between Pt and MnO2 were analyzed using transmission electron microscopy (TEM), X-ray diffraction (XRD), and inductively coupled plasma optical emission spectroscopy (ICP-OES), respectively.
Results
Two models had a similar Pt to MnO2 ratio. The Pt-covered model showed more dispersed Pt nanoparticles in the composites with less thickness of the 2D MnO2 layer assembly. The Pt-covered model revealed a lower electron transfer number for the oxygen reduction reaction compared to the Pt-exposed model, highlighting the possibility of controlling the catalytic pathway by changing the local structure of the composites.
Conclusion
In this study, we synthesized two model structures of Pt nanoparticles and 2D MnO2. Through ORR measurement, we observed that the catalytic activity varied depending on the structural differences. This indicates that the selectivity of catalytic reactions can be adjusted by controlling the catalyst structure. The detailed structure-relationship of the two models will be discussed.

Keywords:

Catalyst,support,2Dnanosheets,Oxygen reduction reaction

Reference:

[1] PNAS, 2014, 111(48), 17023-17028.

1342

Application of dual-beam microscope with TOF-SIMS in characterization of ceramic coatings deposited on filtration membranes

PhD Piotr Wiecinski[1], Professor Halina Garbacz[1], PhD Joanna Kacprzynska-Golacka[2], Profefssor Jerzy Smolik[2], Professor Andrzej Krasiński[1]
[1]Warsaw University of Technology, Warsaw, Poland, [2]Lukasiewicz Research Network – Institute for Sustainable Technologies, Radom, Poland

Poster Group 1

Filtration technologies are of the highest interest to human civilisation since they decrease air pollution and can expand access to drinking water. In the case of application in the food industry, bacteria and microorganisms' growth are the additional factors that influence the lifetime of membranes. Appropriate materials can be deposited on the membrane surface to limit these phenomena. However, such coatings shouldn't affect the filtration parameters of the membranes. During the work, different types of nanocrystalline ceramics coatings (CuO, AgO, ZnO and Cu+ZnO, Ag+ZnO, Ag+AgO, AgO+CuO) were deposited using two magnetron sputtering techniques: DC MS (Direct Current) and HPIMS (High Power Impulse). The influence of deposition parameters on coating thickness, surface morphology, microstructure and chemical composition was analysed. The distribution of the deposited material on the membrane surface, the interface between the coating and substrate, and antibacterial properties were analysed. The investigation evidenced that the obtained coatings were characterised by homogeneous, nanocrystalline structures, but they had different microstructures and morphology. For example, CuO coatings exhibit columnar or needle-like structures, while nano-grains in AgO coatings have more equalized shapes. Moreover, in multicomponent coatings (AgO+CuO), changes in the cathode (copper or silver) power result in differences in coating microstructure. The use of two sources leads additionally to the composite structure (matrix and fine particles) of the coating. The performed investigation also revealed that the application of the HPIMS technique allows the deposit of coatings of more homogeneous and less porous microstructure with smaller grain size compared to the DC MS technique. Coatings exhibits good antibacterial properties.

Acknowledgement: The research was financially supported by the Polish National Centre for Research and Development, grant no. TECHMATSTRATEG-III/0005/2019-00

Keywords:

Filtration membranes, composite coatings, dualbeam